USC UNIVERSITY OF SOUTHERN CALIFORNIA

Image Processing and Informatics Laboratory (IPI)

USC UNIVERSITY OF SOUTHERN CALIFORNIA

Annual Progress Report
February 2010

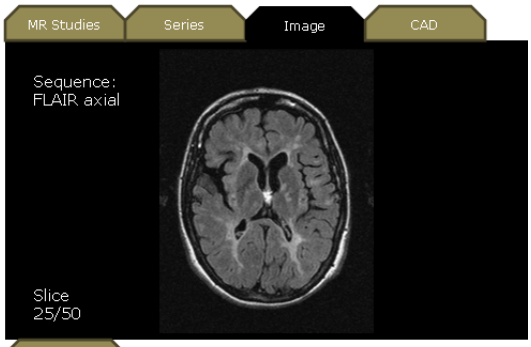

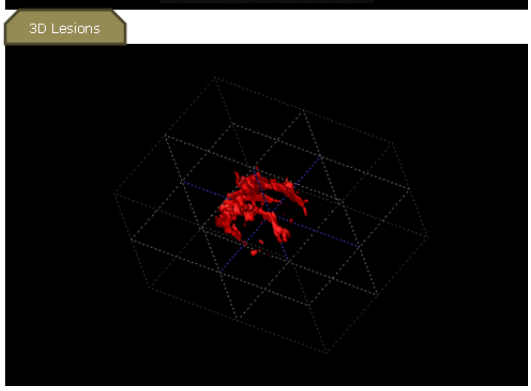

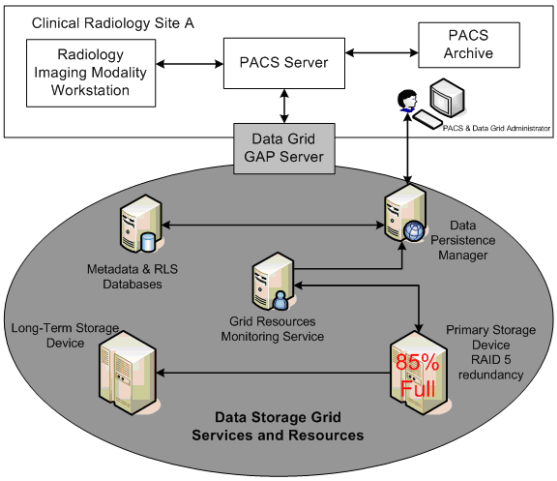

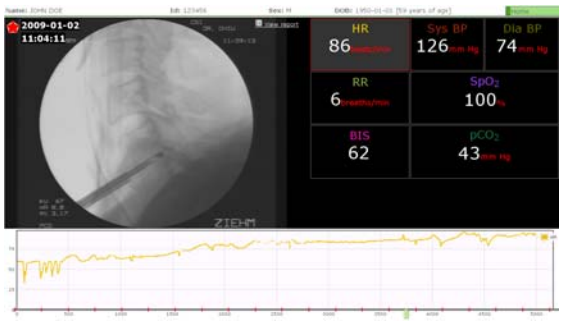

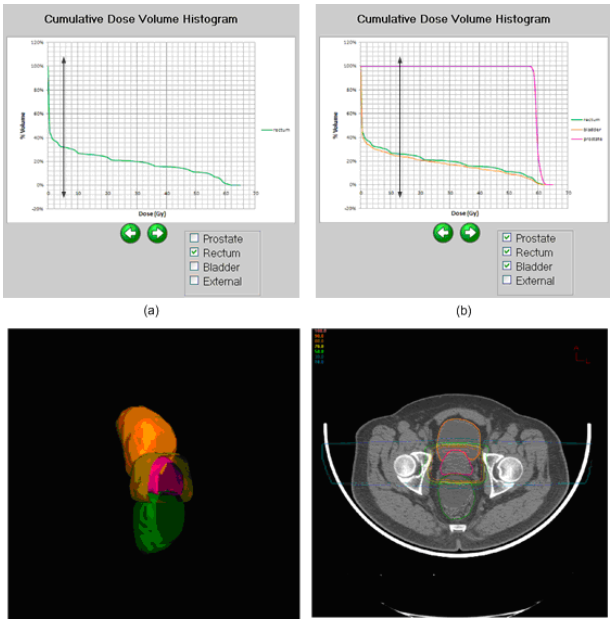

Image Processing and Informatics Lab
Department of Radiology, Keck School of Medicine
University of Southern California
Suite 105, CSC/IGM, 2250 Alcazar St, Los Angeles, California 90033
323 442-2928 Office, 323 442-2575 Fax

DEPARTMENT OF RADIOLOGY AND BIOMEDICAL ENGINEERING
UNIVERSITY OF SOUTHERN CALIFORNIA

2010 Annual Report

Image Processing and Informatics Laboratory

2250 Alcazar Street, CSC 105, Los Angeles, CA 90033. Tel: (323) 442-2928 Fax: (323) 442-2575

SUMMARY

The Image Processing and Informatics Laboratory (IPILab) continues to thrive within the Health Science Campus, USC in the hub of major clinical healthcare and research facilities such as the University Hospital, Healthcare Consultation Centers I and II, Norris Cancer Center, and the Zilka Neurogenetic Institute. IPILab has continued to maintain its course with research support and establishing new collaborations and hosting visitors interested in Imaging Informatics training and research. Some of the accomplishments are detailed:

1. Education and Training

IPILab is entering its fifth and final year of a T32 Training Grant from the National Institute of Biomedical Imaging and Bioengineering (NIBIB), National Institutes of Health (NIH), DHHS entitled: "Biomedical Imaging Informatics Training Program" effective September, 1, 2005 – August 31, 2010, totaling about US$1.6 million. Existing trainees continue receiving recognition as first author in national presentations, proceedings papers and peer-reviewed chapters and papers. We have successfully recruited four additional T32 trainees – Three are T32 Postdoctoral Fellows, 1) Jorge Documet, Ph.D., graduating from USC Biomedical Engineering Department, Viterbi Engineering School; 2) James Fernandez, MD, who graduated from University of Hawaii School of Medicine and accepted to the USC Radiology Residency Program. He postponed his residency training and has returned for a second year training working on computer-aided diagnosis; and 3) Ali Maziad, MD who completed his Orthopedic Surgery Residency at Ain Shams University Medical School, Egypt working on clinical aspect of MISS. As for the pre-doctoral fellows, Syed Ashrafulla, who graduated from University of Texas and is currently a PhD student in the Viterbi School of Engineering, USC working on informatics aspect of image reconstruction, has joined us. Two current USC BME Ph.D. students, Jasper Lee working on Data Grid of molecular imaging, and Kevin Ma working on Informatics model of Multiple Sclerosis, are continuing in the T32 training program.

Summer activities are the height of our academic year for recruiting new and young blood into the IPILab for research collaborations. IPILab welcomed Mr. Colin Jacobs, a Biomedical Engineering Master's student from the University of Eindhoven in the Netherlands to a 15-week internship where he collaborated on image processing and system design for Multiple Sclerosis CAD. The USC Summer Undergraduate Research Programs continues to fund our efforts to recruit and to foster bright young undergraduate students searching for future academic research directions. The previous summer we were able to recruit two undergraduate students from the BME program who remained as Student Assistants in IPILab after the summer. These students were accepted into the Master's Program for both the Electrical Engineering and the Biomedical Engineering departments respectively to continue their graduate career. In addition, an entering USC freshman was recruited this last summer, who was the youngest intern ever in the history of IPILab. Finally, Chiafen Tsai, MD, a visiting faculty from the Department of Psychiatry, Taipei Veterans General Hospital and National Yang-Ming University Schools of Medicine collaborated with us in Imaging Informatics research during her stay here with the Department of Neurology, USC and presented a joint project with our lab at RSNA in November 2009.

Other new additions to our lab, which are a direct result of being closer on the Health Science Campus, include Ruchi Deshpande, Young Woo Park, Alex Zhong, and Kruti Shah, all Master's student interns from the BME graduate program.

In addition to the milestones mentioned above in the T32 training program, Dr. Jorge Documet completed his Ph.D. in BME and is now a T32 Post Doctoral fellow with IPILab. Two other of our BME Ph.D. students have passed their qualifying Ph.D. examinations. Dr. Brent Liu continues in the position as co-Chair for the "Advanced PACS-based Imaging Informatics and Therapeutic Application" Conference of the SPIE Medical Imaging Conference.
Finally, last but not least, Dr. Bernie Huang completed and published his long-awaited and new book titled "PACS and Imaging Informatics" Second Edition, John Wiley & Sons, Publisher January 2010. The cover of the book is included in this annual report for reference. Bernie has just become Professor Emeritus, USC.

2. Research Projects

We have continued in our areas of Medical Imaging Informatics research: 1) a DICOM-RT based ePR system with Decision Support for Managing patients treated with Proton Beam Therapy; 2) CAD systems for Multiple Sclerosis detection in MRI and for small Acute Intracranial Hemorrhage detection on CT; 3) CAD-PACS Integration Toolkit; 4) A surgical ePR system for Image-Assisted Minimally Invasive Spinal Surgery (MISS), the the first system has been used in daily surgical operation at the California Spine Institute, 2009; and 5) The development of an eFolder System for MS Patients, and 6) dedicated breast MRI Data Grid system (BIDG). This year we had two papers accepted for publication in JCARS for both the CAD-PACS Toolkit and the surgical ePR system for MISS. We enjoyed another successful RSNA conference in November 2009 with a total of seven presentations. In addition, one paper was accepted to the ASTRO conference immediately preceding the RSNA conference. Other existing long term research projects such as the Data Grid have continued to progress, and have expanded clinical applications in imaging-based clinical trials, small animal imaging, and Breast Cancer imaging. Some of the research work continues to be supported by extramural finds including NIH, U.S. Army Medical Research and Materiel Command, and the private industry. We are establishing new collaborations in the area of Rehabilitative Science and Physical Therapy since multi-media data is utilized in the research field in addition to Patient-related imaging informatics data.

3. Industrial Collaborations

IPILab has continued R & D collaborations with the private industry including but not limited to: Fujifilm, USA in the development of PACS tools; Calgary Scientific, Inc. in 3-D thin-client server system with iPhone display technology; and SurgMatix, USA in the development of an ePR System for minimally invasive spinal surgery; and Southern Taiwan University of Technology, Taiwan and Aurora Imaging Technology, Boston in collaborating on a dedicated breast imaging data grid for healthcare of mobile breast cancer patients.

As described in the Table of Contents, this 2010 Annual Report includes materials related to the IPILab, IPILab R & D plans and current results, selected published and in-press peer-reviewed

papers during the year, as well as preprints to appear in the *Proceedings of the International Society for Optical Engineering (SPIE) in Medical Imaging*, San Diego, California, February 13-18, 2010.

Our research has been supported by:

- NIH/NIBIB R01 EB 00298
- NIH/NLM Training Grant T15 LM07356
- NIH/NIBIB Biomedical Imaging Informatics Training Grant T32 EB 00438
- USAMRMC/Henry M. Jackson Foundation Subaward 53-5149-5600
- USAMRMC/TATRC AAMTI Walter Reed Medical Center Subaward 2007011185
- USC Undergraduate Research Award No. 22-2149-6044
- USCRA Research Fund 3051-00
- Southern Taiwan University of Technology, Taiwan
- Fujifilm, USA
- MI^2, USA
- SurgMatix, USA

Table of Contents

PACS and Imaging Informatics: Principles and Applications. 2nd Ed
John Wiley & Sons, Publisher January 2010
H.K. Huang 191

STAFF AND COLLABORATORS

Faculty and Administration	
Edward G. Grant, M.D., FACR. Professor and Chairman, Department of Radiology **H.K. Huang, D.Sc., FRCR (Hon.), FAIMBE** Professor Emeritus of Radiology and BME Chair Professor of Medical Informatics, Hong Kong Polytechnic University; and Honorary Professor, Shanghai Institute of Technical Physics, The Chinese Academy of Sciences **James William Hill, M.D., J.D.** Clinical Assistant Professor, Department of Radiology **James Sayre, Ph.D.** Professor of Biostatistics and Radiological Science, University of California, Los Angeles (UCLA) Consultant **Cammy Huang, Ph.D.** Lecturer, Computer Science Dept, Director of Scientific Outreach, WGLN Stanford University Consultant **Angelica Virgen** Administrative Manager	**Michael C.K. Khoo, Ph.D.** Professor and Chairman, Department of Biomedical Engineering (BME) **Brent J. Liu, Ph.D.** Associate Professor of Radiology and BME Director, IPILab **Greg T. Mogel, M.D.** Associate Professor of Radiology, Asst Prof. of BME **Ewa Pietka, Ph.D. D.Sc.** Professor, Technical University of Silesia, Poland Visiting Professor of Radiology **Jianguo Zhang, Ph.D.** Professor, Shanghai Institute of Technical Physics, The Chinese Academy of Science Visiting Professor of Radiology, USC **Maria YY Law, MPhil, BRS, Ph.D.** Associate Professor, Hong Kong Polytechnic University President, Hong Kong College of Radiography and Radiation Therapy Visiting Associate Professor of Radiology, USC **Heinz U. Lemke, Ph.D.** Technical University Berlin Visiting Research Professor of Radiology, USC
Visiting Fellows	**Post Doctoral Fellows**
Tao Chan, M.D., Ph.D. Assistant Professor, Department of Radiology Hong Kong University **Marco A. Gutierrez, Ph.D.** Invited Professor Heart Institute of University of San Paulo Visiting Distinguished Research Fellow	**Jorge Documet, Ph.D. (T32 Fellow)** Lab Manager **Paymann Moin, M.D.** Radiology Fellow **James Fernandez, M.D. (T32 Fellow)** Radiology Resident **Ali Maziad, M.D (T32 Fellow)** Surgery Fellow
Research Assistants/PhD Candidates	**Graduate Student Assistants**
Anh Le, M.S. Ph.D. Candidate **Jasper Lee, M.S. (T32 Fellow)** Ph.D. Candidate **Kevin Ma, M.S. (T32 Fellow)** Ph.D. Candidate **Syed Ashrafulla, B.S. (T32 Fellow)** Ph.D. Student	**Ruchi Deshpande, B.E.** **Young Woo Park, B.S.** **Colin Jacobs, B.S.** University of Eindhoven, The Netherlands **Alex Zhong, B.S.** **Kruti Shah, B.S.**

IPILAB NEW LOCATION & COLLABORATIONS

2250 Alcazar Street, CSC 105, Los Angeles, CA 90033

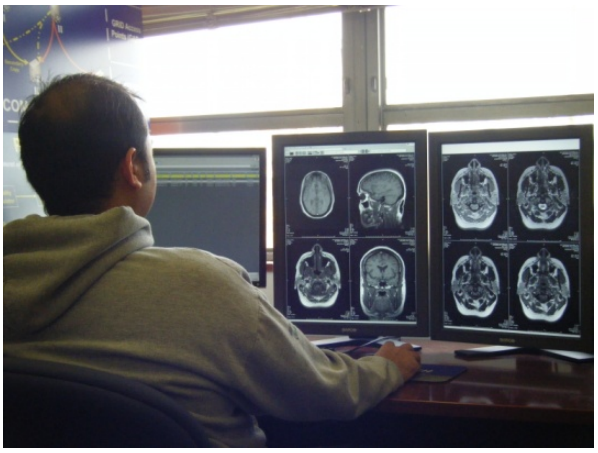

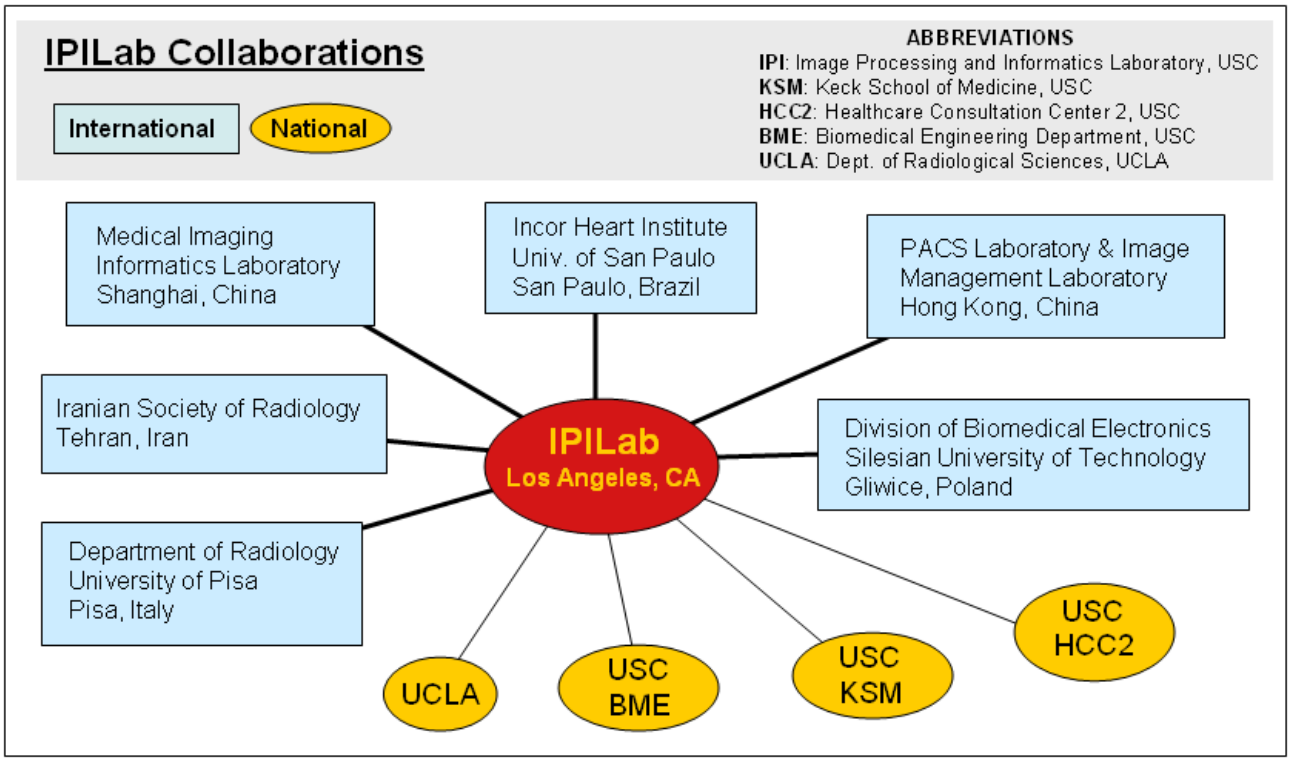

IPILAB WEBSITE

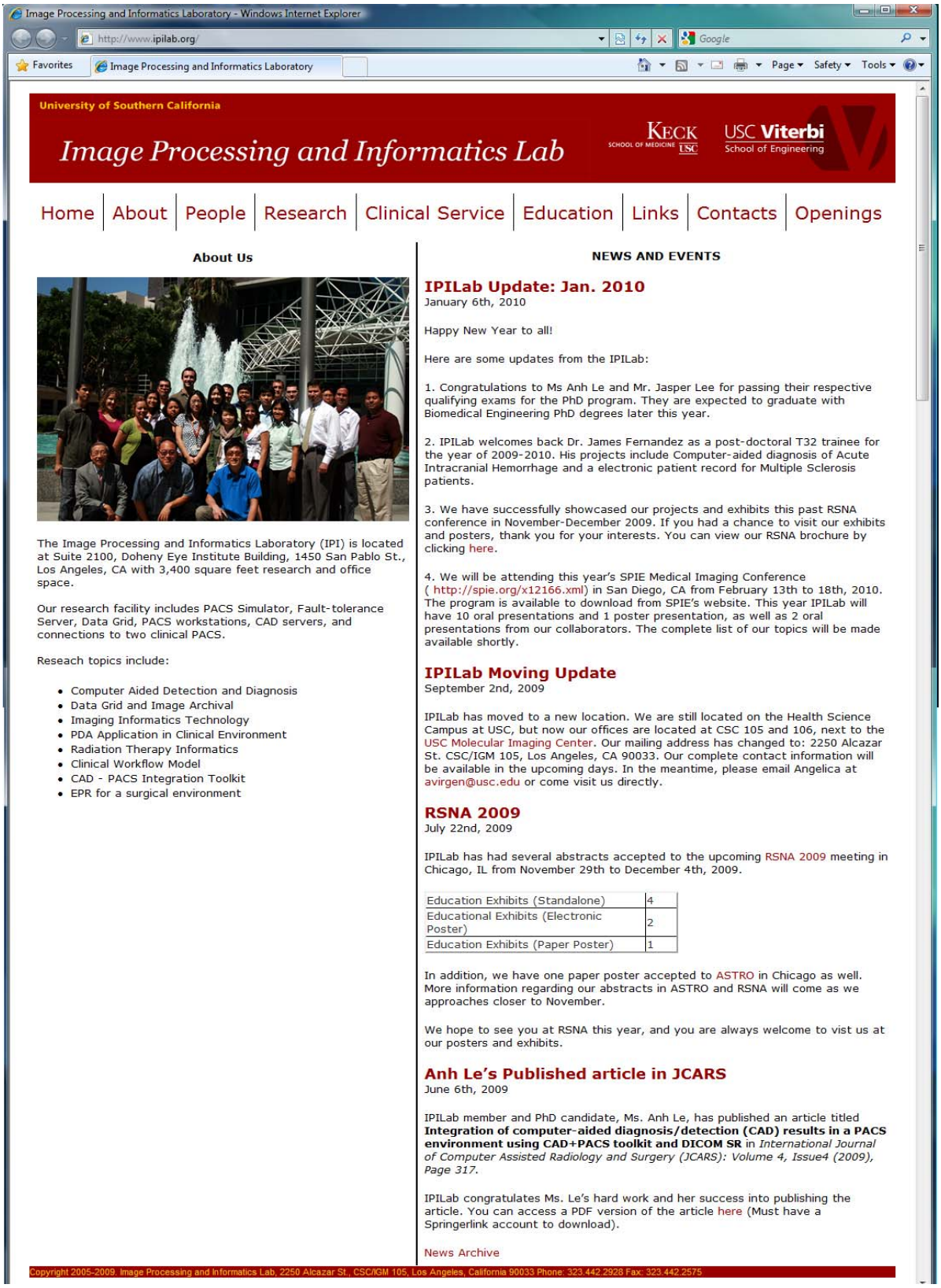

RSNA 2009 POSTERS AND PAMPHLET

UNIVERSITY OF SOUTHERN CALIFORNIA

Image Processing and Informatics Laboratory

Department of Radiology, Keck School of Medicine

RSNA 2009 Quality Counts

RSNA 2009

Education Exhibits & Presentations

November 29 – December 4, 2009
McCormick Place,
Chicago, Illinois

USC Viterbi School of Engineering

KECK SCHOOL OF MEDICINE USC

2250 Alcazar St. CSC 105
Los Angeles, CA 90033
Tel: (323) 442-2928
Fax:(323) 442-2575
http://www.ipilab.org

Contents

STAFF AND COLLABORATORS

Faculty and Administration	
Edward V. Grant, MD, FACR Professor and Chairman, Department of Radiology	**Michael C.K. Khoo, PhD,** Professor and Chairman, Department of Biomedical Engineering (BME)
H.K. Huang, DSc, FRCR (Hon.) Professor of Radiology and BME Director, IPI	**Brent J. Liu, PhD** Associate Professor of Radiology and BME
Vicente Gilsanz, MD Professor of Radiology and Pediatrics	**Greg T. Mogel, MD** Assistant Professor of Radiology and BME
James William Hill, MD, J.D. Clinical Assistant Professor, Department of Radiology	**Ewa Pietka, PhD, DSc** Professor, Technical University of Silesia, Poland *Visiting Professor of Radiology*
James Sayre, PhD Professor of Biostatistics and Radiological Science, UCLA *Consultant*	**Jianguo Zhang, PhD** Professor, Shanghai Institute of Technical Physics, The Chinese Academy of Science *Visiting Professor of Radiology*
Cammy Huang, PhD Director of Scientific Outreach, Wallenberg Global Learning Network, Wallenberg Hall *Consultant*	**Maria YY Law, MPhil, BRS, PhD** Associate Professor, The Hong Kong Polytechnic University *Visiting Associate Professor of Radiology*
Angelica Virgen Administrative Assistant	**Heinz U. Lemke, Professor** Technical University Berlin *Research Professor of Radiology*
Postdoctoral and Visiting Fellows	
Jorge Documet, PhD Lab Manager	**Marco A. Gutierrez, PhD** Invited Professor, Heart Institute of University of San Paulo
Paymann Moin, MD	**Heston K. Kwong, MD, MBA, MS** PhD Candidate, Hong Kong Polytechnic University
Tao Chan, MD, PhD Hong Kong Polytechnic University	**James Fernandez, MD**
Richard Lee, MD	**Ali Maziad, MD**
Research Assistants & PhD Candidates	*Graduate Student Assistants*
Anh Le, MS	**Ruchi Deshpande, BE**
Jasper Lee, MS	**Young Woo Park, BS**
Kevin Ma, MS	**Colin Jacobs, BS** University of Eindhoven, The Netherlands

IPILAB NEW LOCATION & COLLABORATIONS

2250 Alcazar Street, CSC 105, Los Angeles, CA 90033

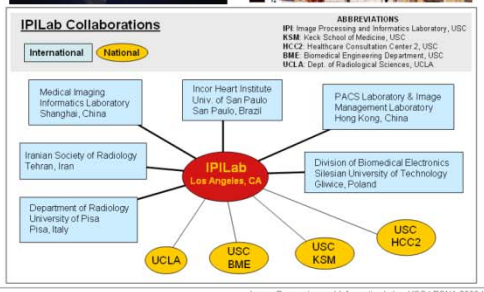

EDUCATION EXHIBITS – STAND ALONE PRESENTATIONS

LL- IN3538: Dynamic Digital MR Image Visual Templates for Grading White-Matter Lesions from Vascular Dementia in a PACS Environment

K C Ma, MS, Los Angeles, CA; C C Tsai, MD; P Moin, MD; J Lee, MD; B J Liu, PhD (kevincma@usc.edu)

BACKGROUND

Age-related white matter degradation is a sign of vascular dementia. Dementia severity is often quantified by the degree of white matter degradation observed in brain MR images. Currently, grading vascular dementia involves subjective uses of a hardcopy template, and the grading method and scale are not standardized. In order to create a standardized grading of white matter changes in vascular dementia and a more convenient method in the digital imaging environment, we designed and implemented a digital and dynamic library of brain MR templates accessible from diagnostic workstations in an enterprise PACS environment.

EVALUATION

A web-based user interface of digital brain MR templates has been designed. The digital template contains multiple MR studies showing various degrees of white matter change. Each image set is carefully selected and evaluated by radiologists at USC; subjects contain both genders with varying age groups. The digital template has been integrated with PACS review workstations in a healthcare enterprise, accessible directly from the PACS application. Radiologists can compare the template images from the web-based GUI with images from PACS. The GUI enables dynamic image manipulation, such as zooming, window/level, pan, and scrolling. Evaluations of the digital template are completed by two radiologists, comparing the printed hardcopy templates with the digital template.

DISCUSSION

The web-based digital template has been successfully designed and implemented in the lab setting, which includes a simulation of the PACS environment. The evaluation workflow has been demonstrated. The performance of the web-based templates is evaluated, and the successful results show that the dynamic digital template improves accessibility and convenience as compared to hardcopy paper templates.

CONCLUSION

The digital template is a comprehensive and useful tool to assist radiologists in grading white matter changes relating to vascular dementia. It addresses the need to have a reliable and a more systematic approach to the evaluation. Future works include implementation in a clinical setting and automatic quantification of white matter in relation to brain matter for an objective approach.

LL-IN3550: An Image-Intensive Breast Cancer Data Grid Infrastructure for Data Mining and Outcomes Research

B J Liu, PhD, Los Angeles, CA; J Documet, PhD; M Y Law, PhD; J Lee, MS; X Hong, PhD; P Moin, MD; K Ma, MS; H K Huang, DSc (brentliu@usc.edu)

PURPOSE/AIM

The utilization of breast MRI is increasing in the diagnostic evaluation of suspicious breast findings. As more imaging centers implement dedicated breast MR, the need for managing data on a large-scale is apparent. We propose an overall solution utilizing data grid and ePR system technologies as an infrastructure for data mining and research.

CONTENT ORGANIZATION

Present the data grid for DICOM images and DICOM-SR data and the image-intensive web-based ePR system technologies. Present the current three-site dedicated breast MR outpatient centers as the clinical application. Show how the implementation of the two technologies can provide a global solution that is portable for the Breast Cancer patient including aggregation of Mammo, US, MR, CAD, BI-RADS, and clinical related reports data to form a powerful platform for data mining and outcomes research.

SUMMARY

The data grid implemented with a web-based ePR system can provide a robust platform for managing Breast Cancer Patient's globally and providing an infrastructure for imaging informatics data that provides future outcomes and data mining research. Specifically we showed a data mining and outcomes example where Mammo studies with dense breasts and corresponding MRI studies with findings of BIRADS 3-5 and correlated biopsy/pathology results were queried/retrieved and compared the findings of both.

LL-IN3551-R: Mind Over Matter: Using a Neuroheadset to Interact with a PACS Workstation

P Moin, MD, Los Angeles, CA; R Deshpande, BE (pmoin@usc.edu)

BACKGROUND

Evolving modalities and the demands of efficient interpretation are increasingly at odds with each other necessitating a revisit of the image interpretation process.

EVALUATION

The Emotiv neuroheadset is adapted for use with a clinical PACS system in an effort to replicate basic functions. Objectives are to reduce repetitive motions, increase productivity, and eventually allow complex commands to be initiated in a single step. In addition, the reduction of repetitive motions using a mouse will reduce the prevalence of associated musculoskeletal fatigue/injuries that may result.

DISCUSSION

We seek to participate in the development of next-generation of human-machine interface tools. The eventual endpoint of interaction between humans and electronic devices is a direct neural-machine interface. We hope this is the start to that process in radiology. In addition, advancement of such functionality could allow more efficient image viewing in other situations such as in the operating room where a surgeon could review and manipulate relevant images intraoperatively while maintaining a sterile field.

CONCLUSION

Continued development of the Emotiv neuroheadset functionality could eventually make the use of a mouse obsolete, increase image interpretation efficiency and allow the proliferation of image intensive medical applications outside of the radiology reading room.

LL-IN3559: Imaging Informatics Beyond Radiology: Clinical experiences from a 6-month Implementation of a DICOM Multimedia Electronic Patient Record (ePR) System for Image-Assisted Minimally Invasive Spinal Surgery

J Documet, PhD, Los Angeles, CA; B J Liu, PhD, A Le, MS, J Chiu, MD, H K Huang, DSc (documet@usc.edu)

PURPOSE/AIM

To present an image and data intensive Electronic Patient Record (ePR) tailored to improve the efficiency of clinical procedures for Image-Assisted Minimally Invasive Spinal Surgery, which is a new frontier in imaging informatics. Conclusions from a clinical implementation of the ePR that has been in place for over six months will be presented.

CONTENT ORGANIZATION

The main stages of clinical procedures for Minimally Invasive Spinal Surgery will be presented including Pre, Intra and Post Operative phases, which provide a variety of data types, such as images (e.g. C-Arm, Endoscopic images, MRI, CR), patient information, videos, waveform data points and pain assessment forms. All these data are acquired and stored on a fault-tolerant and reliable ePR system. Clinical implementation of this ePR system including pitfalls and challenges will also be addressed.

SUMMARY

A novel ePR system tailored to collect and integrate relevant imaging and informatics data from patients who undergo Minimally Invasive Spinal Surgery is presented. The collection of the different data types during the span of the entire clinical procedure opens a rich new area of research opportunities and improving overall workflow efficiency. Similarities between PACS and ePR system clinical implementations were highlighted.

EDUCATION EXHIBITS – ELECTRONIC PRESENTATIONS

LL-UR4738: A Benchmark Study to Measure Native Client-side Image Manipulation Performance Utilizing Firefox 3.5, Safari 4, Chrome 2, and Internet Explorer 8

J Documet, PhD, Los Angeles, CA; R Lee, MD, K Ma, MS; B Liu, PhD (documet@usc.edu)

PURPOSE/AIM:

Viewing medical imaging studies via a web browser has become predominant in the past years and is usually done using a thin client or AJAX (Asynchronous JavaScript and XML) technologies. With significant improvements in Javascript engines by most of current web browser vendors, we explore how well they perform medical imaging manipulation natively.

CONTENT ORGANIZATION:

A cross-platform and stand-alone methodology to measure image manipulation performance utilizing a set of web browsers will be presented with a specific number of tests that are performed. These tests include: zoom, pan, window/level and inverting an image. A set of a 5 jpeg images for each CT, MRI, US and CR will be utilized during the performance evaluation. A virtual machine with Windows XP Home will host all the different web browsers. A final performance evaluation will be presented.

SUMMARY:

This unique benchmark methodology will provide quantitative information about the performance of the latest versions of most used web browsers when performing medical image manipulation which will ultimately allow developers and users to make better decisions on which technology to choose for web-based image viewing. The image manipulation will be performed on the jpeg format instead of native DICOM due to the lack of natively rendering DICOM images on web browsers.

EDUCATION EXHIBITS – POSTER

LL-IN3052: Pre-clinical Implementation and Disaster Recovery Evaluation of a Medical Imaging Informatics Data Grid Used as a Tier 2 Enterprise PACS Back-up Solution at the USC Academic Medical Center

J Lee, MS, Los Angeles, CA; K Wang; B J Liu, PhD (jasperle@usc.edu)

PURPOSE/AIM

To address clinical challenges and performance concerns of a Data Grid based on the Globus Toolkit used as a tier 2 enterprise PACS back-up solution. Topics include methods to integrate with a thin-client PACS, HIPAA-compliance within the enterprise PACS, and disaster recovery performance.

CONTENT ORGANIZATION

1. Introduce design and requirements of the IPILab's Medical Imaging Informatics Data Grid
2. Overview the enterprise PACS infrastructure at the USC Academic Medical Center, consisting of four facilities and two thin-client PACS
3. Discuss system integration methods of the Data Grid with the two PACS
4. Discuss HIPAA concerns and data access-control using the Data Grid's distributive technology
5. Evaluate workflow and performance of the Data Grid in two PACS down-time scenarios

SUMMARY

The Data Grid utilizing the Globus Toolkit is a novel design for an enterprise PACS environment looking for a tier 2 backup solution. It can be integrated into an existing PACS and maximizes the SAN infrastructure. Challenges are realized, however, during pre-clinical implementation of the Data Grid and disaster recovery scenarios at the USC Academic Medical Center. System integration, HIPAA-compliance, and disaster recovery workflow and performance are some major challenges to be addressed.

SCIENTIFIC POSTERS – ELECTRONICS

LL-IN2121-D06: Multi-Modality Electronic Patient Record (ePR) for Diagnostic Breast Imaging Centers

Mon Nov 30 2009 12:15PM - 1:15PM ROOM Lakeside Learning Center

K C Ma, MS, Los Angeles, CA; P Moin, MD; X Hong, PhD; M Y Law, PhD; B J Liu, PhD; H K Huang, DSc; et al.(kevincma@usc.edu)

BACKGROUND
Diagnostic breast imaging is often completed at outpatient imaging centers. To eliminate the hassle of patients carrying hard-copy image and clinical data, provide a remotely-accessible and comprehensive database, and reduce cost, a web-based electronic patient record (ePR) system for multi-modality breast imaging has been developed. The system combines patient information, history, and medical images as a total informatics solution. It allows patients to be mobile without carrying or having to coordinate retrieving their entire history and allows radiologists to easily access patient history to aid diagnosis.

EVALUATION
The breast imaging ePR system features a patient record database, a multi-modality image database, a BI-RADS report database, and a web-based GUI that can be accessed securely and remotely within the ePR network. The GUI is designed to display dynamically MR, mammography, and ultrasound images in a web browser with zooming, panning, and scrolling. Image-guided biopsies and biopsy reports are stored. A search function is for image data mining through both patient information and BI-RADS reports. The system has been implemented and evaluated in a laboratory environment, where a workflow simulates the ePR network involving three outpatient breast imaging centers.

DISCUSSION
The infrastructure of patient information and image database has been completed and set up in the lab environment. The GUI is able to display patient information, multiple images, and their diagnostic and/or biopsy reports. The workflow simulation with three outpatient breast imaging centers includes image querying and retrieving, creating new patients, remote access of patient information, report look-up and data search from BI-RADS scores.

CONCLUSION
This study proves that a multi-modality ePR system is a robust information and image archive and retrieval solution for outpatient breast imaging centers. A successful workflow simulation shows the potential in clinical implementations. Future works include evaluations with radiologists and subsequent clinical implementations. The results can be utilized to expand the breast-imaging ePR system for other clinical uses.

TECHNICAL EXHIBIT: DEN @ USC

Booth 7237 (North Building Hall B): USC Viterbi's School of Engineering Master's Programs and the Distance Education Network (DEN)

The USC Viterbi School of Engineering is consistently ranked among the top ten graduate engineering schools in the United States by U.S. News & World Report. Over 50 Master of Science programs are available in broad disciplines and niche areas, including biomedical imaging and imaging informatics, smart oilfield technologies, medical device & diagnostic engineering, and game development.

Whether you are seeking to pursue your M.S. full time or part time, the Viterbi School has options to enable you to advance your degree. We also offer our M.S. programs online via the Distance Education Network (DEN). DEN enables students to continue their education 100% online. DEN caters to the professional engineer by providing over 30 Master of Science degrees online. In addition to Master's degree programs, Graduate Certificates and Professional (non-credit) courses are available online. Students can also choose to come to campus to attend courses and interact with other classmates on campus and off campus through DEN's unique blended delivery systems.

Representatives from USC are here at RSNA to introduce our various graduate degree programs. Most of us here at IPILab are in progress or have completed our training for Masters in Medical Imaging and Imaging Informatics, which is offered on DEN. We highly recommend you to visit the exhibit if you are interested in learning more about our imaging informatics program.

USC Technical Exhibit Schedule	
Sunday, Nov 29	10am-5pm
Monday, Nov 30	10am-5pm
Tuesday, Dec 1	10am-5pm
Wednesday, Dec 2	10am-5pm
Thursday, Dec 3	10am-2pm

Notes

USC UNIVERSITY OF SOUTHERN CALIFORNIA

Image Processing and Informatics Lab

An Image Intensive Breast Cancer Data Grid Infrastructure for Data Mining and Outcomes Research

B Liu, PhD[1]; J Documet, PhD[1]; M Law, PhD[2]; J Lee, MS[1]; X Hong[3], BS; HK Huang, DSc[1]

1 – Department of Radiology, Keck School of Medicine University of Southern California, Los Angeles, CA, USA

2 – Department of Health Technology and Informatics, The Hong Kong Polytechnic University, Hung Hom, Kowloon, HK

3 – Aurora Imaging Technology, Inc. , North Andover, MA, USA

IPILab Data Grid Project

LEARNING OBJECTIVES:

1) Dedicated Breast Imaging Archive using Data Grid Technology for Fault-Tolerant and Real-time Distribution of Multi-modality and Multimedia Imaging Data.

2) Centralized and Secure Management of Global Breast Imaging Patient Data.

3) Integrated Web-based electronic Patient Record system for User-level Data-Mining Tools and Visualization of Clinical Outcomes.

SUMMARY:

The utilization of breast MRI is increasing in the diagnostic evaluation of suspicious breast findings. As more imaging centers implement dedicated breast MR, the need for managing data on a large-scale is apparent. We propose an overall solution utilizing data grid and ePR system technologies as an infrastructure for data mining and research. The data grid implemented with a web-based ePR system can provide a robust platform for managing Breast Cancer Patient's Multi-modality and Multi-media data globally and providing an infrastructure for imaging informatics data that can provide future clinical outcomes and data mining research.

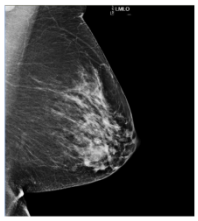

Mammography of Dense Breast

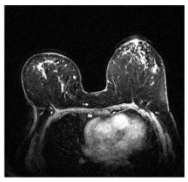

Dedicated Breast MRI

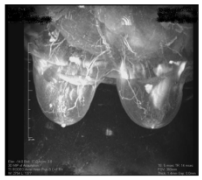

3-D MIP Video

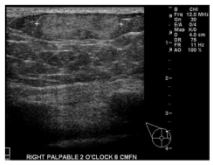

Ultrasound

Breast Imaging Patient Reports

Biopsy/Imaging Results

* Images Courtesy of Aurora Imaging Technology, Inc.

USC UNIVERSITY OF SOUTHERN CALIFORNIA

Image Processing and Informatics Lab

Breast Imaging Data Grid with Integrated ePR Demonstration

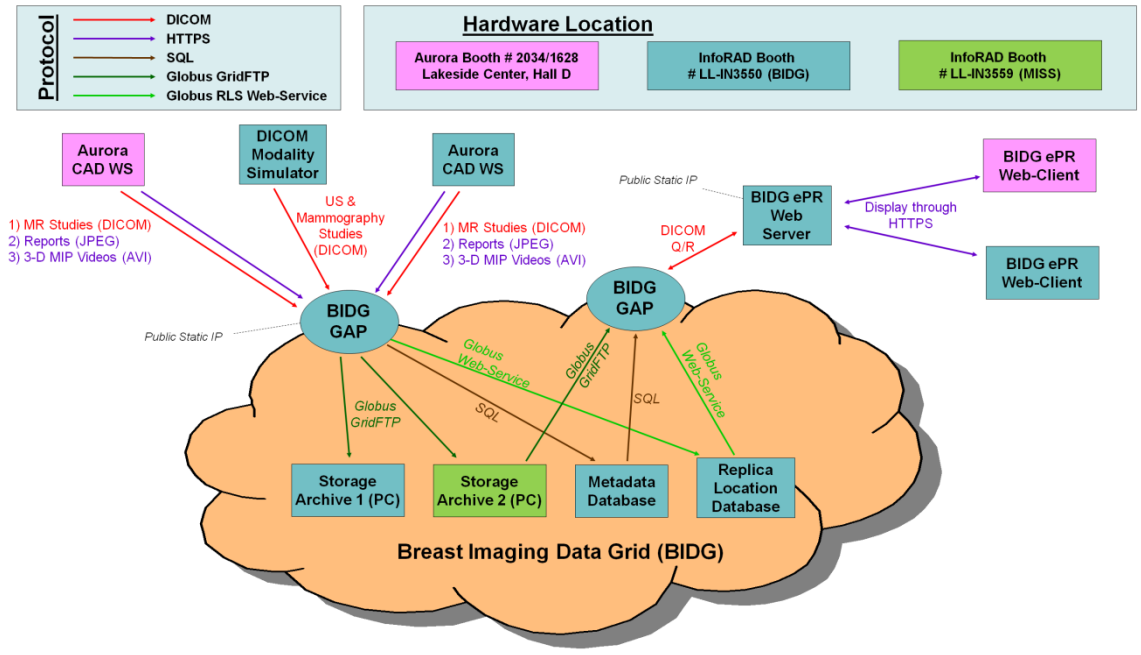

RSNA 2009, McCormick Center – Lakeside Learning Center

This Research is Funded in Part by T32 EB00438 and MII Corp.

USC UNIVERSITY OF SOUTHERN CALIFORNIA

Image Processing and Informatics Lab

Dynamic Digital MR Image Visual Templates for Grading White-Matter Lesions from Vascular Dementia in a PACS environment

K Ma, MS; C Tsai, MD**; J Lee, MD*; A Le, MS*; P Moin, MD*; B Liu PhD**

**Image Processing and Informatics Lab*
Department of Radiology, Keck School of Medicine
University of Southern California, Los Angeles, CA 90033

***Department of Psychiatry, Taipei Veterans General Hospital, Taiwan.*
National Yang-Ming University Schools of Medicine, Taipei, Taiwan

Background:

- Age-related white matter degradation is related to vascular dementia. Recognition of white matter changes may help identify patients with different symptomatology
- Visual rating scales developed by NINDS-AIREN criteria
- White matter degradation rating is performed by comparing patient's images to a hardcopy template with no standardized protocol
- A more practical and convenient method for grading white matter degeneration is needed in today's digital imaging environment

We Propose:

- A digital and dynamic web-based library of brain MR templates accessible from diagnostic workstations in an enterprise PACS environment
- Advantage: Conveniently select the closest-matched brain MR image set to the patient's images
  - readily accessible anywhere within the network
  - Image adjustment and navigation tools allow window/level, zoom, pan
- Integrated with Fuji® Synapse® software:
  - launched within the radiologists' reading workflow and environment
  - Does not disrupt normal workflow

Discussion:

- Implemented and exhibited in a simulated PACS environment and is demonstrated in this exhibit
- Improves accessibility and convenience as compared to hardcopy paper templates while adding dynamic tools
- Presents a reliable and a more systematic approach to the vascular dementia evaluation in radiology
- Future works:
  - implementation in a clinical setting
  - automatic quantification of white matter in relation to brain matter for an objective approach.

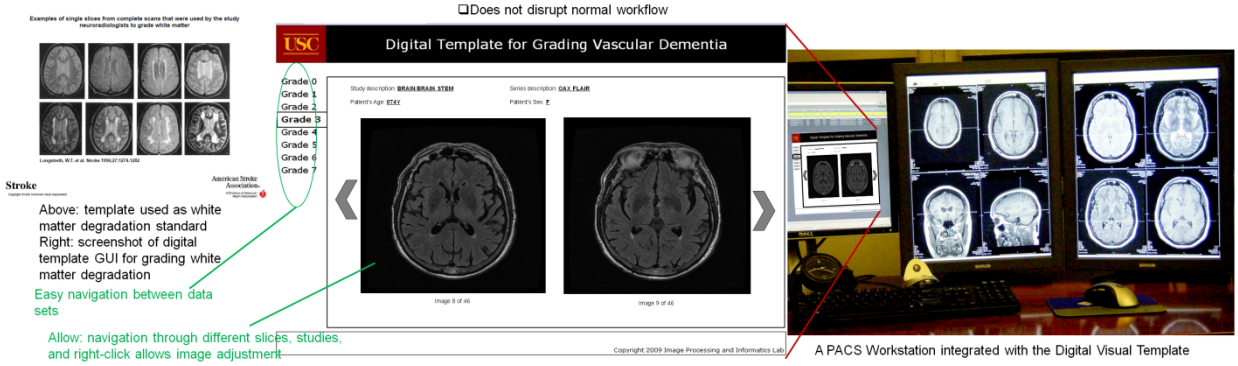

This project has been supported by NIH NIBIB T32 Training Grant

USC UNIVERSITY OF SOUTHERN CALIFORNIA

Image Processing and Informatics Lab

Mind Over Matter: *Using a Neuroheadset to Interact with a PACS Workstation*

Paymann Moin, MD; Ruchi Deshpande, MS; Anh Le, MS; James Fernandez, MD; Brent Liu, PhD
IPILab, Department of Radiology, Keck School of Medicine, University of Southern California, Los Angeles, CA, USA

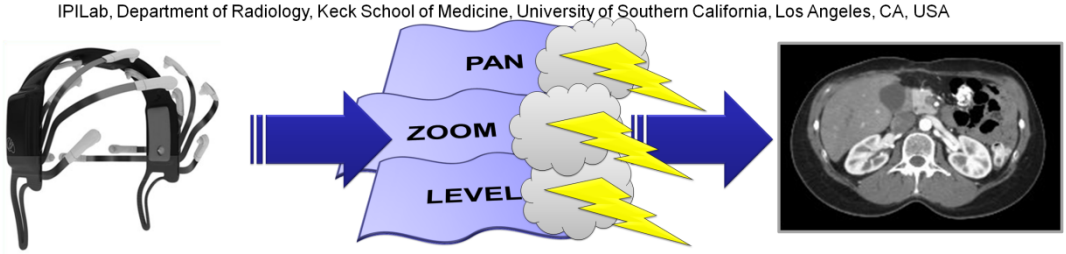

OUR PROJECT

The Emotiv neuroheadset is adapted for use with a PACS system in an effort to replicate basic functions. The headset uses a set of sensors to tune into electric signals naturally produced by the brain to detect user thoughts, feelings and expression.

Our objectives are to investigate the integration of a neuroheadset with a PACS workstation in order to: 1) reduce repetitive motions; 2) increase productivity; and 3) eventually allow complex commands to be initiated in a single step. The reduction of repetitive motions using a mouse will reduce associated musculoskeletal fatigue and injuries that may result.

BACKGROUND

Evolving modalities and the demands of efficient interpretation are increasingly at odds with each other, necessitating a revisit of the image interpretation process.

The development of next-generation human-machine interface tools and their potential are crucial in the evolving radiology workstation and maintaining the relevance of imaging both inside and outside of the radiology reading room.

Paymann Moin, MD and James Fernandez, MD are trainees of the NIH T32 EB00438 grant "Biomedical Imaging Informatics Training."

PROJECT DESIGN

The endpoint of interaction between humans and electronic devices is direct neural-machine interface. Advancement of such functionality in the radiological imaging viewing process will allow for more efficient image viewing and facilitate new situations such as where an interventional radiologist or surgeon could view and manipulate images during a procedure while maintaining a sterile field.

Continued development of headset functionality could eventually make the mouse obsolete, increase interpretation efficiency, and anchor the importance of radiology while allowing the proliferation of image intensive medical applications outside of the reading room.

USC UNIVERSITY OF SOUTHERN CALIFORNIA

Image Processing and Informatics Lab

Imaging Informatics beyond Radiology: Clinical Experiences from a Six-Month Implementation of a DICOM Multimedia Electronic Patient Record (ePR) System for Image-assisted Minimally Invasive Spinal Surgery

J Documet, PhD[1]; B Liu, PhD[1]; A Le, MS[1]; K Wang[1], BS; John Chiu, MD, DSc[2]; HK Huang, DSc[1]

1 – Department of Radiology, Keck School of Medicine University of Southern California, Los Angeles, CA, USA

2 – California Spine Institute, Thousand Oaks, CA, USA

Learning Objectives:

1) Integrate key imaging and informatics data during the pre, intra, and post-operative phases of clinical workflow.
2) Apply the ePR concept to Image-Guided Minimally Invasive Spinal Surgery (IG-MISS) cases.
3) Demonstrate a one-stop source system that has been implemented in the clinical environment for six months and has improved both clinical workflow efficiency and provides a platform for training and patient outcomes analysis.
4) Integrate a variety of still and real-time acquisition systems including X-Ray, CT, MRI, digital fluoroscopy and digital endoscopic video, and waveforms into the ePR.

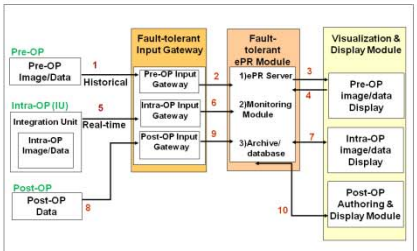

Dataflow of the IA-MISS ePR System

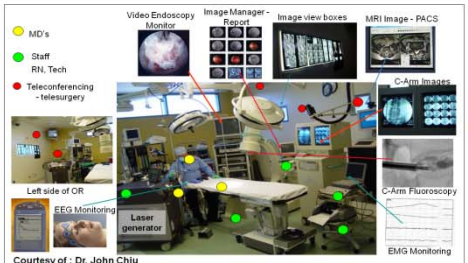

Existing Operating Room (OR) Layout

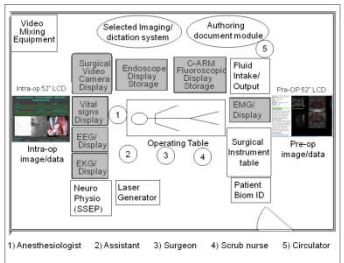

OR Layout w/ ePR System

IA-MISS Workflow Phases

Pre-Op

Intra-Op

Post-Op

USC UNIVERSITY OF SOUTHERN CALIFORNIA

Image Processing and Informatics Lab

Clinical Implementation System

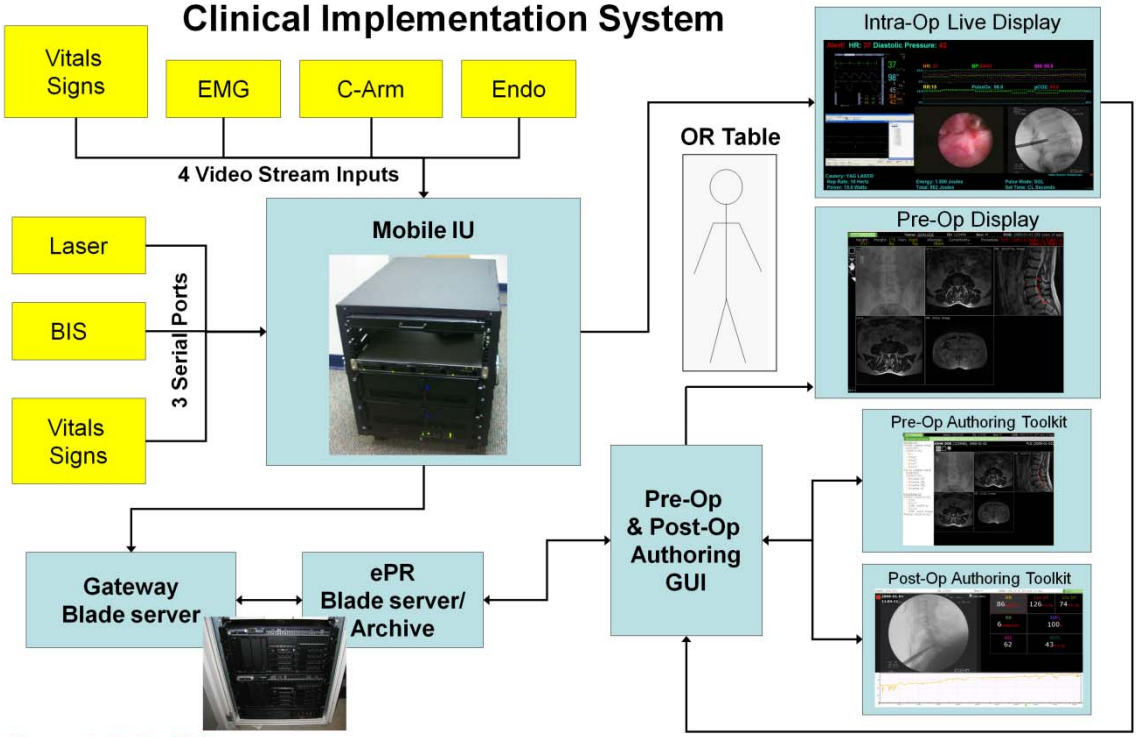

This project is supported by SurgMatix

SPIE 2010 PREPRINTS

Multi-site evaluation of a computer aided detection (CAD) algorithm for small Acute Intra-cranial Hemorrhage and development of a stand-alone CAD system ready for deployment in a clinical environment

Ruchi R. Deshpande[a], James Fernandez[a], Joon K. Lee[a], Tao Chan[b], Brent J. Liu[a], H.K. Huang[a]
[a]Image Processing and Informatics Laboratory, Department of Radiology,
2250 Alcazar Street, CSC 105, Los Angeles, CA 90033
[b]Dept. of Health Technology and Informatics, The Hong Kong Polytechnic University, Hong Kong, SAR, China

ABSTRACT

Timely detection of Acute Intra-cranial Hemorrhage (AIH) in an emergency environment is essential for the triage of patients suffering from Traumatic Brain Injury. Moreover, the small size of lesions and lack of experience on the reader's part could lead to difficulties in the detection of AIH. A CT based CAD algorithm for the detection of AIH has been developed in order to improve upon the current standard of identification and treatment of AIH. A retrospective analysis of the algorithm has already been carried out with 135 AIH CT studies with 135 matched normal head CT studies from the Los Angeles County General Hospital/ University of Southern California Hospital System (LAC/USC). In the next step, AIH studies have been collected from Walter Reed Army Medical Center, and are currently being processed using the AIH CAD system as part of implementing a multi-site assessment and evaluation of the performance of the algorithm. The sensitivity and specificity numbers from the Walter Reed study will be compared with the numbers from the LAC/USC study to determine if there are differences in the presentation and detection due to the difference in the nature of trauma between the two sites.. Simultaneously, a stand-alone system with a user friendly GUI has been developed to facilitate implementation in a clinical setting.

Keywords: Computer Aided Detection, Acute Inter-cranial Hemorrhage, CT, Brain

1. INTRODUCTION

Acute Intra-cranial hemorrhage (AIH) can lead to significant morbidity and mortality unless detected and treated in a timely manner. Heavy emphasis is placed on AIH detection and identification in patients suffering from head trauma and neurological disturbances since it has a direct bearing on further management and treatment strategies. This is especially so in the military and in emergency rooms where triage of patients is crucial. This vital step is often carried out initially by emergency physicians, internists and neurosurgeons. It has been shown that the competence provided by these acute care physicians in reading brain CT scans may not be optimum [1]. Since CT is the modality of choice in diagnosing AIH [2,3], the challenge can be remedied by a computer aided detection system which targets these physicians and enhances their brain CT interpretations. In the event of the AIH lesions being too small or inconspicuous, this system augments the skills of both acute care physicians and radiologists in addition to rendering consistency to their interpretations.

2. THE CAD ALGORITHM

The CAD algorithm for AIH detection was developed and tested with MATLAB (The MathWorks, Inc., Natick, MA, USA). The algorithm accepts a series of CT images in the DICOM format, as input. The system output is again a series of DICOM images, which are secondary captures of the Computer Aided Detection. These images graphically highlight the areas positively identified by the algorithm as AIH lesions. Figure 1 depicts a flowchart of the algorithm, and Table 1 summarizes the image processing techniques involved in each step.

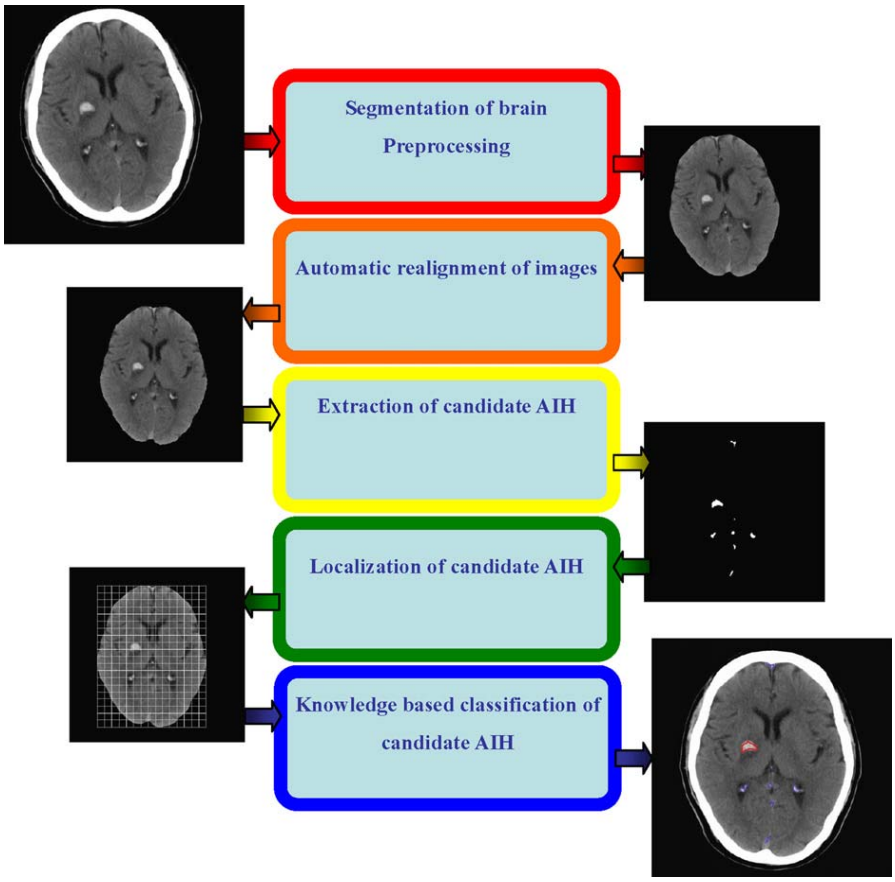

Figure 1: Schematic diagram of the CAD system. Intermediary outputs of an image showing right basal ganglia hemorrhage illustrate the effect of individual steps [4].

Table 1: Details of individual image processing and analysis steps in the CAD system outlined in Figure 1 [4]

Steps	**Methods**	**Purposes**
Segmentation of intracranial contents	Global thresholding and morphological operations Remove structures not contiguous with the main central bulk of intracranial contents	Remove bones of skull and face Remove scalp, orbits, and other head and neck soft tissue
Preprocessing of intracranial contents	Median filtering Adjustment of intensity according to distance from the skull	Denoising Correction for CT cupping artifacts
Automatic realignment of images	Automatic localization of limits of brain, ventricles, floor of anterior intracranial fossa, mid-sagittal plane	Align the brain into normal position
Extraction of candidate AIH	Top-hat transformation Subtraction between the two sides	Highlight local high density regions Extract asymmetrically high density regions
Localization of candidate AIH	Registration of the brain in question against a normalized coordinate system	Render the candidate AIH anatomical information
Knowledge-based classification of AIH	Rule-based system with inputs of image features and anatomical coordinates of the extracted candidates	Distinguish genuine AIH from false positives resulting from noise, artifacts, and normal variants

3. DEVELOPMENT OF A CAD SYSTEM FOR INTEGRATION WITH A CLINICAL ENVIRONMENT

The previous implementation of the CAD algorithm was a static MATLAB program which needed to be run manually for each series in each study individually; following which, the results were pulled up and linked to the unprocessed images by the user. There was no facility for cataloguing image metadata; no service which maintains a link between the unprocessed and processed studies; and no interface for viewing processed results. The goal of building an automated system is to facilitate integration of a stand-alone CAD system into a clinical environment for testing, and ultimately, for long term use.

3.1 Design issues to be considered when building an automated system for CAD

(1) Ensuring that only the appropriate studies sent by PACS to the workstation get accepted. For instance, this application should only accept CT head image studies.

(2) Once accepted, they must be sorted and stored in a suitable file folder hierarchy and relevant metadata must be recorded somewhere for future reference

(3) A continuous check must be carried out for recently acquired images in order to process studies as and when they arrive

(4) There needs to be a mechanism to post-process the results to resolve any metadata conflicts, and to store the results in a pre-determined manner such that the resultant series are linked to the unprocessed, original series.

(5) The CAD process needs to run continuously in the background. On the front end, a graphical user interface is required to enable browsing through the acquired and processed studies, and to attach notes or comments to the results.

(6) A web server is required for remote access to the CAD workstation.

3.2 System Architecture

The automated CAD package is comprised of the following components integrated into one system, the components of which will be described in more detail below, each component being represented by the Red Circle Numbering as shown in Figure 2.

1. DICOM Receiver

The DICOM Receiver is a service which listens on a specified port for incoming DICOM studies and routes them to a pre-specified folder – the “raw” repository. This is the root folder that the control service scans every 5 minutes to check for new images.

2. Pre-processing unit

The studies received from PACS may not be ready for being processed by the CAD algorithm. The studies may be non brain CT studies, sent to the CAD workstation erroneously. Such studies need to be weeded out before they crash the system. The DICOM metadata of the received images must be scanned to ensure that it will be accepted by the algorithm. Once these conditions are satisfied, the images may be passed on to the Control Service.

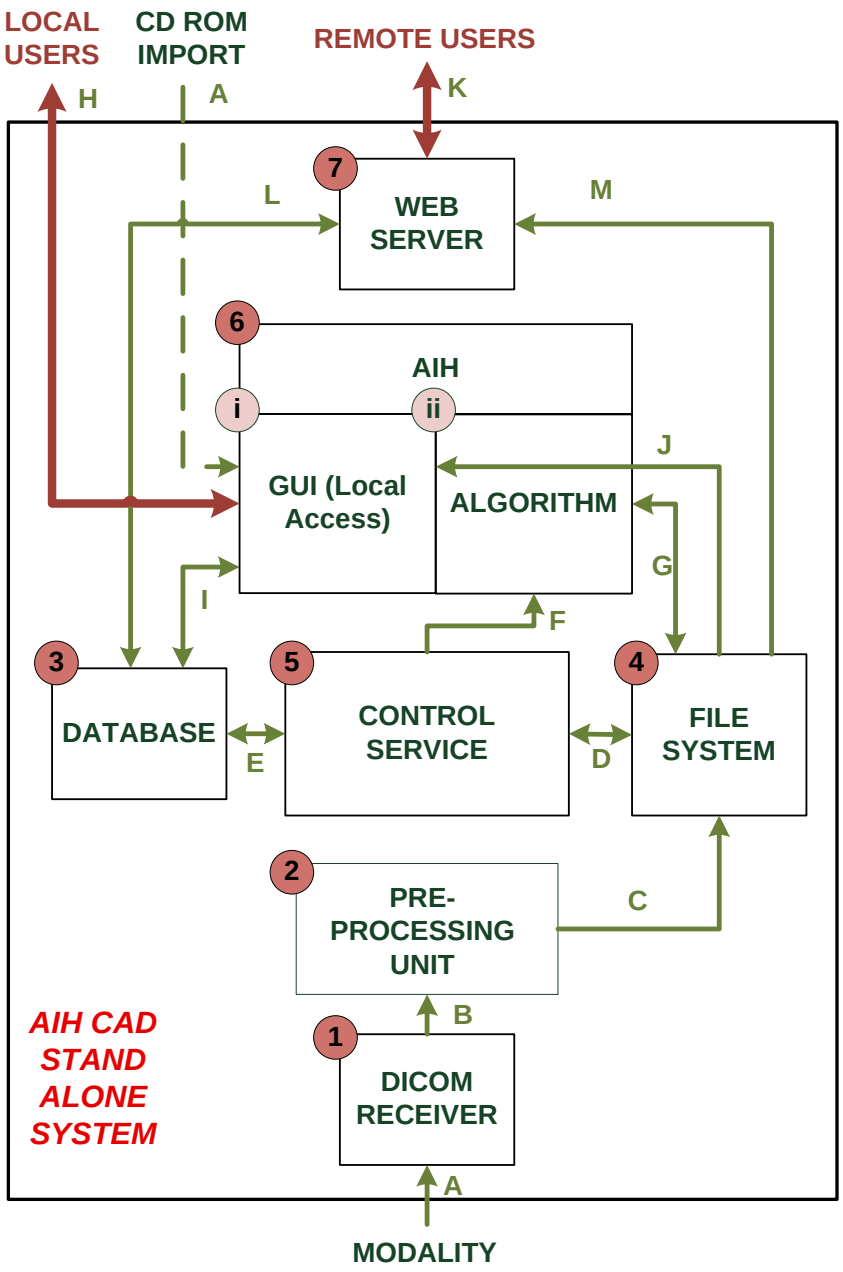

Figure 2: Architecture and workflow diagram for an automated Acute Inter-cranial Hemorrhage Computer Aided Diagnosis System

3. Database

The data model, outlined in Figure 3 was formed along the lines of the DICOM data model of the real world. The figure illustrates that there may be two types of series – unprocessed (original) and processed (secondary captures).

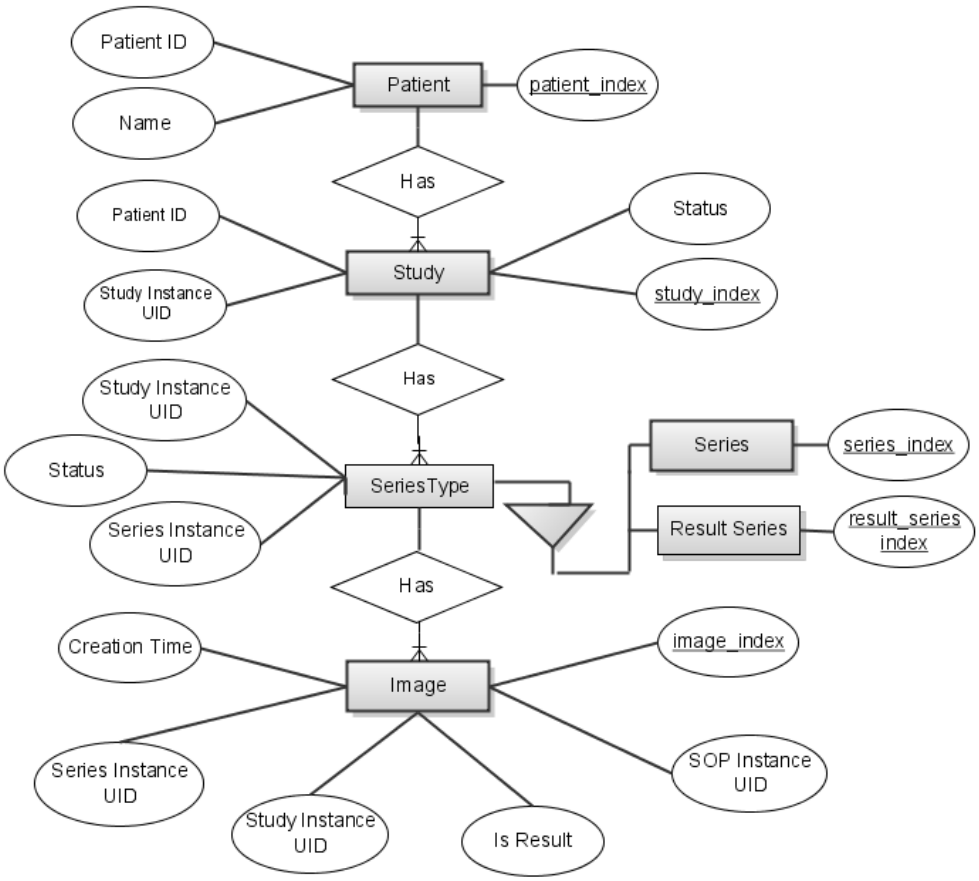

Figure 3: The data model for the CAD application developed along the lines of the DICOM model of the real world, with a few additional non DICOM parameters. As shown, there are two types at the series level – the original, unprocessed series and the resulting, processed series.

4. File System

The storage system is divided into two main partitions – the raw repository, which gathers all the DICOM files received from the CT/ PACS; and the "sorted" repository, which contains the same files as in the raw repository organized in a file-folder hierarchy which mimics the DICOM model of the real world.

5. Control Service

The Control Service is the heart of the automated CAD system, and recurs at a time interval specified in the configuration file, coordinating dataflow between individual components of the system. It sorts the incoming files into an appropriate hierarchy of folders; catalogues DICOM metadata and other non-DICOM attributes in the database; initiates the running of the algorithm at regular time intervals by keeping track of which studies are complete and ready for processing; thus regulating the automation.

6. (i) GUI

The graphical user interface provides a view of the original unprocessed series juxtaposed with the secondary capture series, and the mouse wheel is programmed to navigate through the images in a series. The interface can be used both for

viewing the results generated by the control service, or to intercede and run a series through the CAD manually. The study list is programmed to update itself automatically every 5 minutes, and can also be refreshed manually.

7. Web Server

The web server will enable viewing of CAD results remotely, eliminating the need for users to physically man the workstation. This piece of the application is currently in a developmental stage.

3.3 Workflow

The green arrows and alphabetical indicators in Figure 2 illustrate the workflow of an automated CAD system.

A. Head CT studies are sent by the PACS to the DICOM Receiver unit in the workstation. Alternatively, studies may be imported from a CD ROM manually via the GUI into the temporary storage area.

B. The DICOM Receiver passes the studies to the Pre-processing Unit which removes and flags suspicious files. If studies are imported from a CD ROM drive, the user needs to carry out this step manually.

C. Files cleared by the Pre Processing unit are then routed to a temporary storage sector on the file system, where they lie unsorted.

D. Studies situated in the temporary storage area are then pulled up by the control service, parsed, sorted, and placed in the permanent section of the file system.

E. Metadata retrieved in step D is inserted into the database.

F. The control service directs the algorithm in the AIH module to pull up specific studies from the storage area, process them, and save the results at a particular location.

G. The algorithm processes the required studies as directed by the Control Service in step F, and saves the results.

H. The user runs the GUI.

I. The GUI queries the database for existing studies and creates a work-list.

J. The GUI retrieves studies and results from the file system as per the user's requests.

K. Users access the system through a web GUI.

L. The web server routes queries to the database and returns the results.

M. The web server retrieves appropriate files from the file system for remote users to view.

3.4 Technical Specifications

The system runs on a Windows XP/Vista platform, and requires the .NET Framework Run Time Environment. The workstation will also require a MySQL server. The DICOM receiver module from DCM4CHE was utilized. The control service was built in Visual C#, and incorporates the original MATLAB CAD code compiled to a dynamic link library.

4. MULTI-SITE VALIDATION AND EVALUATION

To verify the efficacy of the CAD algorithm, a two part validation study was conducted. The first part of the study dealt with cases from the Los Angeles County/University of Southern California Hospital System, while the second part dealt with cases from Walter Reed Army Medical Center, Washington DC. These cases were matched with an equal number of normal control cases and processed by the CAD program. The results were then analyzed in order to identify trouble

spots which need fine-tuning, to provide insight into developing a CAD package for installation at a clinical site, and most importantly, to ascertain the effectiveness of the algorithm.

Performance of the algorithm was evaluated both on a per patient and on a per lesion basis. Evaluation on a per patient basis is of greater clinical relevance because the presence or absence of AIH dictates triage and further clinical management. On a per patient basis, if at least one lesion was correctly identified, the case was counted as one amongst the true positives irrespective of whether the rest of the lesions were false positives or not. If the algorithm detected AIH, but there was none, the case was classified as a false positive. If the algorithm did not detect lesions which did exist, the case was counted as a false negative, and if it did not detect lesions where none were present, that counted as a true negative. The gold standard for determining presence of lesions was the radiologists' report.

Another factor that demands consideration is that the algorithm correctly identified lesions at times, but incorrectly classified them as not being AIH. This could arise due to incorrect registration, which would then lead to incorrect application of the knowledge based rules, ultimately resulting in false negatives.

4.1 Evaluation at LAC/ USC

One hundred and thirty five CT head studies of patients diagnosed with AIH were obtained from LAC/USC and matched with a hundred and thirty five normal cases (also from LAC/USC). These studies were captured with a Picker PQ 5000 or 6000 single-slice CT scanner with 5 mm collimation, at 130 kV, and with beam currents of 30 mA.

Results

Table 2: Summary of CAD results for LAC/USC cases on per patient and per lesion bases [4]

	Overall Sensitivity	Sensitivity after considering correctly identified by incorrectly categorized lesions
Per patient basis	77%	89.6%
Per lesion basis	69.6%	84.2%

The control cases yielded a 100% false positive result majorly around the falx, most likely due to incorrect registration and alignment.

4.2 Evaluation at WRAMC

Eight CT head studies of patients diagnosed with AIH were obtained from WRAMC and matched with eight normal cases (also from WRAMC). Another 13 CT head studies of patients diagnosed with AIH and matched with 13 normal cases has been obtained and are currently being evaluated at the time of the writing of this report.

Results

Table 3: Summary of CAD results for WRAMC cases on a per patient basis

True Positives	10/10
False Positives	7/10
True Negatives	1/10
False Negatives	0/10

Table 4: Summary of CAD results for WRAMC cases on per patient and per lesion bases

	Overall Sensitivity	Sensitivity after considering correctly identified by incorrectly categorized lesions
Per patient basis	100%	100%
Per lesion basis	100%	100%

The control cases yielded a 87.5% false positive result majorly around the falx, likely due to reasons mentioned above.

4.3 Conclusion

The system was tested with cases from both LA County Hospital and Walter Reed Army Medical Center. The results generated by the automated system match the results generated by the fundamental MATLAB encoded program. Consequently, a conclusion may be drawn that the new system retains the integrity of the original system while significantly improving the clinical and research workflow efficiency.

Although the initial sample size obtained from WRAMC is small, the CAD system was highly sensitive in detecting AIH. At this time it is difficult to make a comparison between those studies obtained from LAC/USC and WRAMC due to the small size of the WRAMC image data set. Such comparison can be done in the future as the WRAMC dataset is increasing and currently being evaluated by the CAD system.

5. FUTURE WORK

In summary, a Computer Aided Diagnosis algorithm has been developed and validated across two clinical sites, and incorporated into a system which automates the workflow, facilitating its utilization in a clinical environment. Future work includes installing the system at WRAMC to carry out a small pilot study for evaluating both the algorithm and the system.

REFERENCES

[1] Perry JJ, et al., “Attitudes and judgment of emergency physicians in the management of patients with acute headache,” Acad Emerg Med 12(1), 33-7 (2005).
[2] Perry JJ, et al., “Attitudes and judgment of emergency physicians in the management of patients with acute headache,” Acad Emerg Med 12(1), 33-7 (2005).
[3] Mader TJ, Mandel A., “A new clinical scoring system fails to differentiate hemorrhagic from ischemic stroke when used in the acute care setting,” J Emerg Med 16(1), 9-13 (1998).
[4] Chan T., “Computer aided detection of small acute intracranial hemorrhage on computer tomography of brain,” Computerized medical Imaging and Graphics 31, 285-298 (2007).
[5] Joon K. Lee, et al., “Evaluation of a computer-aided detection algorithm for timely diagnosis of small acute intracranial hemorrhage on computed tomography in a critical care environment.”

ePR for Data Grid Breast Imaging: design and specifications

Jorge R. Documet*[a], Brent J. Liu[a]
[a]Image Processing & Informatics (IPI) Laboratory, Radiology Department, University of Southern California, Los Angeles, CA 90033, USA

ABSTRACT

The utilization of breast MRI is increasing in the diagnostic evaluation of suspicious breast findings. As more imaging centers implement dedicated breast MR, the need for managing data on a large scale, nationally and even some times internationally, has become more apparent. Our design proposal is to utilize the data grid for managing the storage of the medical images and an ePR that provides the interface to manage the health data of Breast Cancer Patients. In this paper, we present the data grid for DICOM images and DICOM-SR data and the image-intensive web-based ePR system technologies utilizing the simulation of a three-site dedicated breast MR outpatient centers as the clinical application. The implementation of the two technologies the ePR system together with the Breast Imaging Data Grid (BIDG) can provide a global solution that is portable for the Breast Cancer patient including aggregation of Mammo, US, MR, CAD, BI-RADS, and clinical related reports data to form a powerful platform for data mining and outcomes research.

Keywords: ePR, System Integration, Breast Imaging, Data Grid

1. INTRODUCTION

More than 250,000 women are newly-diagnosed with breast cancer in the United States each year. Currently, conventional mammography is the imaging modality of choice to evaluate the extent and size of the breast cancer prior to surgery. The surgeon largely relies on the mammogram to delineate the extent of the cancer and identify additional tumor foci. Unfortunately, the accuracy of mammography to detect cancer decreases as the breast density increases and dense breast tissue is more common in pre-menopausal women. Contrast Enhanced (CE) MRI of the breast is becoming a significant imaging adjunct to mammography because of its high sensitivity (93-100%) in the detection of malignancy. The ability of CE-MRI to depict symptomatic "macroscopic cysts" may lead to the prevention of unnecessary biopsies through its characterization of target masses and breast anatomy and possibly provide a higher detection rate of other lesion types including solid lesions and carcinomas. Additionally, it is of great clinical importance to successfully preoperatively identify women who need wider surgical excision or a mastectomy, as complete tumor removal is mandatory to avoid tumor recurrence and improve survival.

Grid computing is the integrated use of geographically distributed computers, networks, and storage systems to create a virtual computing and communication system environment for solving large-scale, data-intensive problems, for example, in various medical image applications [1]. This paper focuses on the Data Grid, a subset of Grid computing. The Image Processing and Informatics Laboratory (IPILab) has been on the forefront for developing applications of the Data Grid for both Tier-2 Enterprise storage as well as Imaging-based Clinical trials of clinical imaging data. The application in this paper is to develop a system that simulates a multi-site enterprise level fault-tolerant Breast Imaging Data Grid (BIDG) to support standalone dedicated breast MRI imaging systems and related quantitative breast imaging data for archive and image distribution management. The Globus 4.0 [2] five-layered open source toolkit for Grid Computing integrated with customized DICOM [3] technology and IHE (Integrating the Healthcare Enterprise) [4] workflow profiles forms the infrastructure of the BIDG.

The benefits of BIDG for current and future developments are:

1) It provides an enterprise-level dedicated breast MRI fault-tolerant archive and image/data distribution capability.

2) It allows the integration of all related breast images and data of every patient belongs into a central repository by means of a patient record in an open architecture DICOM Web-based ePR system. This record can be retrieved systematically from any workstation that has access to the central repository.

3) It possesses data mining capability to perform individual and group patient outcome analysis.

2. METHODS AND MATERIALS

2.1 The BIDG

The DICOM-based Breast Imaging Data Grid (BIDG) is an innovative infrastructure that supports an enterprise level Web-based ePR (Electronic Patient Record) system for large-scale breast imaging archive and distribution management. The BIDG has the following functions:

1) It archives 3-D dedicated breast MRI images, and patient records related to the MRI study including other modality type breast images in DICOM format and diagnostic reports.

2) The Data Grid provides fault-tolerance to all archived data.

3) The BIDG also utilizes DICOM Structured Report (SR) standard and IHE workflow profiles linking special quantitative DICOM metadata, reports and breast images for patient record distribution through the ePR.

4) Within the BIDG, any site can access patient record including images and reports from other sites provided permission has been granted by the enterprise. In addition, access rights to patient records from different sites can be controlled through security protocols within the BIDG.

5) Following Item 4, any CAD or Post-processing workstation (WS) can display 3-D dedicated breast MRI images from other sites including the quantitative metadata through DICOM-SR.

6) This work has been done in collaboration with AURORA, an specialized vendor for dedicated breast MRI.

2.2 The components of the BIDG

The BIDG utilizes open source software Globus 4.1, DCIOM image standard, IHE (Integrating the Healthcare Enterprise) Workflow profiles, and SAN storage technology [5] for customized clinical and research applications. This technology has been developed in our Laboratory for over four years, and has been applied as a solution for second-tier PACS backup, Imaging Center Resource for clinical trial, and Molecular Imaging Center Archive. Figure 1 bottom right depicts the concept of the customized Breast Imaging DATA GRID (BIDG), the SAN P2 dedicated to the Data Grid for the backup archive of other sites connected to the BIDG, and additional components required in each of the three proposed clinical sites.

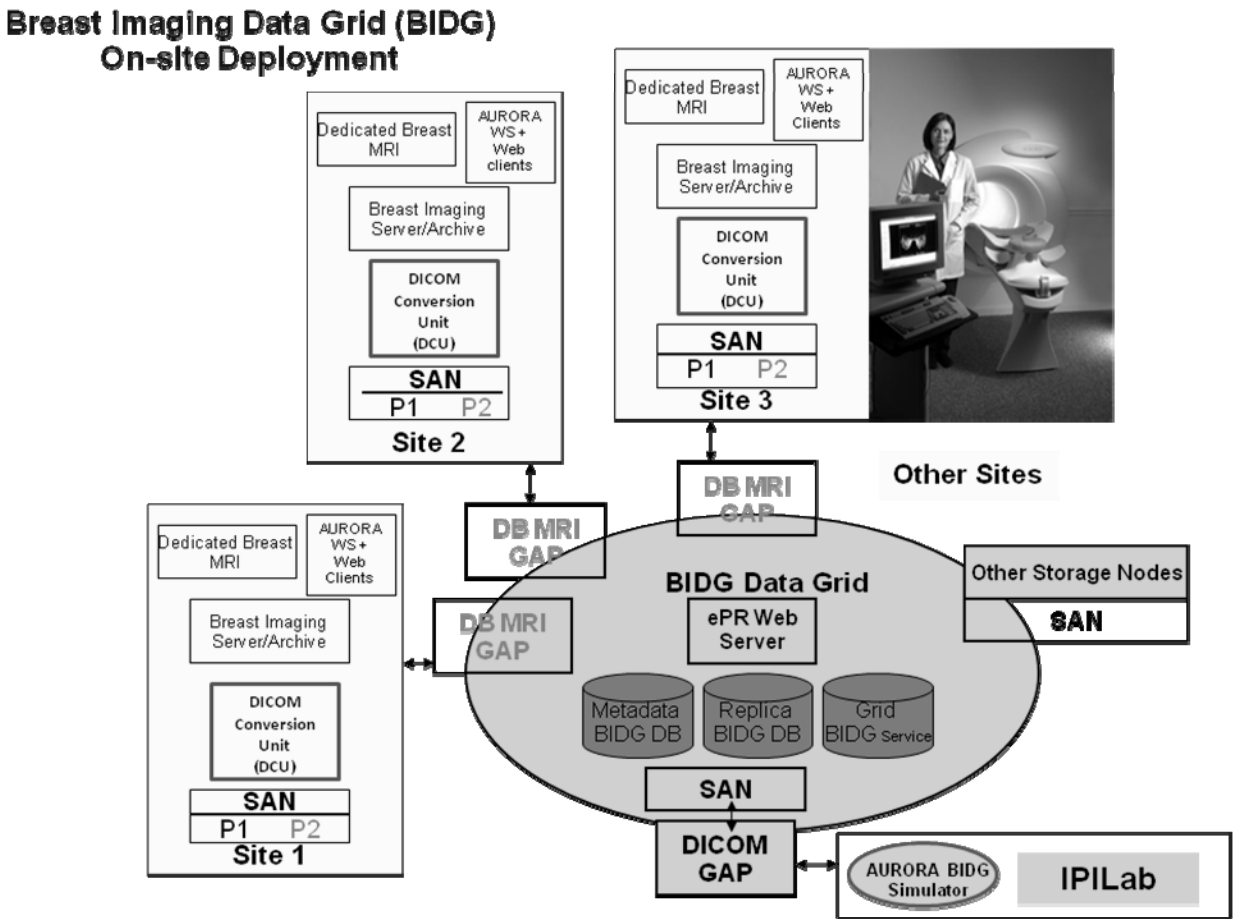

Figure 1. The infrastructure of a three-site Dedicated Breast (DB) MRI Systems (more sites in the future) enterprise. Three Dedicated Breast Imaging sites operate independently and separately and are connected by the Breast Imaging Data Grid. Each site has a standalone DB Breast MRI System with its own server and storage device. It can also acquire other breast imaging related data of the same patient. Aurora workstations (WS) display 3-D MRI breast images. SAN (Storage Area Network) is used for its own archive (P1), and storage backup for other sites (P2). In the enterprise Breast Imaging Data Grid (BIDG), a WS at each site can Q/R images from its own SAN for image display. A WS of any three systems can also Q/R images from any sites belonging to the BIDG. The BIDG maintains interconnectivity of these three systems in real-time without human intervention. There are two types of dedicated breast DB GAP (Grid Assess Point) in this architecture, DICOM GAP (bottom) and DB GAP (middle left). The former is for DICOM WS to transfer from other DICOM-compliant breast imaging systems, the latter can be customized to transfer MRI images to the Data Grid.

2.3 Breast Imaging Data Grid and Related Components

1) Storage Nodes: Server/SAN storage devices provide storage resources for the Data Grid. In this case, each acquired image at a site has three copies, the primary one is in its own SAN P1 (Site 1), and two backup copies are in two other SANs P2 (Sites 2 and 3) within the Data Grid.

2) Database Services: A Service that keeps track of DICOM metadata as well as file locations of different storage nodes within the Data Grid (See components within the big ellipse from Figure 1). Dynamic and robust access to data is provided by the Data Access Interface (DAI) in the Globus toolkit integrated with the database.

3) Dedicated Breast (DB) MRI and DICOM Grid Access Point (GAP): The DB MRI GAP provides Storage and Query/Retrieve services for any DICOM-compliant WS of any Breast Imaging system to access data within the Data Grid. There are multiple GAPs in the Data Grid and can be used as the backup for each other. The DICOM

GAP provides the transfer of DICOM files from other DICOM-compliant breast imaging modality. If the multi-site enterprise conforms to the DICOM standard in the foreseeable future, the DICOM GAP may not be necessary.

4) ePR Web Server: A Web-based electronic patient record system manages all breast patients in the enterprise as well as the BIDG services and components. In addition, any CAD or Post-Processing WS can easily access a patient's record at any site from the BIDG through a DG MRI GAP. The ePR also keeps a log of all patient records transaction within the Data Grid. This function can be used for future data mining applications and patient outcome studies. In addition, the ePR web server can perform diagnostics and management of the BIDG and related components.

2.4 Additional Components at each site

1) Web Clients: A web client is used for easy access to the ePR Web Server for patient records including breast imaging data and quantitative DICOM metadata. In addition, the web client can access the ePR web server for diagnostics and management logs of the BIDG and related components.

2) DICOM Conversion Unit (DCU): The DCU converts 3-D MRI images or any other related breast images (DM, US, and others) of the patient to DICOM standard if necessary. It also converts a specialized MRI report to DICOM Structured Report (SR) format allowing the linkage between the report, images, and quantitative metadata. This feature allows a) tracking the patient progress from multiple studies, b) performing data mining for patient outcome analysis, and c) developing breast imaging teaching files. The converter also coverts 3-D MRI DICOM images to CAD or Post-Processing WS display format.

3) SAN with P1 and P2 partitions: The SAN storage device at each site is divided into two partitions, P1 and P2. P1 is used for its own patients' records, and P2 is contributed to other sites for their backup archive within the BIDG. Each image in each site has three copies, one in its own SAN P1 and two in SANs P2 of two other sites that are stored within the BIDG. Note that P2 in each SAN is physically located in the SAN of the site, however, logically, once P2 is committed to the BIDG for other sited backup, it serves only the BIDG.

2.5 The workflow

The BIDG has three major functions: image/data archive and backup, query/retrieve, and disaster recovery.

1) Archive and Data Backup

Under normal operation condition (Figure 2, left, solid lines), the first copy of MRI 3-D breast images after acquired at Site 1 are sent to Partition 1 of its own SAN, the second and third backup copies are sent utilizing the GAP 1 to P2 of SAN 2 and P2 of SAN 3 contributed by other clinical sites to the Data Grid. The fault-tolerance (FT) of the GAP can be depicted by the dotted lines in Figure 2. During the backup procedure, suppose GAP 1 fails (cross-lines), then the Data Grid would automatically assign GAP 2 to replace GAP 1. GAP 2 would then complete the task original assigned to GAP 1 by storing copy 2 to P2 of SAN 2, and P2 of SAN 3.

2) Query/Retrieve (Q/R)

Figure 3 solid lines (left) shows the normal operation of DICOM Q/R from WS at Site 1. If the image file is in its own SAN 1 P1, then it is normal PACS operations. The FT of SAN 1: If SAN 1 P1 fails, Q/R will go through GAP 1 to SAN 2 P2, or SAN 3 P2 for Site 1 images.

If the image file is from other clinical sites, then the Q/R will be initiated with GAP 1 to the Data Grid to query and then retrieve the image file from the storage nodes, in this example, SAN 2, P1. The FT of SAN 2 P1: If during the process, SAN 2 fails (cross-lines), Data Grid can identify SAN 3, P1 with the image file, from which the file is then retrieved (dotted lines). If during the off site Q/R, GAP 1 fails, GAP 2 will replace the function of GAP 1 as described in Figure 2.

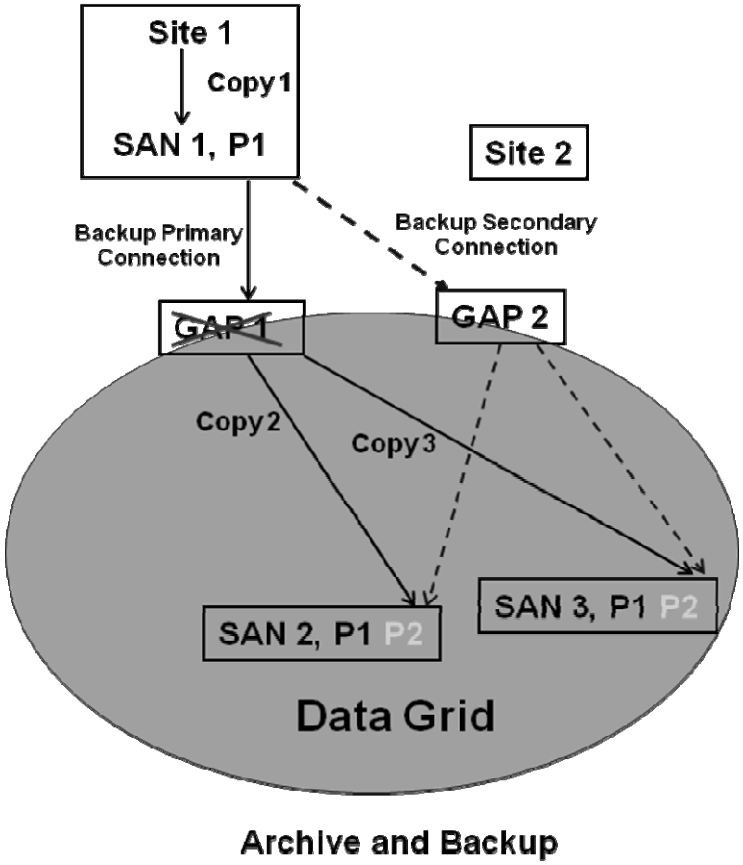

Figure 2. Image archive and backup: Solid lines (left), show the normal archive and backup operations, the first copy of the image file is sent from the MRI acquisition to its SAN 1 P1, and two backup copies to the Data Grid SAN 2 P2, and SAN 3 P2 for backup storage through its designated GAP1. Dotted lines show when GAP 1 fails (cross-lines), and GAP 2 takes over GAP 1 functions automatically.

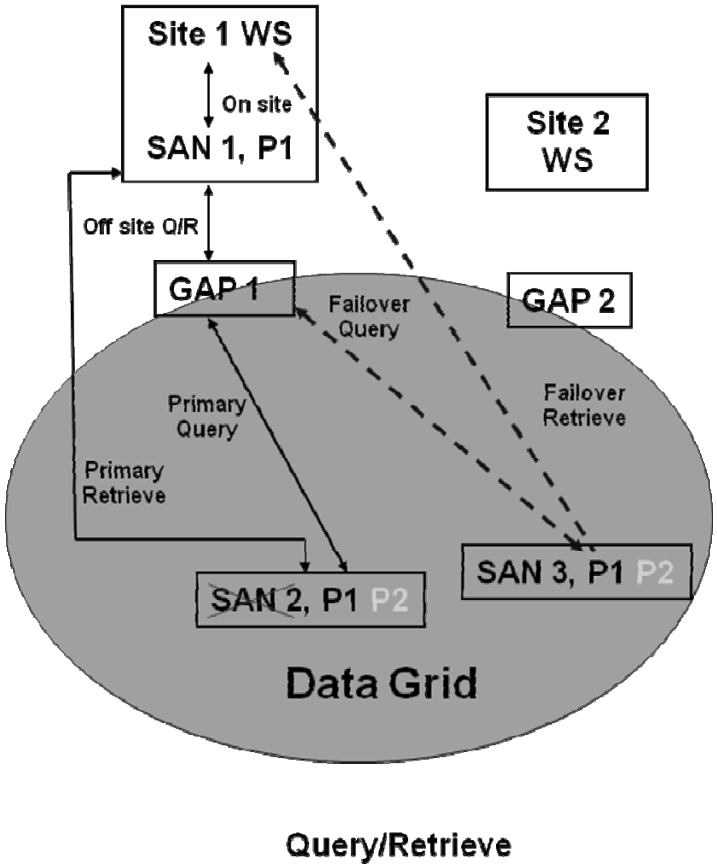

Figure 3. Query/retrieve: Solid lines (left) show the normal operation, WS queries Site 1 images from SAN 1, P1. Off-site images are Q/R from SAN 2, P1 in the Data Grid through GAP1. Dotted lines show if SAN 2 fails (cross-lines), GAP 1 finds SAN 3 automatically and completes the Q/R task from SAN 3 P1 (dotted lines).

3. RESULTS

Currently the BIDG system has been designed and developed based on the application for three clinical sites. We utilized data obtained from an AURORA CAD workstations as well as an Aurora dedicated breast MRI system to test and evaluate the BIDG simulator. In addition we evaluated other modality types including breast US and digital Mammography studies in DICOM format to create a virtual patient record by utilizing the IPILab PACS Simulator.

The BIDG Simulator is currently being evaluated together with the breast ePR system utilizing workflow scenarios including:

1) Storing of dedicated breast MR studies into the BIDG
2) Storing of Post-Processed data into the BIDG
3) Storing of report into the BIDG
4) Storing of other DICOM studies such US and Mammo
5) Querying and Retrieving of dedicated breast MR studies
6) Querying and Retrieving of Post-Processed data
7) Querying and Retrieving of reports

8) Querying and Retrieving of other DICOM studies

9) Displaying all breast imaging patient cases in the ePR system

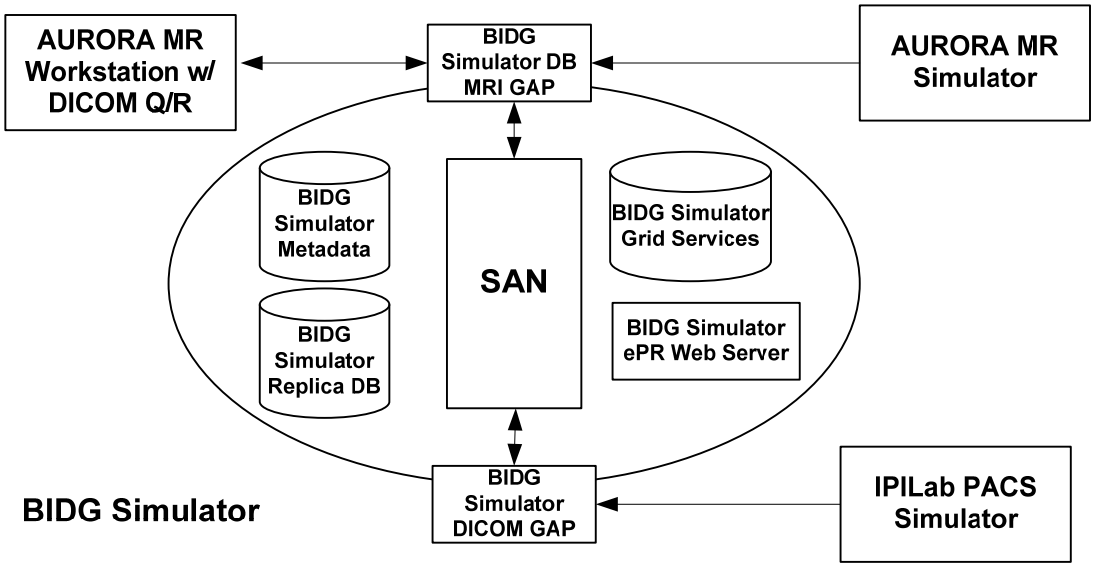

Figure 4. The schematic for the BIDG Simulator. At the top the components that simulate the DICOM data coming from the Breast MRI. The components inside the ellipse simulate the Data Grid. At the bottom, the other GAP acts as the entry point for the devices present in the IPILab PACS Simulator.

4. CONCLUSION

The data grid implemented with a web-based ePR system can provide a robust platform for managing Breast Cancer Patient's globally and providing an infrastructure for imaging and informatics data that provides future outcomes and data mining research. Future work includes extending the BIDG simulator from the laboratory environment into a three-site clinical environment and evaluating the testing results.

REFERENCES

[1] Foster I, Kesselman C, Nick J, Tuecke S, The Physiology of the Grid: An Open Grid Services Architecture for Distributed Systems Integration. In Open Grid Service Infrastructure WG, Global Grid Forum, June 22, 2002.

[2] Globus Toolkit 4, http://www.globus.org/toolkit/docs/4.0/

[3] DICOM, http://medical.nema.org/, accessed on February 1, 2010.

[4] SAN Technology: http://www.storage.ibm.com/ibmsan/whitepaper.html

[5] IHE, http://www.ihe.net/, accessed on February 1, 2010.

Migration from a prototype ePR for IA-MISS system to alpha version

Jorge R. Documet*[a], Anh Le[a], Brent J. Liu[a]
[a]Image Processing & Informatics (IPI) Laboratory, Radiology Department, University of Southern California, Los Angeles, CA 90033, USA

ABSTRACT

Last year we presented a paper that describes the design and clinical implementation of an ePR (Electronic Patient Record) system for Image-Assisted Minimally Invasive Spinal Surgery (IA-MISS). The goal of this ePR is to improve the workflow efficiency by providing all the necessary data of a surgical procedure from the preparation stage until the recovery stage. The mentioned ePR has been implemented and installed clinically and it has been in use for more than 16 months. In this paper, we will describe the migration process from a prototype version of the system to a more stable and easily-to-replicate alpha version.

Keywords: ePR, System Integration, Pre-, Intra-, and Post-Op Surgical Workflow, Image-Assisted Minimally Invasive Spine Surgery

1. INTRODUCTION

1.1 Current Challenges in Image-Assisted Minimally Invasive Spinal Surgery

Image-Assisted Minimally Invasive Spinal Surgery (IA-MISS) is a microdecompressive spinal discectomy procedure for decompressing nerve roots constricted by spinal disc protrusions. This image-assisted procedure utilizes a variety of still and live real-time imaging devices and methods including X-Ray, CT, MRI, 3-D modeling, digital fluoroscopy and digital endoscopic video. These techniques, when integrated, provide magnification, guidance and real-time course intervention to assist the surgeon with the insertion of a small tube (6 mm diameter) into the disc to remove its offending portion. IA-MISS is different from standard spinal disc surgery because there is no traumatic muscle dissection, bone removal, or bone fusion. The incision is tiny enough to close with sutures and then covered with a small band-aid. Therefore, most of the complications that occur with conventional spine surgery are virtually eliminated with the IA-MISS procedure. Over the past eight years, there have been stepwise technical and clinical advances in IA-MISS demonstrating the potential for significantly improved spinal surgical outcomes. However, there still remain large gaps along the clinical continuum from diagnosis to surgical treatment to postoperative follow-up that can be more fully addressed by the integration of a variety of advanced medical and imaging informatics technologies. The following paragraphs in this chapter will first introduce the IA-MISS workflow, data utilized, and the challenges relating to this clinical procedure. Then, a general introduction to the concept of the image-intensive electronic patient record (ePR) will be presented as a potential solution for IA-MISS and related issues.

1.2 Current Challenges in Image-Assisted Minimally Invasive Spinal Surgery

Despite the overall benefits from MISS in terms of recovery time and successful patient outcomes, there are still challenges remaining that need to be addressed and are described as follows:

1. Current scattered systems within the operating room (OR) including multiple sources of images, video, and waveforms. This is similar to general surgery.
2. The need for enhanced workflow with data acquisition, management, and distribution all in a single system.
3. The need for an integrated data repository in a one-stop source during all stages of the surgical workflow (eg, before, during, and after).
4. The need to develop outcomes analysis for patients undergoing MISS since it is a relatively new field of expertise.

5. The need for training of new adopters in MISS.

1.3 General workflow for Image-Assisted Minimally Invasive Spinal Surgery

The following paragraphs describe the general workflow with the steps involved in a typical MISS procedure. Figure 1 depicts this workflow.

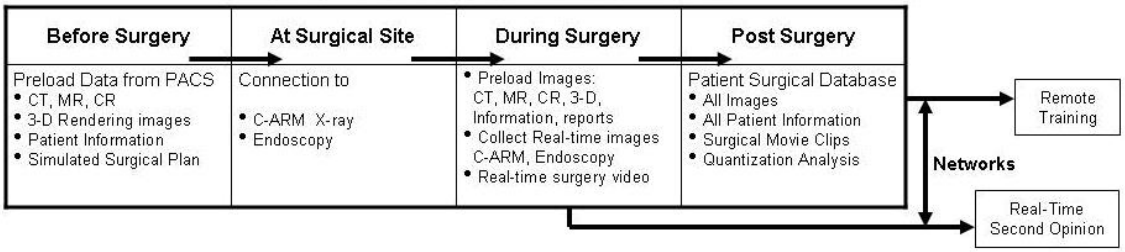

Figure 1 The Workflow of the MISS procedure showing all the different stages: before surgery, during the surgery (including the preparation) and post surgery

The workflow can be broken down into three phases:

1) Pre-Op (Before surgery), which is the phase in the surgical workflow when the patient goes for consultation and is determined that the patient needs to undergo surgery. At this time, the physician assistant(s) in agreement with the surgeon(s) plan the surgical procedure with the assistance of information gathered from different sources such as medical images (CR, CT, MRI) and patient's relevant information including pain sources, allergies, weight and height.

2) Intra-Op (During surgery), which is the phase when the surgeon performs the surgery on the different disc(s) in order to alleviate the patient's pain. While the surgery occurs, the ePR system is continuously acquiring data from the different assisting devices that are present in the OR, and these data is displayed live while at the same time is archived in the ePR for later review. A clinical surgery last in average 30 minutes per vertebrae.

3) Post-Op (After surgery), which is the last stage of the clinical procedure where the patients recover from the surgical procedure. A set of pain assessment forms are handled to the patients to gather the new intensity levels of pain (if any) in order to make a judgment of the success of the operation; these pain forms are entered digitally into the ePR. The recovery period after surgery lasts from 45 minutes to one hour, after that the patient is discharged. Therapy can begin the next day and the patient can go back to work within 2 to 3 days.

1.4 Need for data integration

As mentioned before there exists challenges that need to be covered in order to improve the overall workflow efficiency of IA-MISS and patient outcomes. One such concept that addresses these challenges and shed some light on possible advancements within the field is the concept of an image-intensive ePR (Electronic Patient Record) system with image distribution.

2. METHODS AND MATERIALS

2.1 The ePR System for IA-MISS

The ePR system serves the purpose of integrating clinical data into a single source, by combining data from different sources to a centralized server. Even though ePR servers have been implemented by initiatives coming from different departments, such as radiology or cardiology; there is currently no such ePR system that has been specifically tailored for surgical data. This concept was first proposed in 2001 [1], but required technologies were not readily available for system design and clinical implementation. The efforts done this year were aimed to improve the user experience when using the ePR and at the same time being more robust and reliable.

The proposed ePR for MISS has been designed to overcome the challenges presented in section 1.2 which are currently not being designed or implemented by any available system, either from the research arena or as a commercial product.

- Scattered systems in the OR: The proposed ePR acquires all Pre-Op, Intra-Op, and Post-Op pertinent available data and presents them on two organized large LCD monitors, one for Pre-Op and the second for

real-time Intra-Op. The data is also organized and saved in the ePR based on the DICOM (Digital Imaging and Communications in Medicine) data model.

- The need for enhanced workflow: The proposed ePR can perform workflow analysis of a surgical procedure in OR. Additionally, it provides the necessary infrastructure to properly acquire, manage and distribute all contents to the users. Another important aspect of the workflow is regarding proper patient verification at the OR and filling out survey pain in digital form; both aspects have been considered and implemented in this Alpha release.
- The need for an integrated data repository: The proposed ePR keeps all relevant information from Pre-Op, Intra-Op, and Post-Op, and stores the data in a database with a filesystem. In addition, the system keeps biometric information of the patients in the form of fingerprints.
- The need for training of new personnel for MISS: The proposed ePR is aimed to be a simple-to-use but powerful application that will make the utilization of MISS more attractive for general surgery personnel to adopt. This ePR is currently being implemented at a clinical site.
- The need to develop outcomes analysis: The proposed ePR brings a new and unique application in MISS surgery that will allow patient surgical outcomes analysis. Actual data collection for the outcomes analysis is in progress.

2.2 Standards used

Interoperability of devices is important when data needs to be shared, accessed, and stored in an efficient and convenient manner. In addition, standards are a comprehensive set of rules that allow devices and especially software components to communicate between each other. Thus, standards become crucial for a robust system integration that will eventually lead to reduced costs, risks, and developmental time.

The proposed ePR has been designed with the concept of utilizing available standards whenever possible. Currently we are using the following standards:

1. DICOM (Digital Imaging and Communications in Medicine): As previously mentioned in the ePR data model design, DICOM is the de facto standard for communications in medicine for medical images. Even though it was originally mainly utilized by Radiology, other clinical departments are beginning to utilize it on a daily basis. For the proposed ePR system the DICOM standard is used as the communication protocol when receiving images from the PACS (Picture Archiving and Communication System) archive in addition to the aforementioned data model design.
2. HTTPS (Hypertext Transfer Protocol Secured): The ePR itself is a web application that allows users to obtain clinical information about patients from a single interface. The users connect to the ePR server and utilize a client browser, (ie Internet Explorer or Mozilla Firefox). All the communication are established using HTTPS for security reasons. This protocol also serves as the foundation for the communication protocol used to transfer the data from the Integration Unit (IU) to the ePR.
3. JPEG (Joint Photographic Expert Group), GIF (Graphics Interchange Format) and PNG (Portable Network Graphics): Due to the web-based nature of the ePR and the lack of native support of DICOM images on web browsers, all images are converted to formats web browsers can understand. The format of choice for medical images is jpeg. For other type of images such as icons the gif or png formats are used.
4. RS-232 (Recommended Standard 232): This standard is used by some of the peripheral devices on the OR to transmit data out, however, even though the transmission is standard, the protocols from machine to machine can vary significantly. Thus, it is important to note that currently the vendors do not have implemented a common standard protocol to share the acquired data (data point values and video streams) for the devices within the OR. This has been a major challenge in the clinical environment and one of the major reasons for this research work in system integration and ePR development.

2.3 System architecture

From the system architecture point of view, the ePR system should be designed for efficiency, effectiveness, and reliability of system operations. For these reasons, although system workflow is separated into Pre-Op, Intra-Op, and Post-Op stages, some modules which handle multiple workflow stages may be combined to share system workload and reliability. For example, the fault-tolerant requirement of each component in the system is better designed to

support other existing components of the system for easy system back-up and cost containment. Also, although there are four major components and three operational workflow phases in the ePR system, many of the software have similar design backbones, and some software may be bundled together for easier programming effort and faster system execution time. For these reasons, the ePR System architecture has been designed from the dataflow shown in Figure 2.

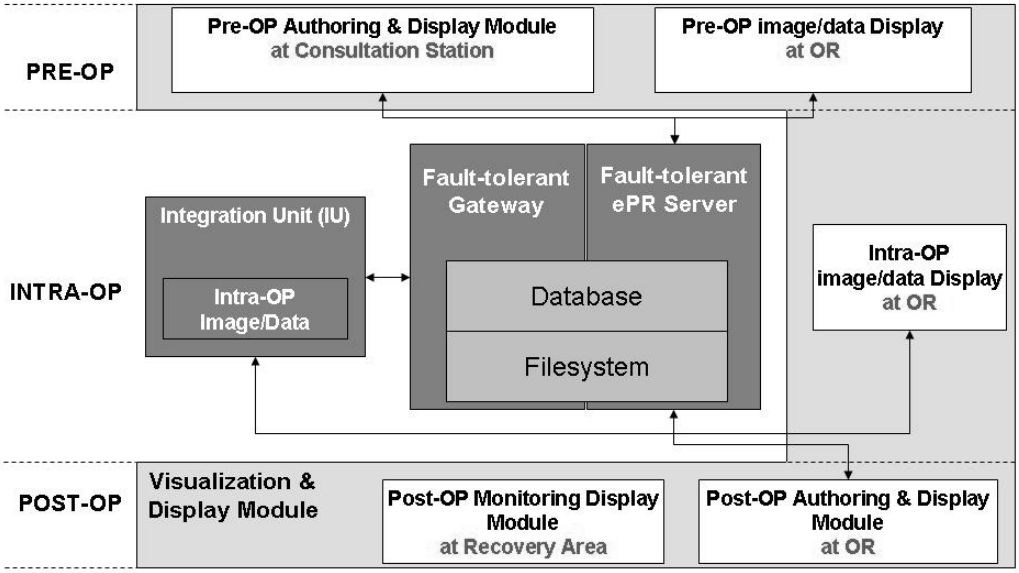

Figure 2 The ePR system architecture showing three operation phases: Pre-Op, Intra-Op and Post-Op (Left); as well as four operation modules, some modules are bundled up together for ease of data transfer and fault-tolerant back-up. The arrows show the data flow during the three phases of operation. The outside light gray color side-way "U" band is the Display module backbone with five subunits. Inside the opening of the "U" in dark gray are the Integration Unit (IU), Fault-tolerant Gateway, and Fault-tolerant ePR Server. Within the Gateway and the ePR Server, the Database and Filesystem software are interrelated and shared by both components.

The four major components in the MISS ePR System are: 1) Data Input Integration Unit (IU); 2) Fault-tolerant Gateway server; 3) Fault-tolerant ePR Server, and 4) Visualization and Display. Both the Input Gateway and the ePR Server include data storage and archive, system database, system security, system fault-tolerance, continuous availability and failover. The GUI and display module resides within the ePR Server. All data input systems like medical imaging, surgical video, vital signs waveform recorders, and textual data recorder generate Pre-Op, Intra-Op, and Post-Op data, and they are all categorized as input data. The imaging and data systems that generate information are existing peripheral surgical supported equipment already within the OR but they do not belong to the MISS ePR system. However, the ePR system must integrate these systems in order to receive the input data that is acquired before, during, and after surgery to support the surgical procedure.

2.4 Improvements for the Alpha version of the ePR

The following aspects went through a redesign for the Alpha version of the ePR. The previous version will be referred to as Prototype 1:

- The Integration Unit (IU): The IU improvements come in two different aspects of this component.
    - Software:
        - Saving both video sources: The IU Alpha version of the ePR stores both image sources at the same time for a surgical procedure compared to a single source being saved in the Prototype 1. In the Prototype 1 version of the IU the users had to manually select which video source was active (selecting between C-Arm and endoscope) which sometimes led to having the unused video feed as selected when was not used at that moment. With both sources of video being stored in the ePR we also added the benefit of comparison when the surgeon wants to take a C-ARM image while utilizing the endoscope device.

- Additional timestamps: In order to address the challenge of performing outcome analysis, as mentioned on the section 1.2, we needed to accurately and reliably store the beginning and ending timestamps for each surgical procedure.
- Data acquisition using multi-threads: Alpha version of the ePR was improved significantly with the development of data acquisition from different devices in parallel using multiple threads as compared to the sequential mode used for Prototype 1. This improvement allowed us to collect data in 1-second intervals.
- Communication protocol between the IU and the ePR: The communication protocol used to store all the data captured by the IU (images and datapoints) was migrated from a proprietary protocol to web services. With this change we gained flexibility and reliability for the data collection.

o Hardware: The main goal for the hardware change was to provide system redundancy in case of failure; all the different data sources have dual inputs to the IU, thus, in case one of the servers in the IU fails, the other will take over from that point further. However, at the time of writing, the failover is done via manual switching between the servers. We are studying the feasibility to provide an automatic mechanism for this task. The new mobile IU is shown in Figure 3.

Figure 3 The Mobile IU at the OR with the different pieces that .

- Patient Biometrics: We implemented a biometrics registration and verification toolkit to provide an easier way to launch the clinical Pre-Op data for a patient in the OR while at the same time reducing any possibility of patient misidentification. This module was implemented using CrossMatch fingerprint scanners and a corresponding SDK.
- Post-Op Authoring toolkit: Having the IU being able of collecting more data, by means of higher frequency collection intervals and saving both video feeds at the same time, the Post-Op had to be redesigned as well. The main challenge was to include both sources of video in the screen while showing the waveforms in a synchronized manner. Figure 6 in the Results section show the screenshot of the new Post-Op Authoring toolkit.

3. RESULTS

Since October 2008, the ePR system has been deployed at a clinical site, California Spine Institute (CSI). For the Pre-Op stage the users can register new patients, create new surgical procedures, add key images to those procedures with their corresponding annotations, add patients' surveys form into the ePR, and include whiteboard data. All these data are being displayed during live surgical procedures. The Intra-Op module is currently under clinical

evaluation and data from the surgical procedures are being collected for analysis and Post-Op authoring module evaluation. Due to the high sensitivity of the data being displayed, the IU is undergoing some performance improvements to handle different input sources adequately and more efficiently. The feedback loop is being carried on with the clinical staff. Certain refinements related to interconnectivity of some peripheral surgical devices are being done with clinical feedback. The 3 major stages on the surgical workflow: Pre-Op, Intra-Op, and Post-Op are explained below with the developed GUI and corresponding screenshots.

1. The Pre-Op stage of a MISS procedure is where all necessary information prior to the surgery procedure is collected and organized in a patient e-folder. The Pre-Op happens days prior to the surgery and involves querying, interviewing, collecting, and storing of pre-surgical medical images, patient demographic information as well as other pertinent data value that would assist the surgery during the procedure, such as patients' fingerprints. Figure 4 below shows a screenshot of this stage utilizing the Pre-OP authoring toolkit.

Figure 4 The Neuro-navigator tool, which is a part of the Pre-Op authoring toolkit, allows the correlation of the position of the lesion in the sagittal (left) and the axial view (right).

2. The Intra-Op stage is defined by the time during which the surgical procedure is being performed by the surgeon in the OR. All information collected during the Pre-Op are displayed in the Pre-Op display Monitor in OR. In addition live data from different input devices during the surgery are collected by the Integration unit (IU) and displayed in the Intra-Op monitor screen. Before the surgery starts, the patient's fingerprint is captured in the OR and verified with the biometric data acquired during the Pre-Op stage. This is an important step towards reducing errors and insuring correct patient identification prior to surgery. Figure 5 below depicts a screenshot of the Intra-OP Live Display.

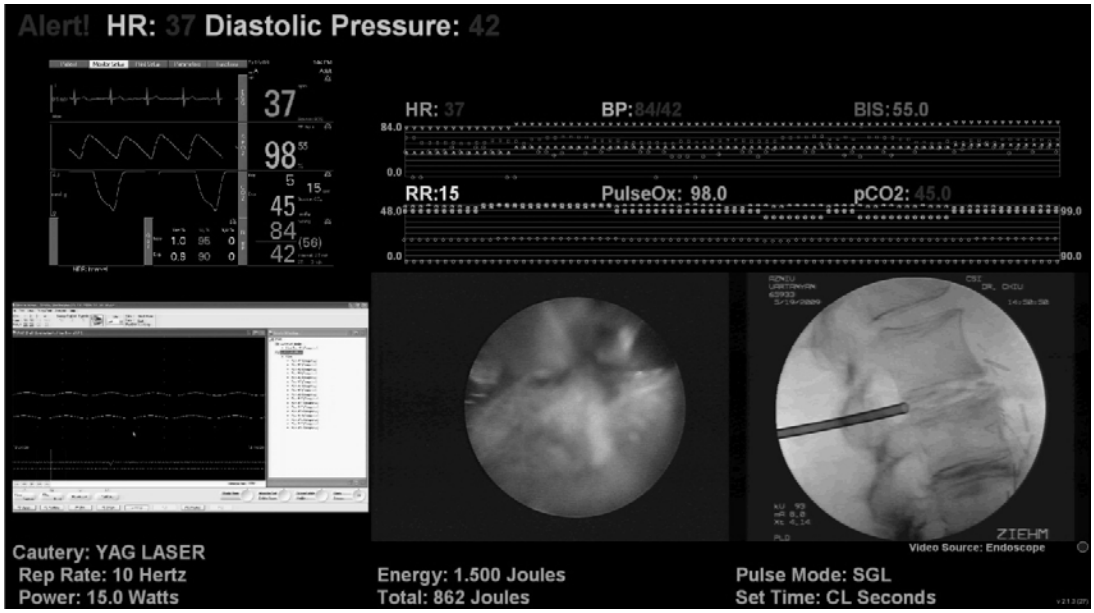

Figure 5 A mock-up example of the Intra-Op Live Display as seen on the Intra-Op large monitor in OR. Top row: Waveforms of six vital signs, BIS, and IVF, the horizontal axis is time. Middle row: Waveform of EMG, Fluoroscopic image, and endoscopic image. Bottom row: Laser output values.

3. The Post-Op stage takes place after the completion of the surgical procedure. There are three substages: 1) Patient in the recovery area and then discharged, 2) the Surgeon documents the surgical results, and 3) follow up pain surveys. In addition, with the Post-Op authoring toolkit, the surgeon can create image reports which can include important Pre-Op and Intra-Op data.

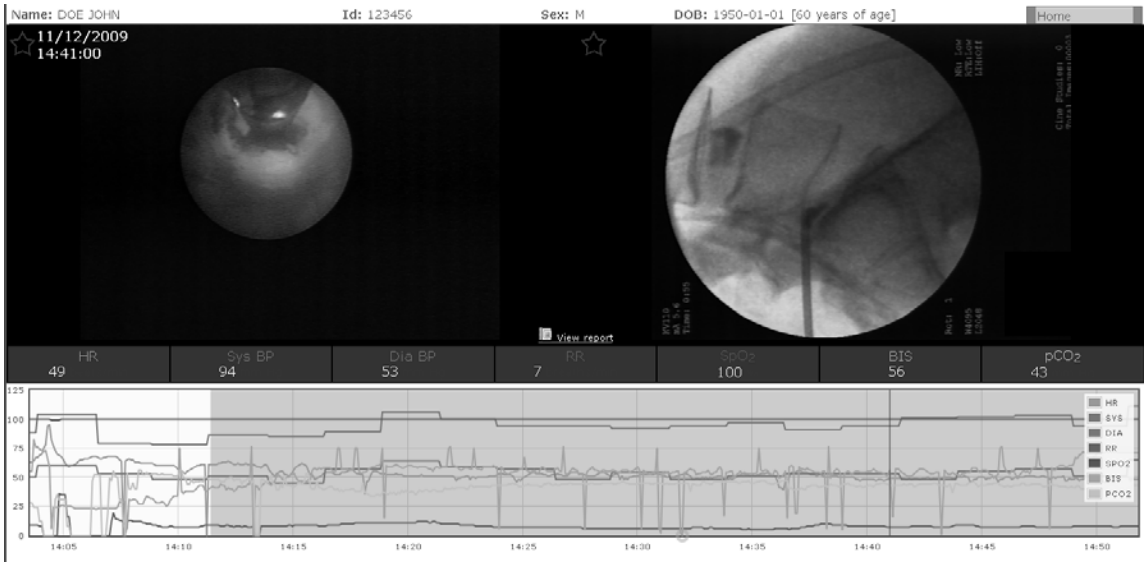

Figure 6 The Post-Op interface that shows the different waveforms from the vital signs datapoints collected during the surgical procedure. This interface also shows the 2 video feeds that were captured by the IU. All the data shown above is synchronized in time for easier review. The darker section at the right of the displayed waveforms indicates the actual duration of the clinical procedure from the time the surgeon initiates the procedure until the end of it.

4. CONCLUSION

An ePR system tailored for Minimally Invasive Spinal Surgery has been migrated from its prototype version 1 to a more robust and mature alpha release. The data model still follows the DICOM standard with new data objects designed specifically to address the surgical procedure; in addition, the database schema has been modified to include all the datapoints and image captures acquired during a surgical procedure. The system was implemented at a clinical site that performs MISS and the surgical data is currently being captured and stored within the ePR system. From the technical point of view, the ePR system is more stable and robust due to the fact of migrating to a more reliable communication protocol between the IU and the ePR/Gateway servers. The Alpha release of the system was implemented in October last year and the evaluation and analysis of the data collected is currently ongoing. The total number of cases performed since the inception of the Alpha version of the ePR system is 22 cases.

REFERENCES

[1] Huang H.K., 2001. PACS, Informatics, and the Neurosurgery Command Module. J. Mini Invasive Spinal Technique. Vo1 1, 62-67

An automatic quantification system for MS lesions with integrated DICOM structured reporting (DICOM-SR) for implementation within a clinical environment

Colin Jacobs[a], Kevin Ma[b], Paymann Moin[b], Brent Liu[b]
[a]Eindhoven University of Technology, Den Dolech 12, 5612 AZ, Eindhoven, The Netherlands
[b]Image Processing and Imaging Laboratory, Department of Radiology, USC, 2250 Alcazar Street, CSC 105 Los Angeles, CA 90033

ABSTRACT

Multiple Sclerosis (MS) is a common neurological disease affecting the central nervous system characterized by pathologic changes including demyelination and axonal injury. MR imaging has become the most important tool to evaluate the disease progression of MS which is characterized by the occurrence of white matter lesions. Currently, radiologists evaluate and assess the multiple sclerosis lesions manually by estimating the lesion volume and amount of lesions. This process is extremely time-consuming and sensitive to intra- and inter-observer variability. Therefore, there is a need for automatic segmentation of the MS lesions followed by lesion quantification. We have developed a fully automatic segmentation algorithm to identify the MS lesions. Characterized quantification of the lesions is performed. The quantification results, which include lesion volume and amount of lesions, are stored in a structured report together with the lesion location in the brain to establish a standardized representation of the disease progression of the patient. The development of this structured report in collaboration with radiologists aims to facilitate outcome analysis and treatment assessment of the disease and will be standardized based on DICOM-SR. The results can be distributed to other DICOM-compliant clinical systems that support DICOM-SR such as PACS. In addition, the implementation of a fully automatic segmentation and quantification system together with a method for storing, distributing, and visualizing key imaging and informatics data in DICOM-SR for MS lesions improves the clinical workflow of radiologists and visualizations of the lesion segmentations and will provide 3-D insight into the distribution of lesions in the brain.

Keywords: Multiple Sclerosis, MR, white matter, lesion, segmentation, quantification, DICOM-SR

1. INTRODUCTION

1.1 Multiple Sclerosis

Multiple Sclerosis (MS) is a common neurological disease affecting the central nervous system. It is considered as an inflammatory autoimmune disease that is characterized by several pathologic changes including demyelination and axonal injury. The disease affects approximately 2,500,000 people worldwide between the age of 17 and 65 years old, according to the National Multiple Sclerosis Society in the USA. A recent study has confirmed the traditional thought that MS occurs more in women than in men and more in regions more distant from the equator.[1] At present, the exact cause of MS remains unknown. The life expectance of MS patients is nevertheless not lower than the unaffected population although certain consequences of the disease could lead to early death.

As mentioned, the disease is characterized by demyelination, and this causes the axons to be unable to effectively conduct signals through the brain. This is leading to a broad range of symptoms including sensorial, visual, cerebellar and motor symptoms. These symptoms often occur intermittent and the periodicity of the symptoms differs strongly among patients. After the demyelination, the damaged myelin sheath degenerates and forms scar tissue (sclerosis). The areas of scar tissue are referred to as "plaques" or lesions and the amount and size of the lesions give an indication of the disease condition and progression. The size of a lesion is usually referred to as lesion load. MS lesions occur primarily in the white matter (WM) of the brain with a preference in the periventricular area. However, lesions are also frequently found in the corpus callosum, subcortical region, brain stem, U-fibers, optic nerves and the visual pathway.

1.2 Multiple Sclerosis and MRI

Multiple sclerosis lesions can be detected with MR imaging with great sensitivity and this has proven to be an important clinical tool to assess the condition of the disease in a patient. After a patient undergoes a MR examination, the radiologists will observe the acquired images and investigate the patients for MS lesions. During this process, the radiologists manually contour the lesions and try to estimate the size and amount of lesions that are present in the patient's brain. This will give insight into the disease condition and using follow-up studies, the progression of the disease can be studied. However, the quantification of the MS lesions is difficult, time-consuming and sensitive to intra- and inter-observer variability. For those reasons, a lot of research has been done into designing either manual, semi-automatic of fully automatic MS lesion segmentation algorithms. The different research projects have been using different input images such as PD-weighted images, T1-weighted images, T2-weighted images or Fluid Attenuated Inversion Recovery (FLAIR) images. In addition, the projects could be focused either on 2-D images or 3-D datasets.

1.3 Computer Aided Diagnosis for Multiple Sclerosis

In this project, a fully automatic Computer Aided Diagnosis (CAD) algorithm is designed and developed. The focus of the algorithm will be on T1-weighted, T2-weighted and/or Fluid Attenuated Inversion Recovery (FLAIR) three-dimensional datasets. MS lesions occur as hyperintense on T2-weighted images, but the distinction between lesions and cerebrospinal fluid (CSF) is difficult because CSF occurs as hyperintense as well. However, the CSF is suppressed with the FLAIR sequence thereby making the border between CSF and lesions clearly visible on these images. On T1-weighted images, the lesions normally appear as isointense to the normal white matter although certain circumstances such as chronic tissue injury or severe inflammatory edema can lead to a hypointense signal.[2] The algorithm uses the intensity values and spatial information from the three different MR sequences to determine a classification for each voxel in the MR image. To do this accurately, several preprocessing steps are applied to guarantee spatial correlation between the different datasets. When a successful CAD algorithm is designed, the CAD algorithm will be integrated into an e-Folder system together with other clinical related data. The e-Folder system is a disease centric clinically tailored imaging and informatics system in a health care enterprise which has many functions such as accepting direct digital input of patient data and providing clinical decision support. By integrating the CAD algorithm and its results, the system is able to provide key clinical imaging informatics data for outcomes analysis and treatment assessment.

1.4 DICOM Structure Reporting

The MS e-Folder that is described in further detail in "The Development of a Disease Oriented eFolder for Multiple Sclerosis Decision Support," a fellow SPIE 2010 conference presentation. The CAD algorithm produces output data that needs to be standardized and integrated with other system components as well as querable. DICOM structured reporting (DICOM-SR) provides templates to include quantification results in a standardized format[3]. The structured reporting would allow searching, storage, and comparison with other similar data better than traditional paper report format. A sample diagram of how a sample DICOM-SR is modeled.

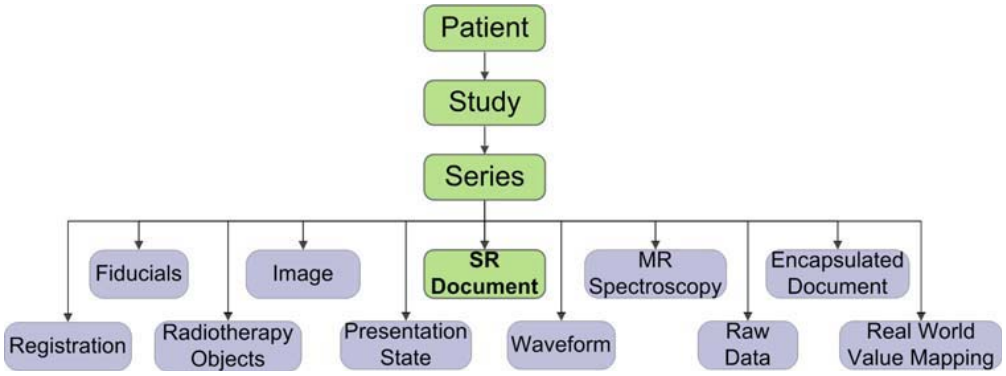

Figure 1. DICOM-SR model in the real world.[8]

Integrating CAD results with Picture Archiving and Communication System (PACS) using DICOM-SR has been accomplished previously[4]. The CAD-PACS toolkit was designed to streamline the CAD workflow in PACS, from generating CAD worklist from RIS/PACS to storing CAD results in PACS as DICOM-SR objects. For this project, an integration of MS CAD with DICOM-SR is designed and implemented to directly store CAD results in a tabulated format in the database, as well as to produce DICOM structured reports that may be displayed from a PACS workstation and stored in a conventional PACS.

2. METHODS

2.1 Image alignment using the midsagittal plane

A first and crucial aspect of the algorithm is that the different images have to correspond spatially, because the final classification evaluates the different voxel intensities and positions in the T1-weighted image, T2-weighted image and FLAIR image. Evidently, a voxel at a certain position in the T1-weighted image has to correspond to the same position in the brain in the T2-weighted image and so on. Therefore, the images are aligned according to the midsagittal plane. The extraction of the midsagittal plane is fully automatic and is based on an algorithm designed by Hu et al. in 2003[5]. Using the midsagittal plane, the different yaw, pitch and roll angles are calculated and a rigid body transformation is applied to ensure registration of the different images.

2.2 Brain segmentation

After aligning the images, a segmentation of the human brain is needed to select the region of the head where the MS lesions can occur. Although Multiple Sclerosis lesions occur mainly in the white matter, the choice is made to segment both the gray matter as the white matter. The reason for this is mainly because the distinction between white matter and gray matter is difficult and lesions can also occur on the border of gray and white matter which makes the decision to segment both white and gray matter obvious. The segmentation of the brain is based on an article by Shan et al. in 2002 [6]. The authors describe an automated histogram-based brain segmentation algorithm that uses T1-weighted three-dimensional MR head images. Although the authors bring out a high accuracy using the T1-w images only, the brain segmentation in this system uses the FLAIR images also. The main reason for this is that the FLAIR sequence generates a better distinction in intensity between CSF and GM which is of major importance in the algorithm.

2.3 Probabilistic segmentation of multiple sclerosis lesions

After the brain is extracted from the 3-D volume data, a method is designed to classify the voxels within the brain mask. As mentioned in the introduction, the method uses the information from the T1-weighted, T2-weighted and FLAIR image. The classification method is based on an article by Anbeek et al. in 2003[7]. The authors proposed a method in which they use K-Nearest Neighbor classification to build a fully automatic segmentation algorithm for white matter lesions. KNN classification is a non-parametric classification technique often used in image processing which builds a feature space and calculates the nearest neighbors to a certain target point within this feature space. The amount of neighbors that is searched for is defined by K. The actual classification is performed by comparing the target to its K nearest neighbors to attain an estimate for the class of the target.

Using the information from the MR images, each voxel can be represented by a six dimensional vector containing the intensity values in respectively the T1-w, T2-w and FLAIR image and the spatial position coordinates x, y and z. So, the feature space is a six dimensional space wherein a voxel can be represented as a point in this space. Using this feature space, the probability that a voxel is an MS lesion is in concept calculated by the fraction of the classes of its nearest neighbors in the feature space that are considered to be part of a MS lesion. To be able to do a classification, a feature space has to build from other datasets in which the classification of the voxels is known. These datasets are referred to as learning datasets. In a particular learning dataset, all voxels are classified either to be part of a MS lesion or not and these voxels are put into the feature space. When a sufficient amount of learning points are put into the feature space, a voxel is classified by placing in into the feature space and calculating its K nearest neighbors. Subsequently, the fraction of the K nearest neighbors that are classified as part of a MS lesion determines the probability of the target voxel to be part of a MS lesion. In principal, the brain of a radiologist does the same thing since radiologists also compare and relate a case to

other cases from their past and knowledge to make a diagnosis. Finally, thresholding of the probability map will give you to the final binary segmentation containing the MS lesions. Figure 2 depicts the probabilistic segmentation process.

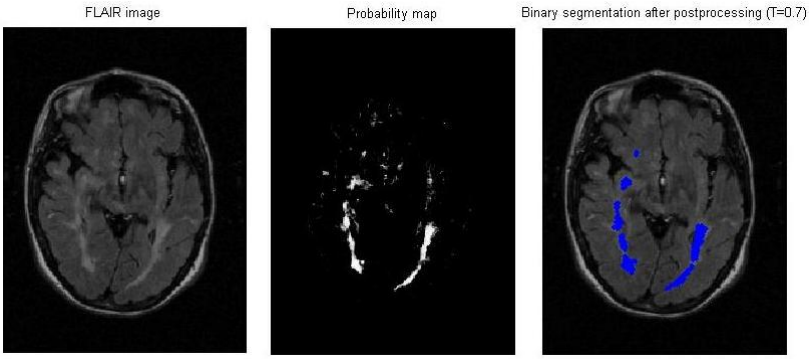

Figure 2. Example of probabilistic segmentation of the multiple sclerosis lesions. The left image is the FLAIR image where the lesions are clearly visible. The middle image displays the probability map for this specific slice. The right image shows the segmentation which is acquired by applying a threshold of 0.7 to the probability map.

In addition, we use kd-trees to accelerate the KNN classification process. Using this kd-tree technique, a more intelligent nearest neighbor search can be done on this tree structure which allows you to only search a few of the 'leafs' of the total tree and thereby saving a lot on computation time.

2.4 Quantification

The voxels in the binary segmentation are clustered in 3-D using 26-connectivity and all clusters smaller than 10 voxels are removed from the segmentation. Subsequently, the lesion load and the number of lesions can be calculated using these clusters. Evidently, the amount of clusters corresponds to the amount of lesions that are present. The lesions are divided into several groups. These groups are created to supply information about the size of the different lesions. The lesion load of each lesion is calculated by multiplying the number of voxels by the voxel size which can be extracted from the DICOM-headers. Finally, the total lesion load is calculated. In conclusion, the final result of the algorithm will contain the amount of lesions of the different groups and the total lesion load in cm^3.

2.5 DICOM Structured Reporting for CAD Output

The initial output of the MS CAD program is a text file containing total lesion load, lesion coordinates, volume of each lesion, number of lesions, 2D MR slices containing lesions and lesion representation in 3D space.

A DICOM-SR template is required for converting CAD outputs. The MS CAD DICOM-SR template is presented in Figure 3.

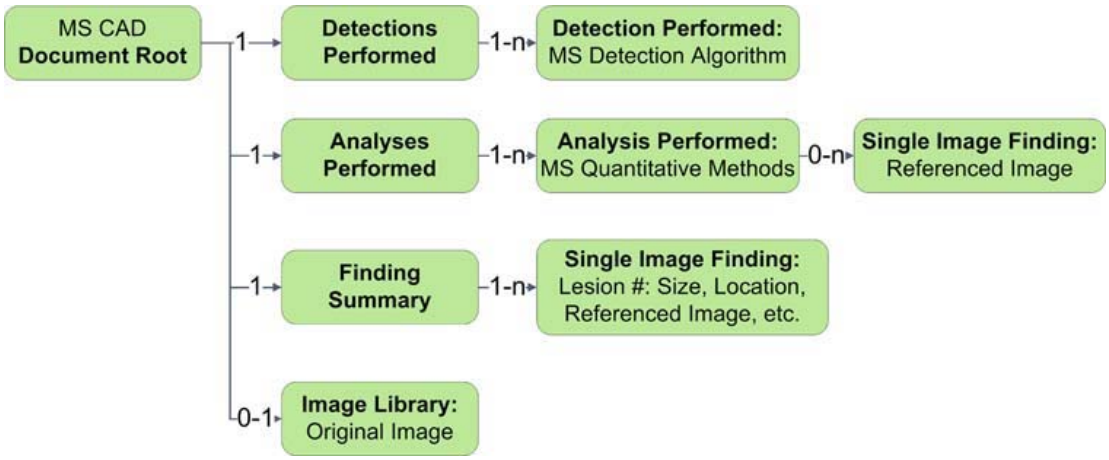

Figure 3. DICOM-SR template used for MS CAD application[8], as published by Le, A. (2009). The figure shows the tree structure that can be stored in DICOM-compliant file structure.

There are four parent nodes in the template: detections, analyses, finding summary and image library. Under each parent nodes, different numbers of child nodes are attached based on number of actions performed in the case. The detection branch records the detection methods used, the analyses branch records all quantitative analyses performed, and the finding summary branch records the detection and analyses results. The structure format is obtained directly from the DICOM standard, as detailed in DICOM supplement 23[9].

3. RESULTS

More than 20 cases are collected from USC Health Consultation Center in Los Angeles, CA. Each case are of different patients. Slice thickness are 3mm without no gaps in between slices, which is important for voxel size calculation and quantification accuracy. Each image sequence has around 50 slices. In those cases, four are used for training purposes and 10 cases total are used in outputting data for the MS eFolder, complete with patient information. MS CAD has been performed on the 10 image cases and lesion detection results are computed. Table 1 lists the quantifiable data of CAD results. Figure 4 is a screenshot of CAD result in 3D space, displayed by the open-source ITK-SNAP tool[10].

Table 1. Sample MS CAD output of one patient

Total lesion load	32.63 cm^3
Total Number of lesions	12
Number of Lesions < $1cm^3$	10
Number of Lesions > $1cm^3$ but < $5cm^3$	0
Number of Lesions > $5cm^3$	2

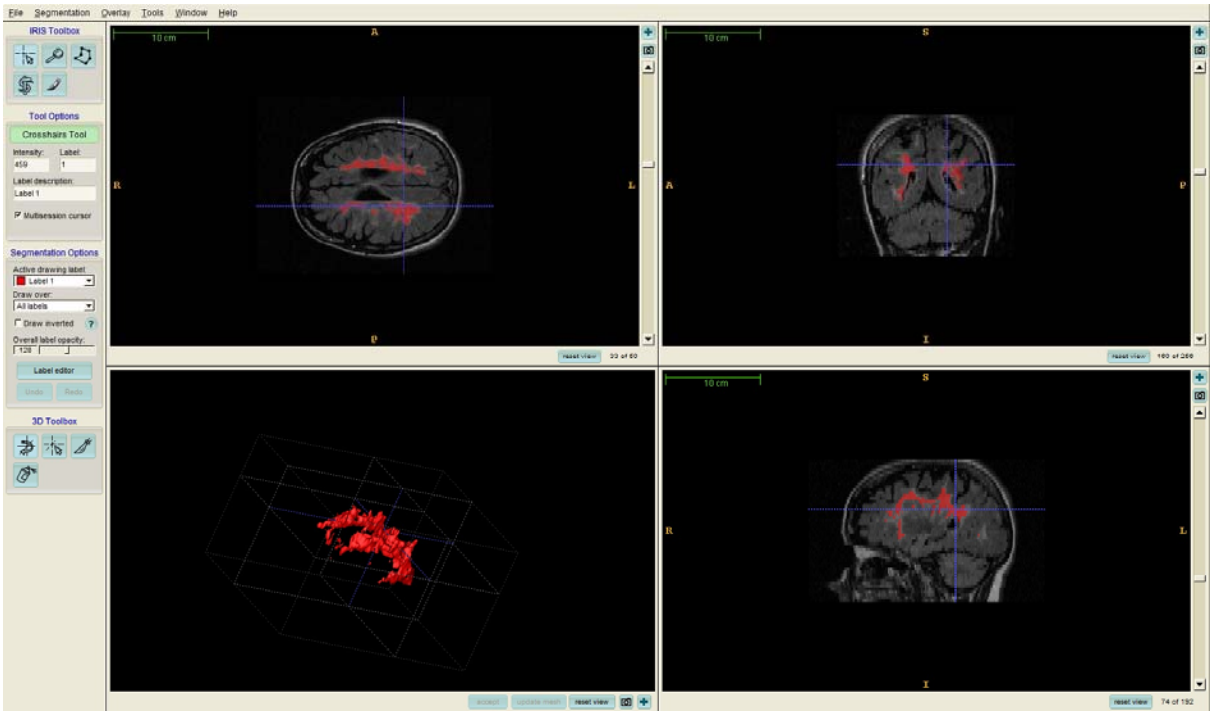

Figure 4 Screenshot of identified MS lesion voxels being rendered three-dimensionally by ITK-SNAP tool. The top left image is the axial viewof the FLAIR sequence (original image), while the top right image is the coronal view and bottom right image is the sagittal view, which are calculated from the axial view. The bottom left image is the 3D rendered image of lesion voxels. The rendered image can be rotated to view from different angles.

While the CAD algorithm is written in MATLAB®, the use of ITK-SNAP tool is to more easily present the 3D view of lesions. The DICOM MR images are converted to ANALYZE files for easier ITK-SNAP handling and lesion image overlapping. As of the time of this writing, the CAD results have not been validated with radiologists and neurologists. There remains some shortcomings of the CAD algorithm, such as the long runtime to do numerous recursive calls by MATLAB. The speed aspect of MS CAD performance is described in detail in SPIE 2010 project titled “Performance evaluation for volumetric segmentation of multiple sclerosis lesions using MATLAB and computing engine in the graphical processing unit (GPU).”

The quantification results are successfully incorporated into a structured report based on DICOM-SR using the developed MS module. Figure 5 presents a series of screen shots of resulting DICOM-SR outputs.

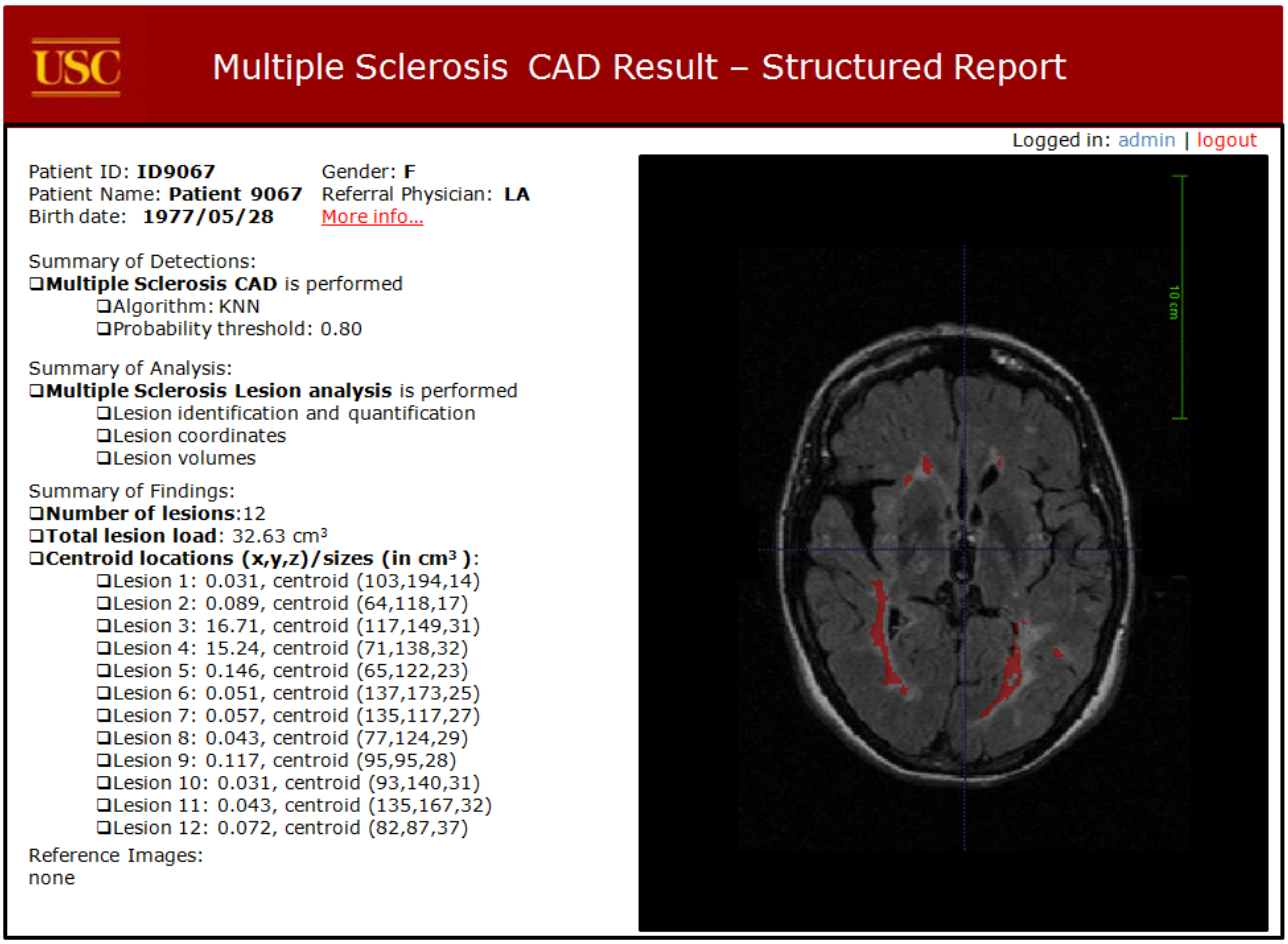

Figure 5. Screenshot of sample DICOM-SR for MS CAD results

The structure report is stored in the MS eFolder database as the output of CAD algorithm. DICOM-SR result is currently in the prototyping stage and has not been tested with other DICOM-compliant tools, such as PACS. The in-lab simulation of DICOM-SR workflow is still ongoing.

4. CONCLUSION

This paper presents a novel approach of a standardized representation of the disease condition of Multiple Sclerosis using DICOM-compliant structured reporting of quantification results derived by fully or semi-automatic quantification of MS lesions from MR images. The structured report is based on DICOM-SR and this makes it suitable for distribution among other DICOM-compliant systems that support DICOM-SR such as PACS. With DICOM-SR, quantification results can be queried by lesion load, locations of lesions, and volume of each contour. This allows data mining for cases with specific criteria previously not available to clinicians and researchers. The workflow of the radiologists can be improved and accelerated using the CAD system. Besides that, the quantification of the MS lesions is extremely helpful for outcome analysis and disease treatment. The results for the CAD algorithm will be integrated into an e-Folder system together with other clinical related data and this will create a system that provides key clinical imaging data to specialists. Furthermore, the system provides additional data to radiologists in the decision-making process.

Future works include a clinical validation of the MS CAD method, an improvement in CAD performance in terms of efficiency and practicality, and the clinical validation of fully-integrated MS CAD with DICOM-SR in a PACS

environment. The DICOM-SR output will also be integrated and stored into the MS eFolder database, where the contents of CAD results can be queried and displayed within the Ms eFolder system.

REFERENCES

[1] Alonso A. and Hernn. M.A. “Temporal trends in the incidence of multiple sclerosis: a systematic review.” Neurology, 71(2):129-135, Jul 2008.

[2] Ge Y. Multiple sclerosis: “The role of MR imaging.” American Journal of Neuroradiology, 27:1165-1176, Jun-Jul 2006.

[3] Hussein, R., Engelmann, U. et al. “DICOM Structured Reporting” Radiographics, 24, 891-896 (May 2004)

[4] Zhou Z, Liu B, Le A. “CAD-PACS Integration Tool Kit Based on DICOM Secondary Capture, Structured Report and IHE Workflow Profiles” Computerized Medical Imaging and Graphics, 31(4): 346-352

[5] Qingmao Hu and Wieslaw L. Nowinski. “A rapid algorithm for robust and automatic extraction of the midsagittal plane of the human cerebrum from neuroimages based on local symmetry and outlier removal.” NeuroImage, 20(4):2153{2165, Dec 2003.

[6] Zu Y. Shan, Guang H. Yue, and Jing Z. Liu. Automated histogram-based brain segmentation in t1-weighted three-dimensional magnetic resonance head images. NeuroImage, 17(3):1587{1598, Nov 2002.

[7] Petronella Anbeek, Koen L. Vincken, Matthias J.P. van Osch, Robertus H.C. Bisschops, and Jeroen van der Grond. “Probabilistic segmentation of white matter lesions in MR imaging.” NeuroImage, 21(3):1037{1044, Mar 2004.

[8] Le A, Liu B, Huang HK, “Integration of computer-aided diagnosis/detection (CAD) results in a PACS environment using CAD-PACS toolkit and DICOM SR” Int J CARS (2009) 4:317-329

[9] Digital Imaging and Communications in Medicine (DICOM) Supplement 23: Structured Reporting Storage SOP Classes http://medical.nema.org/Dicom/supps/sup23_lb.pdf

[10] Paul A. Yushkevich, Joseph Piven, Heather Cody Hazlett, Rachel Gimpel Smith, Sean Ho, James C. Gee, and Guido Gerig. User-guided 3D active contour segmentation of anatomical structures: Significantly improved efficiency and reliability.*Neuroimage* 2006 Jul 1;31(3):1116-28.

Decision support tools for proton therapy ePR: intelligent treatment planning navigator and radiation toxicity tool for evaluating of prostate cancer treatment

Anh H. Le*, Ruchi Deshpande, Brent J. Liu
Image Processing and Informatics Laboratory, 2250 Alcazar Street, Los Angeles, CA, USA 90033; Depts. of Radiology and Biomedical Engineering, University of Southern California, Los Angeles, CA, USA 90033

ABSTRACT

The electronic patient record (ePR) has been developed for prostate cancer patients treated with proton therapy. The ePR has functionality to accept digital input from patient data, perform outcome analysis and patient and physician profiling, provide clinical decision support and suggest courses of treatment, and distribute information across different platforms and health information systems. In previous years, we have presented the infrastructure of a medical imaging informatics based ePR for PT with functionality to accept digital patient information and distribute this information across geographical location using Internet protocol. In this paper, we present the ePR decision support tools which utilize the imaging processing tools and data collected in the ePR. The two decision support tools including the treatment plan navigator and radiation toxicity tool are presented to evaluate prostate cancer treatment to improve proton therapy operation and improve treatment outcomes analysis.

Keywords: DICOM-RT, DICOM-RT-ION, ePR, Proton Therapy, Prostate, Decision Support

1. INTRODUCTION

The current workflow of proton therapy has four main phases: Consultation, Treatment Planning, Treatment Delivery and Follow-up. After the Follow-up phase, patient data are usually collected by research department to do further analysis for improvement in treatment methodology and quality of care.

Many treatment protocols used in radiation therapy needs to go through an acceptance process whether a protocol is adequate to deliver the total dose to patient without new side effects or radiation toxicity. At the James M. Slater, M.D. Proton Treatment and Research Center, the escalation dose treatment protocol, in which the current total dose has been increased to 80 Gy, has been utilized in clinical treatment for many years and this protocol has proven to have minimum radiation toxicity compared to lower dose. The current practice is to give the patient one fraction, 2 Gy, of total dose each day, five days a week until the patient receives all prescribed dose. This treatment duration usually consists of 40 fractions in 40 days, approximately 2 months. The duration has been a problem for many patients since most of them are not local. Another treatment protocol has been introduced and is undergoing evaluation and acceptance process. This new method, called hypo-fractionation dose protocol, allows patient to receive higher dose per day; therefore, decreases the total fractions of PT. [1]

In order of evaluate the new protocol for prostate cancer, researchers need to collect all the clinical information, images and treatment plans data. The problem arises when the data is scattered among many systems. Furthermore, there is no system to collect all the data in one source for doing outcome analysis and QA in treatment planning that can be transferred to multiple locations. The ePR is an effective system that provides a centralized archive for all data of prostate cancer patient treated with proton therapy. On top of that, the ePR is constructed with decision support tools which foster the process of treatment planning and data analysis. Two examples will be discussed in this paper are an intelligent treatment plan navigator (ITPN) and radiation toxicity tool (RTT).

*anhhle@usc.edu; phone 1 323 442-2936; fax 1 323 442-2575; ipilab.org

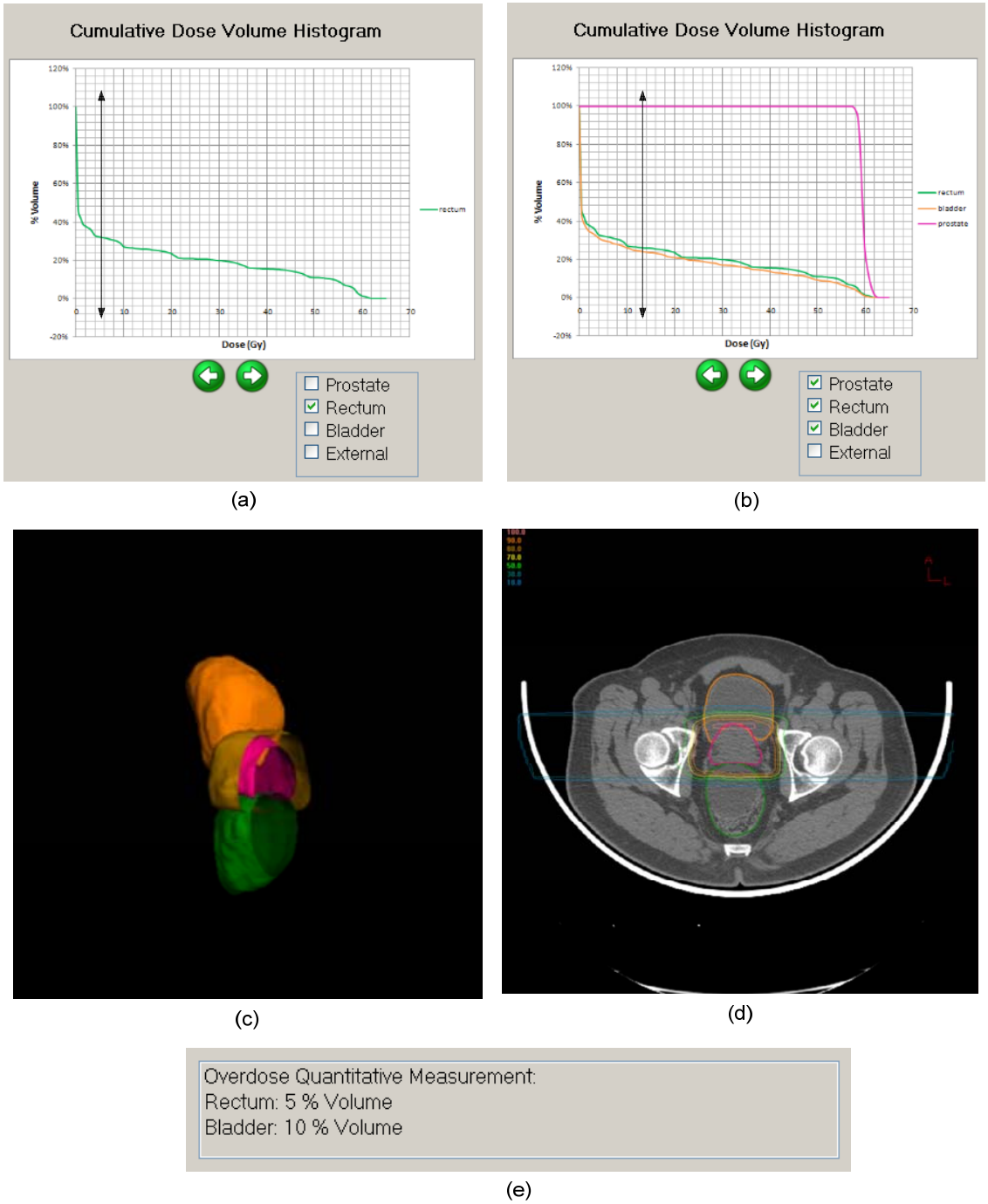

Figure 1. Screenshots illustrate ITPN workflow (a) Feature 1: Single DVH curve navigation along x-axis and y-axis using arrow buttons; (b) Feature 2: Multiple DVH curves navigation; (c) Feature 3: Display 3D surface of chosen critical structure, dose distribution; (d) Feature 4: Display 2D CT Images with contours and isodose curve overlaid; (e) Feature 5: Display quantitative measurement of overdose volume in critical structures. (Orange-bladder; Green-rectum; Pink-prostate; Brown-isodose surface).

2. METHODOLOGY

2.1 The ePR Architecture

We have developed an ePR system with DICOM compliance that can archive patient images and related treatment planning and clinical outcomes data. The visualization tools, such as MR/CT image fusion, RT and RT-ION objects interpretation module, and a knowledge database to foster treatment planning process, are developed based on DICOM images, DICOM-RT and DICOM-RT-ION objects with clinical collaboration from James M. Slater, M.D. Proton Treatment and Research Center, Loma Linda, CA and its oncologists and physicists. The data includes two DICOM image objects and four DICOM RT and RT-ION objects. In addition, clinical outcomes data collected from select PT cases are included in the overall database knowledge for future outcomes analysis. For example, the ePR provides an interface for clinician to input follow-up data and outcome data, and uses these data to determine the rectal toxicity based on the Common Terminology Criteria for Adverse Events v3.0 (CTCAE). Through analysis of rectal toxicity of previous patients, clinicians can improve treatment plans on current patient who has similar characteristics, such as age, prostate size and radiated rectal volume. A Graphical User Interface (GUI) application embedded in the ePR allows clinicians to manipulate DICOM images, review contours, isodose and dose-volume histogram (DVH) curves, and render 3D dose images. The ePR system utilizes the Web-based technology; hence, the patient data can be visualized through web browser and distributed across multiple locations by the local area network and Internet. [2-4]

2.2 The Intelligent Treatment Plan Navigator Design

In order to plan the treatment of hypo-fractionation and dose escalation protocols, both physicist and oncologist need to ensure that the 90% isodose curve needs to cover entire prostate gland; the critical structures, such as bladder and rectum, fall under approved clinical ranges; and the plan has no overdose regions. The current treatment tools are limited in their ability to provide intelligent navigation of data for the necessary evaluation. Therefore, we designed and developed the ITPN utilized the DICOM-compliant ePR platform and patient data stored in ePR database to enhance the treatment planning process, therefore, improve PT workflow.

The features of the INTP include:

- Navigate along a single DVH curve to verify dose of the tumor and critical structures along with correlated dose distribution volumes in 2D and 3D,
- Navigate through multiple DVH curves with the same corresponding volume or dose along with correlated dose distribution volumes in 2D and 3D,
- Visualization and quantification of overlapped or non-overlapped region between the structure volume and isodose using 3D surface rendering,
- Automatic visualization and quantification of overdose regions in critical structures.

Figure 1 shows the features of the Intelligent Treatment Plan Navigator (ITPN) with examples of what the graphical user interface (GUI) provides for each of the features.

2.3 Radiation Toxicity Tool

In order to assess the effectiveness of the hypo-fractionation protocol, one must analyze the outcome data, which are depicted by the radiation toxicity of the treatment. The radiation toxicity is usually graded on a scale from 1 to 5. Grade refers to the severity of the adverse event (AE). The Cancer Radiation Therapy Program, National Cancer Institute has published the Common Terminology Criteria for Adverse Events (CTCAE) (formerly known as Common Toxicity Criteria) as standards used to grade, assign attribution and report side effects or radiation toxicity experienced by patients in clinical trials. The version used in the Radiation Toxicity Tool of the ePR is CTCAE v.3 published on August 9, 2006, including all AE applicable to all oncology trials regardless of chronicity or modality [5]. The radiation toxicity is usually graded on a scale from 1 to 5. Grade refers to the severity of the adverse event (AE).

The toxicity grade is most important measurement for the effectiveness and efficiency of PT treatment in radiation treatment. However, the current method of determining this grade is to manually read the CTCAE guideline and assign a

grade for each symptom dependent on its severity. This process is not only tedious and time consuming but also prone to mistakes due to human error. Furthermore, user cannot query or relate patient data and toxicity grade with treatment plans to do futher analysis. The Radiation Toxicity Tool (RTT) is developed to eliminate problem in this process using simple database table and query approach.

The RTT uses the CTCAE v.3 as a guideline to create the ctacaemap table, as shown in Figure 2, for querying the toxicity grade according to the AEType, AE and severity of these AEs. Figure 2 also shows examples of information stored in this table.

The features of the radiation toxicity tool include:

- A digital form for clinician to enter outcome data,
- A automatic engine to determine radiation toxicity grade according the CTCAE v.3 guideline,
- A report graphical user interface to show the patient outcome summay and worst toxicity grade.
- A query tool to relate toxicity grade and patient treatment plan data.

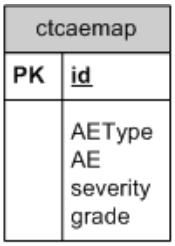

id	AEType	AE	severity	grade
11	Gastrointestinal	Colitis	Asymptomatic, pathologic or radiographic findings only	1
12	Gastrointestinal	Colitis	Abdominal pain; mucus	2
13	Gastrointestinal	Colitis	Abdominal pain, fever, change in bowel habits with ileus; peritonea	3
14	Gastrointestinal	Colitis	Life-threatening consequences (e.g., perforation, bleeding, ischemi	4
15	Gastrointestinal	Colitis	Death	5
16	Gastrointestinal	Constipation	Occasional or intermittent symptoms; occasional use of stool soften	1
17	Gastrointestinal	Constipation	Persistent symptoms with regular use of laxatives or enemas indicat	2
18	Gastrointestinal	Constipation	Symptoms interfering with ADL; obstipation with manual evacuation i	3

Figure 2. Radiation toxicity tool database schema. Top: ctcaemap table structure contains the information published in CTCAE v.3 to evaluate radiation toxicity grade. Bottom: examples of data stored in ctcaemap table.

3. DATA

The ePR system is a centralized system that integrates all disparate data and provides a “one-stop-shop” for data of prostate cancer patients treated with proton therapy. All the data utilized in my research is collected at the James M. Slater, M.D. Proton Treatment and Research Center, Loma Linda University Medical Center (LLUMC).

A prostate cancer patient’s data set includes an Initial Data Form, CT images, a RT Dose, a RT Structure Set, a RT ION Plan, one or two RT Images, RT ION Treatment Record, and Initial Data Form and Follow-up Data Forms. Table 1 summarizes all data collected from one patient. Currently, there are more than 30 patient data sets in total of 50 patient data sets has been collected. These data is used to evaluate the ePR system, including the intelligent treatment plan navigator and radiation toxicity tool. The 50 patient data sets will be used in a pilot study of evaluation hypo-fractionation treat

Table 1. Proton therapy data collected from one prostate cancer patient.

Name	Media	Type	Digital Format	Location
Patient Initial Data Form	Text	Pre-treatment Clinical Data	No	Research Spreadsheet
CT	DICOM Files	Image	Yes	PT Data Server
RT Structure Set	DICOM File	Contours	Yes	TPS WS
RT-ION Plan	DICOM File	Plan	Yes	TPS WS
RT Image	DICOM File	RT Image	Yes	TPS WS
RT Dose	DICOM File	Dose Image	Yes	TPS WS
RT-ION Treatment Record*	DICOM File	Treatment Record	No	Patient Chart
Follow-up Data Form	Text	Outcome Data	No	Research Spreadsheet

(* not currently collected since this data type is not significant for current status of the system)

4. RESULTS

The 30 collected patient data sets, mentioned in Section 3, are imported into the ePR system to evaluate the system and testing the two developed tools. The following sections will discuss the graphical user interface (GUI) and interaction steps of the ITPN to evaluate treatment plan and RTT to assess outcome data.

4.1 Intelligent Treatment Plan Navigator GUI

The ITPN allows a user to intelligently navigate between DVH curves and corresponding 3D dose distribution volumes along with quantified volume data of overdosed regions for better evaluation of complex treatment plans. Figure 3 shows a clinical example of graphical user interface (GUI) of ITPN and below are steps that the user can interact with the GUI to evaluate the treatment plan.

1. Step 1: Utilizing the ITPN, the user can first review the DVH curves of the tumor and critical structures (rectum and bladder), in region (1) of the GUI.
2. Step 2: In addition to the DVH curve, the corresponding 3D dose distribution is displayed together with the prostate and critical structures in region (3). In this case, the 3D dose distribution (see the blue arrow) shows some dose outside of the prostate volume indicating possible dose to neighboring critical structures.
3. Step 3: The user can then include the DVH of the rectum critical structure in region (1). Again, the corresponding 3D volume of the rectum critical structure is displayed showing how the 3D dose distribution volume overlapped into the 3D rectum critical structure volume in region (3).
4. Step 4: The 3D views are also accompanied by 2D slice views with isodose curves overlaid. The user can use the function toolbox, region (2), to control the appearance on both the 2D view and the 3D view to properly assess any overdose regions
5. Step 5: Additionally, the quantified volume of dose that is overlapped into the rectum critical structure volume is displayed in region (5) along with the results as shown in the DVH curve.

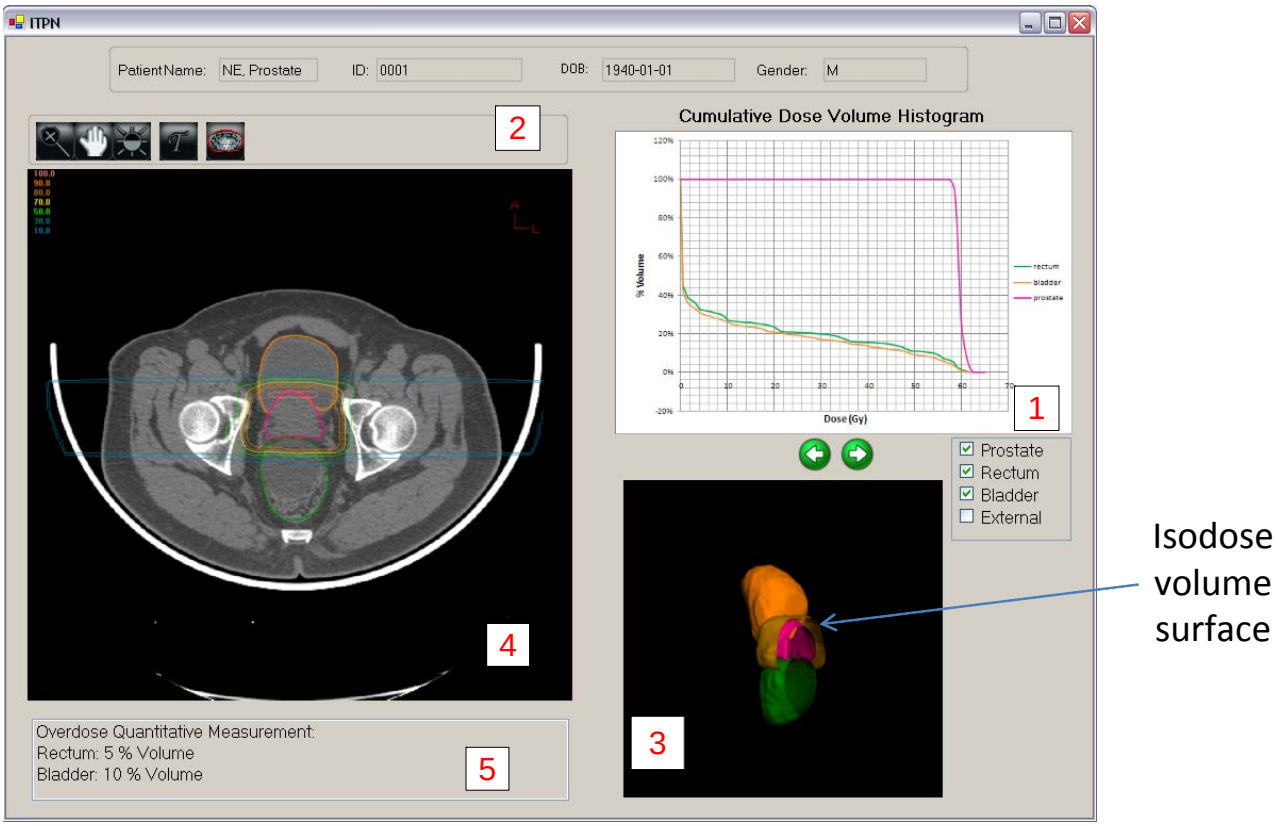

Figure 3. Prototype GUI of ITPN (1) Function toolbox; (2) DVH display region; (3) 3D Rendering image display; (4) 2D image display with contours and isodose curve overlaid; (5) Quantitative measurement display.

4.2 Radiation Toxicity Tool Usage

The radiation toxicity tool (RTT) allows the user to enter five adverse event types (AEType) for query purposes, which are gastrointestinal, urinary, skin, constitutional and sex function. These AEs are specifically collected for prostate cancer patients treated with proton therapy at LLUMC. Figure 4 shows the RTT GUI. Before completing the form using the "Submit" button, the user will do the following:

- Enter the prostate specific antigen (PSA) level ,
- Choose the date for the form,
- Choose the AEType,
- For each AEType, a list of adverse event (AE) will appear, the user will then select severity of each AE from the drop down list.

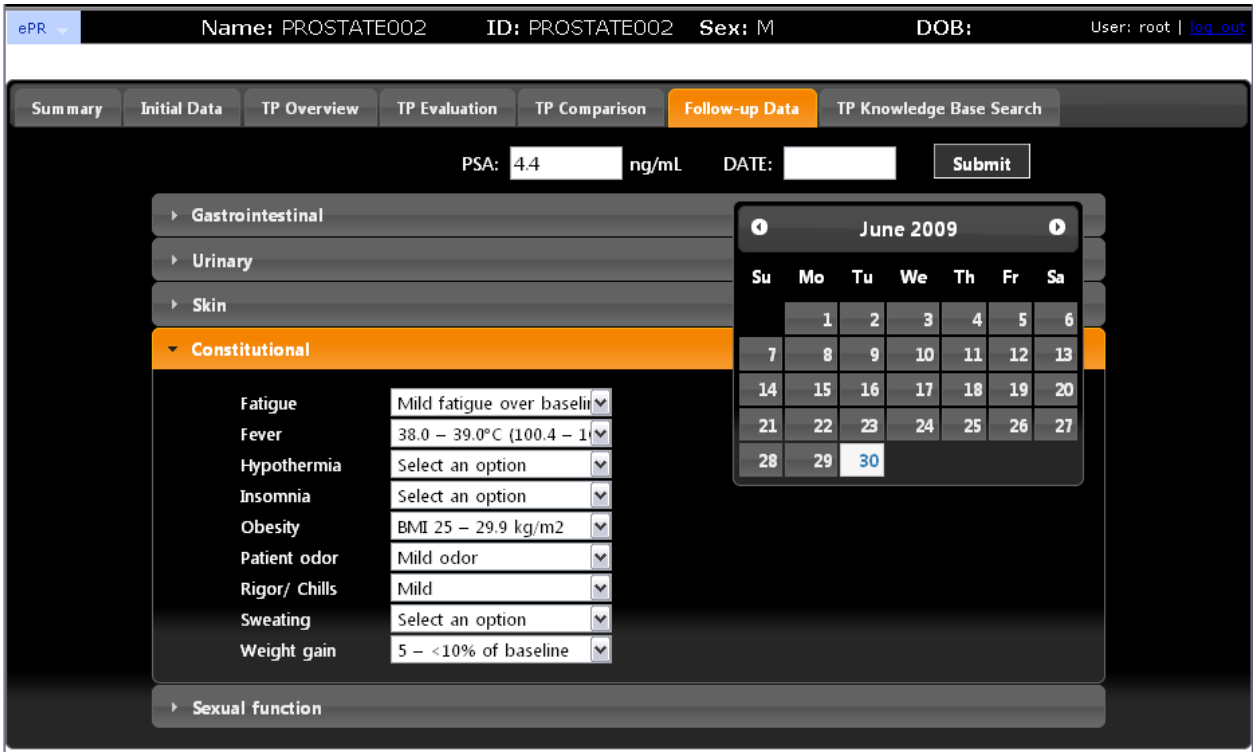

Figure 4. Digital form for user to determine radiation toxicity grade. On this figure, the Constitutional Criteria is currently opened, the left shows the list of AE in this criteria and the drop box list contained the severity of each AE. Using this form, the user can also select the data for the form and enter prostate specific antigen level.

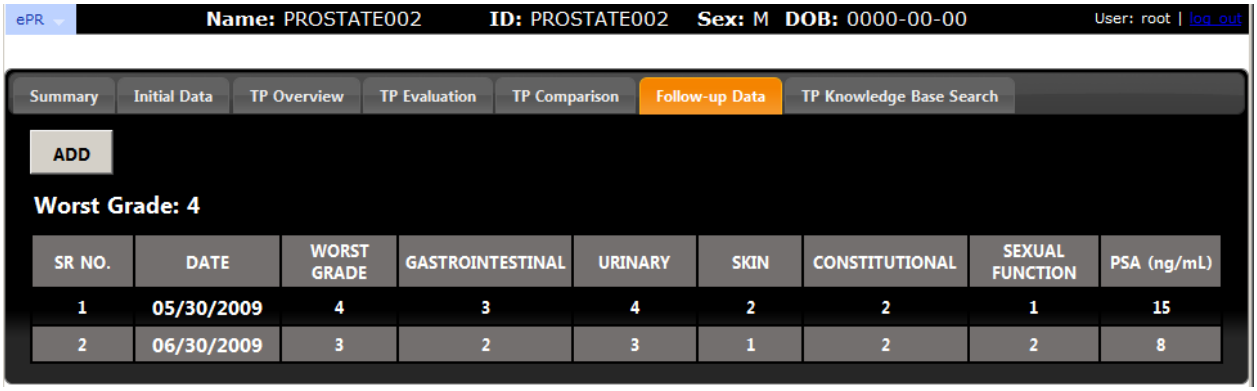

SR NO.	DATE	WORST GRADE	GASTROINTESTINAL	URINARY	SKIN	CONSTITUTIONAL	SEXUAL FUNCTION	PSA (ng/mL)
1	05/30/2009	4	3	4	2	2	1	15
2	06/30/2009	3	2	3	1	2	2	8

Figure 5. The summary page includes outcome data from different dates with determined radiation toxicity grade.

After the user submits the form, the RTT automatically determines the radiation toxicity grade for each AEType and determine to worst grade for that patient's outcome. This calculation is based on ctcaemap stored the CTCAE v.3 guideline. After the calculations are completed, an outcome data summary page is generated, as shown in Figure 5. The summary page shows all the forms with different dates have been filled for that current patient.

The RTT also provides user a GUI to query existing patient data stored in ePR to give insight for treatment of the new patient. Assuming there is a new case prostate cancer patient who will be treated with hypofractionation protocols and receives 60 Gy in total we can perform the following search: Find all patients with toxicity grade greater than 3 that have received 60Gy total dose, as shown in Figure 6. The query gives a list of patients who has toxicity grade 3 and had

received total dose of 60 Gy. At that moment, user will use the ITPN to review the plan and make adjustment to new patient treatment plan to possible improve outcome of new patient or ensure the new patient get the same minimize radiation toxicity grade.

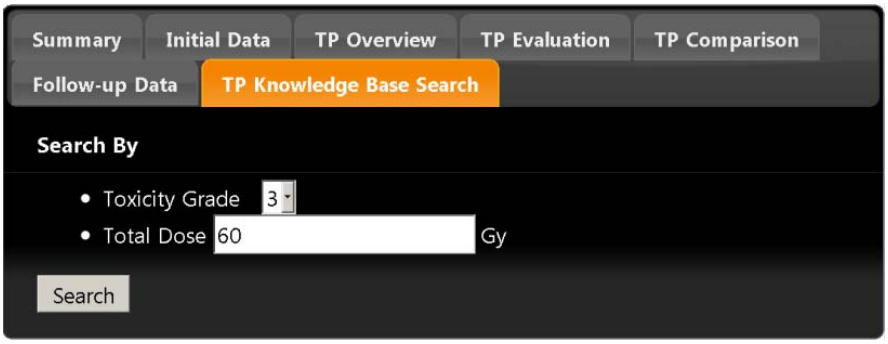

Figure 6. Query GUI illustrates data mining query for patient with toxicity grade greater than 3 and received 60Gy total dose.

5. CONCLUSIONS

The proton therapy ePR with images and clinical data has been developed and currently deployed at LLUMC for initial ePR system evaluation. The INTP and RTT are two decision support tools has been developed and tested within the ePR system. The successful implementation of these tools will facilitate the proton workflow for both treatment planning and outcome analysis. The centralized ePR system not only provides methods for physician and physicist to review and evaluate treatment plans but also decision support tools for researcher to access images, treatment plans and outcome data more efficient and improve the acceptance process of new treatment protocol.

REFERENCES

[1] Slater, J.D., Schulte, Reinhard W., "Proton-Beam vs Intensity-Modulated Radiation Therapy: Too Soon for a Randomized Trial." Oncology 22(7), (2008).

[2] Le, A., Documet, J., Sullivan A., and Liu, B., "A prototype of image-guided outcome analysis for prostate proton therapy patients based on DICOM-RT ePR," Proc. SPIE 7264, 72640L (2009), DOI:10.1117/12.813909

[3] Liu, B.J., et al., "Image-assisted knowledge discovery and decision support in radiation therapy planning." Computerized Medical Imaging and Graphics, 31(4-5), 311-321 (2007).

[4] Le, A., Liu B., "A Proton Therapy Electronic Patient Record Based On DICOM-RT And DICOM-RT-Ion For Archiving, Distributing And Visualizing Treatment Plans And Outcome Data". Presented at the 51st ASTRO Annual Meeting November 1-5, 2009, West McCormick Place, Chicago (2009).

[5] "National Cancer Institute. Cancer Therapy Evaluation Program: Protocol Development." 2009 [cited 2010 Janurary 31]; Available from: http://ctep.cancer.gov/protocolDevelopment/electronic_applications/ctc.htm.

Performance evaluation for volumetric segmentation of multiple sclerosis lesions using MATLAB and computing engine in the graphical processing unit (GPU)

Anh H. Le*, Young W. Park, Kevin Ma, Colin Jacobs, Brent J. Liu
Image Processing and Informatics Laboratory, 2250 Alcazar Street, Los Angeles, CA, USA 90033;
Depts. of Radiology and Biomedical Engineering, University of Southern California, Los Angeles, CA, USA 90033

ABSTRACT

Multiple Sclerosis (MS) is a progressive neurological disease affecting myelin pathways in the brain. Multiple lesions in the white matter can cause paralysis and severe motor disabilities of the affected patient. To solve the issue of inconsistency and user-dependency in manual lesion measurement of MRI, we have proposed a 3-D automated lesion quantification algorithm to enable objective and efficient lesion volume tracking. The computer-aided detection (CAD) of MS, written in MATLAB, utilizes K-Nearest Neighbors (KNN) method to compute the probability of lesions on a per-voxel basis. Despite the highly optimized algorithm of imaging processing that is used in CAD development, MS CAD integration and evaluation in clinical workflow is technically challenging due to the requirement of high computation rates and memory bandwidth in the recursive nature of the algorithm. In this paper, we present the development and evaluation of using a computing engine in the graphical processing unit (GPU) with MATLAB for segmentation of MS lesions. The paper investigates the utilization of a high-end GPU for parallel computing of KNN in the MATLAB environment to improve algorithm performance. The integration is accomplished using NVIDIA's CUDA developmental toolkit for MATLAB. The results of this study will validate the practicality and effectiveness of the prototype MS CAD in a clinical setting. The GPU method may allow MS CAD to rapidly integrate in an electronic patient record or any disease-centric health care system.
Keywords: Multiple Sclerosis, GPU, Matlab, CAD

1. INTRODUCTION

1.1 Multiple sclerosis and multiple sclerosis computer-aided diagnosis

Multiple Sclerosis (MS) is a progressive neurological disease affecting myelin pathways in the brain. According to the National Multiple Sclerosis Society, USA, this disease affects approximately 2,500,000 people worldwide between age of 17 and 65 years old. The affected patients usually have multiple lesions in the while matter which can cause paralysis and severe motor disabilities. The symptoms include changes in sensation, visual problems, muscle weakness and depression. The exact cause of MS currently remains unknown [1].

At present, MRI T1 and FLAIR pulse sequence are used for radiological diagnosis. In these images, MS appears as multiple white lesions in the white matter of the brain. MRI can also be used to follow-up and monitor progress of the disease and the effectiveness of the drug therapy treatment. Since MRI provides excellent delineation of MS, it is fairly easy for radiologist to make a diagnosis. However, due to large number of multiple lesions in the MRI 3-D volume set of the brain, it is tedious and time consuming to identify the 3-D aspect of each lesion and quantify the number and size of these lesions. Furthermore, the quantitative reproducibility is not consistent due to human-observance variability [2]. Therefore, augmenting computer aided detection (CAD) with imaging informatics methods, a 3-D CAD MS package would facilitate the physician's timely diagnosis, improve accuracy, and assess quantitatively the progress of drug therapy treatment. Despite the highly optimized algorithm of imaging processing that is used in CAD development, MS CAD integration and evaluation in clinical workflow is technically challenging due to the requirement of high computation rates and memory bandwidth.

*anhhle@usc.edu; phone 1 323 442-2936; fax 1 323 442-2575; ipilab.org

1.2 Graphical Processing Unit

A Graphical Processing Units (GPU) is a specialized processor attached to a graphics card dedicated to performing graphics rendering from the microprocessor. A GPU implements a number of graphics primitive operations; therefore, makes the graphics drawing directly to the screen much faster than using the host computer processing unit (CPU) [3].

Figure 1. The diffecence in CPU and GPU architecture (ALU: Athrimetic Logic Unit)

Figure 1 shows the architecture different of CPU and GPU. A CPU is expected to process a task as fast as possible whereas a GPU must be capable of processing a maximum of tasks on a large scale of data. The priority for the two is not the same, their respective architectures show that point. GPU increase the number of processing units and the CPU develop control and expend its cache.

Currently, a GPU contained a much higher number of microprocessors than on a CPU, allowing a higher number of computational processes to be performed in the same amount of time. Utilizing this characteristic, one could develop a CAD specifically used the computational power of GPU.

In this paper, we investigate challenges of using a computing engine in the graphical processing unit with MATLAB for parallel computing in MS CAD

2. METHODS AND MATERIALS

We have developed a CAD system that automatically quantifies MS lesions, displays 3-D lesion map to original images according to current DICOM standard. The CAD is currently developed under MATLAB environment and MATLAB imaging processing toolbox. A second version of MS CAD is also developed using computation engine within the NDIVIA graphic card with the CUDA toolkit. The algorithm of MS CAD developed is discussed in more detail in SPIE 2010 project titled “An automatic quantification system for MS lesions with integrated DICOM structured reporting (DICOM-SR) for implementation within a clinical environment.”

2.1 Hardware

The performance evaluation MS CAD utilized the GPU power is performed on a dedicated Lenovo workstation with NVIDA card installed. The specification of this workstation include two Intel® Xeon X5560 CPU at 2.8 GHz , 16.0 GB installed memory, Windows 7 64-bit operating system, and a NVIDIA Tesla C1060, a dedicated GPU computational card. The Lenovo workstation and NVIDIA Tesla card were donated to Image Processing and Informatics Laboratory, University of Southern California by Lenovo, USA [4] and NVIDIA Professor Partnership Program [5], respectively.

Another regular workstation is used to run the CAD for performance comparison. The specification of this workstation is as follows: Intel® Core2 6420 at 2.13 GHz, 3GB installed memory, Windows Vista 32-bit operating system, and a NVIDIA GeForce 8600 GT graphics card.

2.2 NVIDIA CUDA Architecture

CUDA (Compute Unified Device Architecture) is a parallel computing architect developed by NVIDIA. NVIDIA provide a fully SDK (Software Development Kit) for a high layer programming. The NVIDA CUDA Architecture, as shown in Figure 2, shows both a low level API (Application Programming Interface) and a high level API support from CUDA SDK. They provide libraries, comparator and specific driver to take care of all the communication between applications with the graphics card.

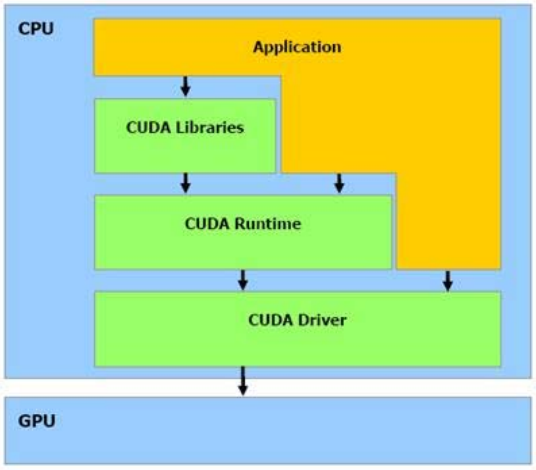

Figure 2. NVIDIA CUDA Architecture

2.3 GPU Implementation using Jacket

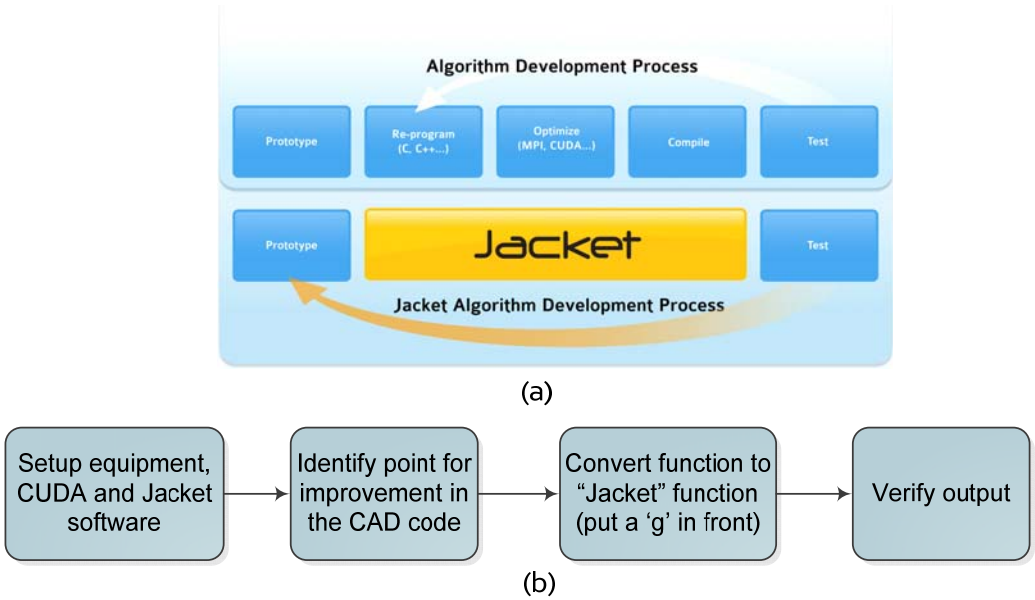

Figure 3. GPU Implementation using Jacket; (a) Jacket algorithm development process; (b) Jacket implementation steps

Using Accelereye software's Jacket plugin [6], implementation of CUDA was done in relatively easy processes. Figure 3a shows the algorithm development process of an application using Jacket; developer can bypass the steps of compiling, functions optimization and re-programming. Using Jacket's built in functions, variables could be declared on GPU's onboard and executed using GPU core. For example, while the function "ones()" declares a double array in system's memory, function "gones()" declares an array of doubles in GPU space. Jacket can also perform distributed

parallel processing using functions such as “gfor()” for performing loops function. The steps of using Jacket developing Matlab application are shown in Figure 3b.

2.4 GPU Implementation using Matlab-MEX

Implementation of CUDA within Matlab could also be done using Matlab’s MEX tool, which allows Matlab to access functions written using c/c++ - based languages. Utilization of CUDA through MEX were made possible by using CUDA’s C/C++ libraries and CUDA-MEX compiler executable called “NVMEX”, which are available in nVidia’s website. CUDA incorporated C/C++ codes were compiled using NVMEX and made system calls to the Matlab environment for execution [7].

As shown in Figure 4, after the initial equipment setup and software installation, the implementation of CUDA-MEX was done in two steps. First, conversion of existing Matlab based k-nearest neighbor function was converted in C++ code to run under regular MEX environment without GPU. Once conversion to C-based code is completed, incorporation into CUDA using CUDA libraries was performed to implement CUDA-MEX.

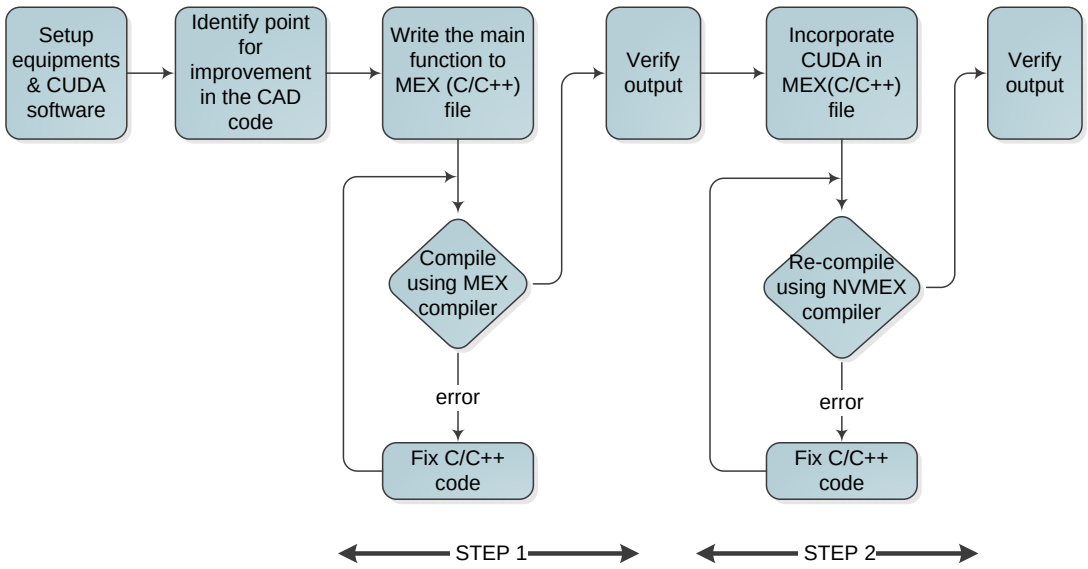

Figure 4. GPU implementation steps using Matlab-MEX

2.5 Performance Evaluation

The performance experiments were to evaluate the CAD performance between a high power workstation (Lenovo brand workstation with Intel® X5560 CPU) and a regular workstation (with Intel® 6420 CPU) using non-GPU implementation, and between non-GPU and GPU implementation on a high power workstation. In the first evaluation, total four MS cases were used to run the MS CAD on two workstations. A total time variable is implemented in the CAD source code to output the time from beginning to the end of running each MS case into a file. The second evaluation is performed in a similar fashion, except two application packages, a non-GPU version and a GPU version, were used to run four cases on the same high-power workstation. The conclusions would be drawn from the average elapsed time in seconds of four cases.

The MS cases used in these evaluations were collected from the USC Health Consultation Center in Los Angeles, CA.

3. RESULTS AND DISCUSSION

3.1 Preliminary Results

For the first evaluation, figure 5 shows the time performance of running MS CAD with non-GPU implementation on a normal desktop computer and dedicated Lenovo WS, mentioned in Section 2.1. The total execution time of the MS CAD was cut by one-third on a Lenovo Workstation. According to PassMark Computer BenchMark, a computer benchmarking tool, the CPU scores of the Intel Xeon X5560 is over 9 times faster than the Intel Core2 6420 [8]. This finding suggested that an increase in CPU power is not proportional to the CAD running time. In fact, this time improvement does not justify the cost and the power of the high end CPU workstation. Furthermore, the 5.5 hour average running time of MS CAD on a high end workstation with non-GPU implementation are not yet feasible to integrate the MS CAD in clinical environment.

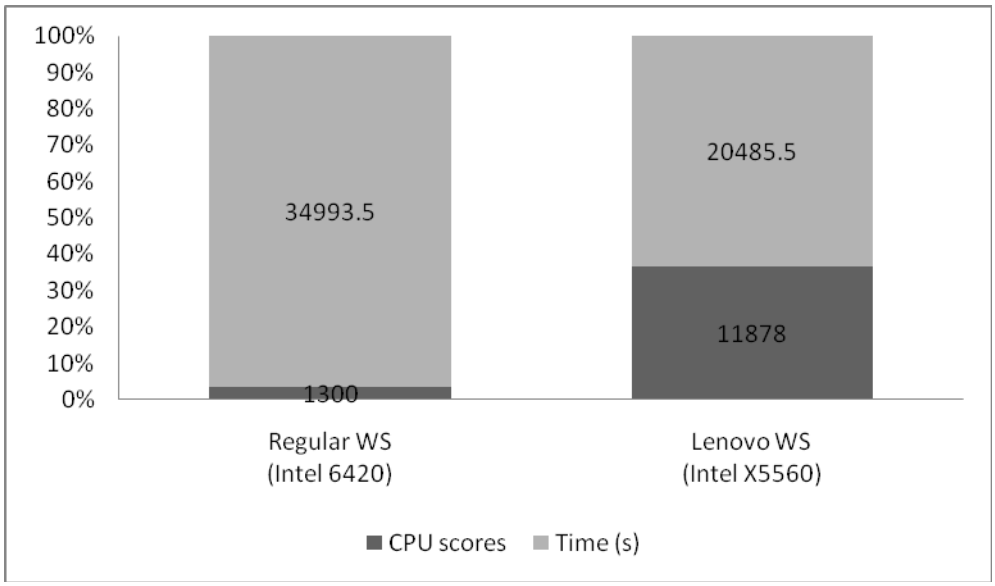

Figure 5. Computer benchmark in relation to CAD time performance in two workstation (WS)

For the second evaluation, the MS CAD was divided into five different tasks for time measurement. Table shows status and time duration of each task for only one MS case. The results show that the GPU implementation was slightly better in the brain segmentation task but failed in performing KNN classification to find MS lesions.

Table 1. Time measurement of each CAD tasks in GPU implementation vs. non-GPU implementation

Tasks	GPU Time (s)	non-GPU Time (s)
File Import	14.2	14.4
Image Alignment	89	88
Brain Segmentation	9	29
Probabilistic segmentation of MS lesions (using kd-trees and KNN classification)	(failed to run)	36443
Total Time	n/a	36620

3.2 GPU implementation challenges

The segmentation of MS lesion is mainly based on classification of features space using K nearest neighbors (KNN) method. Each voxel in the 3-D volume set needs to be compared to the features space to determine whether it belongs to

an MS lesion. In order to accomplish this, the conventional non-GPU implementation uses the recursive call for each voxel. However, the CUDA does not allow for recursion due to the nature of GPU architecture with limited stack size and memory preserved for each calculation. Recursion is unattractive in a massively parallel kernel because providing stack space for the tens of thousands of threads that may be active would require substantial amounts of memory. Serial algorithms that are normally expressed using recursion, such as quicksort, are typically best implemented using nested data parallelism rather than explicit recursion [9-10].

This is a significant challenge because current KNN search implementation in current MS CAD heavily relies on recursive calling. Even though two methods have been tested, one using commercial Matlab plug-in and one using NVMEX calling directly in Matlab environment, both methods could not successfully run without crashing the CAD application.

4. SUMMARY

We have investigated two methods of GPU implementation using CUDA library indirectly through a commercial Matlab plugin and directly though MEX functionality and C/C++ code. The time evaluation of MS CAD on two different systems suggested that the CAD development would not be efficient using just CPU power of high end workstation. However, the evaluation experiment of using GPU for KNN lesion classification was not successful due to using recursive calls. It is important to notice that the GPU is a highly parallel architecture designed with more processing units than allocated memory in cache and smaller size control units for computation than a CPU.

It has been well established that the GPU technology is beneficial for 3D display and parallel computations. However, for some image processing algorithm, i.e. recursion, utilizing lots of memory and requiring more processing control, the results of this study show that the GPU does not perform significantly better as compared to conventional CPU systems and even fail to perform the calculation due to memory overloading. Even though recursion methods are attractive towards reducing CPU running time, these methods require the system to provide cache for thousands of threads running in multiple microprocessors of a GPU which ultimately negates its computation power capabilities. Serial and parallel computation should also be addressed carefully in implementing an algorithm for CAD using GPU technology, lots of processing units, smaller size cache and limited size control units.

REFERENCES

[1] Alonso A. and Hernn. M.A. “Temporal trends in the incidence of multiple sclerosis: a systematic review.” Neurology, 71(2), 129-135 (2008).

[2] Moin, P., Ma, K., Amezcua, L., Gertych, A., and Liu, B., “The development of an MRI lesion quantifying system for multiple sclerosis patients undergoing treatment” Proc. SPIE 7264, 72640J (2009)

[3] http://www.pcmag.com/encyclopedia_term/0,2542,t=GPU&i=43886,00.asp

[4] ThinkStation Workstation. http://www.lenovo.com (2010)

[5] NVIDIA Professor Partnership Program. http://www.nvidia.com/page/professor_partnership.html (2010)

[6] AccelerEyes - MATLAB GPU Computing. http://www.accelereyes.com/ (2010)

[7] MATLAB plug-in for CUDA. http://developer.nvidia.com/object/matlab_cuda.html (2010)

[8] http://www.cpubenchmark.net/

[9] http://queue.acm.org/detail.cfm?id=1365500

[10] Garcia, V., and Nielsen, F., [Computer Vision/Computer Graphics CollaborationTechniques] “Searching High-Dimensional Neighbours: CPU-Based Tailored Data-Structures Versus GPU-Based Brute-Force Method.”, Springer, Berlin, , 425-436 (2009).

Data Migration and Persistence Management in a Medical Imaging Informatics Data Grid

Jasper Lee*[a], Jorge Documet [a], Brent Liu [a]
[a] Image Processing & Informatics Laboratory, USC 90033, CA

ABSTRACT

The Medical Imaging Informatics Data Grid project is an enterprise infrastructure solution developed at the University of Southern California for archiving digital medical images and structured reports. Migration methodology and policies are needed to maintain continuous data availability as data volumes are being copied and/or moved within a data grid's multi-site storage devices. In the event a storage device is unavailable, a copy of its contents should be available at a live secondary storage device within the data grid to provide continuous data availability. In the event a storage device within the data grid is running out of space, select data volumes should be moved seamlessly to a tier-2 storage device for long-term storage, without interruption to front-end users. Thus the database and file migration processes involved must not disrupt the existing workflows in the data grid model. This paper discusses the challenges, policies, and protocols required to provide data persistence through data migration in the Medical Imaging Informatics Data Grid.

Keyword: Data Grid, PACS, Data Migration, Data Persistence, Continuous Availability

1. INTRODUCTION

1.1 Data Grid in the Clinical PACS Environment

The clinical application of data grid technology in the medical imaging informatics field, specifically in radiology, is gradually becoming more usable and robust over the past few years. Its progress has been encouraged by the increased utility of the Internet in medicine, and the push for digitized and sharable medical health records. Since 2005 at the University of Southern California, the Image Processing and Informatics Laboratory has developed a Medical Imaging Informatics Data Grid for radiology by building DICOM compliant software packages upon an open-source grid backbone called the Globus Toolkit (GTK). The Data Grid can connect radiology imaging studies securely and seamlessly between multiple Picture Archiving and Communication Systems (PACS) in an enterprise radiology environment. The results have been off-site back-up of sensitive patient imaging studies that is cost-effective for clinical radiology institutions by utilizing existing SAN infrastructure, and an enterprise DICOM image sharing solution for multi-site PACS consortiums.

Major components in the first version of the Medical Imaging Informatics Data Grid system were designed to achieve preliminary tasks to meet DICOM compliance, create a metadata database modeled for real-world DICOM objects, and secure DICOM file delivery across the wide-area-network (WAN) using GTK packages. Functionality at the user-level, including DICOM C-Store, C-Find, and C-Move, were implemented using DCM4CHE tools[1]. Figure 1 below diagrams this system architecture with its components and services categorized into 5 design layers – application, collective, connectivity, resource, and fabric.

*jasperle@usc.edu; phone 1 323 442-2928; fax 1 323 442-2575; www.ipilab.org

1.2 Data Migration and Persistence Management

The Data Grid design now includes data file management features such as long-term data migration and data persistence management of imaging studies archived within the Data Grid. In a data grid system, data persistence is achieved through redundancy of all data content stored at two or more distinct storage locations in order to provide higher data availability in the event of primary hardware or network failure at a participating grid site. This paper discusses the new components, highlighted in Figure 1 in boxes, and data management features that have been added to the Medical Imaging Informatics Data Grid. The ability to monitor, handle, and maintain continuous availability of data amongst the multiple storage devices are important in a Data Grid for implementation in the clinical environment. This new system infrastructure with data management services has added dynamics, policies and dataflow, and will be presented in the following methodology section.

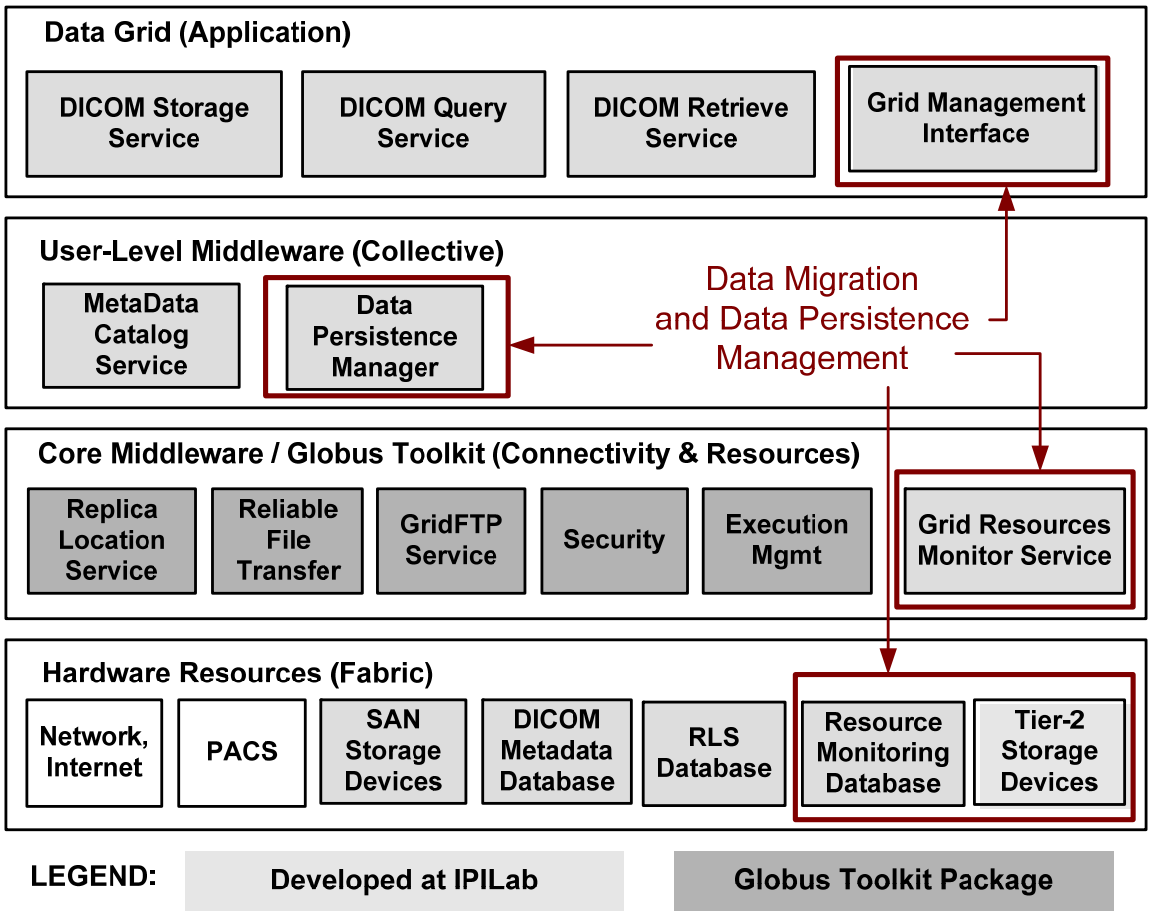

Figure 1 IPILab Data Grid 5-Layered Infrastructure Integrating Globus Toolkit and DICOM.

2. METHODOLOGY

Native data management in medical imaging informatics systems requires integration with clinical workflows such that internal movement of data does not negatively impact data availability and performance of essential user functionality. The objective of the Medical Imaging Informatics Data Grid system in radiology is to provide an enterprise solution that enables multiple PACS at geographically distributed healthcare provider sites to share and retrieve patient DICOM images for authorized radiologists, clinicians and referring physicians. Local PACS systems at each site remain the primary image archive and provider for all local patient imaging requests, while the Medical Imaging Informatics Data Grid is accessed to retrieve or recovery patient imaging studies archived in its internally distributed storage devices. Thus, data management features for the Medical Imaging Informatics Data Grid should optimize data and storage resource availability within the Medical Imaging Informatics Data Grid without compromising performance and data

security in storage and retrieval of DICOM studies. Figure 2 below is a general use-case overview to demonstrate utilization of the Medical Imaging Informatics Data Grid in an enterprise healthcare provider environment.

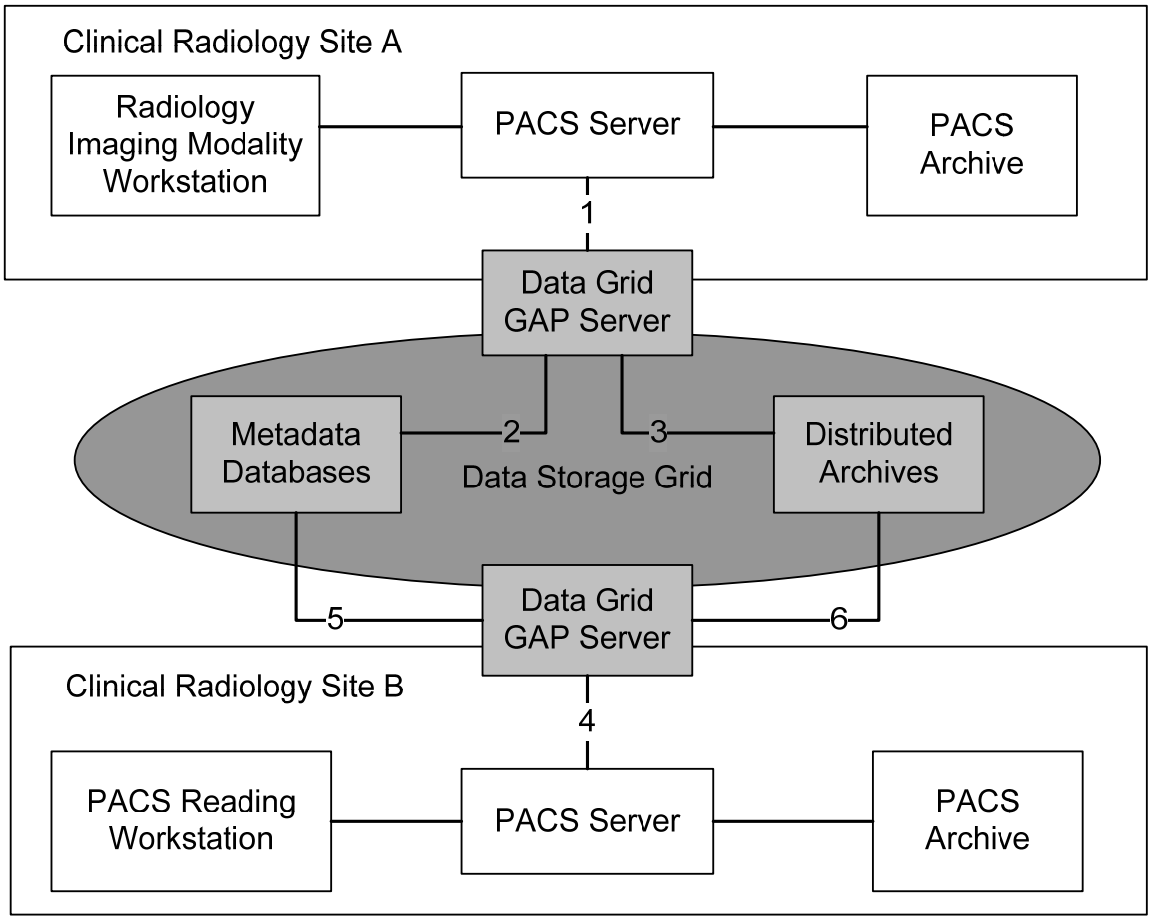

Figure 2 Components, connectivity, and general dataflow with two clinical radiology sites sharing a Medical Imaging Informatics Data Grid implementation. Step 1) New imaging studies in the local PACS server at site 'A' are replicated to the local GAP server. Step 2) Services in the GAP server update the Data Grid databases with DICOM and file metadata. Step 3) DICOM images are securely and efficiently sent to one or more storage repositories in the grid. Steps 4,5,6) PACS administrators at site 'B' query and retrieve imaging studies to be downloaded over DICOM to their local PACS server for radiologist, clinicians, and referring physicians to access.

2.1 System Architecture

The system architecture shown in Figure 1 has 5 data management components that have been added to the Medical Imaging Informatics Data Grid design. These components are a web-based user interface at the application layer, a Data Persistence Manager at the collective layer, Grid Resources Monitoring service at the core middleware layer, and Resource Monitor database and tier-2 storage devices at the fabric layer.

The web-based user interface is used by PACS administrators to query and select archived imaging studies to be retrieved into their local PACS servers. The user interface is run in a web-server on the local GAP server and requires users to log-in, creating an audit trail of all user activity. Another purpose of the web-based user interface is for authorized Medical Imaging Informatics Data Grid administrators to selectively migrate antiquated imaging studies to dedicated long-term storage devices, also belonging to the Medical Imaging Informatics Data Grid, so as to free up storage space on a primary storage device.

The Data Persistence Manager in the collective layer is a group of services installed on primary data grid storage devices to conduct two data management services - data migration for long-term data archival and data persistence for

guaranteeing data redundancy within the Medical Imaging Informatics Data Grid. The details and dataflow for these two services are presented in the following sections.

At the connectivity and resources layer, grid resource monitoring services are automated to periodically ping the DICOM metadata database, Replica Location Service database, and multiple storage devices to monitor uptime and real-time storage capacities. The findings are written to a centralized and redundant database, and thereby enabling the Data Persistence Manager at the collective layer to intelligently copy or move DICOM imaging studies from one remote storage device to another.

In the event of component or network failures, achieving data persistence and long-term storage guarantees a secondary physical storage location of all files which can be queried to retrieve a DICOM study to a remote site. Support for tier-2 storage devices in the fabric layer means antiquated imaging studies can be migrated from local primary storage devices to off-site long-term storage solutions that are more cost-effective than purchasing additional primary disk infrastructure.

2.2 Data Persistence

In order to maximize hardware utilization, the Data Persistence Manager is installed on every primary storage server and designated for managing only data content residing within its local storage device. The process of maintaining two or more copies of all DICOM imaging studies archived in the Medical Imaging Informatics Data Grid requires the Data Persistence Manager to have access to shared metadata databases, Globus file transfer services, and all storage device repositories. Each Data Persistence Manager instance periodically scans the Medical Imaging Informatics Data Grid's Replica Location Service (RLS) databases for the existence of a second copy of files already residing on its local storage device. If a second remote copy of an imaging study is missing, the Data Persistence Manager will schedule and initiate replication of that local file automatically to a second primary storage device within the Medical Imaging Informatics Data Grid. The selection of that second copy's destination device is drawn from the Grid Resources Monitoring database and is based on the storage device with highest storage capacity percentage remaining. Upon successful replication of its files to the second location, the initiating Data Persistence Manager will update the RLS databases of the new file instance.

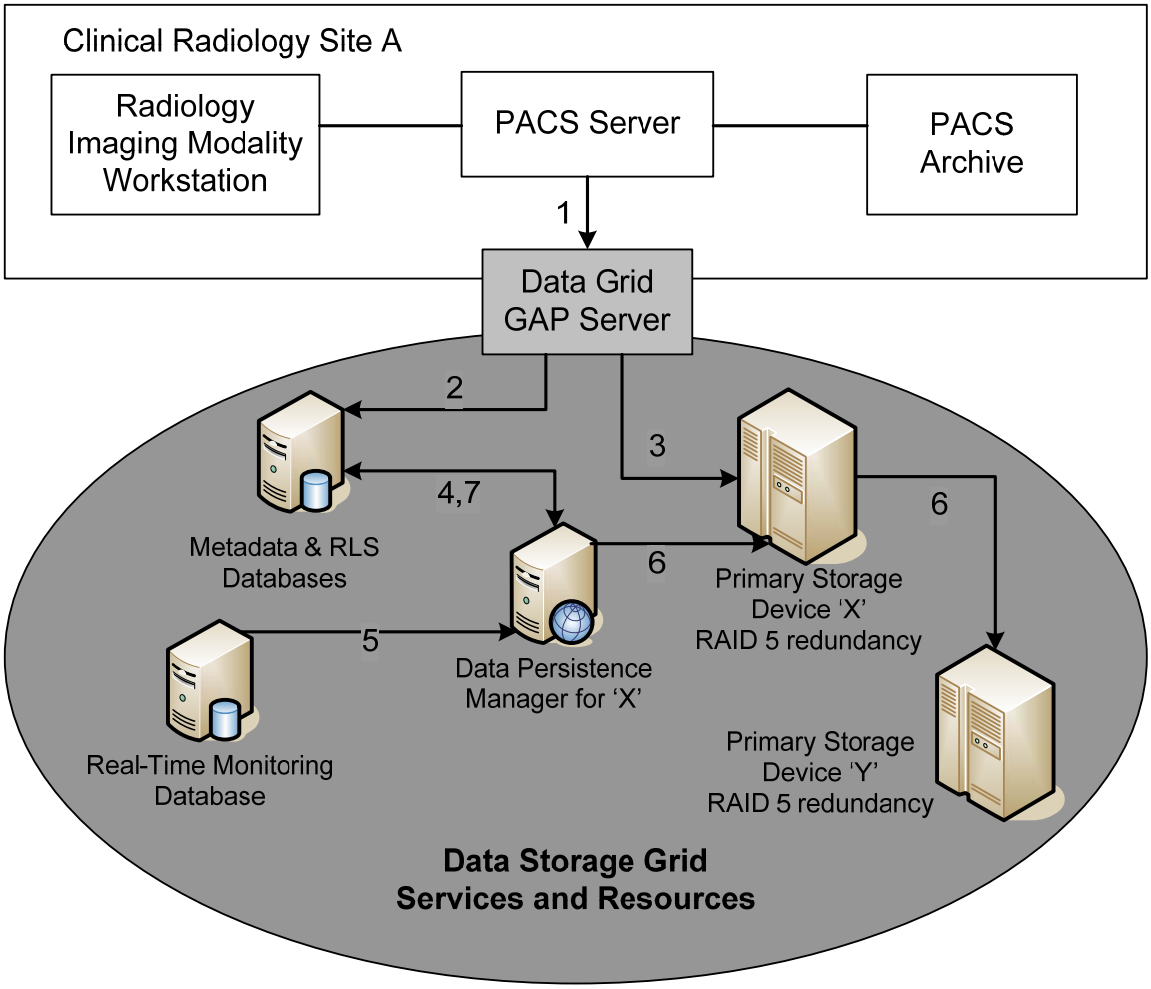

Figure 3 Data Persistence Manager Dataflow

Steps:

1. DICOM imaging studies are sent into the GAP server from the PACS server at site 'A'
2. Metadata and Globus Replica Location Service (RLS) databases are updated for the new imaging studies
3. Imaging study files are archived to a primary storage device with RAID 5 redundancy
4. Data Persistence Manager for storage device 'X' periodically queries the RLS database for files archived on 'X', looking for files without a second copy
5. Data Persistence Manager queries the real-time grid monitoring database to find another primary storage device 'Y' with highest storage capacity percentage remaining
6. Data Persistence Manager performs GridFTP file transfer from 'X' to 'Y'
7. New second copy of imaging study files are written into RLS databases

2.3 Data Migration

In order to give grid administrators the option of allocating long-term storage to a remote and dedicated long-term storage device within the Medical Imaging Informatics Data Grid, as opposed to adding disks to an existing site's SAN infrastructure, a data migration service is needed for the Medical Imaging Informatics Data Grid. When a storage capacity threshold is exceeded in a primary storage device, the Data Persistence Manager's data migration service on that server will query the shared metadata database and select imaging studies that have not been accessed for more than a given period of time, such as two years. Thereafter, a grid administrator can log into the Data Persistence Manager's web-based user interface and authorize, or deny, the migration of these selected studies to a designated tier-2 storage device within the Medical Imaging Informatics Data Grid.

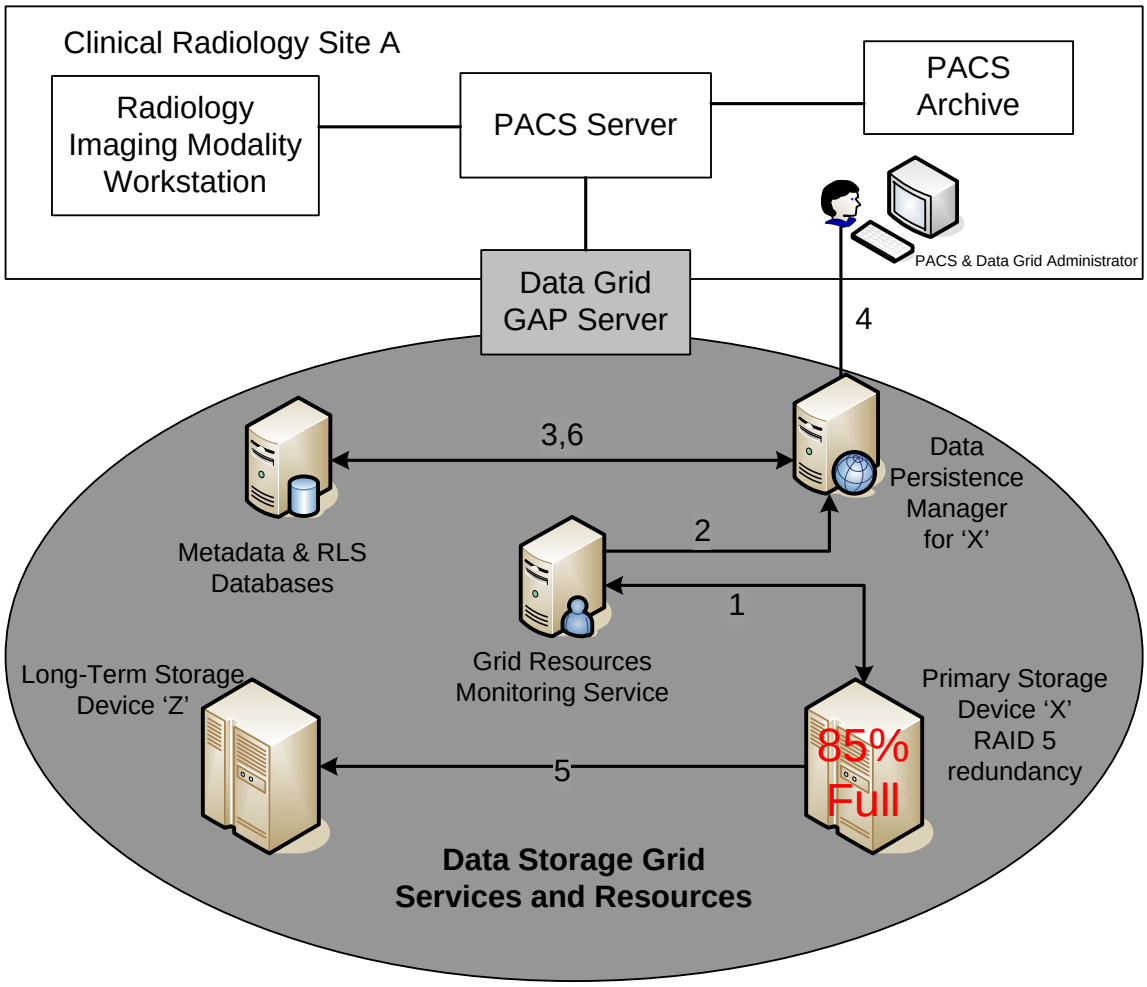

Figure 4 Long-Term Data Migration Dataflow

Steps:

1. Grid Resources Monitoring Service identifies primary storage device 'X' as running out of storage space
2. Data Persistence Manager is notified of the lack of remaining storage capacity
3. Data Persistence Manager searches the Metadata database for imaging studies residing on 'X' with a last-accessed date older than a given duration (ex. 2 years)
4. PACS & Data Grid administrator logs into the web-based interface of the Data Persistence Manager for 'X' to authorize or deny the migration of antiquated imaging studies to long-term storage device 'Z'
5. Authorized imaging studies for migration are moved from 'X' to 'Z', and the source copy is deleted upon completion of the file migration
6. Changes in file location due to the migration are reflected in the RLS databases

3. RESULTS and DISCUSSION

A method to manage a growing data volume set within a multi-node Medical Imaging Informatics Data Grid is being evaluated in the laboratory environment at the University of Southern California's IPILab. The data sample includes DICOM imaging studies from clinical imaging modalities and post-processing applications. The test environment is made up of three PACS simulators and a single Medical Imaging Informatics Data Grid implementation connecting them. Within the data grid are three Grid-Access-Point servers, for communicating with each simulated PACS site, a database server, a Globus services server, and three digital storage devices. Two of the storage devices act as primary archives with RAID 5 data redundancy, and the third storage device acts as the secondary and long-term archive without

any internal data redundancy. A Data Persistence Manager is initiated at both of the two primary storage devices. Using testing scenarios described below, evaluation of the Data Persistence Manager is currently ongoing. Networking and hardware limitations must be factored into both evaluations.

3.1 Evaluating Data Persistence

Data persistence is being evaluated for the length of time a study is archived in the data grid, but not replicated at two distinct storage devices. There are two possible scenarios for evaluation. When a DICOM imaging study is sent into the Medical Imaging Informatics Data Grid for the first time, and when a copy of a study is deleted due to simulated network or storage device failure. It takes the Data Persistence Manager at least one scan cycle before file replication is initiated from one storage device to the second. Thus, measured length of time is taken from initial completion of archival, or deletion of an existing copy, until the completion of full redundancy.

3.2 Evaluating Data Migration

Data migration is being evaluated for the length of a physical copy of a DICOM study is unavailable due to the data migration processes. For simulation purposes, archived studies that have been kept at a primary storage location for longer than one week is marked as antiquated by the Data Persistence Manager. The antiquated study is then migrated to the designated long-term storage device, and consequently removed from the primary storage's physical disk upon completion. The length of time measured is the time of initialization to completion of data migration, during which the physical dataset is unavailable to Grid-Access-Point servers for retrieval.

4. CONCLUSION

A data migration policy and protocol is designed and presented for handling data persistence of DICOM imaging studies within the Medical Imaging Informatics Data Grid infrastructure. The data management techniques will ensure continuous availability of storage space and optimizing the persistence of data stored on data grid storage nodes by maintaining at least two copies of all imaging studies archived within the Medical Imaging Informatics Data Grid. Due to the extensible number of storage devices and varying storage capacities within the Medical Imaging Informatics Data Grid, an automated data management tool is essential to the maintenance and robustness of the Medical Imaging Informatics Data Grid system in the clinical environment.

5. REFERENCES

[1] Huang, H.K., "Utilization of Medical Imaging Informatics and Biometrics Technologies in Healthcare Delivery," Int J CARS. 3:27-39 (2008).

[2] Huang HK, Zhang A, Liu BJ, et al., "Data Grid for Large-Scale Medical Image Archive and Analysis," Proceedings of the 13th ACM International Conference on Multimedia. pp 1005-1013 (2005).

[3] Zhou, Z., Lee, J., Huang, H.K., et al., "A Data Grid for Imaging-based Clinical Trials," Proc. SPIE 6516, (2007).

[4] Chervenak, A., Foster, I., Kesselman, C., et al., "The Data Grid: Towards an Architecture for the Distributed Management and Analysis of Large Scientific Datasets," Journal of Network and Computer Applications, 23:187-200 (2001).

[5] Zhou, Z., Documet, J., Chan, L., et al., "The Role of a Data Grid in Worldwide Imaging-Based Clinical Trials," USC UPU: Marina del Rey (2006).

[6] Liu, B., Zhou, Z., Documet, J., "Utilizing Data Grid Architecture for the Backup and Recovery of Clinical Image Data," Computerized Medical Imaging and Graphics 29, 95-102 (2005).

A Study-Centric Database Model for Organizing Multimodality Images and Metadata in Animal Imaging Research Facilities

Jasper Lee[*a], Alparslan Gurbuz[b], Brent Liu[a]
[a] Image Processing & Informatics Laboratory, USC 90033, CA
[b] Molecular Imaging Center, USC 90033, CA

ABSTRACT

Research images and findings reports generated during imaging-based small animal imaging experiments are typically kept by imaging facilities on workstations or by investigators on burned DVD's. There usually lacks structure and organization to these data content, and are limited to directory and file names to help users find their data files. A study-centric database design is a fundamental step towards imaging systems integration and also a research data grid infrastructure for multi-institution collaborations and translational research. This paper will present a novel relational database model to maintain experimental metadata for studies, raw imaging files, post-processed images, and quantitative findings, all generated during most imaging-based animal-model studies. The integration of experimental metadata into a single database can alleviate current investigative dependency on hand-written records for current and previous experimental data. Furthermore, imaging workstations and systems that are integrated with this database can be streamlined in their data workflow with automated query services. This novel database model is being implemented in a molecular imaging data grid for evaluation with animal-model imaging studies provided from the Molecular Imaging Center at USC.

Keywords: Animal-Model Imaging, Data Mining, Database Model

1. INTRODUCTION

1.1 Imaging-Based Animal-Model Research

Medical research today almost always involves a pre-clinical trials phase that precedes testing in humans, and quite often requires in vivo and in vitro imaging of animal models. This phase is a proof-of-concept step that must be carried out and validated before any pharmaceutical or therapeutic experimentation can be done on humans. Therefore the imaging facilities, often called molecular imaging centers, and resources that provide investigators with these services are many and specialized. Most medical research institutions operate an animal imaging facilities for its researchers to use. However, regardless of the experimental factors and objectives, animal-models are purchased, prepared, and scanned by scientific investigators in a generic scientific workflow at animal imaging facilities. The essence of this workflow is to capture images of a live animal's physiological and pathological activity and identify the biomarkers in the image that can be used for quantitative and/or qualitative conclusions. Figure 1 outlines this generic workflow that is followed in most animal-model experiments by investigators and in collaboration with staff at the small animal imaging facilities.

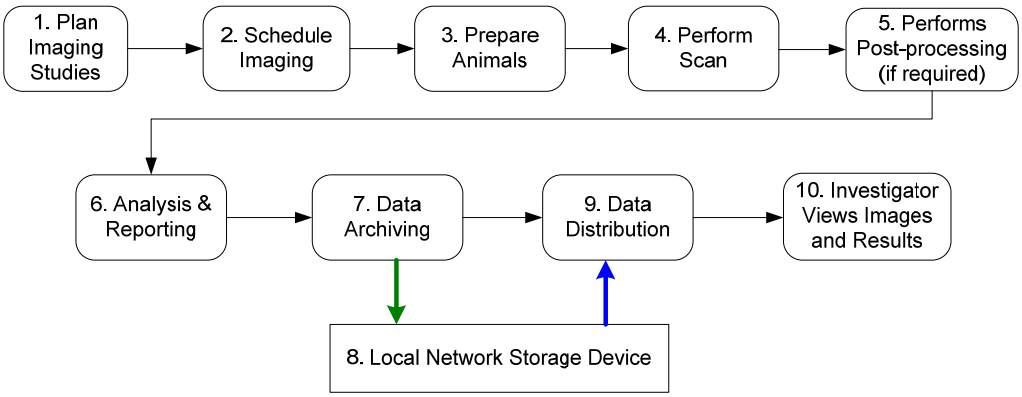

Figure 1. General workflow of imaging-based animal-model experiments

*jasperle@usc.edu; phone 1 323 442-2928; fax 1 323 442-2575; www.ipilab.org

With discoveries of new radiopharmaceutical labels and higher-resolution imaging modalities, the utility of animal-model imaging studies and the quantity of data being generated across research is expanding. Being able to archive these datasets and share them in a long-term archiving repository would be invaluable to new and established medical investigators. However, the current limitations in storage archive solutions hinder animal-model imaging datasets from being stored long-term and shared after publication.

1.2 Imaging Informatics in Animal Imaging Facilities

Most animal imaging facilities provide on-site imaging workstations for investigators to process, visualize, and analyze their images. Depending on the modality and type of image file format, such as 2-dimension optical images or 3-dimension microCT volume sets, investigators at the animal imaging facilities use different and often dedicated software to access these images. Consequently, the animal imaging workstations, software applications, and data files are not usually well integrated with one another and limit the organization and sharing capabilities of image datasets, even within a single animal imaging facility.

1.2.1 Imaging Modalities

Most of the imaging modalities in animal imaging facilities are similar to the modalities used in clinical radiology. For example, the microCT, microPET, micro-ultrasound, and microMR are fundamentally the same as the human-sized modalities, only with smaller bore diameters and higher resolutions. The autoradiography modality, shown in Figure 2.f, is essentially a digital x-ray machine with digitized film cartridges. Optical imaging, shown in Figure 2.e, is the main animal imaging modality that is not popularly used in clinical radiology due to its shallow-to-surface imaging capability.

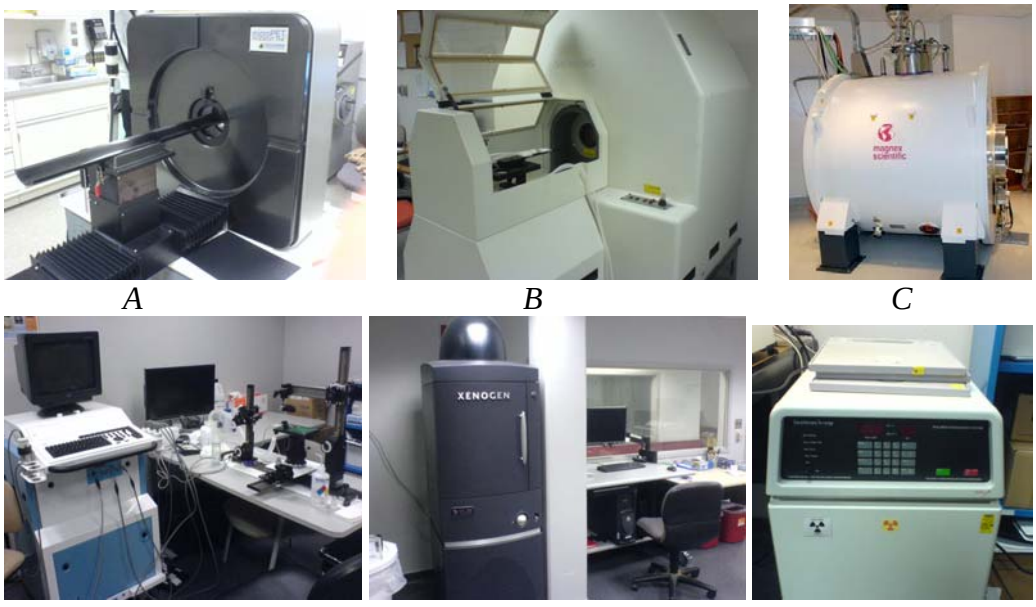

Figure 2. a) MicroPET b) MicroCT c) MicroMRI d) MicroUS e) Optical Imaging f) Autoradiography
Courtesy of Molecular Imaging Center, USC for Fig. 1 a,b,d,e,f, and
Molecular Imaging Program at Stanford, Stanford University for Fig.1c.

Despite these physical similarities in modality design, the workflow and software tools surrounding the animal imaging scanners are not as sophisticated and well integrated as in radiology. The lack of file format standards and the emphasis on keeping pre-processed raw datasets has translated into proprietary visualization methods and limited understanding of foreign data between users and software applications. With little accessibility and utility outside of an experiment's scope, these animal-model imaging data files are typically kept untouched at these animal imaging facilities or burned onto DVD's for investigators. The results are lost experimental datasets and redundant experimentation on animals.

1.2.2 Data Storage Solutions

Current informatics solutions in animal imaging facilities vary between institutions based on investigator pool size, data accessibility requirements, and workflow protocols. Facilities with more investigators using their modalities, workstations and services typically have log-in user domain accounts on their workstations and some form of user interface on their workstations for scheduling their experiments and accessing created data. Facilities on a smaller operational scale may perform most of their scans by staff, where investigators participate in the imaging and analysis processes. The storage solutions for these animal imaging facilities, however, are typically the same. A central networked storage device is shared internally by the facility's workstations for archiving new image data files under investigator names and study folders. Files of diverse formats are copied into the storage device from modality and post-processing workstations, and copied out for post-processing, viewing, or analysis at user software workstations. Experimental logs, parameters and findings are primarily recorded on individual log-books because there lacks an integrated archiving system and database for maintaining such metadata. This paper presents a study-centric metadata database model for animal imaging datasets that can be used to catalog and navigate previously unorganized multi-modality imaging data files.

2. METHODOLOGY

2.1 Data Object Formats

Due to non-standardized file formats in animal-model imaging studies, the archival and sharing of data in animal imaging facilities have been a challenge. Raw acquisition images, acquisition header files, intermediate reconstruction files, post-processing workflow files, analysis ROI files, and varying display formats all have metadata associated with them and add to the complexities of creating a centralized database archive for organizing and finding imaging datasets. Table 1 lists some common modalities, and their file formats and descriptions, based on the USC Molecular Imaging Center facility. With these different file formats identified, a database model can be built to describe the metadata fields attached to each modality file type.

Table 1. Common file formats for five small animal imaging modalities.

Modality Type	File Format	Description
MicroPET	*.lst +*.lst.hdr *.scn + *.scn.hdr *.img + *.img.hdr	Image Acquisition files Histogram Reconstruction Final Reconstruction
MicroCT	*.cat + *.cat.hdr *.img + *.img.hdr	Image Acquisition files Final Reconstruction
MicroPET/CT	*.img *.img *.xif	PET Input file CT Input file Final Co-registered Image
Optical	*.tif *.txt *.png	Acquisition files Processing Parameters Final Overlay Image
Ultrasound	*.avi *.tif *.dcm	Recorded video clips Screenshots Screenshots

2.2 Database Schema

Creating a metadata database schema enables data-mining and study-specific management of animal-model imaging files. To accommodate multi-modality and multi-vendor acquisition parameters and post-processing parameters in molecular imaging, the proposed metadata database schema utilizes a linked series of tables that is both comprehensive and extensible in design. The parent table for the entire database schema is the 'study' table, containing metadata descriptors for each imaging study with fields such as the unique study ID, study description, region-of-interest, and study status. Imaging investigators are given an investigator ID that is pointed to the imaging studies they have access to, forming a unique primary key combination in the 'investigator' table. A child of the 'study' table is the 'subject' table that describes the animal groups used in each study. One study may have multiple subject groups, each requiring an

authorization IACUC [3] number. Another child of the 'study' table is the 'report' table that lists analysis files and report files, but is limited in its data field content, due to the variable nature of experimental objectives, to analyst's name, the report filenames, and the date of when a particular report file was created.

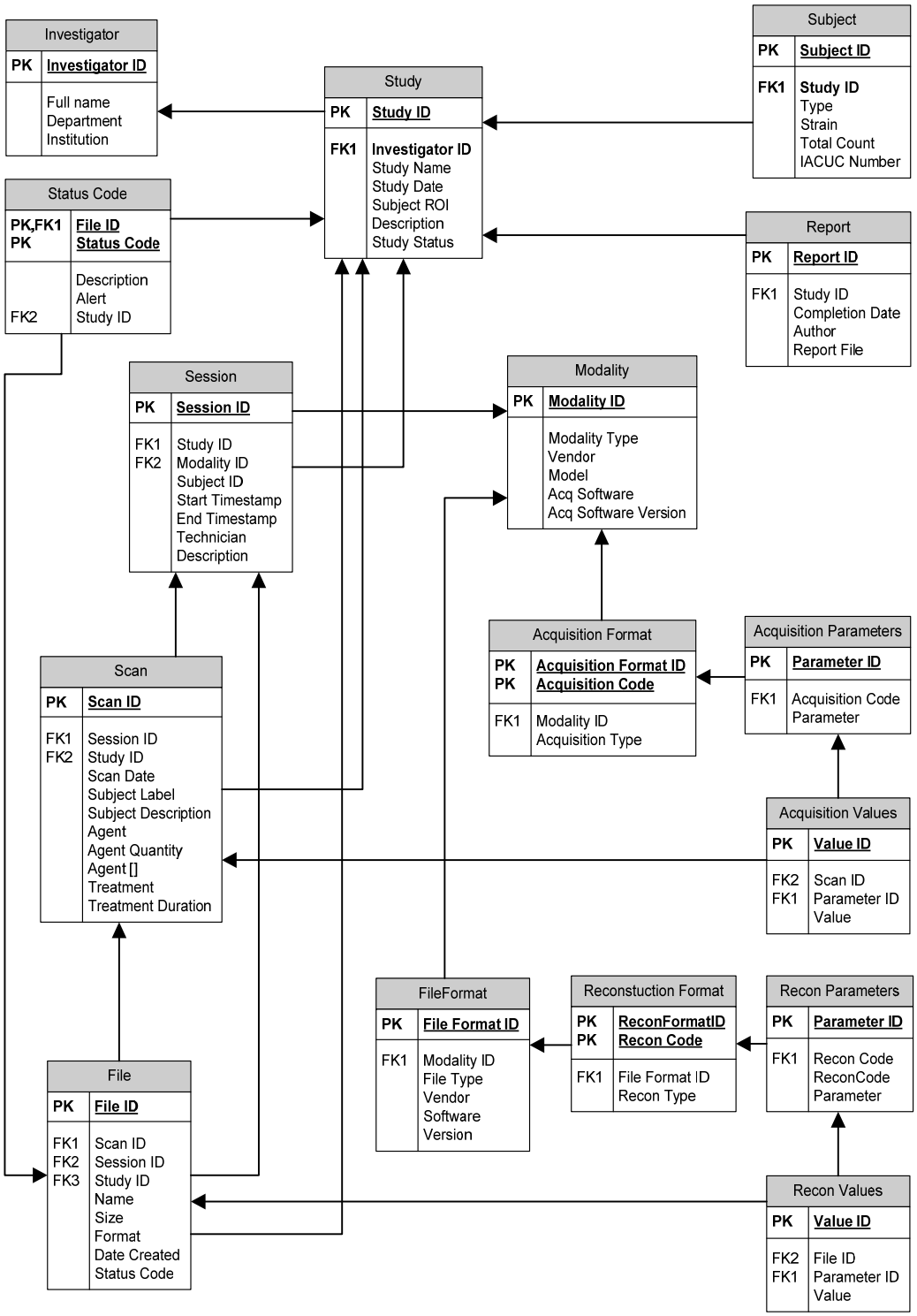

Figure 3. Database Model for Animal Imaging Datasets

For each modality type, there may be different acquisition formats between vendors and even between acquisition software versions; so the 'acquisition format' table is a mapping of modality ID's to one-or-more acquisition types. For each acquisition type, there are one-or-more parameters that need to be recorded such as bin factors and scan duration; so the 'acquisition parameters' table is a mapping of acquisition types to parameters. And finally, the 'acquisition values' table records the actual parameter values associated with each scan ID. A similar series of table structures is used for organizing file reconstruction parameter values. Each modality has different reconstruction methods, listed in the 'reconstruction format' table; each reconstruction method has its own set of parameters, listed in the 'recon parameters' table; and the actual reconstruction values are recorded in the 'recon values' table, along with the unique file ID.

3. RESULTS

This metadata database model is implemented in a molecular imaging data grid at the Image Processing and Informatics Laboratory at USC. The metadata database supports imaging studies from microPET, microCT, micro-ultrasound, and optical imaging modalities. Small animal imaging studies are uploaded and archived into the data grid through a web-based user interface, which allows study-related metadata and experimental findings can be inputted along with the imaging files. Ten sample datasets from each of the five supported modalities are used for evaluation, and include study images and comprehensive experimental metadata. The collected study datasets vary in disease type, experimental scope, and animal subject type to test support for diverse experimental objectives. Metadata from image files are extracted and updated to a centralized metadata database server before the physical files are archived into the grid's storage devices.

3.1 Data Searching and Retrieval

The ability to search for complex imaging studies in the molecular imaging data grid has been enabled by the metadata database. Through a web-based interface, authorized users enter filtering parameter values, such as animal type and disease type, to search the data grid's metadata database for specific study datasets archived in the data grid. Resulting study datasets that meet those search parameters can be retrieval and downloaded through the same web-based interface, alleviating investigators imaging facility staff from relying on written records for accessing historic and published imaging data files. The metadata database significantly reduces the workflow for investigators trying to mine for data.

3.2 Data Management

The internal management of imaging datasets within a small animal imaging facility is improved with study-specific information provided by the metadata database model, such as file creation timestamps, study status updates, and inter-file relationships. Data management features such as long-term data storage can be automated for studies with complete and published datasets. Furthermore, any unfinished analysis reports or post-processing files can be quickly identified as the cause for incomplete studies and corrected by the animal-imaging facility staff through monitoring of individual study status'. Therefore, maintaining complete datasets for each animal-model imaging study is more attainable and the archival of these datasets within integrated storage infrastructure is more automated.

4. CONCLUSIONS

We have implemented a study-centric database model to consolidate small animal imaging metadata, files and findings into a database schema around the investigators. Providing more information about a small animal imaging facility's archived files is the first step towards improved systems integration and interoperability of multimodality data in pre-clinical medical research. Specifically, a metadata database makes data accessible for data management, post-processing, and data-mining in translational sciences. With a growing interest in multimodality datasets, yet a myriad of incompatible file formats, a study-centric database model is essential to organizing, centralizing and streamline the data workflow in small animal imaging facilities.

5. REFERENCES

[1] Yang, J., Yang, M., Arabnia, H., Deng, Y., "Genomics, molecular imaging, bioinformatics, and bio-nano-info integration are synergistic components of translational medicine and personalized healthcare research," BMC Genomics. 9:Suppl 2:I1 (2008).

[2] Mabry, P., Olster, D., Morgan, G., Abrams, D., "Interdisciplinarity and Systems Science to Improve Population Health," Am J Prev Med. 35:S211-S224 (2008).

[3] Stout, D., Chatziioannou, A., Lawson, T., et al, "Small Animal Imaging Center Design: The Facility at the UCLA Crump Institute for Molecular Imaging," Mol Imaging Biol. 7:393-402 (2005).

[4] Tulipano, K., Tao, Y., Millar, W., et al, “Natural Language Processing and Visualization in the Molecular Imaging Domain,” J Biomed Informatics. 40:270-281 (2007).
[5] Peng, H., “Bioimage Informatics: a new area of engineering biology,” Bioinformatics. 24:17:1827-1836 (2008)
[6] Nikiforidis, G.C., Sakellaropoulos, G.C., Kagadis, G.C., “Molecular Imaging and the Unification of Multilevel Mechanisms and Data in Medical Physics,” Med Phys. 35:8:3444-3452 (2008).

A Zero-Footprint 3D Visualization System Utilizing Mobile Display Technology for Timely Evaluation of Stroke Patients

Young Woo Park*[a], Bing Guo[b], Monique Mogensen[b], Kevin Wang[b], Meng Law[b], Brent Liu[a]
a. Image Processing and Informatics Laboratory, Univ. of Southern California, 2250 Alcazar St., CSC/IGM 105, Los Angeles, California 90033
b. Department of Radiology, Univ. of Southern California, 1520 San Pablo Street, Los Angeles, CA 90033

ABSTRACT

When a patient is accepted in the emergency room suspected of stroke, time is of the utmost importance. The infarct brain area suffers irreparable damage as soon as three hours after the onset of stroke symptoms. A CT scan is one of standard first line of investigations with imaging and is crucial to identify and properly triage stroke cases. The availability of an expert Radiologist in the emergency environment to diagnose the stroke patient in a timely manner only increases the challenges within the clinical workflow. Therefore, a truly zero-footprint web-based system with powerful advanced visualization tools for volumetric imaging including 2D. MIP/MPR, 3D display can greatly facilitate this dynamic clinical workflow for stroke patients. Together with mobile technology, the proper visualization tools can be delivered at the point of decision anywhere and anytime. We will present a small pilot project to evaluate the use of mobile technologies using devices such as iPhones in evaluating stroke patients. The results of the evaluation as well as any challenges in setting up the system will also be discussed.

Keywords: Stroke, Mobile display technologies, Web-based visualization tools

1. INTRODUCTION

1.1 Background information on stroke

Stroke has become one of major health issues in the modern society. According to American Stroke Association, about 795,000 Americans suffer from stroke annually. Among them, more than 137,000 cases have resulted in death, making stroke third most common cause of death behind heart diseases and cancer. There are two major types of strokes: hemorrhagic and ischemic strokes. Hemorrhagic stroke makes up for about 13 percent of all stroke cases. Ischemia results in death of brain tissue, and therefore is often called as cerebral infarction (tissue death) instead. Ischemic stroke makes up for 87 percent of all stroke cases.

There are several guidelines for treatment of stroke patients. American Heart Association/ American Stroke Association (AHA/ASA) guideline[1], which is observed by many hospitals, specifies following timelines when treating stroke patients. In stroke cases, speed is one of the most important factors in determining the success of treatment in patients. The infarct brain could suffer irreplaceable damage as soon as three hours after the onset of stroke symptoms. rtPA, which is the only drug approved by Food and Drug Administration (FDA) for treatment of cerebral infarction, should ideally be administered within 3 hours of symptom onset[2]. The following table shows the benchmark treatment time for NIH – National Institute of Neurological Disorders and Stroke (NINDS) for cerebral infarction with rtPA.

Table 1. Maximum Intervals Recommended by NINDS

Maximum Intervals Recommended by NINDS	
Door-to-doctor first sees the patient	10 min
Door-to-CT completed	25 min
Door-to-CT read	45 min
Door-to-thrombolytic therapy starts (rtPA)	60 min
Physical Examination	+15 min

Neurosurgical expertise available	+2 hours
Admitted to monitored bed	+3 hours

The above chart assumes that from the onset of the stroke to arrival and transportation of stroke patient to hospital took slightly less than two hours. If discovery and transportation of the patient has taken more than two hours, hospital workflow should be hastened to accommodate the delay. As shown in the above chart, CT read should be completed in 20 minutes or less to ensure that thrombolytic therapy could start within 3 hours from the onset of infarction.

1.2 Current workflow for treating stroke patients

At LA County – USC (LAC+USC) hospital, where all stroke patients around metro LA are sent, the stroke patient treatment workflow follows the guideline set by AHA/ASA. Figure 1 summarizes workflow involving stroke patients at LAC+USC hospital from the onset of the stroke to review step by neurologists for determining treatment options.

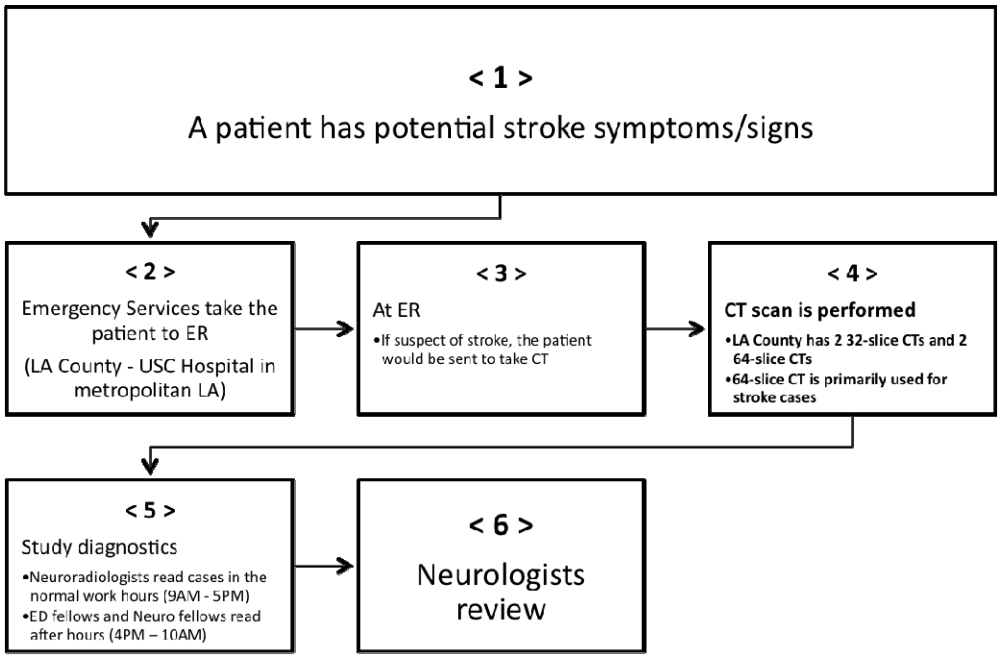

Figure 1. Stroke Patient Workflow at LAC+USC Hospital

<1> Stroke occurs and emergency services are called in.

<2> Emergency crews arrive for stroke patient; in metropolitan Los Angeles, they would take the patient to LAC+USC hospital's ER.

<3> At the ER, the patient would be sent to CT if suspected of stroke after examination by attending physician.

<4> CT scan is performed on the patient: LAC+USC hospital currently has 2 32-slice and 2 64-slice CT scanners, with 64-slice scanners being primarily used on stroke cases.

<5> Once images are taken and ready to be reviewed at a PACS workstation, neuroradiologists will review the study and prepare the report. During after hours when neuroradiologists are not available, ED and/or neuro fellows will read the study instead.

<6> After the study is read, it will be sent to neurologists to have them decide which treatment should be taken next.

Because many different procedures and personnel are involved in handling stroke cases, there are many factors that could cause delays from the onset of the stroke to the review by neurologists. For example, if the patient suffers stroke during non-business hours, (i.e. after 6PM until 9AM the following day) ED and neuro-fellows, instead of

neuroradiologists will be in attendance to read CT scans (Step 5). If fellows would want a second opinion during off hours, they would either have to page neuroradiologists to come in, wait until the regular business hours to proceed, which would result in additional delays. Additionally, there could also be delays between Steps 5 and 6, in which neurologists face delays in accessing CT images. This could cause further delays in determining and starting treatment for stroke patients.

Mobile display technology could improve stroke treatment experiences by reducing aforementioned delays. During after hours, neuroradiologists could review cases over their mobile phones when requested, which would eliminate the need to halt the procedure until the next business day. In addition, mobile display technology could allow neurologists to access stroke images conveniently anywhere with cellular phone coverage, and set up treatment plans if they are not present at the hospital.

1.3 Mobile Display technology

One possible solution to overcome aforementioned issues would be to employ a mobile display technology using PDAs and smartphones. Mobile technology could enhance treatment experiences by reducing the time for studies to be evaluated by radiologists, especially during non-work hours. However, since imaging information that's being shared across devices contains patients' private medical information, implementing mobile display technology in the field of medicine should comply with HIPAA Security Guidance for Remote Use of and Access to Electronic Protected Health Information (EPHI)[3]. The guideline specifies that mobile devices should employ security measures such as encryption and password protection as well as leaving minimal data (cache) on the device itself to avoid loss of private data when the device is lost.

Many mobile medical display options adhere the first two requirements on encryption and password protection. However, avoid creating local cache is a difficult option because of retrieving and handling DICOM image format. Many currently available mobile medical display solutions implemented solution that store downloaded medical images on the devices' memories. The advantage of this solution is it allows fast and smooth access to images once they are downloaded to devices' memories. However, this solution may cause security concerns if the device is lost or stolen and loss of patients' EPHI. Because of such risks, applications with local cashing of EPHI may not comply with requirements set out in the HIPAA security guideline.

One possible solution for mobile display technology, while meeting HIPAA requirements, is to employ zero-footprint technology. Zero-footprint solution is a type of implementation, where any relevant information is stored in the server and accessible only at the time of use. No software application installation is required, all the image manipulation is done at the server side and a jpg (the most suitable for medical images) is displayed on the web browser. Because there is no application data cached on the device, there is no EPHI on the device after execution, which complies with the HIPAA security guideline. However, the downside for zero-footprint solution is its heavy reliance in network connectivity, as it requires an Internet access to operate and retrieve information. This type of approach has the following characteristics:

a. It is less restricted to the browser vendor used. Some browser incompatibilities issues might need to be resolved but it has the benefit of working in a variety of Operating Systems (OS) and browsers.
b. Quality of the images is not enough for Radiological readings; however it is suitable for review and training.
c. Standard web protocols are used, no extra knowledge is required for handling the communication between the server and the client.
d. The cache mechanisms are inherent from the browsers and the settings set by the user. This could be an issue if a high number of images are needed to be downloaded.
e. The bandwidth usage can be considered low because there is no need to send the native DICOM images to the client, only the jpeg images.
f. Minimal requirements are set for the hardware of the client PC. Because the processing is done at the server side, the clients do not require having high-end components in order to display the images.

Figure 2 shows the communication scheme in a thin-client or "zero footprint" system.

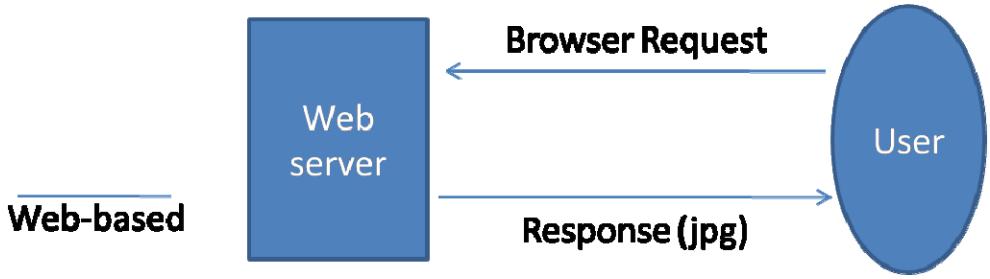

Figure 2 – True Thin Client or "zero footprint" communication scheme

In this study, we employed Calgary Scientific Inc's zero-footprint mobile display solution for iPhone and iPod touch devices and examined the feasibility of incorporating the technology in time-critical applications such as stroke-diagnosis.

2. METHODS

2.1 Hardware Overview

For this trial, we used iPhone 3GS devices with 3.5-inch display with 480-by-320-pixel resolution at 163ppi. All devices were under AT&T 3G (UMTS/HSDPA) coverage and equipped with Wi-Fi (802.11b/g) capability. The CSI server which processed the 3D volumes and supports the zero footprint technology is a Xeon 8-way SMP 3.2 GHz multiple processor server with 16GB RAM and 4GPU NVIDIA 9800GX2 graphics card with a 2.5 TB RAID running 64bit OS. The medical images were first collected in the CD forms and loaded onto experimental Fuji PACS at Healthcare Consultation Center 2 (HCC2). Then, images were pushed from Vincent PACS to a server provided by Calgary Scientific where DICOM images were converted and ready to be reviewed on iPhone mobile devices. Finally, PC workstations with grayscale LCD display of 1600 x 1200 pixels (163ppi) were used to view CT stroke images in traditional radiology viewing conditions.

2.2 Clinical Evaluation of using mobile device

For this pilot project, a retrospective study on stroke cases from LAC+USC hospital were utilized. Three fellowship-trained neuroradiologists (R1, R2 and R3) from USC radiology department reviewed studies using their iPhone displays, and then their diagnoses with iPhones were compared with actual radiology reports to find any discrepancies between the two. After completion of iPhone display diagnosis, radiologists checked their iPhone-based reads against results using full PACS workstation to see any differences in their reads.

A total of 33 stroke cases were used for this retrospective study. Studies were collected from LAC+USC hospital, with 33 cases of non-contrast CT-head scans of the patients presenting to the emergency department with signs of an acute stroke.
Radiology reports of each study were also collected and used to identify and categorize patients. Four main categories were identified including hemorrhage, normal, subtle and obvious infarctions.

Out of 33 studies used:

Table 2. Four main categories

TOTAL	**33**
Hemorrhagic	8
Subtle Infarct	9
Obvious Infarct	8
Normal	8

Lists of patients from the 4 different sub-groups were combined to form a single list. Then the list was re-arranged alphabetically based on last names of stroke patients. This was to ensure that radiologists were not biased when filling out the survey form. All radiologists were asked to record any abnormalities after reviewing the cases,

locations of each abnormality (if exists), and the confidence score between 1 (lowest) and 4 (highest) of their diagnostics. Also, they recorded location of affected area, adjacent effect and grading of stroke from scale of 1 (Least severe) to 3 (Most severe) based on its size and severity (Table 3).

Table 3. Sample Evaluation Sheet

Last Name	First Name	Infarct (Y/ N/ Indeterminate)	Location	Adjacent effect	Hemorrhage (y/n)	Grading 1-3 (Size/ Severity)	Read Date (mm/ dd/ yy)	Read Started (Time)	Confidence (1 lowest, 4 highest)	Misc Comments
DOE	JOHN	Y	L cerebellum	Mass effect with compression 4th vent	N	3	10/21/ 09	22:03	4	WiFi

Retrospective CT images used during this study were not officially randomized like in a true receiver operator characteristic (ROC) study. This was just an initial pilot feasibility study to determine the mobile technology and whether it could be used in emergency clinical environments.

Additionally, radiologists were asked to run the software in various locations, using both cellular (AT&T 3G UMTS/HSPA) and Wi-Fi network modes to gather their feedback on accessibility in various conditions.

2.3 Gathering Feedback on diagnosing strokes on the mobile device

Another survey form was handed out to radiologists to gather their feedback on using the software and possible room for improvements. Feedback survey form was created and distributed electronically (Table 4). The result will be discussed in Results and Discussion section.

Table 4. Feedback Survey Form

1 (greatly diminished), **2** (somewhat diminished), **3** (equivalent), **4** (improved)	
Display characteristics	
Display size	
Resolution	
Contrast	
Brightness	
Comments	
Viewing functionality - 2D	
Window/level	
Slice scrolling	
Pan	
Zoom	
Comments	
Viewing functionality - 3D	
Window/level	
Visualizaton presets	
Volume rotation	
Pan	
Zoom	
Comments	
Solution characteristics	

Mobility of solution	
Access to patient imaging data	
Potential as collaborative tool	
Time to diagnose (from page)	
Time to diagnose (once read started)	
Image quality	
Product performance (Wi-Fi)	
Product performance (3G)	
Intuitiveness of viewing interface	
In-product viewing instructions	
Comments	

3. RESULTS AND DISCUSSION

Between October and December of 2009, three (R1, R2 and R3) radiologists reviewed 33 stroke cases over their mobile devices (iPhones) as well as PC workstations at the HCC2. Results were then compared against a grading sheet compiled using radiology reports of individual cases from LAC+USC hospital to evaluate the accuracy of iPhone reads.

Simple intra-observer agreement between the interpretation on iPhone and PC workstation was high for all readers (R1=100%, R2=91%, R3=94%). There were no discrepancies (100% in R1, R2 and R3) between reports from LAC+USC hospital and PC workstation, and therefore interpretation agreement between iPhone and reports were same as previous case (R1=100%, R2=91%, R3=94%). Differences in simple agreement were primarily secondary to subtle infarcts not seen during interpretation on the mobile device. All acute abnormalities reported on the mobile device were seen on the standard PC workstation clinical application.

Average confidence levels of interpretations on the mobile device versus the PC workstation were as follows: R1=3.60 versus 3.79, R2=3.73 versus 3.91, and R3=3.40 versus 3.73, in a range of 1 to 4 with 1 lowest and 4 highest level confidence in reading (Is this scoring range correct? Please verify). The result highlights that all radiologists had higher confidence levels with studies read on PC Workstation than with their iPhones. However, the confidence levels with iPhones are still above three and showed it maintained a good level of confidence from all three radiologists.

User experience gathered from feedback survey form (Table 4) showed that while all three radiologists were satisfied with the mobility and the software's ease of access, there were some issues in the hardware limitation, software functionality and network connectivity. Radiologists found iPhone's screen too small to view images, as they needed to constantly zoom in and out of slides. Additionally, radiologists wanted some changes in the interface layout and inclusion of several features such as contrast presets for stroke cases.

The network connectivity was the most critical issue as poor performance over AT&T's cellular network hindered the use of the application. Since the software was a zero-footprint solution, which needed to pull image data frequently from the server, delays in cellular network (3G/EDGE) caused delayed responses in almost every aspect of the application, including browsing and zooming of slides, and changing contrasts. However, the application's performance over Wi-Fi connections was significantly better than over cellular network, which resulted having most of the reads for this study to be done under Wi-Fi.

4. CONCLUSION

The results of this pilot study shows that while reading studies from mobile devices such as iPhones were lacking compared to reading studies from radiology workstations, the performance were still competitive enough. This is shown by the fact that reads over iPhone and PC workstation did not completely agree on two out of three radiologists. In addition, reads on the iPhone had lower overall confidence score over a PC workstation, which shows radiologists still preferred reviewing cases on PC workstations. However, more than 90% agreements for all

readers (R1=100%, R2=91%, R3=94%), and confidence score of over 3 (R1=3.60 versus 3.79, R2=3.73 versus 3.91, and R3=3.40 versus 3.73) on the iPhone, showed that reviewing cases over iPhones were competitive against reviewing on PC workstations. Therefore, mobile display technology could successfully be integrated into radiology workflow of diagnosing and treating stroke patients.

In contrast, there were some issues with regard to using a zero-footprint solution for mobile display. The zero-footprint solution's heavy reliance on network connection became an issue when the connection was not perfect. All radiologists found the application to be slow and lagging over cellular connection, and had to use Wi-Fi connection to complete their reads for this trial. Mobile display technology should be accessible anywhere, in order for the mobile display to be effective. Because Wi-Fi has limited range, sometime the iPhone must rely on cellular technology to retrieve information.

Calgary Scientific has been improving their mobile display solution with incorporation of many features we requested during this pilot study, including performance enhancement. They are looking at having a temporary image cache on the device's RAM to ease application's network traffic and have faster interface interactions.

Mobile display's competitive results during this study, as well as possible improvements from Calgary Scientific have shown that the device could successfully be integrated into stroke workflow. Therefore, future work includes a prospective trial of stroke patients at LAC+USC hospital in 2010.

REFERENCES

[1] Summers, D., et al., "Comprehensive Overview of Nursing and Interdisciplinary Care of the Acute Ischemic Stroke Patient: A Scientific Statement From the American Heart Association," Journal of American Heart Association, Retrieved from http://stroke.ahajournals.org/cgi/content/full/40/8/2911, (2009).

[2] Bederson, J.B., et al. "Guidelines for the Management of Aneurysmal Subarachnoid Hemorrhage: A Statement for Healthcare Professionals From a Special Writing Group of the Stroke Council, American Heart Association," Journal of American Heart Association, Retrieved from http://stroke.ahajournals.org/cgi/content/full/40/3/994, (2009).

[3] U.S. Department of Health and Human Services – Centers for Medicare and Medicaid Services., "HIPAA Security Guidance for Remote Use of and Access to Electronic Protected Health Information," Retrieved from http://www.cms.hhs.gov/SecurityStandard/Downloads/SecurityGuidanceforRemoteUseFinal122806rev.pdf, (12/28/2006).

Computer-aided Bone Age Assessment for Ethnically Diverse Older Children Using Integrated Fuzzy Logic System

Kevin Ma*[a], Paymann Moin[a], Aifeng Zhang[b], Brent Liu[a]
[a]Image Processing and Informatics Laboratory, Dept of Radiology, Univ. of Southern California, 2250 Alcazar St. Los Angeles, CA 90033
[b]Dept of Psychiatry-CS, Univ. of Illinois at Chicago, Chicago, IL 60612

ABSTRACT

Bone Age Assessment (BAA) of children is a clinical procedure frequently performed in pediatric radiology to evaluate the stage of skeletal maturation based on the left hand x-ray radiograph. The current BAA standard in the US is using the Greulich & Pyle (G&P) Hand Atlas, which was developed fifty years ago and was only based on Caucasian population from the Midwest US. To bring the BAA procedure up-to-date with today's population, a Digital Hand Atlas (DHA) consisting of 1400 hand images of normal children of different ethnicities, age, and gender. Based on the DHA and to solve inter- and intra-observer reading discrepancies, an automatic computer-aided bone age assessment system has been developed and tested in clinical environments. The algorithm utilizes features extracted from three regions of interests: phalanges, carpal, and radius. The features are aggregated into a fuzzy logic system, which outputs the calculated bone age. The previous BAA system only uses features from phalanges and carpal, thus BAA result for children over age of 15 is less accurate. In this project, the new radius features are incorporated into the overall BAA system. The bone age results, calculated from the new fuzzy logic system, are compared against radiologists' readings based on G&P atlas, and exhibits an improvement in reading accuracy for older children.

Keywords: bone age assessment, image processing, fuzzy logic system, system integration

1. INTRODUCTION

This project presents an objective and automated computer-aided diagnosis (CAD) system for bone age assessment (BAA). The system aims to improve current clinical practices of bone age assessment and introduces the use of fuzzy logic algorithm for computing CAD outputs.

1.1 Bone Age Assessment

Bone Age Assessment (BAA) of children is a common clinical procedure performed in pediatric radiology to evaluate the stage of skeletal maturation of children. The clinical importance of BAA can help diagnose endocrinological problems and growth disorders of children. A difference between the chronological age and the skeletal age of the subject suggests abnormal development. BAA can also be used in monitoring growth hormone therapies and may be used in pediatric surgeries.

The current standard for BAA in the United States is for radiologists to compare the patient's left hand radiograph with the Greulich & Pyle (G&P) Hand Atlas[1]. The atlas contains left-hand radiographs of normal children of both male and female ranged from newborn to 18 years of age. G&P Atlas, while widely accepted, have some disadvantages. First, the atlas contains left hand images that were collected over 50 years ago. Previous studies have shown that there have been discrepancies between the G&P atlas and the development stages of modern children[2]. Second, the subjects were only Caucasians from the American Midwest region. In today's urban environment and ethnic diversity, the Atlas may not be adequate enough to evaluate childrens of different races. Thirdly, because BAA is based on visual comparison of closest matched image to the Atlas, there are inter- and intra-personal reading discrepancies. Using the G&P atlas, inter-observer readings can differentiate from 0.37 to 0.6 years, and intra-observer differences can range from 0.25 to 0.47 years[3,4]. Based on the shortcomings, a solution is needed that both defines a new standard for today's ethnically diverse population and eliminates subjective comparison analysis for assessing bone age.

1.2 Computer-aided Diagnosis of Bone Age

A complete computer-aided diagnosis for bone age assessment has been previously designed and implemented. The project has taken place over the span of more than ten years, from data collection to algorithm development and clinical validation and implementation of web-based CAD system in a clinical setting. The detailed history and components of BAA CAD system are listed here.

1.2.1 Digital Hand Atlas

In order to develop an objective BAA CAD system, data collection of normal children's left hand images is needed to replace the G&P Atlas as the standard and the first option for BAA. The result is a digital hand atlas (DHA). DHA is a collection of 1400 normal children's left-hand radiographs[2]. Subjects include both male and female children of different ethnic backgrounds: African American, Asian American, Caucasian, and Hispanic. The subjects are aged from zero to 18 and are all from the Greater Los Angeles area. The result is an ethnically diverse and rich hand atlas that is more suitable for today's children in an urban setting. The data collection process began in the late 1990s and continued through the middle of 2000s. The subjects were considered having normal skeletal development based on trunk heights, body height and weight, and tanner index, the latter of which was used by clinical endocrinologists.

The images are taken at Children's Hospital of Los Angeles, and film images are digitized using a film scanner (Array, Tokyo, Japan). In DICOM header fields, patient's demographic information was manually entered, along with patient's physical measurements. The data was obtained in two cycles: the first cycle contained a set number of hand images per age group, gender, and ethnicity, while the second cycle was completed to complement the first cycle results by increasing the number of cases for children between the ages of 5 to 14, due to the rapid development of bone features during this developmental stage.

The database of digital hand atlas is viewable online at http://www.ipilab.org/BAAweb. The DICOM images are converted to JPEG format for online viewing. Figure 1 is a screenshot of the DHA database showing all cases of 10-year-old Asian female subjects.

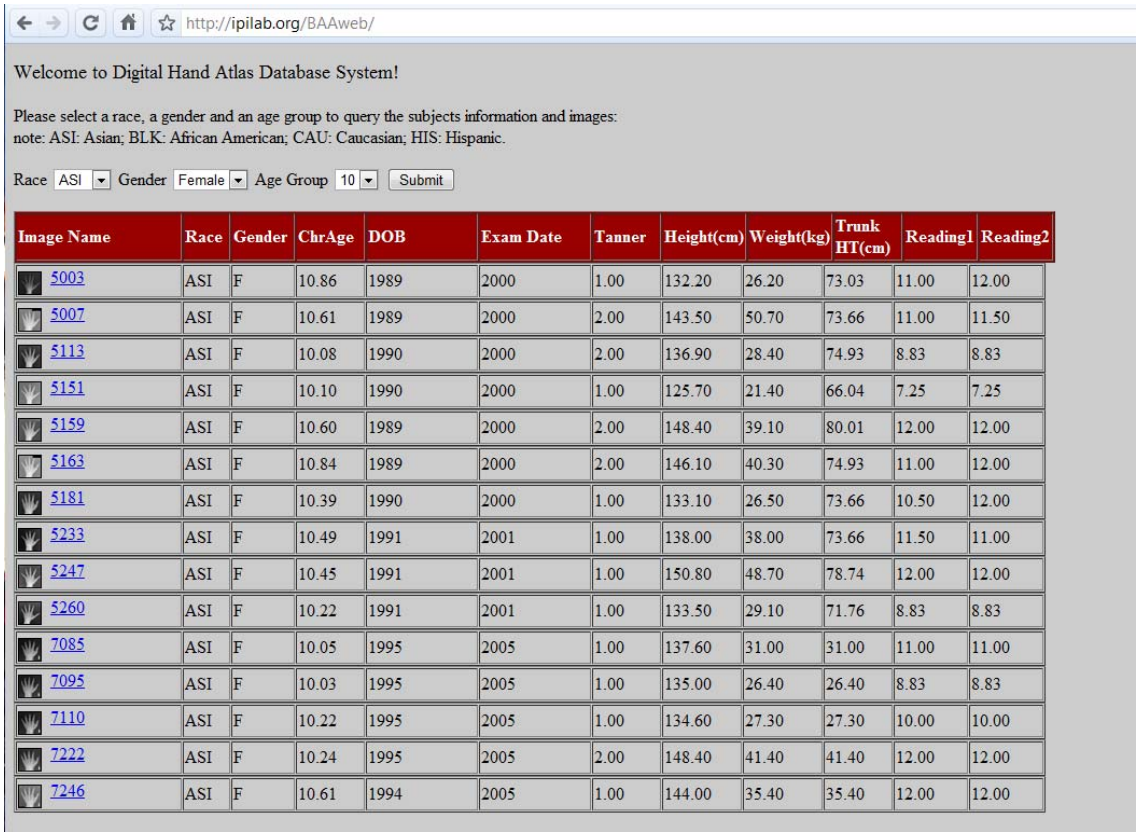

Image Name	Race	Gender	ChrAge	DOB	Exam Date	Tanner	Height(cm)	Weight(kg)	Trunk HT(cm)	Reading1	Reading2
5003	ASI	F	10.86	1989	2000	1.00	132.20	26.20	73.03	11.00	12.00
5007	ASI	F	10.61	1989	2000	2.00	143.50	50.70	73.66	11.00	11.50
5113	ASI	F	10.08	1990	2000	2.00	136.90	28.40	74.93	8.83	8.83
5151	ASI	F	10.10	1990	2000	1.00	125.70	21.40	66.04	7.25	7.25
5159	ASI	F	10.60	1989	2000	2.00	148.40	39.10	80.01	12.00	12.00
5163	ASI	F	10.84	1989	2000	2.00	146.10	40.30	74.93	11.00	12.00
5181	ASI	F	10.39	1990	2000	1.00	133.10	26.50	73.66	10.50	12.00
5233	ASI	F	10.49	1991	2001	1.00	138.00	38.00	73.66	11.50	11.00
5247	ASI	F	10.45	1991	2001	1.00	150.80	48.70	78.74	12.00	12.00
5260	ASI	F	10.22	1991	2001	1.00	133.50	29.10	71.76	8.83	8.83
7085	ASI	F	10.05	1995	2005	1.00	137.60	31.00	31.00	11.00	11.00
7095	ASI	F	10.03	1995	2005	1.00	135.00	26.40	26.40	8.83	8.83
7110	ASI	F	10.22	1995	2005	1.00	134.60	27.30	27.30	10.00	10.00
7222	ASI	F	10.24	1995	2005	2.00	148.40	41.40	41.40	12.00	12.00
7246	ASI	F	10.61	1994	2005	1.00	144.00	35.40	35.40	12.00	12.00

Figure 1. Collection of hand images in Digital Hand Atlas, available online

Performance of DHA has been evaluated. Two radiologists read all of the DHA cases using the G&P atlas for Asian American (AS), African American (AA), and Hispanic subjects (HI) of both genders, and the results have been stored in the DHA database to show cross-racial reading discrepancies between G&P atlas and normal skeletal development[5].

1.2.2 CAD module: Image Processing Algorithm

BAA CAD system uses data collected from Digital Hand Atlas to establish an objective and reliable algorithm that assesses bone age of children. The goal of CAD is to aid radiologists performing BAA by offering a second opinion that is consistent for all cases. The system examines three regions of interests: carpal bones, phalanges, and wrist joint. Each region of interests display different level of importance in evaluating bone age for different age groups. Table 1 displays the three regions of interests and the area of where they are most effective in.

Table 1. Clinical reliability of using the three ROIs for BAA in different age groups

Age group	Phalangeal ROIs	Carpal ROI	Distal Radius ROI
0 – 5 (female) **0 – 7 (male)**	Feature analysis of epi-metaphysis - **NOT reliable**	Size & shape analysis of carpal bones - **Reliable**	
6 – 13 (female) **8 – 15 (male)**	Feature analysis of epi-metaphysis - **Reliable**	Degree of overlapping of carpal bones - **NOT reliable**	
14 – 18 (female) **16 – 18 (male)**	Feature analysis of epi-metaphysis - **NOT sufficient**		Feature analysis of epi-diaphysis - **Reliable**

The phalangeal ROI is one of the first criteria in assessing bone age. The shape, size, and development of epiphysis in relation to metaphysis in the middle three fingers are used to evaluate bone development. During infancy, the epiphysis has not been formed and thus cannot be used in BAA. As bone ages, the epiphysis would start to increase in size, and finally it fuses with metaphysis when the subject enters adolescence. Therefore, the phalangeal ROI analysis is best suited for children in the middle age groups.

The carpal ROI is more reliable for younger children of less than 5 years old for female and less than 7 year old for male children. Carpal bones grow as the infant grows, and the bones begin to overlap with each other starting at the age of 5. The difficulty in distinguishing different carpal bones in the ROI makes the method only suitable for BAA of younger children.

After the epiphysis and metaphysis have fused in the phalangeal ROI, epiphysis and metaphysis do not fully fuse in the wrist joint region until the child's development is fully mature. In other words, analysis on the degree of fusion between epiphysis and metaphysis on radius is used best for BAA of older children.

1.3 Use of Fuzzy Logic in computing Bone Age

The BAA CAD system needs to intelligently put weight on results from the three ROI analyses to accurately assess bone age. Relationship between extracted features and assessed bone age is also nonlinear. The three analysis components are arranged in a modular fuzzy logic system that integrates results and computes bone age for patients of different age, gender, and ethnicity. The fuzzy logic concept is derived from inherently imprecise measurements that exist in the natural, biological world[9]. A fuzzy logic system uses a set of rule-based classifications (various if…then.. statements) and mathematical equations to derive outputs evaluating imprecise outcomes. Fuzzy logic is commonly used in engineering as a means for computing systems to output qualitative assessment, rather than quantitative data[11].

For BAA CAD, a rule-based fuzzy logic system has been developed to compute outputs from feature analyses. The results need to be aggregated and a final bone age is computed from the integrated fuzzy logic system. Previously, CAD algorithm has been completed for each components and fuzzy logic has been designed for each components. This paper focuses on the development of the complete algorithm that has been used in developing the BAA CAD system,

incorporating all three ROI analyses, and to include the implementation and results of an integrated fuzzy logic system for results analysis.

2. METHODS

2.1 Data Collection

Normal left-hand images are collected from the Digital Hand Atlas. All DHA images are collected for training of the algorithm. Additionally, around 75 of both normal and abnormal cases are collected at LAC+USC Medical center as recent as 2008. The images are normal hand images in DICOM format and have been determined by radiologists using the G&P atlas for visual comparison. The LAC images are used for system evaluation.

2.2 Feature Extractions

The overall CAD system contains three components. Figure 2 shows how each components are evaluated in the CAD system.

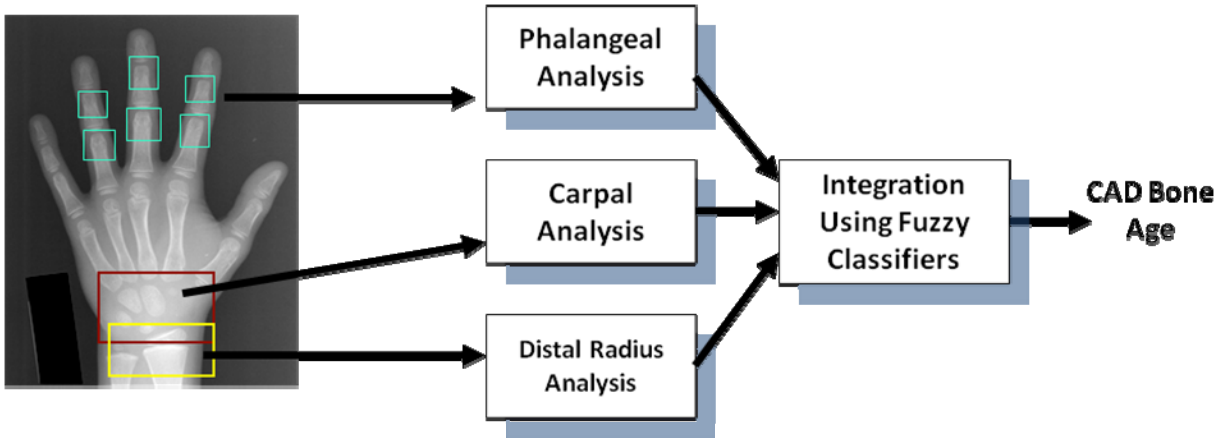

Figure 2. The BAA CAD system workflow diagram

The left hand image first goes through the pre-processing step. In this step, the hand is segmented, and a knowledge-based segmentation step is used to identify the three regions of interests.

2.2.1 Phalanges ROI

The middle and distal epimetaphyseal regions of the middle three digits are localized and extracted from the hang image. A total of six sub-regions of interest are identified and segmented. Region features are then acquired: eight quantitative size and shape features and ten wavelet features (once the epiphysis starts to fuse with metaphysis). Wavelet features, in image processing, are used in determining texture and pattern of the examined image, making it suitable for examining degree of fusion in the epimetaphyseal regions[13]. Figure 3 summarizes the features extracted, the quantitative calculations involved, and the aggregation of all six sub-ROIs for the bone age assessment based on only phalanges ROI. The bone age output from phalange analysis is named BA1.

2.2.2 Carpal ROI

Two bones, the capitates and hamate, are the focal points in the carpal ROI analysis. The two bones are the first to ossify during development in the carpal region, thus making it ideal candidates for assessing bone age for small children. The two bones are segmented during carpal ROI analysis, and size and shape features are extracted. The two features are aggregated and passed through a fuzzy logic classifier for assessing the bone age based solely on carpal ROI analysis results. Figure 4 presents the summary and diagram of how BA is calculated based on carpal region. The bone age output from this analysis is BA2.

2.2.3 Wrist Joint ROI

Wrist joint ROI analysis consists of evaluating the growth plate region of the radius, which is similar to what has be done in the phalangeal ROI. Ten wavelet features are extracted from the wrist ROI, which has been segmented and

radius has been identified. Figure 5 shows the diagram of wrist joint ROI analysis in computing the BAA output. In addition, the correlation coefficients of the ten wavelet features are computed to determine if each feature are independent of each other. Independent features are then input into the fuzzy classifier to computer BA3.

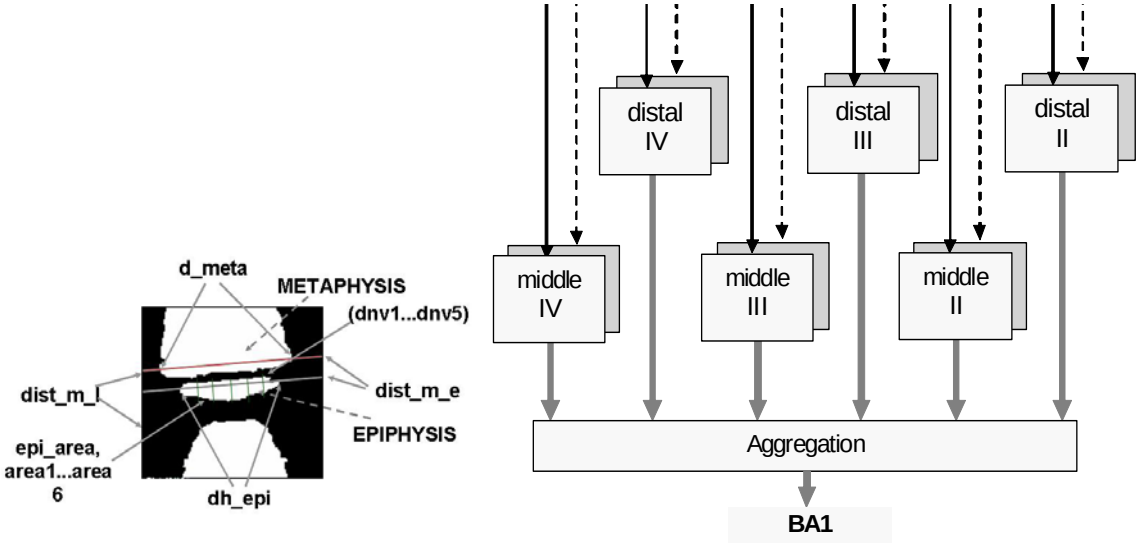

Figure 3. Diagrams of feature extraction from phalangeal ROI. Left: quantifiable features extracted from one epimetaphyseal sub-ROI[2].

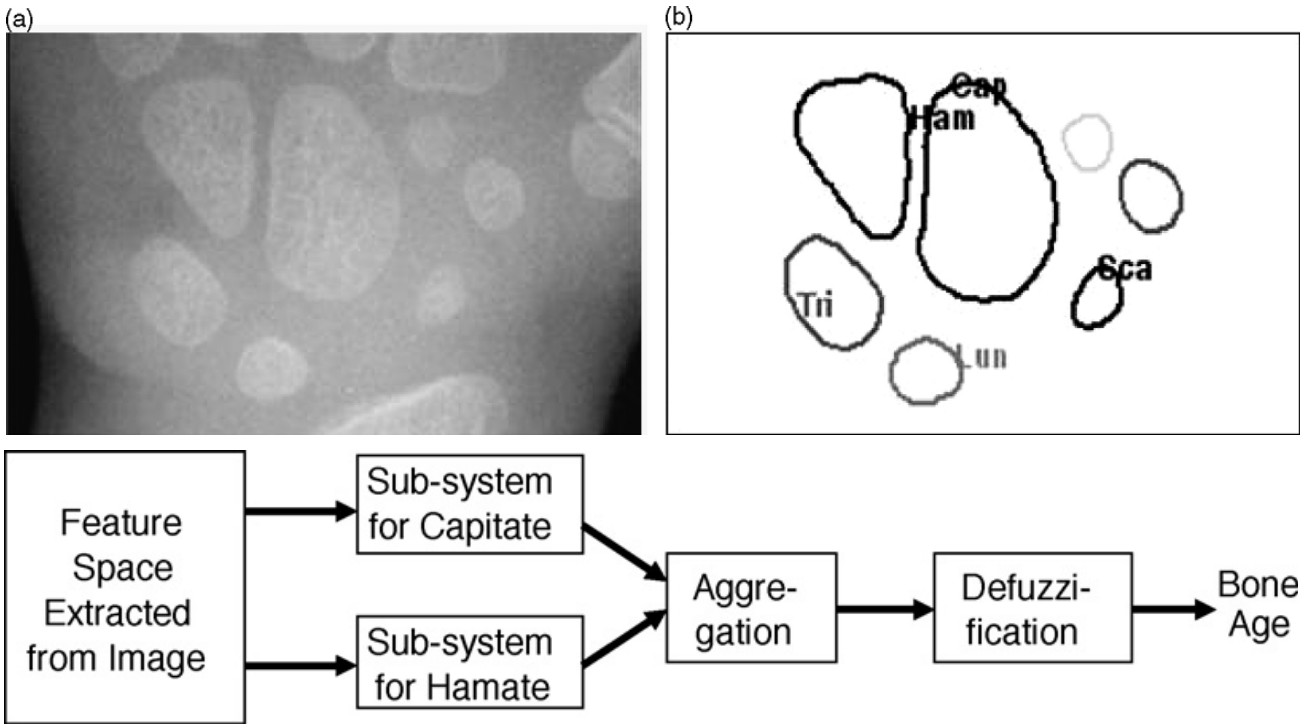

Figure 4. Diagram of carpal ROI region analysis. The top two images are the carpal ROI on the original image and the segmented outline of carpal bones. The bottom diagram shows how features extracted from capitates and hamate are used to calculate bone age.

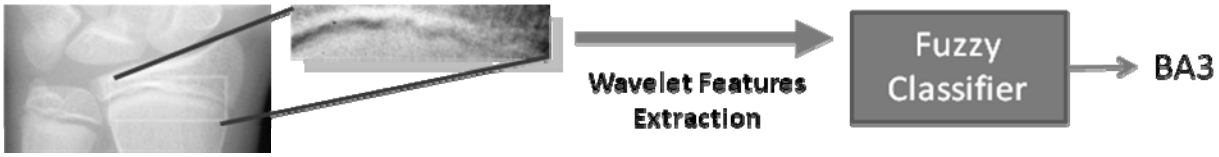

Figure 5. Diagram of Wrist Joint Analysis and computation of BA3.

2.3 Fuzzy Logic Subsystems Design

As mentioned in the previous sections, each ROI analysis is completed by a fuzzy logic classifier at the end to compute a bone age based on the features unique to those ROIs alone. In this section, fuzzy logic classifiers' designs are explained in more detail.

Each fuzzy logic classifier employs rules-based membership functions that categorize output results based on the input values. Because of the diverse ethnicity and different genders, eight fuzzy subsystems are separately designed and trained for an ROI fuzzy system: (ASM, ASF, AAM, AAF, CAUM, CAUF, HIM, and HIF). In the second step, the rules are generated based on input data used for training. Using the carpal ROI analysis for example, one of the defining tules can be that if the output of capitates subsystem is A and hamate subsystem is B, then the output bone age is C. Table 2 illustrated the inference rules that govern the carpal fuzzy logic system.

Table 2. Six inference rules of capitate sub-system for Caucasian males. Numeral represents the age group.

Rule 1: If (size is 0 1) and (eccentricity is 0 1) and (triangularity is 0 1) then (Age is 0 1)
Rule 2: If (size is 2) and (eccentricity is 2 3) and (triangularity is 2) then (Age is 2)
Rule 3: If (size is 3) and (eccentricity is 2 3) and (triangularity is 3) then (Age is 3)
Rule 4: If (size is 4) and (eccentricity is 4) and (triangularity is 4) then (Age is 4)
Rule 5: If (size is 5) and (eccentricity is 5 6 7) and (triangularity is 5) then (Age is 5)
Rule 6: If (size is 6 7) and (eccentricity is 5 6 7) and (triangularity is 6 7) then (Age is 6 7)

Fuzzy logic contains membership functions that compute the probability of the patient being under a certain age group. Each age group is represented by one membership function from 0 to 1. The larger the membership value is, the more the input feature reflects the corresponding age group. Each membership function is Gaussian distributed, and the training method is to automatically perform feature extraction on all images corresponding to the target group (gender, race, and age), find the mean and standard deviation, and construct the membership function. Figure 6 shows a sample membership function distribution for size feature of capitates for Caucasian boys seven years old and younger.

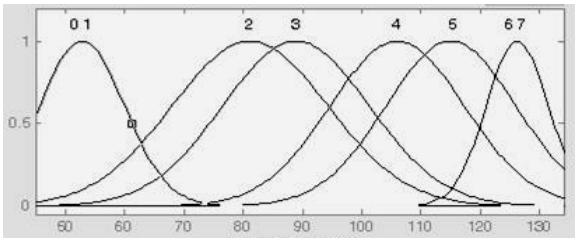

Figure 6. Membership function distribution of capitates size corresponding to bone age assessment for Caucasian boys. The vertical axis shows the membership function value between 0 to 1, and the horizontal axis is the value of corresponding feature.

2.4 Integrated System

Figure 7 shows the aggregation process of assessing the final bone age output using an integrated fuzzy logic system.

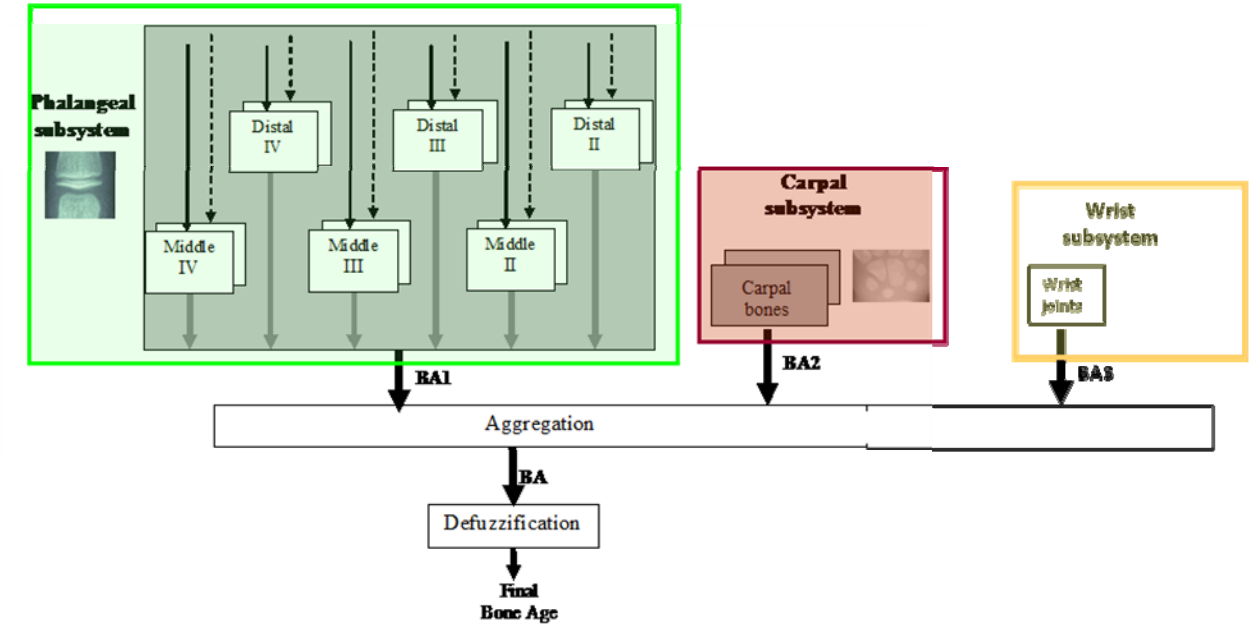

Figure 7. Diagram of final bone age assessed by all three ROI analyses

The integrated fuzzy logic is designed to take the three BA outputs and calculate the final bone age. However, since not all regions of interests are used to assess all of the age groups, new rules are put in the system: when assessed bone age is more than 14 years old for male and 12 years old for female, then BA2 from carpal ROI analysis is not included in the evaluation because of its ineffectiveness in evaluating bone age of older children. If the subject is older than 5years for female and 7 years for male, then wrist joint ROI system is not included. The selective BAA criteria aim to improve on assessment accuracy. Using only BA subsystem outputs as aggression inputs may not be robust enough; thus the aggregated fuzzy logic system evaluates the features and other input values used to create BA1, BA2, and/or BA3. However, too many inputs can also blur set differences between membership functions, and thus the number of inputs is being limited.

Since the wrist joint subsystem is newly completed, BAA results of older children are specifically evaluated.

3. RESULTS AND DISCUSSION

The system has been designed and implemented using MATLAB's Fuzzy Logic Toolkit. The integrated fuzzy logic system features from phalangeal, carpal, and wrist regions and assesses the bone age. Eight different fuzzy logic classifiers are created based on different ethnicities and genders.

The first phase of fuzzy logic system evaluation is to assess BA of the DHA cases. The integrated CAD results are compared with the average of two radiologists' readings and the chronological age. Figure 8 shows the BAA comparison graphs of both Asian and Caucasian males. Table 3 shows the mean difference between CAD and the chronological age for Asian male and Caucasian male. The other six evaluations are still ongoing at time of writing. Additionally, the evaluation process will include comparing CAD results with integrated fuzzy logic system and CAD results with the three individual fuzzy logic subsystems.

The results show that while BAA CAD is able to assess bone age of children of different ethnicity, the results are still not as accurate as radiologists' readings from the G&P hand atlas. It should be noted that CAD results follows the radiologists' readings more closely than the chronological ages.

There are several future works to be completed. The system's performance will be evaluated from cases other than DHA cases. Integrated fuzzy logic system has room for adjustments in input values, rule defining, and membership functions. Not all ROIs are successfully segmented, thus the image processing algorithm has room for improvements.

Table 2. CAD evaluation for two genders with four races combined. Values in the table are the mean differences between chronological age and each reading, and CAD result in year.

Mean Difference with Chr. Age	**F**	**M**
Reading 1	0.932	0.745
Reading 2	0.935	0.767
CAD BA	1.137	1.098
No. of Cases	700	690

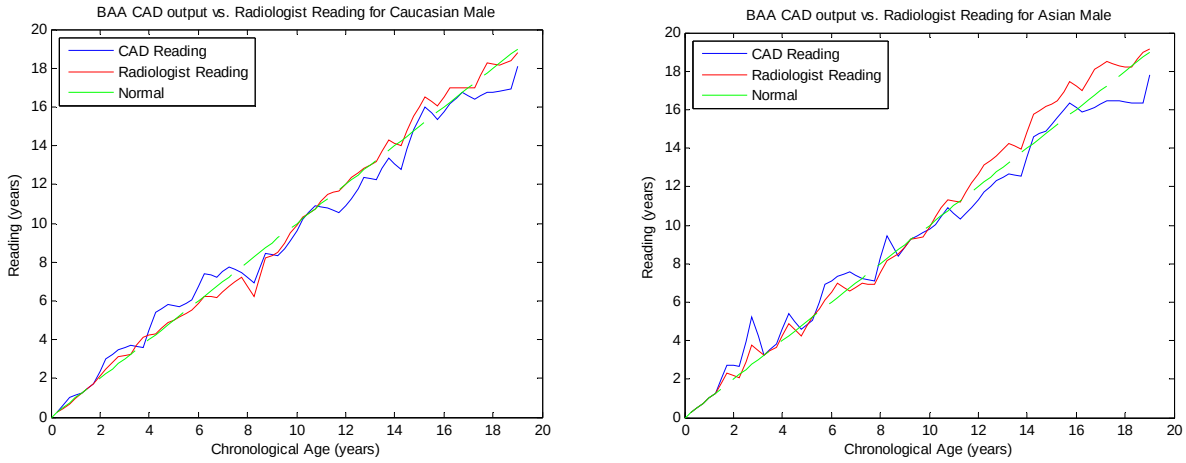

Figure 8. Left: CAD results for Caucasian male, versus radiologists' readings from G&P atlas and the chronological age. Right: Results for Asian male Both graphs are linearly interpolated to show the linear graphs.

4. CONCLUSION

The standard of bone age assessment in the US has been the use of Greulich & Pyle Hand Atlas, which is outdated and not suitable to evaluate skeletal development of children of other ethnicities. Digital Hand Atlas has been created as an alternative method for BAA. Based on DHA, an automated and objective CAD algorithm has been designed. The system uses fuzzy logic classifiers on both subsystem and systematic levels to convert image processing results into assessed bone age. In this paper, design and development of fuzzy logic systems have been presented and discussed. Integration of three different ROI analyses have been completed. With refinements in CAD algorithm and fuzzy logic system design, the BAA CAD system shows promise as a second opinion for radiologists to consult.

REFERENCES

[1] Greulich W. and Pyle S. Radiographic atlas of skeletal development of hand wrist. Stanford, CA: Stanford University Press, (1959)

[2] Gertych, A., Zhang A., Sayre, J et al. "Bone age assessment of children using a digital hand atlas" Computerized Medical Imaging and Graphics 31:322-331 (2007)

[3] Roch A., Rochman C. Davila G. “Effect of training of replicability of assessment of skeletal maturity (Greulich-Pyle)”. Am J Roentgenol 108:511-515 (1970)
[4] King D., Steventon D., O’Sullivan M., et al. “Reproducibility of bone ages when performed by radiology registrars: an audit of Tanner and Whitehouse II versus Greulich and Pyle methods”. Br J Radiol 67:848-851 (1994)
[5] Cao F., Huang H., Piettka E. et.al. “Digital hand atlas and web-based bone age assessment: system design and implementation” Comput Med Imag Graph 24:297-307 (2000)
[6] Cao F, McNitt-Gray M, Pietka E, et. al. “Computer-assisted phalangeal analysis in skeletal age assessment.” IEEE Trans Med Imag 10:616-620 (1991)
[7] Pietka E, Kaabi L, Kuo M, et al. “Computer assisted bone age assessment: image preprocessing and ROI extraction”. IEEE Trans Med Imag 20:715-729 (2001)
[8] Pietka E, Gertych A, Pospiech S, et. al. “Computer automated approach to the extracton of epiphyseal regions in hand radiographs.” J Digit Imag 14:165-172 (2001)
[9] Zadeh L., “Knowledge representation in fuzzy logic”, IEEE Trans Knowl Data Eng 1:98-100 (1989)
[10] Mamdani E., “Application of fuzzy algorithms for control of simple dynamic plant”. Proc IEEE 121:1585-1588 (1974)
[11] Baldwin, J. “Fuzzy logic and fuzzy reasoning”, in Fuzzy Reasoning and Its Applications, E.H. Mamdani and B.R. Gaines (eds.) London: Academic Press, 1981
[12] Zhang A, Gertych A, Liu B. “Automatic bone age assessment for young children from newborn to 7-year-old using carpal bones.” Comput Med Imag Graph 31:299-310 (2007)
[13] Ma W., and Manjunath B., “A comparison of wavelet transform features for texture image annotation” Int Conf on Image Process (1995)

The Development of a Disease Oriented eFolder for Multiple Sclerosis Decision Support

Kevin Ma*[a], Colin Jacobs[b], James Fernandez[a], Lilyana Amezcua[c], Brent Liu[a]
[a]Image Processing and Informatics Laboratory, Dept of Radiology, Univ. of Southern California, 2250 Alcazar St. Los Angeles, CA 90033
[b]Eindhoven University of Technology, Den Dolech 12, 5612 AZ, Eindhoven, The Netherlands
[c]Dept. of Neurology, Univ. of Southern California, 1520 San Pablo St. Los Angeles, CA 90033

ABSTRACT

Multiple sclerosis (MS) is a demyelinating disease of the central nervous system. The chronic nature of MS necessitates multiple MRI studies to track disease progression. Currently, MRI assessment of multiple sclerosis requires manual lesion measurement and yields an estimate of lesion volume and change that is highly variable and user-dependent. In the setting of a longitudinal study, disease trends and changes become difficult to extrapolate from the lesions. In addition, it is difficult to establish a correlation between these imaged lesions and clinical factors such as treatment course. To address these clinical needs, an MS specific eFolder for decision support in the evaluation and assessment of MS has been developed. An eFolder is a disease-centric electronic medical record in contrast to a patient-centric electronic health record. Along with an MS lesion computer aided detection (CAD) package for lesion load, location, and volume, clinical parameters such as patient demographics, disease history, clinical course, and treatment history are incorporated to make the e-Folder comprehensive. With the integration of MRI studies together with related clinical data and informatics tools designed for monitoring longitudinal multiple sclerosis studies, it provides a platform to improve the detection of treatment response in patients with MS. The design and deployment of MS eFolder aims to standardize MS lesion data and disease progression to aid in decision making and MS-related research.

Keywords: multiple sclerosis, electronic patient record, database design, computer-aided detection, system integration, MRI

1. INTRODUCTION

The goal of this paper is to present the development of an imaging informatics-based eFolder specifically for multiple sclerosis patients. The system would store MS patients' data, such as demographics, social history, clinical findings, disease history, as well as patients' MR images and quantitative results of MS lesion detection including lesion load, volume, and location. This comprehensive informatics tool can benefit physicians and radiologists in decision support, treatment assessment, outcome analysis, quantified lesion tracking, and a data repository for clinical researches.

1.1 Multiple Sclerosis

Multiple Sclerosis (MS) is an autoimmune neurological disease that affects approximately 2.5 million people worldwide. The body's own immune system attacked the central nervous system, causing damages and scar tissues in the brain, spinal cord, and optic nerves[1]. Its symptoms vary greatly and in the most severe cases can be disabling and life-threatening. MS manifests itself differently amongst different ethnicities[2], such as different prevalent symptoms, differences in disabilities, MS lesion locations, and response to treatments[3]. Factors in environmental exposures also may result in MS taking different forms and progressions.

Magenetic Resonance Imaging (MRI) is a commonly-used tool in diagnosing and detecting MS. Studies have shown that the mean time between first brain MRI to first clinically isolated MS syndrome is 2.3 years[4]. Scarred tissue, or lesion, in white matter appears hyperintense in MR sequences T2 and FLAIR, while lesions may appear hypointense in T1 sequences. Figure 1 shows a MS patient's MRI in the three sequences.

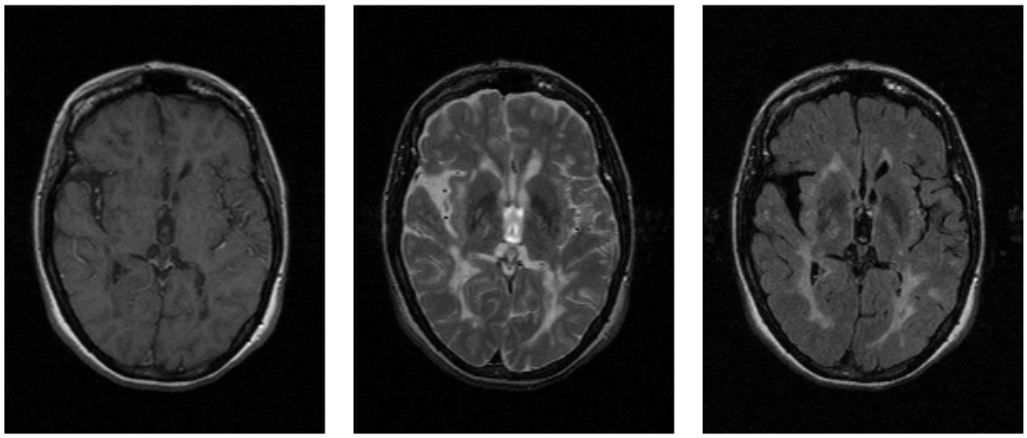

Figure 1. MR brain images of a multiple sclerosis patient. From left to right are T1, T2, and FLAIR sequences. Lesions appear brighter in FLAIR, which suppresses intensity of CSF

1.2 Importance for developing a comprehensive tool for MS treatment and research

In evaluating severity of MS using MRI, radiologists need to quantify MS lesions in the MR images, and in the current protocol, rulers are used manually to measure a lesion volume. The process is tedious and often prone to human errors. In a longitudinal study, comparison with historical cases of the same patient is also completed by hand. In order to have a more accurate and objective way of tracking patient's MS progression, there is a need for a lesion detection and analysis tool that objectively quantifies lesions. With accurate and efficient lesion tracking, the patient's disease progression can be accurately reported. The results may help with treatment planning and decision support. An example would be a physician may be able to research for the best and most effective course of treatment for a patient by looking up other patients with similar conditions and backgrounds.

The imaging and quantification data, combined with patient demographic data, social and medical history, can provide a powerful data repository for clinical research. Data can be queried based on a variety of search criteria, including lesion location, treatment, personal backgrounds, medical history, etc. An automated quantification tool can also be used as a data mining tool for clinical trials, to effectively and objectively quantify any improvements based on the treatment trials.

Based on the needs, we propose an imaging informatics-based comprehensive system to integrate patient information, images, and computer-aided detection (CAD) to aid clinicians and researchers in various tasks related to multiple sclerosis treatment and research.

1.3 eFolder Concept

The concept of eFolder is derived from electronic patient records (ePR). EPR is a comprehensive patient record database that includes patient's demographic information, medical history, disease history, and any information that is needed in today's clinical environment. The advantages of ePR are 1. it is paperless and easily accessible anywhere with a connection to the database server 2. is comprehensive and can be designed to hold any information and 3. allows telecommunications between different departments using the same system, acting as a record-keeping and master database for the enterprise environment.

The eFolder differs from ePR in several ways. First, the eFolder is specifically designed for patients diagnosed for a specific disease, in this case, MS. The system thus is required to store data that are related to the disease. ePR, on the other hand, is designed for patients in a certain geographical environment or a certain facility. Second, the eFolder is designed for data mining for the specific disease characteristics. This allows a more powerful tool for gather data for

research specifically on the disease. The eFolder, therefore, has a unique capability of decision support and treatment planning for the disease.

The proposed MS eFolder combines three components: patient data database, patient images, and CAD results into one comprehensive system. The system would simply workflow for physicians in making follow up evaluations of multiple sclerosis patients, decide course of treatment for patients, track lesion changes over several imaging studies, and making objective comparison studies for patients of different backgrounds and ethnicities.

2. METHOD

This section describes how the system is designed, and how each component connects with each other to present information required by the users. The system is designed as a tool for several ongoing research projects, including a study for Hispanic MS patients and how MS symptoms and lesions are presented differently in the Hispanic population in the Los Angeles area.

2.1 Database Design

The most basic component of the MS eFolder system is the database. It stores text data such as patient history, images, and CAD results. The text data follows the HL7 standard, while the images are stored in DICOM format, and CAD outputs are stored in both text and structured reports (DICOM-SR). The system is written in MySQL for its open source environment and easy web-based development. The database design consists of three parts:

2.1.1 Patient Demographic Data

The patient demographic data is the center of database, as all other information is based on the single patient's records. The information stored in demographic data includes race, sex, ethnicity, birthplace, childhood illnesses, vaccines, and other past medical histories. The database then includes the patient's MS history, consisting of the year of first diagnosis, and family members with MS, MS type, MS symptoms and frequency, treatment history, and so forth. Data gathering is done by patient interviews and paper forms, reading of medical reports, and physician inputs. Columned items are collected on the recommendations of leading neurologists and research project leaders. Several of the stored data follows SNOMED nomenclature to standardize names and codes for symptoms, race, country of origin, vaccines, and etc. This allows an easier and universal way of storing and querying data of that nature.

2.1.2 Imaging Database

The imaging database stores all MR images of the patients. The database structure is designed following the DICOM format: from patient to study, series, and finally images. Since only MR images are stored, studies do not need to be categorized by modality. The columns, such as study instance UID and SOP class UID are taken directly from DICOM headers.

2.1.3 Lesion Quantification Results Database

The paper introduces a novel approach to storing quantification data in the database. The system organizes MS patient data, enables data query by quantification results, and visualizes imaging and CAD results. Quantitative results stored include total lesion load, number of lesions, size of each lesions, 3D location of each lesions, secondary captures of lesion contours overlaid on top of original images, and 3D rendering of the quantification study.

Figure 2 displays the overall database design of MS eFolder. The database is structured such that all tables are interconnected based on individual patients.

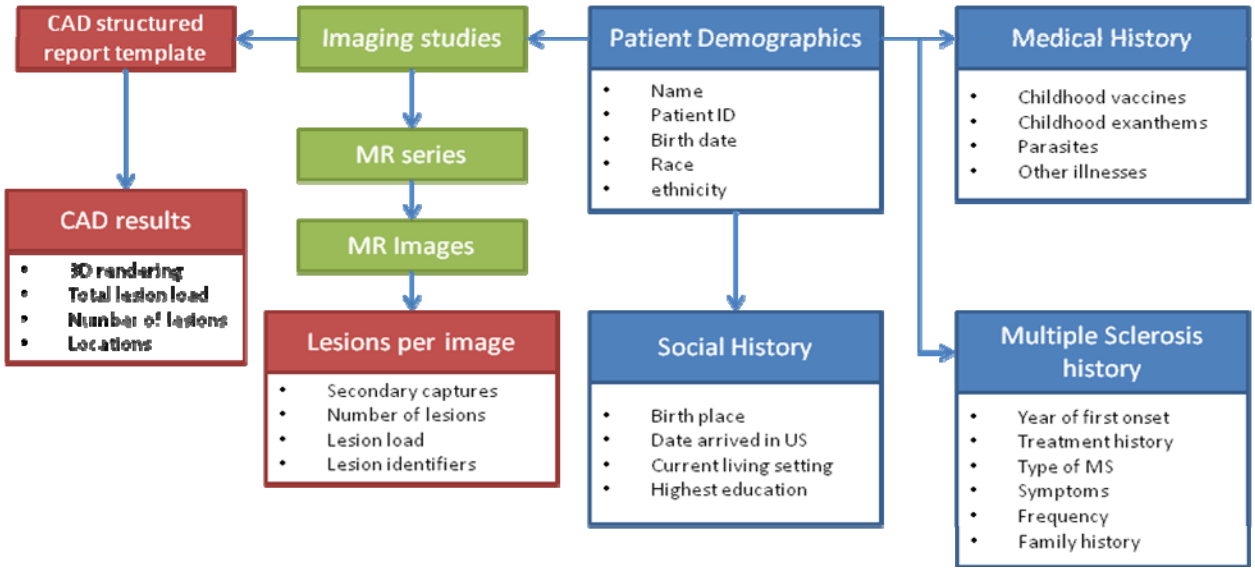

Figure 2. The graph shows the simplified database schema of MS eFolder. The colors indicate the different portions of database: red is the CAD quantified results database, green is imaging database, and blue indicates the patient information database. The arrows show how each table is interconnected with each other.

2.2 Computer-aided Detection

The computer-aided detection uses image processing and analysis to automatically quantify MS lesions in the MR brain images. The CAD algorithm is described in detail in SPIE 2010 presentation "An automatic quantification system for MS lesions with integrated DICOM structured reporting (DICOM-SR) for implementation within a clinical environment". In this section, the CAD algorithm is summarized.

Three MR sequences are used in the CAD algorithm: T1, T2, and FLAIR. The images first go through a preprocessing step. It includes image realignment to the midsaggital plane and brain segmentation.

The second step is to construct probability map of each voxels being lesions in the brain. This is done using the theory of K-Nearest Neighbors, or KNN[5]. Initially, training cases are used to manually segment out lesion voxels. For each voxel, six features are extracted: image intensities in T1, T2, FLAIR, and the voxel coordinates (x,y,z) in 3D space. This training step, once completed, does not need to be repeated each time a CAD analysis is performed.

When the CAD system receives a new set of images and preprocessing is completed, the six features are extracted from each voxels to find the K voxels in the training set that have the most similar features as the current voxel. In this case, K is 100. The number of lesion voxels out of 100 closest neighbors determines the probability of the current voxel being a lesion. Once analysis is completed, a pre-set threshold value is applied to the probability map to filter out non-lesion voxels. After post-processing steps, such as morphological filters and lesion size filters (lesions too small are considered noise signal and thus is thrown out), the result is the lesion voxels for the particular case. Figure 3 shows the KNN process of segmenting lesions.

2.3 Graphical User Interface

A graphical user interface (GUI) is needed to display all the information available in the eFolder, as it ties everything together in a presentable and user-friendly way for navigation. There are three requirements for an eFolder GUI:

- The GUI need to be web-based to allow remote access and requires no additional installing of software. All computations and visualizations are completed on the server side for a light-weight GUI.
- The GUI needs to be comprehensive. It needs to display text data, imaging data, and CAD results on the same interface. It allows physicians and radiologists to access all of the information related to the query.

- The system needs to be dynamic and allow display of 3D images and manipulations of images presented for being more user-friendly. An attractive viewing interface allows a more clarified presentation

A web-based GUI has been designed and is being developed for this purpose. Based on PHP because of its vast functionalities with MySQL databases and large number of libraries, the dynamic GUI guides the user to look up a specific patient's disease history with images, and it allows querying for patients with various different criteria. Viewing of DICOM images allows zoom, pan, window/level, scrolling. The 3D rendering allows users to rotate the 3D image with lesions, and a crosshair pointer allows users to select a specific region to view. The program has been written in PHP and the dynamic element is based on jQuery toolkit in Javascript. Figure 4 shows a screen shot of the current GUI design.

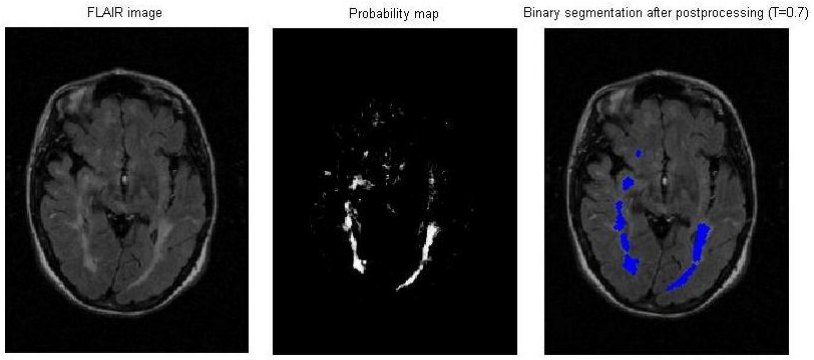

Figure 3. The lesion segmenting process. The left most figure is the original FLAIR image. The middle image is the probability map for lesion voxels, and the right image is the segmented lesion overlaid on the original image. In this case, the applied threshold value is 0.70.

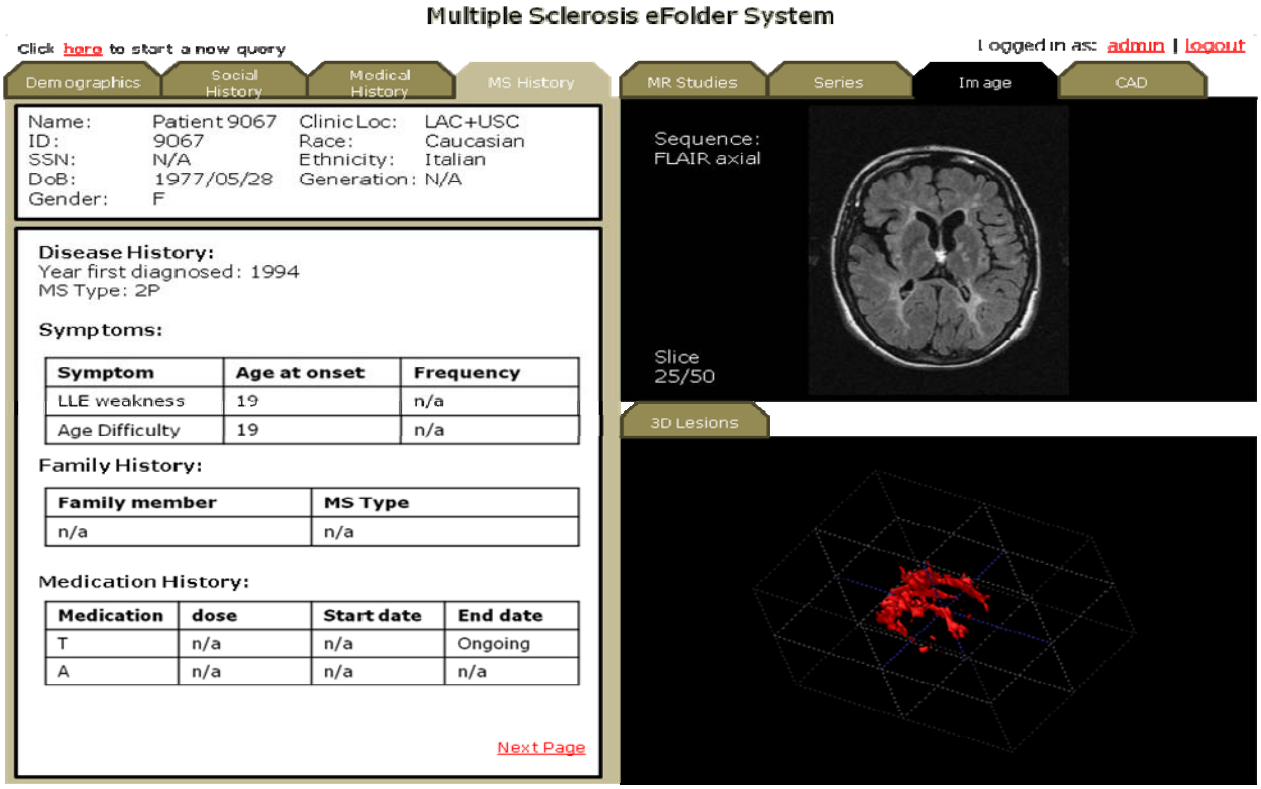

Figure 4. MS eFolder User Interface

3. RESULTS

3.1 Data Collection

A total of 18 MR cases have been collected at the USC Academic Medical Center. The imaging protocol is 3mm continuous slices(no gaps). Among the 18 cases, 10 are accompanied with complete patient interview data and thus have been entered in the eFolder system. The 10 patients are of Hispanic, Caucasian, and African American backgrounds. CAD analysis have been completed on all 10 patients.

3.2 Current status of development for eFolder

At present, the CAD algorithm has been completed and is integrated with the database schema. Four cases have been used for training purposes with more training cases planned in the near future. Because of the complex nature of the algorithm, the CAD program currently takes between 8.5 to 9 hours and thus needs improvement. Results of CAD are in the process of validation by experts in multiple sclerosis.

Several system performance improvements have been implemented and more are being sought upon, such as computing KNN using a tree structure, and exploring the possibility of using graphical processing unit (GPU) to compute the 3-D data. Another SPIE 2010 presentation, "Performance evaluation for volumetric segmentation of multiple sclerosis lesions using MATLAB and computing engine in the graphical processing unit (GPU)", provides details in performance evaluation and improvement of MS CAD.

The graphical user interface is under development including a 3D viewing of lesion contours which is accomplished by using the ITK-SNAP open-source software[8]. Figure 5 shows the ITK-SNAP software used in 3D representation.

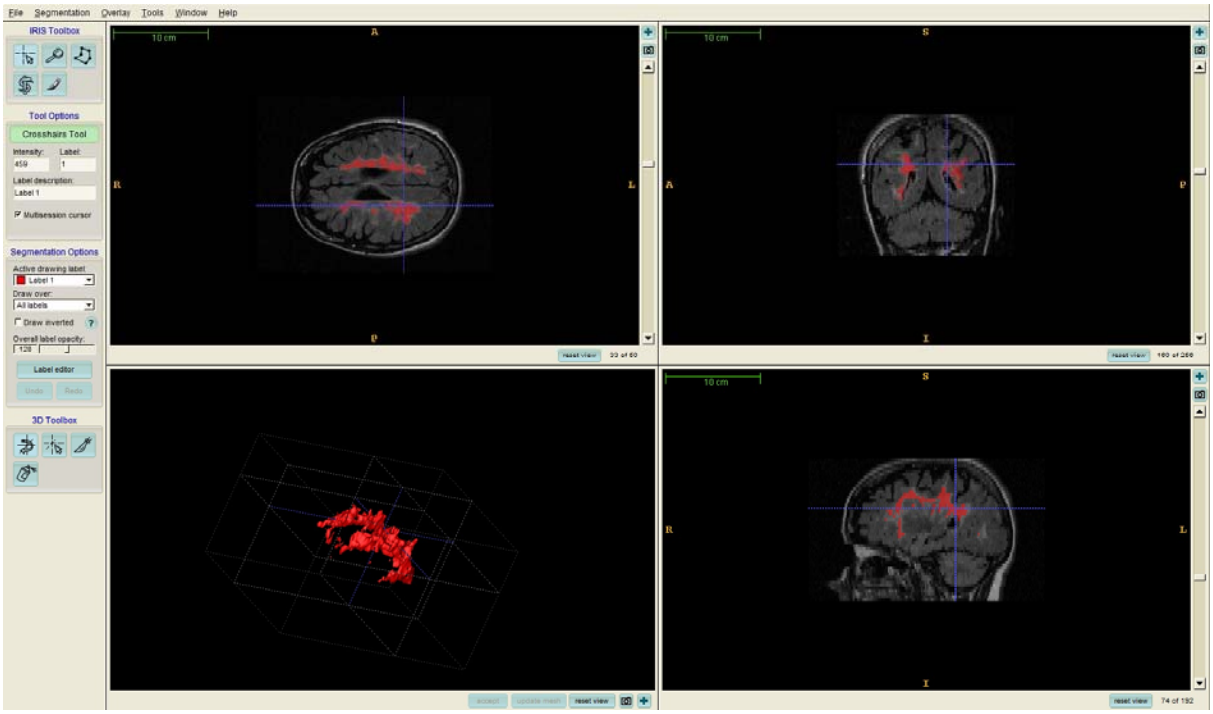

Figure 5. CAD results rendered by ITK-SNAP tool

Data collection is also ongoing to collect 100 MS cases at LAC+USC Hospital and the USC Academic Medical Center. The 100 patients will have longitudinal imaging studies, which will be used to design and evaluate lesion tracking and treatment effectiveness.

3.3 Future work

The MS eFolder system architecture has been designed, and several components have been developed. Additional refinements and pieces can be added into the eFolder system as future work. For example, an image registration

technique needs to be developed in order to standardize all images of the same patient for better lesion tracking. A lesion registration algorithm also needs to be designed and developed in order to pinpoint specific lesion volume changes in a longitudinal study. Several system evaluations include CAD performance evaluation, GUI user feedbacks, and efficiency and time saved from using the system as opposite of manually segmenting lesions and pulling historical data from PACS to do comparison studies.

4. CONCLUSION

This paper describes the design and development a comprehensive imaging-informatics based eFolder system for Multiple Sclerosis decision support. It combines the concept of electronic patient record along with disease-centric database design, MR images, and an objective automated lesion quantification tool for an easier, more efficient system for disease tracking and decision support, specifically for multiple sclerosis patients. The eFolder serves as a evaluation tool and data repository for conducting MS research, including differences of MS between different racial and ethnic groups. The system is HL-7 and DICOM-complaint, while being completely web-based to allow remote access and telemedicine. The prototype MS lesion detection and quantification system has been developed in MATLAB, using the concept of K-Nearest Neighbors. Imaging data and patient disease data have been collected and inputted in the system, while a graphical user interface is being developed to bring ease of access and user-friendliness to the MS eFolder. While the current state of development is incomplete and several improvements are needed, the eFolder concept aims to improve on MS diagnosis, tracking, and research. The eFolder will bring a novel and comprehensive approach to observe longitudinal Ms lesion changes in MR, and deciding treatment plans that best suit the MS patient's profile.

REFERENCES

[1] National Multiple Sclerosis Society http://www.nationalmssociety.org/about-multiple-sclerosis/index.aspx

[2] Cree B, Khan O, Bourdette D, et al. "Clinical characteristics of African Americans vs Caucasian Americans with Multiple Sclerosis" Neurology 63:2039-2045 (2004)

[3] Yamasaki K, Kira J, Kawano Y et al. "Western versus asian types of multiple sclerosis: Immunogenetically and clinically distinct disorders" Annals of Neurology 40:4 569-574 (2004)

[4] Lebrun C, Bensa C, Debouverie M, Wiertlevski S, Brassat D, de Seze J, et al. Association between clinical conversion to multiple sclerosis in radiologically isolated syndrome and magnetic resonance imaging, cerebrospinal fluid, and visual evoked potential: follow-up of 70 patients. *Arch Neurol*. Jul 2009;66(7):841-6.

[5] Petronella Anbeek, Koen L. Vincken, Matthias J.P. van Osch, Robertus H.C. Bisschops, and Jeroen van der Grond. "Probabilistic segmentation of white matter lesions in MR imaging." NeuroImage, 21(3):1037{1044, Mar 2004.

[6] Wong A, Gertych A, Zee CS, Guo B, Liu BJ, "A CAD system for assessment of MRI findings to track the progression of multiple sclerosis," Proceedings of SPIE Medical Imaging, 65142U-1-7 (2007).

[7] Moin P, Ma K, Amezcua L, et al. "The Development of an MRI Lesion Quantifying System for Multiple Sclerosis Patients Undergoing Treatment" Proceedings of SPIE Medical Imaging, Vol. 7264-72640J (2009)

[8] Paul A. Yushkevich, Joseph Piven, Heather Cody Hazlett, Rachel Gimpel Smith, Sean Ho, James C. Gee, and Guido Gerig. User-guided 3D active contour segmentation of anatomical structures: Significantly improved efficiency and reliability.*Neuroimage* 2006 Jul 1;31(3):1116-28.

Content-based numerical report searching for image enabled case retrieval

Liang Xue, Tonghui Ling, Jianguo Zhang

Laboratory for Medical Imaging Informatics, Shanghai Institute of Technical Physics, Chinese Academy of Science, Shanghai

Abstract

One way to improve accuracy of diagnosis and provide better medical treatment to patients is to recall or find records of previous patients with similar disease features from healthcare information systems which already have confirmed diagnostic results. In most situations, features of disease may be described by other kinds of information or data types such as numerical reports or a simple or complicated SR (Structure Reports) generated from Ultrasound Information System (USIS) or from computer assisted detection (CAD) components, or laboratory information system (LIS). In this presentation, we described a new approach to search and retrieve numerical reports based on the contents of parameters from large database of numerical reports. We have tested this approach by using numerical data from an ultrasound information system (USIS) and got desired results both in accuracy and performance. The system can be wrapped as a web service and is being integrated into a USIS and EMR for clinical evaluation without interrupting the normal operations of USIS/RIS/PACS. We give the design architecture and implementation strategy of this novel framework to provide feature based case retrieval capability in an integrated healthcare information system.

Keywords: Numerical Record Retrieval, High Dimensional Indexing, VA-Trie, Ultrasound Information System(USIS), Cardiology Examination

1. Introduction

The CBIR (Content-based image retrieval) technology has been proposed for retrieve images for decision support in imaging diagnosis. Also, the text retrieval technology has been used for text reports searching in RIS (Radiological Information System) and CIS (Clinical Information System). However, features of disease may be described by other kinds of information or data types such as numerical reports, a simple or complicated SR (Structure Reports) generated from Ultrasound Information System (USIS) or from computer assisted detection (CAD) components, or laboratory information system (LIS). The content-based searching and retrieval for Structured Report are also crucial for medical professionals to find similar cases from medical information systems. A structured report usually has tables and contains multiple dimension information, e.g., some dimensions just having two values such as 1 or 0, other dimensions being texts to describe the characters of test items, but most dimensions having numerical values measured by specific modalities. Figure 1 shows an ultrasound report about cardiology examination, which contains 8 dimensions of numerical values.

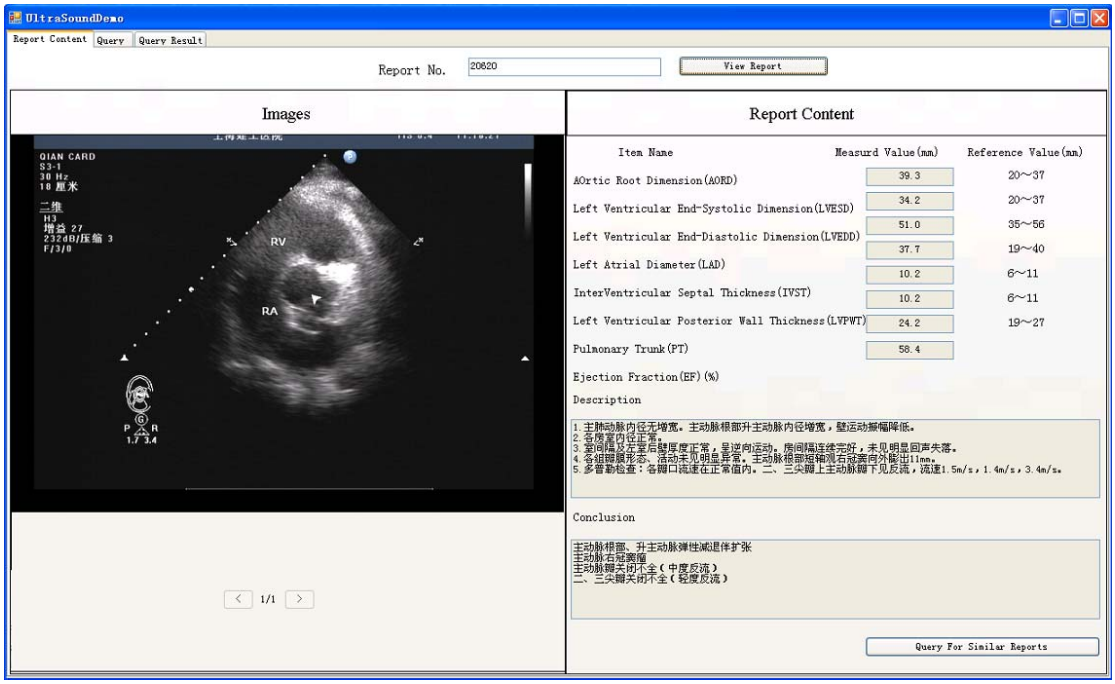

Figure 1. Ultrasound report of cardiology examination

Similarly with RIS, it was usually using key words such as patient ID, study ID, and Procedure codes to search and query USIS to find reports. It is difficult to use multiple dimension numerical values or similar content to search and find the similar cases in USIS.

We had developed a novel method combining text retrieval and typical CBIR techniques to search large-scale medical image database in integrated RIS/PACS for computed aided decision support and presented this research work in PACS and Imaging Informatics of 2009 SPIE conference on Medical Imaging[3]. The text retrieval process in the first phase was used as a navigation method for finding relevant candidate images, and similarity computing was processed between user query image and the candidate images. In this paper, we presented a new approach to search and query image-enabled cases from USIS with content of SR of US, gave the preliminary testing results and discussed how to integrate this capability into clinical environment.

2 High Dimensional Information Indexing

2.1 Brief of High Dimensional Indexing

In last decade, many new technologies have been developed to enable content-based multimedia information retrieva1, and meanwhile, there were still many difficult problems having not being solved, such as high dimensional space indexing efficiently to support large scale high dimensional content-based similarity query and retrieval. So, there are many indexing methods have been proposed to solve this problem，such as R-Tree [1] and A-Tree [2]，VA-File [4], etc. Most high dimensional algorithms are based on data-partitioning such as R-Tree and A-Tree. For example, in the algorithm of R-Tree, neighbor vectors are covered by MBRs (Minimum Bounding Rectangles) which are organized in a hierarchical tree structure. The VA-File (Vector

Approximation File) is another kind of algorithms to index high dimensional vectors. VA-File divides the data space into cells and allocates a bit-string to each cell. The vectors inside a cell are approximated by the cell, and the VA-File itself is simply *n* array of these geometric approximations. During searching, the entire VA-File is scanned to select candidate vectors. Those candidates are then verified by accessing the vector files.

Structured report searching or numerical content-based retrieval has similar problem of high dimension indexing such as CBIR in medical image, but the most CBIR algorithms can't be used here for the following reasons:

(1) Data-partitioning based algorithms can only index and retrieve data with fixed dimensions. For example, if one creates an index with 10 dimensions, one can only fill the index with 10 dimensional vectors, and also one can only retrieval data with 10 dimensional vectors. But in medical records, most structured reports may have numerical data with various data types and various dimensions. In this situation, some dimensions or parameters of a patient report may be null in the report, and others may have values, and other patients may have different parameters in their reports.

(2) We have tested most of high dimensional indexing algorithms and concluded that the performance of query and retrieval was good if the number of dimensions were less 20, but the performance would decrease as the more dimensions were considered. It is well-known as the "dimensional curse"

After doing research on different high dimensional indexing methods, we adopted VA-Trie indexing algorithm in our research for numerical report content-based searching and retrieval.

2.2 Structure, Operation and Advantage of VA-Trie Algorithm

The key of VA-Trie is to adopt the VA concept in VA-File and then employing the Trie structure to organize and manage the approximations.

VA-Trie Structure:

Figure 2 shows the structure of VA-Trie.

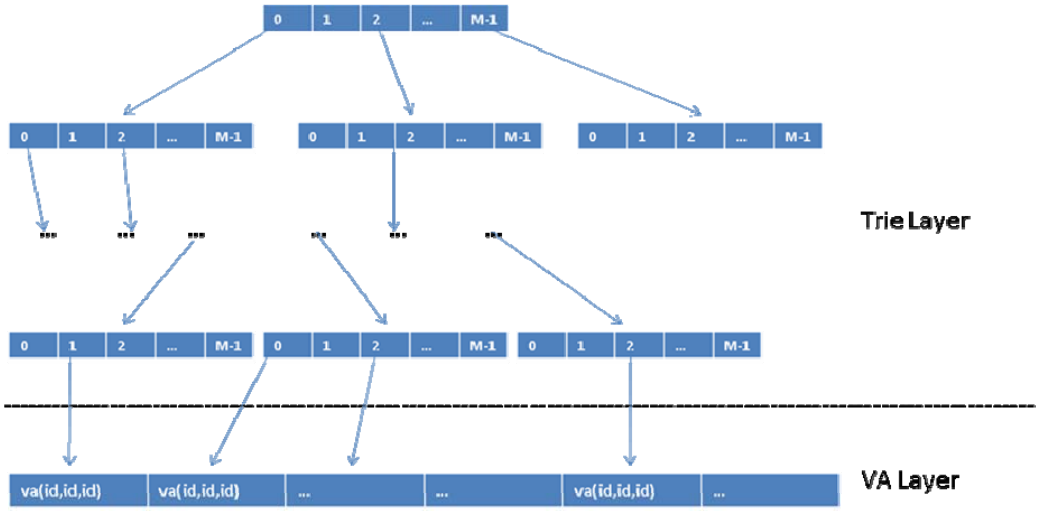

Figure 2. Structure of VA-Trie

The VA-Trie consists of two components: The Trie layer and the VA layer. The Trie layer is used for searching the addresses of vectors on VA layer and the VA layer is used to store approximated vectors.

(1) Trie layer: The Trie layer is a tree structure. The depth of the tree is the same as the dimensionality of the indexed vector. Root node represents the dimension *1* of a vector, the son nodes of the root represent the dimension *2*, and so on. There are *M+1* partition points in dimension *i* to divide this dimension into *M* segments and there is a son node in dimension *i+1* linked to each segment of the nodes in this dimension. The larger tree would be, the higher dimensionality and the number of segments of each dimension are. However, in high dimensional space, only few nodes are not null, so the scale of the tree is limited. There isn't any son node in leaf nodes, but some values point to particular blocks in the VA layer.

(2) VA layer: The VA layer is a file on the hard disk and is consist of blocks. Records stored in one block are site to each other and the size of each block is fixed. If one block is full, a new block will be created to store new record and the former block will have a tag pointing to the new block.

VA-Trie Operations:

Here we introduce two basic operations on VA-Trie: inserting and searching

(1) It is easy to insert a vector into VA-Trie: First, we get an approximation of the vector according to the partition points of each dimension. Second, find out the path of the approximated vector in Trie layer. Third, write the *id* information of the vector into the corresponding block of the path in the VA layer.

(2) The searching algorithm is based on the distance of two vectors. We define the distance between two vectors as follows:

$$D(\vec{\mathbf{q}}(q_1, q_2, ..., q_n), \vec{\mathbf{p}}(p_1, p_2, ..., p_n)) = \sum_{i=1}^{n} | q_i - p_i | \qquad (1)$$

Where *D* is the Manhattan distance, and represents the distance of vector $\vec{\mathbf{q}}$ and $\vec{\mathbf{p}}$. The q_i is the *i-th* component of $\vec{\mathbf{q}}$,*n* is the dimensionality**.**

We also defined a parameter called D_{max} which represents the searching range for a search operation. The search procedure starts from the root node of the Trie layer according to the method shown in Figure 3.

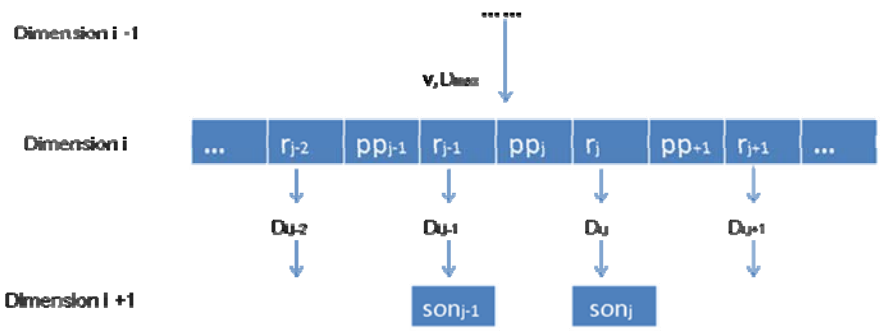

Figure 3. Search algorithm in a Trie node

In Figure 3, the search procedure gets to a node in dimension *i* with query vector $\vec{v}$ and range D_{max}. For range r_j in dimension *i*, we compare $D_{i,j}$ with D_{max}**.**

$$D_{i,j} = \begin{cases} D_{i-1} & pp_j \le v_i \le pp \\ D_{i-1} + |v_i - pp_j| & v_i < pp_j \\ D_{i-1} + |v_i - pp_{j+1}| & v_i > pp_{j+1} \end{cases} \quad (2)$$

Here, D_{i-1} is the distance generated in first *i-1* dimensions, v_i is the *i-th* component of $\vec{v}$ and pp_j is the *j-th* partition point in dimension *i*. The search procedure will switch to corresponding son node of r_j if $D_{i,j}$ is lower than D_{max}. This procedure will continue until we get to leaf nodes. The search procedure in Trie layer will guide us to the position of the approximated vectors on the VA layer and the approximated vectors will be achieved in the returned result set.

Advantages:

(1) This VA based algorithm outperforms data-partitioning algorithms(R- Tree) especially when the dimensionality is high. Also, vectors with some dimensions empty can also been indexed in this algorithm.

(2) The VA-Trie algorithm inherits the method of VA from VA-File. Instead of scanning the entire VA-File for search, it uses a tree structure to manage the cells. It will avoid the unnecessary scanning time when the number of cells becomes very large.

3 Content-Based Numerical Report Searching and Retrieval

In this section, we presented a framework to build content-based searching and retrieval in an integrated USIS/PACS environment using the algorithm of VA-Trie described in section 2. We first discussed the procedure of indexing and searching. Then, we presented a similarity computation algorithm to verify the query results.

3.1 Indexing

The USIS is widely used in ultrasound department to manage the workflow as well as diagnostic reports. In our design for numerical reports or SR searching and retrieval, we created index according to the following steps: First, all ultrasound reports of the specific examination were analyzed statistically on each dimension. Second, we found proper partition points and range on each dimension using the deviation, the maximum value, the minimum value and the statistical distribution from the first step. The best partition of one dimension was to make all reports uniformly distributed in a specific range. Third, we selected the parameters of the VA-Trie with the partition points of each dimension. Last, each report was inserted into the index. Figure 4 shows the indexing procedure.

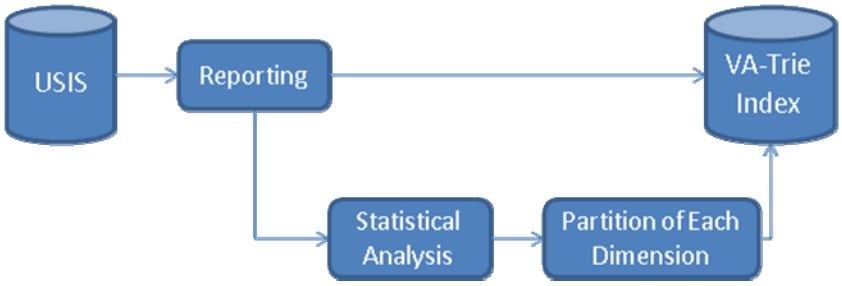

Figure 4: Indexing procedure

3.2 Searching and Retrieval

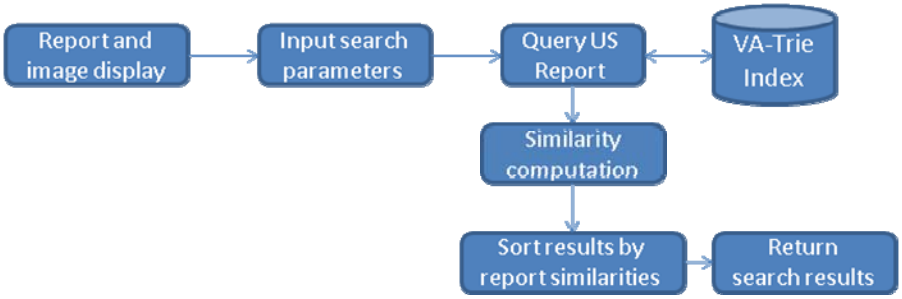

Figure 5: Retrieval procedure

Figure 5 shows the searching and retrieval procedure. When a new case was available from a modality or a clinical PACS and was viewed on PACS/USIS workstation, the doctor might want to find the similar cases with similar measured parameters from USIS and PACS. So, the query parameters input from user should contain the following information: the query vector of the report($\vec{v}$), the query range(D_{max}), and weight of each dimension($w_1, w_1, \ldots w_n$).

We did some improvements to the Manhattan distance of two vectors:

$$D'(\mathbf{q}(q_1, q_2, \ldots, q_n), \mathbf{p}(p_1, p_2, \ldots, p_n)) = \sum_{i=1}^{n} w_i \cdot | q_i - p_i | / s_i \qquad (3)$$

s_i is the deviation of dimension i. We introduced deviation here because of the difference between the statistical distribution of dimensions. The w_i is the weight of dimension i and represents the importance of dimension i in this search.

The output of VA-Trie index is a set of vectors. If the distances between the input vector and the queried vectors are lower than or around D_{max}, then, the candidate report similarity is calculated as follows:

$$S(\mathbf{q}, \mathbf{p}) = \exp(-D'(\mathbf{q}, \mathbf{p})) \qquad (4)$$

The vectors which are near to the input vector will have high similarity. The queried results are then sorted by report similarities and returned to user.

4. Implementation

In our clinical practice, we developed a prototype system of content-based retrieval for US numerical reports or SR about cardiology examination and tested it in Jian-Gong hospital in Shanghai. The System included High Dimensional Retrieval server, PACS and USIS. Figure 6

showed the diagram of the prototype system.

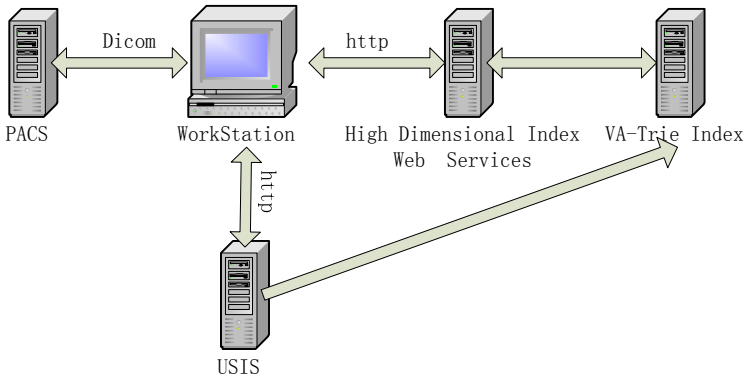

Figure 6. Integration of High Dimensional Index, PACS and USIS

To index the reports, we first scaned the USIS and constructed a vector for each cardiology report. Then we did statistical analysis on each dimension of the vectors and built the structure of the index. Existing Reports of cardiology examination were then inserted into the index. Every new generated cardiology report could be indexed into the index server. The high dimensional index service could be accessed from USIS clients through a web server.

We built a search GUI and integrated it into the USIS workstation. When an user viewed reports and images through USIS workstation, he or she could use search GUI to adjust the parameters and its' ranges for specific pathology. The parameters then input into the high dimensional index server, and a list of similar cases were returned and sorted by similarities. Users could get contents and images of each query result from USIS and PACS. All these works were done without interrupting the normal operation of USIS and PACS.

5. Results

In our preliminary testing, we had 60,000 records included and indexed in the High Dimensional Index Server and each record was 8-dimensional vector. In order to achieve a better performance, we divided the value range of each dimension into 10 segments.

A Dell PowerEdge Server R200 with Intel Xeon 3050 CPU(2.13GHz), 2 GB RAM, and 160GB 7200rpm HD was used to create index and to provide search service to clients, and the operating system of the server was windows server 2003.

Figure 7 shows the images and contents of the query. Figure 8 shows the search GUI and search results with medium query range.

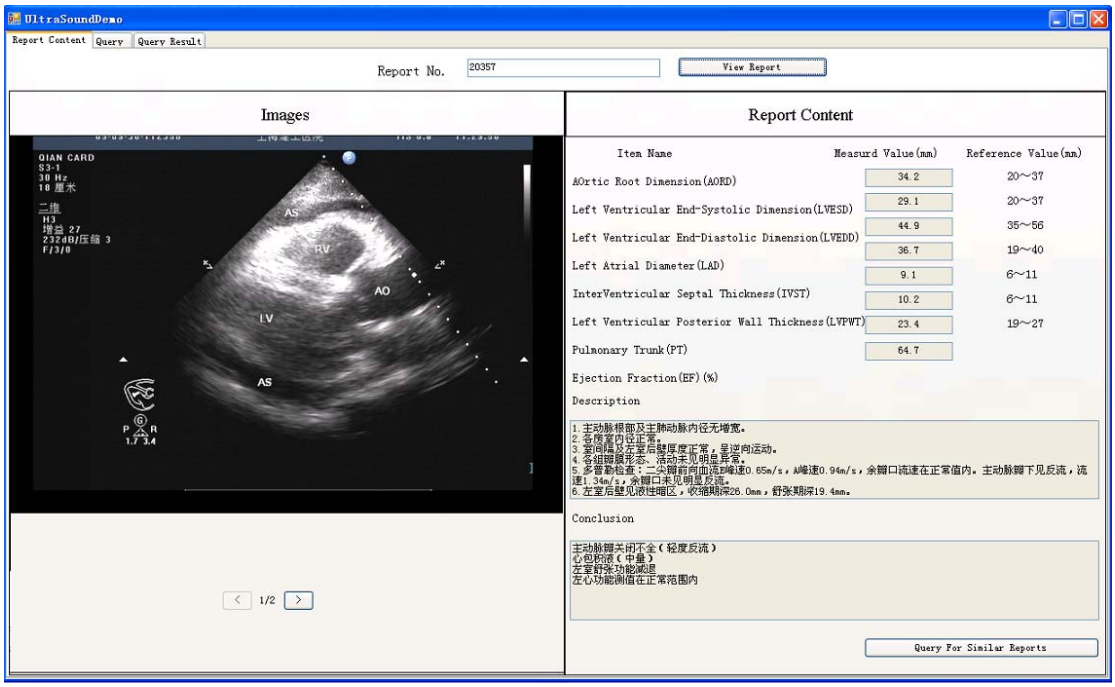

Figure 7. The input report with images

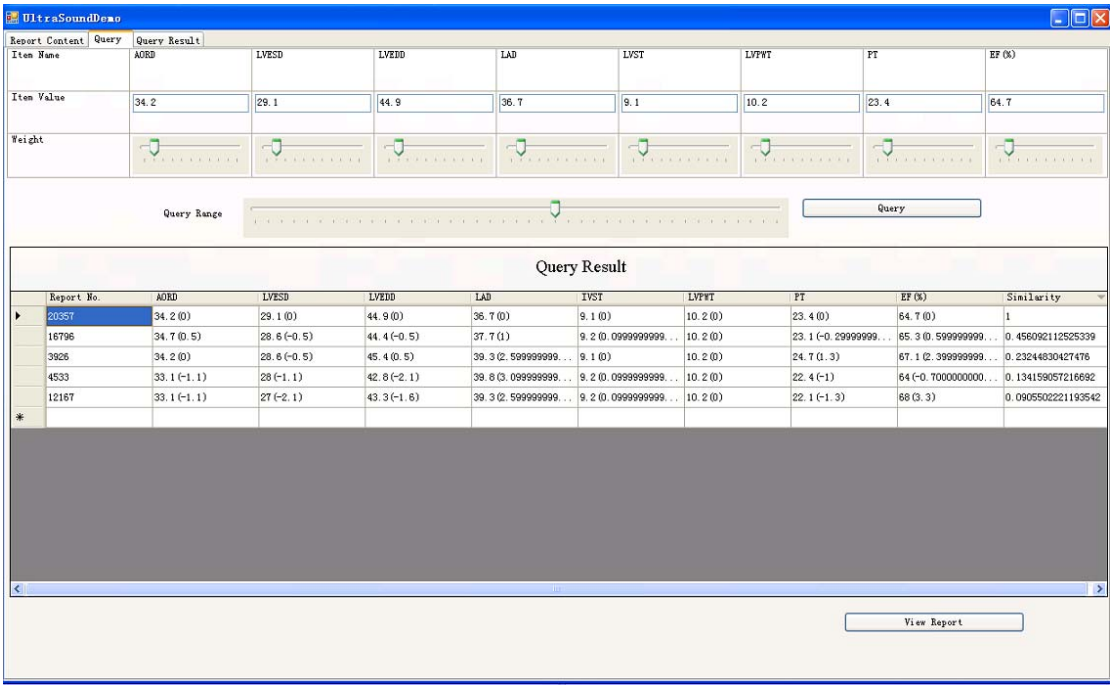

Figure 8. The queried list of results with medium range

In Figure 8, we got 5 similar reports with the various values in each dimension. The last column shows the similarity of each result report. The first row shown in the list is just the query report for a perfect match.

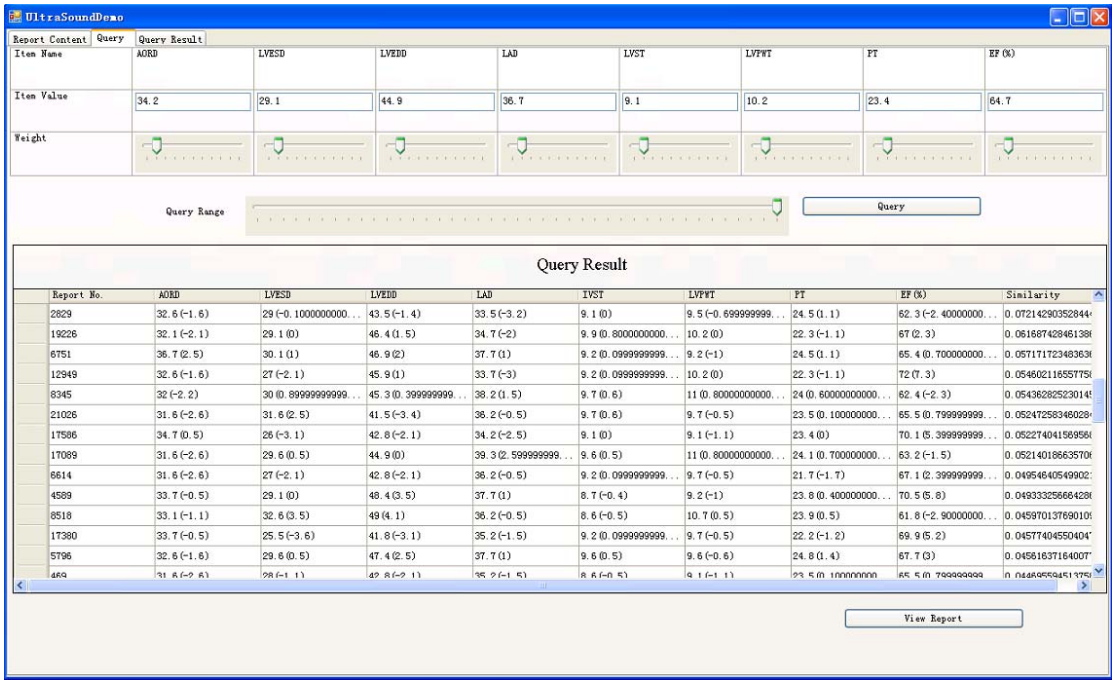

Figure 9. Queried Results with high query range

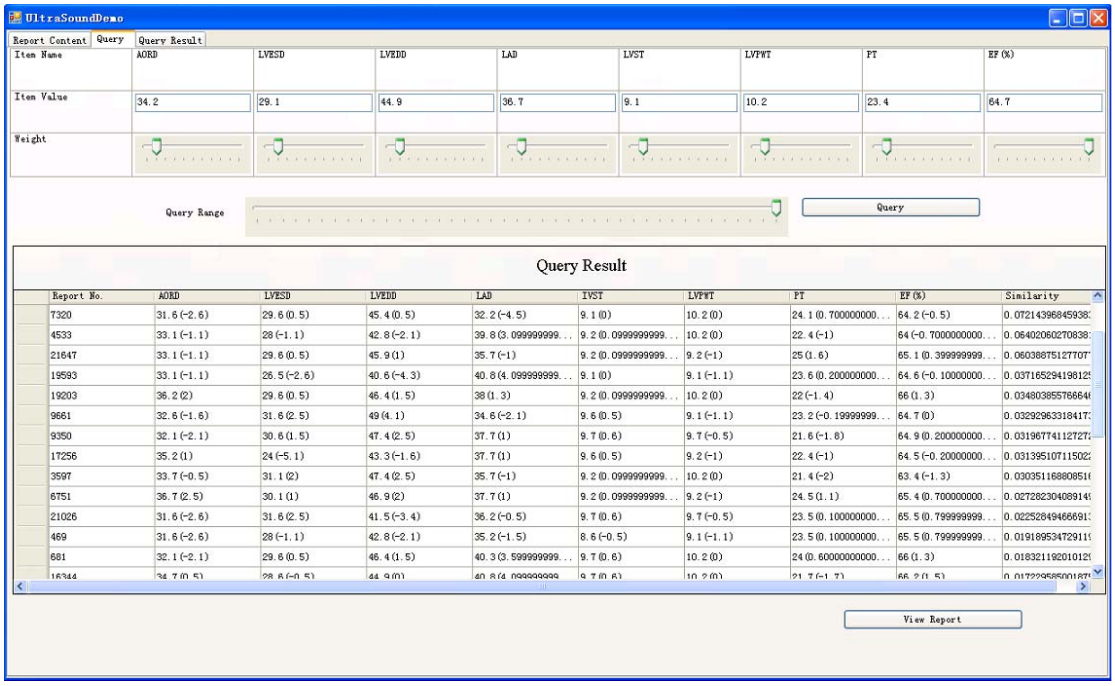

Figure 10. The queried results with high query range and different weights

In Figure 9, we set query range to little bits of high. We got a result set with 79 reports. Comparing with Figure 8, the queried results contained more reports which had lower similarity. In Figure 10, the query range was higher and we set the weight of the last dimension (Ejection Fraction) to 10.0. We got 32 results this time.

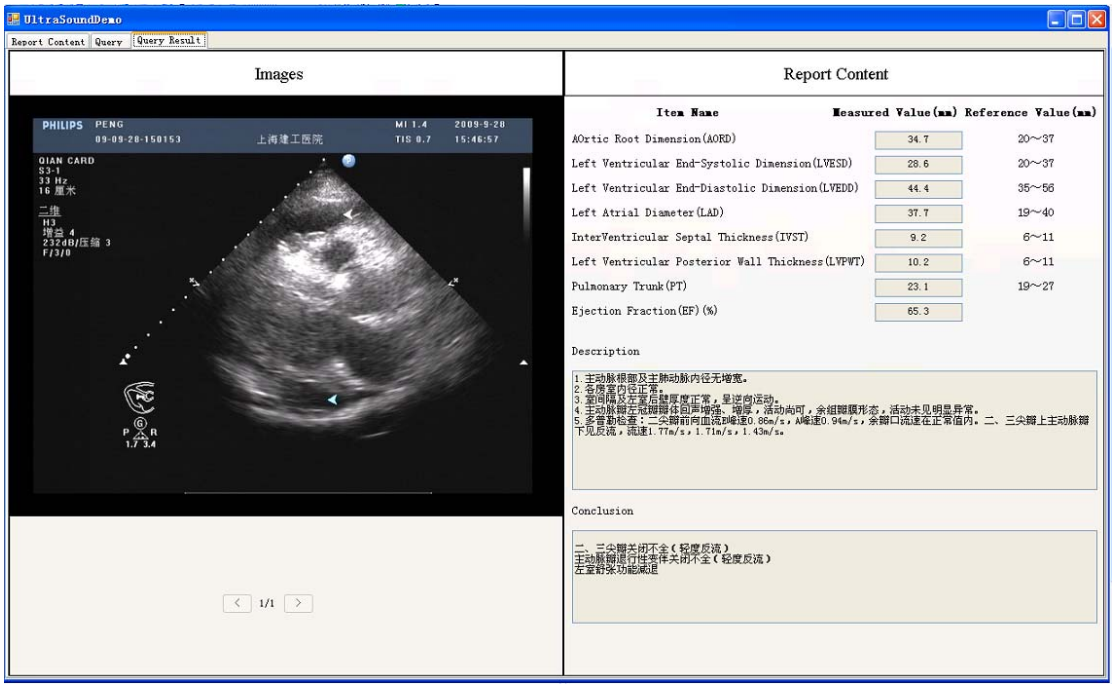

Figure 11. Retrieved report with corresponding images

If the feature similarities of a queried report were close to that of the input report, the pathologies described by queried report may also similar to that described by the input report. Figure 11 shows the report text and image related to the queried report which has a similarity of 0.456 with that of Figure 7 under default weight 1.0. The impresses of both reports showed that these two patients had the same pathologies of:

(1) Declination of diastolic of the left ventricle.

(2) Aortic insufficiency.

(3) Mild regurgitation.

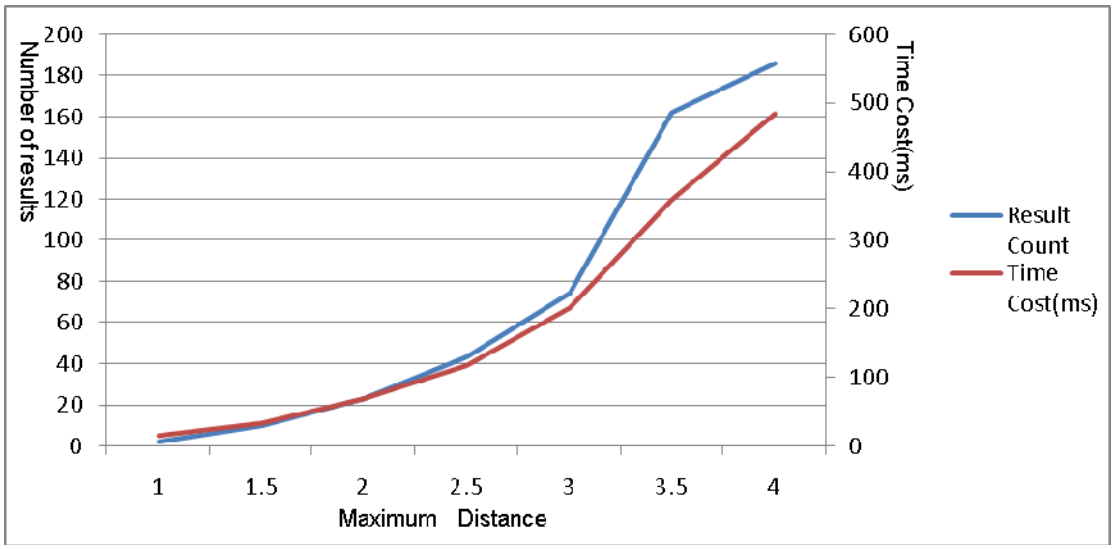

Figure 12. Sensitivity of con

Figure 12 shows the performance of querying different reports in the 60,000 reports which was measured by the average responding times and averaging number of retrieved results v.s.

maximum distance. The horizontal axis shows the maximum distance defined in equation (3) , the left vertical axis shows the number of results, and the right vertical axis shows the time required. In this testing, the weight of each dimension was 1.0, and the maximum distance was changed from 1.0 to 4.0. The querying times depends on the querying range set in dimension. The larger the similarity range between the input and candidate reports, the more number of queried reports would be retrieved, and the longer the responding times would take for searching. So, the developed prototype system would have good performance in content-based numerical report querying and retrieval if the similarities were properly set up.

6. Conclusions

In this presentation, we presented the design method of content-based numerical report searching and retrieval system. We chose VA-Trie as the indexing and searching algorithm and did some improvement for medical applications. We developed a prototype system of content-based retrieval for ultrasound information system which managed US numerical reports. We tested and evaluated this system by using numerical data of cardiology examinations in ultrasound information system (USIS) and got desired results both in accuracy and performance. The accessing interfaces of this system were wrapped as web services, and the developed system could be integrated into a USIS for clinical evaluation without interrupting the normal operations of USIS/RIS/PACS.

7. Acknowledgement

This research was supported in part by National Nature Science Foundation of China (Grant No. 30570512), Department of Science and Technology of Shanghai (No. 05DZ19510), and Department of Science and Technology of China (No. 2007BAH06B01/B02/B03).

8 . Reference

1. A.Guttman, R-trees: a dynamic index structure for spatial searching**,** Proceedings of the 1984 ACM SIGMOD international conference on Management of data Boston, Massachusetts.
2. Sakurai, Yasushi and Yoshikawa, Masatoshi and Uemura, Shunsuke and Kojima, Haruhiko (2000) The A-tree: An Index Structure for High-Dimensional Spaces Using Relative Approximation. VLDB 2000, Proceedings of 26th International Conference on Very Large Data Bases, September 10-14, 2000 .
3. Zhenyu He, Yanjie Zhu, Tonghui Ling, Jianguo Zhang, Combining Text Retrieval and Content-based Image Retrieval for Searching Large-scale Medical Image Database in Integrated RIS/PACS Environment SPIE 2009
4. Weber, Roger and Blott, Stephen (1998) A Quantitative Analysis and Performance Study for Similarity-Search Methods in High-Dimensional Spaces. In VLDB 98: Proceedings of the 24rd International Conference on Very Large Data Bases
5. Dong Daoguo，Liu Zhenzhong，and Xue Xiangyang, VA-Trie: A New and Efficient High Dimensional Index Structure for Approximate k Nearest Neighbor Query, Journal of Computer Research and Development 42(12)2213~2218,2005

SELECTED PEER REVIEWED REPRINTS

Int J CARS
DOI 10.1007/s11548-009-0387-x

ORIGINAL ARTICLE

A multimedia electronic patient record (ePR) system for image-assisted minimally invasive spinal surgery

Jorge Documet · Anh Le · Brent Liu · John Chiu · H. K. Huang

Received: 23 April 2009 / Accepted: 21 June 2009

Abstract
Purpose This paper presents the concept of bridging the gap between diagnostic images and image-assisted surgical treatment through the development of a one-stop multimedia electronic patient record (ePR) system that manages and distributes the real-time multimodality imaging and informatics data that assists the surgeon during all clinical phases of the operation from planning Intra-Op to post-care follow-up. We present the concept of this multimedia ePR for surgery by first focusing on image-assisted minimally invasive spinal surgery as a clinical application.
Methods Three clinical phases of minimally invasive spinal surgery workflow in Pre-Op, Intra-Op, and Post-Op are discussed. The ePR architecture was developed based on the three-phased workflow, which includes the Pre-Op, Intra-Op, and Post-Op modules and four components comprising of the input integration unit, fault-tolerant gateway server, fault-tolerant ePR server, and the visualization and display. A prototype was built and deployed to a minimally invasive spinal surgery clinical site with user training and support for daily use.
Summary A step-by-step approach was introduced to develop a multimedia ePR system for imaging-assisted minimally invasive spinal surgery that includes images, clinical forms, waveforms, and textual data for planning the surgery, two real-time imaging techniques (digital fluoroscopic, DF) and endoscope video images (Endo), and more than half a dozen live vital signs of the patient during surgery. Clinical implementation experiences and challenges were also discussed.

Keywords ePR · System integration · Pre-, Intra- and Post-Op surgical workflow · Minimally invasive spinal surgery

Abbreviations

API	Application program interface
BIS	Bispectral index system
CO_2	Carbon dioxide
CR	Computed radiography
CSI	California Spine Institute
CSS	Cascading style sheet
CT	Computed tomography
DICOM	Digital imaging and communications in medicine
EMG	Electromyography
ePR	Electronic patient record
GIF	Graphics interchange format
GUI	Graphical user interface
HIPAA	Health Insurance Portability and Accountability Act
HIS	Hospital information system
HTML	Hyper text markup language
HTTP	Hyper text transfer protocol
HTTPS	Hyper text transfer protocol secured
ICT	Information and communication technology
IA-MISS	Image-assisted minimally invasive spinal surgery
IPILab	Image Processing and Informatics Laboratory
IRB	Institutional Review Board
IT	Information technology

J. Documet (✉) · A. Le · B. Liu · H. K. Huang
IPILab, Department of Radiology, Keck School of Medicine,
University of Southern California,
1450 San Pablo Street, Suite DEI 2100,
Los Angeles, CA 90033, USA
e-mail: documet@usc.edu

J. Chiu
California Spine Institute Medical Center Inc,
1001 Newbury Road, Thousand Oaks, CA 91320, USA

Published online: 26 July 2009

IU	Integration unit
IVF	Intravenous fluid
JPEG	Joint Photographic Expert Group
LCD	Liquid crystal display
MB	Megabytes
mmHg	Millimeters of mercury
MRI	Magnetic resonance imaging
OR	Operating room
PACS	Picture archiving and communication system
PHP	PHP: hypertext preprocessor
PNG	Portable network graphics
RAM	Random access memory
RIS	Radiology information system
RS232	Recommended Standard 232
SC	Secondary capture
SDK	Software development kit
TB	Terabytes
USC	University of Southern California
VAS	Visual analog scale
VGA	Video graphics array

Introduction

Bridging the gap between diagnostic images and surgical treatment

This paper presents the concept of bridging the gap between diagnostic images and image-assisted surgical treatment through the development of a one-stop multimedia electronic patient record (ePR) system that manages and distributes the real-time multimodality imaging and informatics data that assists the surgeon during all clinical phases of the operation from planning Intra-Op to post-care follow-up. We present the concept of this multimedia ePR for surgery by first focusing on image-assisted minimally invasive spinal surgery as a clinical application. For this particular surgical procedure, in addition to images, clinical forms, waveforms, and textual data for planning the surgery, two real-time imaging techniques (digital fluoroscopic, DF) and endoscope video images (Endo), and more than half a dozen live vital signs of the patient during surgery are needed to assist and monitor the surgery. All these data have to be acquired, displayed and archived in real-time as well.

Minimally invasive spinal surgery

Back and neck pain is the price human beings pay for poor posture, prolonged sitting, lifting, repeated bending, obesity, and injury from accidents. This ailment gives the United States with a massive economic headache. Approximately 85% of inhabitants of the Western world are afflicted with some degree of back or neck pain at some point in their lives [1]. About 25% of our population has been incapacitated for 2 weeks or more due to back pain and an estimated 8 to 10 million people have a permanent disability from it [2–5]. The economic impact is obvious. In most cases, simple treatments such as bed rest, exercise, physiotherapy, and pain medication bring relief. Many sufferers are not so fortunate. If one or more of their vertebral discs ruptures and presses on nerve roots, the pain radiating from the back or neck and down the limbs can be incapacitating and severe. Until recently, the only treatment was surgical removal of part of the ruptured disc, a major operation that required general anesthesia, the dissection of muscle, removal of bone, manipulation of nerve roots, and, at times, bone fusion. In an effort to overcome the disadvantages of traditional surgical techniques, the scientific medical community began exploring the use of endoscopy (arthroscopy) for minimally invasive spinal surgery surgical operation [6,7].

An endoscope provides clear visualization and magnification of deep structures in real-time. With the advancement of scientific technology and miniaturization, including fiber optics, video imaging technology, laser treatment and experience gained through minimally invasive spinal surgery, there is a less traumatic discectomy procedure for some patients with disc problems. In the recent years, development of image-assisted surgery has improved the precision and reduced surgical tissue trauma. Figure 1 depicts the cervical, thoracic and lumbar spines on MRI before (Pre-Op) and after (Post-Op) the endoscopic-guide spinal discectomy. The lesion(s) at each spinal region is clearly cured after the surgery.

Rationale for a multimedia ePR system for image-assisted minimally invasive spinal surgery

Minimally invasive spinal surgery will be the method of choice for future spinal surgery to treat cases of herniated lumbar discs, post fusion junctional disc herniation, neural compression, osteophytes, spinal stenosis, vertebral compression fractures, spinal tumor, synovial cysts and other types of spinal traumas. Despite the overall advantageous and benefits of minimally invasive spinal surgery compared to conventional open spinal surgery, there are challenges remained in minimally invasive spinal surgery including (1) integration of Pre-, Intra-, and Post-Op surgical data from scattered data acquisition systems, (2) overcoming the difficulty of real-time data collection during the surgery, and (3) improving the efficiency of surgical workflow. An integrated real-time multimedia ePR system is an ideal solution to overcome these challenges. If successful, it will take Minimally Invasive Spinal Surgery to a higher level of excellence by combining surgical expertise in minimally invasive spinal surgery with the frontier advancements in imaging informatics.

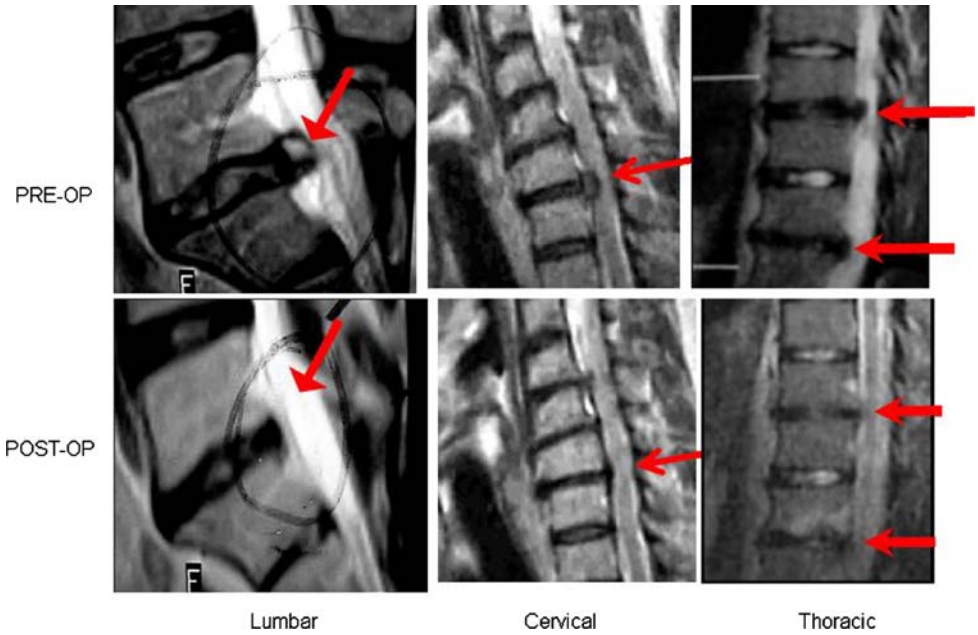

Fig. 1 Minimally invasive spinal surgery on cervical, thoracic, and lumbar spines. *Upper row* Pre-operation arrows show the areas where the disc protrudes the spine. *Lower row* Post-endoscopic-assisted spinal surgery shows the lesions have been cured

The goals of the ePR

The two goals of this research development are:

(1) To develop a totally integrated multimedia ePR system for image-assisted minimally invasive spinal surgery. All data collected for the patient from Pre-Op, Intra-Op and Post-Op will be acquired, displayed, and archived during each clinical phase of the surgical workflow. Any data record of the patient in the ePR can be retrieved instantaneously anytime and anywhere.

(2) To deploy the ePR at a clinical site for daily clinical use. Figure 2 depicts the ePR prototype system running at the Minimally Invasive Spinal Surgery Operating Room (OR) of a clinical site, with two large LCDs (liquid crystal display), one for the Pre-Op consultation integrated display, and the second for the Live Intra-Op integrated display.

Materials and methods

General minimally invasive spinal surgery workflow

The minimally invasive spinal surgery current high-level operation workflow includes pre-surgical consultation, pre-operation preparation, intra-operation image and vital signs acquisition and display, post-surgery documentation to patient recovery monitoring. The workflow can be broken down into three phases [8,9]: (1) before surgery, (2) during surgery (including the preparation) and (3) post surgery. Each of the three clinical phases will be discussed below.

(1) Before surgery (Pre-Op): this phase is the workflow involved prior to the actual surgical procedure. In the Pre-Op workflow, usually the patient presents with a problem and is evaluated by the physician to determine whether Minimally Invasive Spinal Surgery is needed and whether it would be helpful to the patient. If this case is true, then a procedure is scheduled. At this stage the surgeon or surgeons in combination with the physician assistant plan the surgical procedure using digital diagnostic images such as CR, CT and MRI. In addition to the information obtained from the medical studies, the patients also fill out a set of surveys that determine the level of pain that they feel.

(2) During surgery (Intra-Op): during the surgical procedure, the surgeon(s) operate on the different disc(s) that need to be corrected. While operating, there is a significant amount of data being acquired that help monitor the body response of the patient to the procedure. This includes video and image data acquired with the endoscope. A single vertebrae procedure usually lasts 30 min on average.

(3) After surgery (Post-Op): during this Phase the patient recovers from surgery. The patient is continuously monitored in the recovery area to assure all vitals signs are stable. In addition, a set of tests are also performed to assess the outcome of the surgical procedure which includes an additional set of forms that the patient fills out.

The recovery period after surgery lasts from 45 min to 1 h. The patient is then discharged. Therapy can begin the next day and the patient can go back to work within 2–3 days.

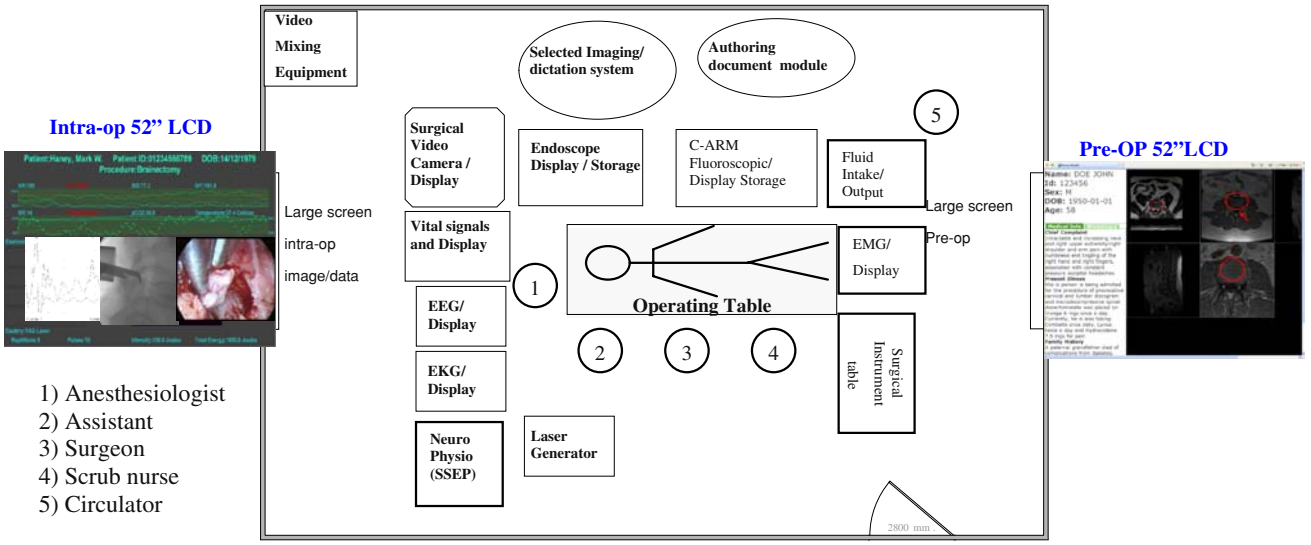

Fig. 2 Schematic of the dynamic multimedia ePR system for image-assisted minimally invasive spinal surgery. The ePR prototype system is running at the minimally invasive spinal surgery OR of CSI, with two large LCDs (liquid crystal display), one for the Pre-Op consultation integrated display, and the second for the Live Intra-Op integrated display

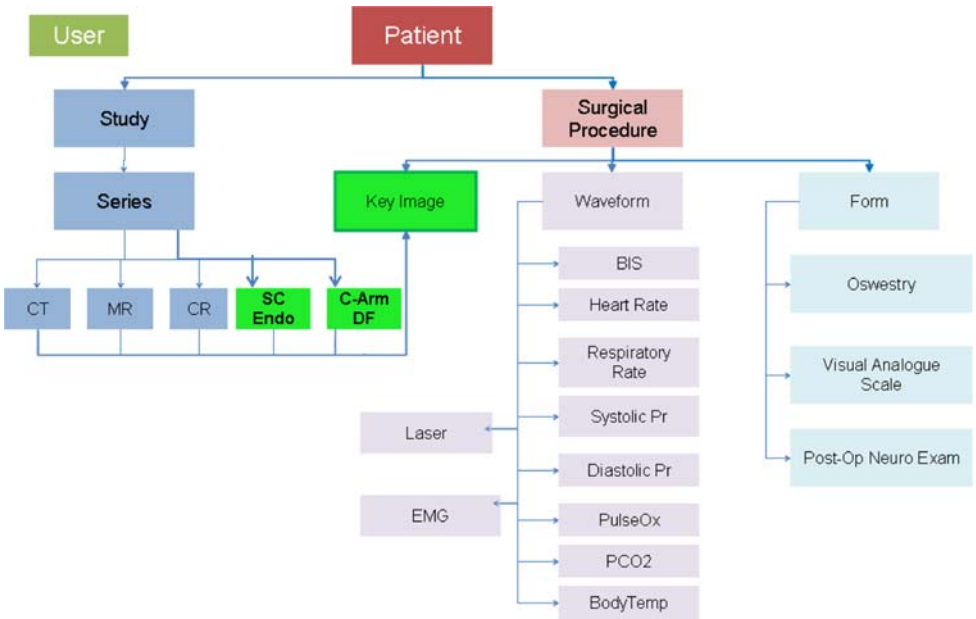

Fig. 3 The data model of the ePR system. It extends the schema of DICOM to accommodate surgical information including live waveform and several standard surgical forms. Additional entities have been augmented to the data model

Data model of ePR system

The data model of the ePR for Minimally Invasive Spinal Surgery has been designed to extend the DICOM data model due to the similarities that exists for medical imaging data at CSI utilizing DICOM. From the DICOM data model the ePR for Minimally Invasive Spinal Surgery follows the relationship between the patient, the medical studies, series and images. The modified data model utilized for the current ePR contains additional entities that describe the data required for minimally invasive spinal surgery. These new elements that are added to the data model include the surgical procedure type, waveforms, the key image, survey forms for pain, and user information for access to the system. The data model is shown in Fig. 3.

The ePR dataflow

The initial data flow utilized by the ePR system was based on the concept of the workflow presented in the general

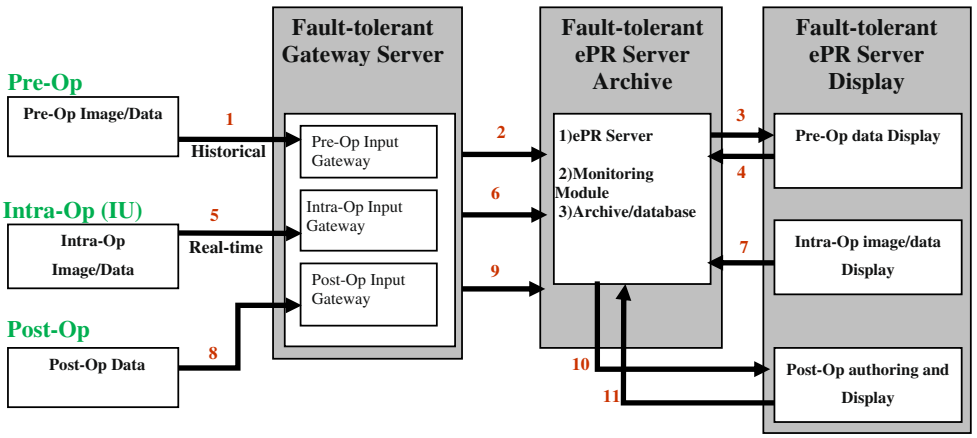

Fig. 4 Dataflow of the ePR system for minimally invasive spinal surgery. There are three time phases (*vertical*): Pre-Op, Intra-Op and Post-Op; and four operational modules (*horizontal*): input units, gateway, ePR Server and database, and visualization and display, which forms a 3×4 matrix. Each *numeral* represents one event in the dataflow explained in the text

minimally invasive spinal surgery workflow and is shown in Fig. 4 where each numeral represents a dataflow event.

There are three time phases, from the top down: the Pre-Op image/data module, the Intra-Op module, and the Post-Op module. Each of these modules contains four components: input module, input gateway, ePR server, and the visualization and display module.

Pre-Op workflow

Following Fig. 4.

(1) Historical medical imaging studies in DICOM format are acquired from the PACS (picture archiving and communications system).
(2) The gateway, which is a component of the ePR system, receives the DICOM images and processes them accordingly. The original image is kept in the ePR and a JPEG version is utilized for display purposes via the web interface of the ePR. All DICOM header information and metadata are extracted and recorded in the database.
(3) Pre-Op authoring is performed by the surgeon(s) and the physician assistants. The surgical procedure information is entered into the ePR. At this Phase the patient's survey pain forms are also entered into the system. The surgeon selects some key images and authors annotations overlaid on the key images that will ultimately be utilized during surgery. The authorized images/data are displayed in the OR utilizing a 52-in. LCD display (see Fig. 1).
(4) Authorized images/data are archived in the ePR server.

Intra-Op workflow

(5), (6) and (7) The integration unit (IU) is connected to all clinical devices in the OR and continuously gathers live data signals from them during the entire surgical procedure, and display them in real-time on the second large 52-in. digital display (see Fig. 1).
(6) The gateway Server receives the data from the IU and stores the data values and images in real-time at the database within the ePR system.

Post-Op workflow

(8) While the patient is in the recovery area, the system continues gathering some vital signs that are transferred to the gateway server.
(9) The gateway server receives the data and stores the data into the database of the ePR system.
(10) The surgeon uses the Post-Op authoring module to create a final report out of the data gathered during the Pre-, Intra-, and Post-Op phases.
(11) The final report will be kept in digital format at the ePR Server as the patients' permanent surgical record.

Minimally invasive spinal surgery ePR system architecture

Recalling Fig. 4 which depicts the workflow and data flow model of the minimally invasive spinal surgery ePR system represented by a 3×4 dimension matrix model. The three rows are Pre-Op, Intra-Op, and Post-Op workflow process Phases; and the four columns are the input data integration unit (IU), input gateway, ePR server, and image/data display. From the system architecture point of view, the ePR system should be designed for efficiency, effectiveness, and reliability of system operations. The fault-tolerant requirement of each component in the system is designed to support other existing components of the system for easy system back-up and cost containment. The ePR System architecture is shown in Fig. 5 and will be discussed in detail in the following paragraphs.

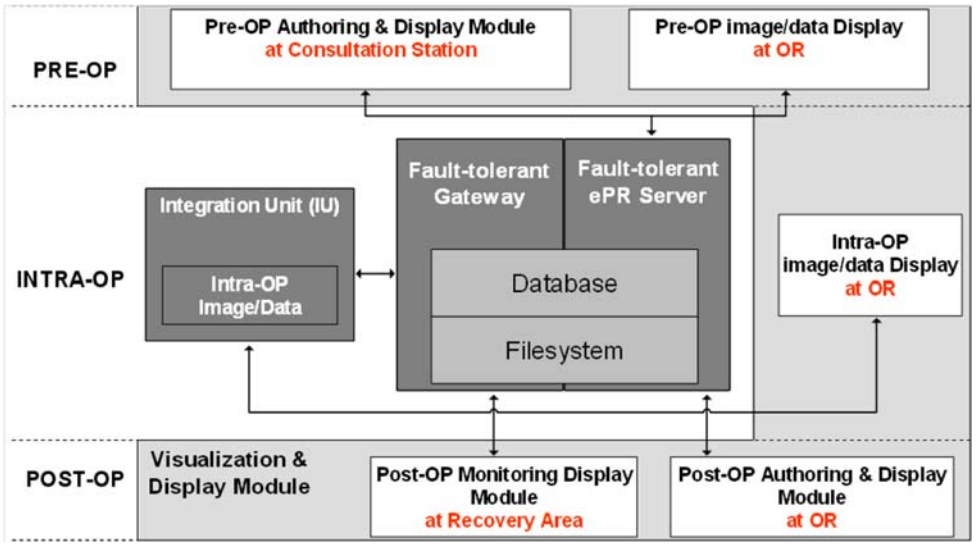

Fig. 5 The ePR system architecture showing three operation phases (first column): Pre-Op, Intra-Op and Post-Op; as well as four operation modules (partitioned and scattered systematically). Some partitioned modules are bundled up together for ease of data transfer and fault-tolerant back-up. The *arrows* show the data flow during the three phases of operation. The outside *light gray color* side-way "U" band is the display module backbone with five *rectangular box* subunits. Inside the opening of the "U" in *dark gray* are the integration unit, fault-tolerant gateway, and fault-tolerant ePR server. Within the gateway and the ePR server, the Database and Filesystem software are interrelated and shared by both components

Four major components in the minimally invasive spinal surgery ePR system

The four major components in the Minimally Invasive Spinal Surgery ePR System are: (1) integration unit (IU), (2) fault-tolerant gateway server, (3) fault-tolerant ePR server, and (4) Visualization and Display. Both the input gateway and the ePR server include data storage and archive, system database, system security, system fault-tolerance, continuous availability and failover. The GUI and display module resides within the ePR Server. All data input systems like medical imaging, surgical video, vital signs waveform recorders, and textual data recorder generate Pre-Op, Intra-Op, and Post-Op data, and they are all categorized as input data. The imaging and data systems that generate information are existing peripheral surgical supported equipment already within the OR but they do not belong to the Minimally Invasive Spinal Surgery ePR system. However, the ePR system must integrate these devices in order to receive the input data that is acquired before, during, and after surgery that support the surgical procedure.

Integration unit (IU)

This component is responsible for acquiring all data from different peripheral devices that are presented in the OR during surgery (Intra-Op) that continuously measure all live vital signs, waveform signals, and surgical related images of the patient undergoing a procedure. The data acquired by the IU from all input devices are synchronized through a master clock and displayed live onto a customized interface using a 52-in. LCD (liquid crystal display) screen (called Intra-Op live display) in the OR. The data gathered during surgery include the following:

- Digital C-ARM fluorographic images
- Digital endoscopic video images
- Waveform signals: EMG (electromyography), BIS (bispectral index), and vitals (blood pressure, heart rate, respiratory rate, pulseOX, body temperature and partial pressure of carbon dioxide).

The images, videos and data points mentioned above are transferred automatically and continuously from the various input sources of the different data devices in the OR during operation that are attached to the data input IU. The data is immediately saved into IU memory. The IU software displays the waveforms, images, and streamed videos properly every second (which is a default value) on the large Intra-Op LCD, and also makes a copy from the memory to the IU local hard drive with 1.5 TB (Terabytes) of storage space every 5 s (which is also a default value). These two default values can be adjusted interactively depending on clinical demands.

Normal procedures for a single vertebra surgery take about 30 min on average. This Intra-Op data is sent continuously to the gateway where the images are processed if needed and then placed in a data folder shared with the ePR server where

they will be permanently archived. The data values are also extracted and saved to the ePR system database.

In addition to the one second input display refresh-rate described in the last section, the IU features a rule-based alert-mechanism that checks each input waveform for data that is out of the normal range. The IU has a set of rules based on clinical accepted medical practice that determines when a given signal is considered within the normal range for a patient. If at any given time during the surgical procedure, a signal falls outside the safe range, the IU will trigger an alert message on the Intra-Op Live display. This assists the surgeon and key personnel in the OR to take necessary actions during the surgical procedure. It is noted that the default values might not be considered normal for all patients; thus, during the Pre-Op patient consultation time, these default values can be revised and properly adjusted as necessary.

The fault-tolerant gateway server

The functions of the input gateway are receiving, staging, managing, and transferring input data during the three clinical workflow phases of the surgery: Pre-Op, Intra-Op, and Post-Op.

Pre-Op phase The gateway receives DICOM images and diagnostic reports from PACS. Once images are received by the gateway, a Pre-Op script is automatically launched by the gateway to properly extract all the information from the headers of the DICOM files. This data is then saved into the database. This whole process is automated at the gateway and does not require any user intervention.

Intra-Op phase During Intra-Op, the gateway receives live data from the IU using an API (application program interface). The transfer protocol used is the HTTPS (hypertext transfer protocol secure) Standard. Before any data is sent to the Gateway, the IU needs to properly authenticate itself in order to avoid conflict with other possible input devices. Once the data is received by the gateway server, the API will place the data in a specific location in the ePR where a script will be executed to process the data accordingly.

Post-Op phase During Post-Op, the patient is under observation in the recovery area by a nurse and the surgeon. The vital signs and other monitoring equipment are used to evaluate the patient Post-Op condition. During the 45 min to 1 h observation, live data of the patient is continuously received and displayed at the bedside monitor by the Post-Op module.

The fault-tolerant ePR server

The ePR Server is the heart of the Minimally Invasive Spinal Surgery ePR System and is the front-end of the system where the users will login to perform all the necessary tasks during the surgical workflow. The ePR Server allows access to the Pre-Op authoring module, the Pre-Op display in the OR and the Post-Op authoring module (see Fig. 5). Administrative tasks such as giving the users access to the system, registration of patient information, scheduling, among others are also included.

The ePR by definition allows the participants to obtain any necessary information about the patient from a single interface, i.e., the information follows the patient. The ePR not only shows information about the medical examinations for the patients, but also any other related data such as clinical history and pain surveys acquired during the surgical procedure.

The ePR is developed utilizing PHP (PHP: hypertext preprocessor) as the backend programming language. The data values are stored using a MySQL database [10]. The web pages are structured with HTML (hyper text markup language), and they are styled using CSS (cascading style sheet). The interfaces are dynamically updated using JavaScript. The web server utilized is Apache 2.2 [11].

Data storage and archive and system database Managing the data acquired by the ePR system is a critical task. Therefore, a dual-system back-up mechanism is implemented as follows. First, the ePR server has the server hardware, and the Gateway has the Gateway hardware. Two identical server software packages are implemented, one in the ePR server hardware as the primary and the other in the Gateway hardware as the back-up. By the same token, two Gateway software packages are implemented, the primary package is in the Gateway hardware, and the secondary package is in the ePR Server hardware as the back-up. Refer to the middle row of Fig. 5, the Gateway and the ePR server each has its own hardware, where each hardware piece is housing both the ePR server software and the Gateway software; one is the back-up of the other. Figure 6 shows the dual-system backup mechanism.

The input data first comes to the Gateway hardware, where the Gateway software categorizes them by images, live waveform information, and textual information. Images include DICOM images in their original DICOM format as well as in JPEG format for web display; as well as endoscopic videos, endoscopic single frame images, and digital C-arm fluoroscopic images. The metadata in the DICOM images and other data are stored in the database disks. All acquired data and metadata are immediately backed up by the ePR Server hardware.

System security The system security has been considered carefully during the design in order to comply with the HIPAA (Health Insurance Portability and Accountability Act) requirement. Only the users who have been granted

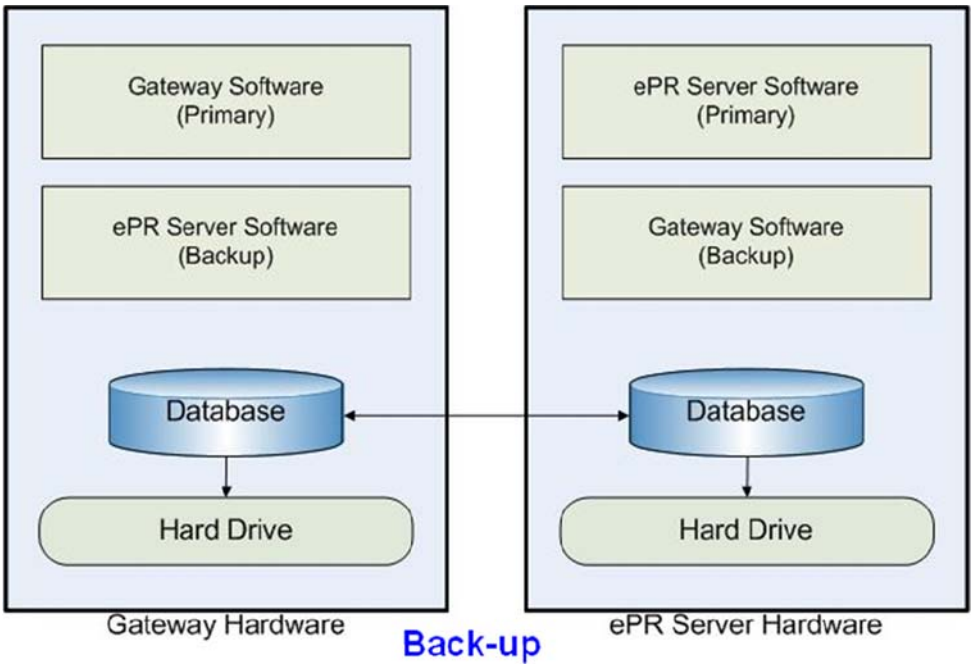

Fig. 6 The dual-system back-up schema with two hardware pieces: ePR server hardware and gateway hardware. Each hardware piece has two components of software: ePR Server software and gateway software; and a tandem database with hard drive for data and metadata archive

permission are allowed access to the system. At the same time the privacy of the communications are kept to avoid any non-authorized receiver to obtain a given patient's private information. To guarantee the security of the data, web access to the ePR is established with HTTPS that encrypts all communication between the server and the clients (web browsers). In addition, the ePR system handles permissions that will allow users to perform different tasks on the system. Different user groups in the system have a different set of enabled permissions, however, permissions can be overwritten for individual users by the system manager if necessary providing a greater level of flexibility.

System fault-tolerance and continuous availability and failover The information that is kept in the ePR is unique and cannot be obtained from any other sources if lost. To overcome any possible loss of data, a fault-tolerant solution that replicates the data of the ePR to more than one place has been implemented. The primary Gateway serves as the backup for the primary ePR server, and vice versa.

In addition to having the data being stored with more than one copy, system redundancy with automatic failover mechanism has been designed to access the data in case of the failure of any component in the system to guarantee system continuous availability.

Visualization and display

The last of the four components in the ePR System is the graphic user interface (GUI) and Display. In order to have the ePR system to be utilized as an effective tool that can improve the workflow of the Surgery Department, it is important to have a user-friendly GUI that presents all necessary contents for the surgery in an easy to use manner. For this reason, the ePR system is designed with this concept to achieve this goal.

Because the entire ePR system operates in three interrelated Phases during a surgical procedure, from planning (Pre-Op), to surgery (Intra-Op), to patient recovery (Post-Op); the interface design between these three Phases are critical. The Display interface design (see Fig. 5) includes the main page, the Pre-Op display at the patient consultation room, the Pre-Op display at the OR, the Intra-Op display at the OR, the Post-Op at the patient recovery area, the Post-Op at the OR for surgical documentation, and the administrative pages.

Pre-Op authoring module The Pre-Op Phase of a minimally invasive spinal surgery procedure is where all necessary information prior to the surgery procedure is collected and organized in a patient e-folder. The Pre-Op happens days prior to the surgery and involves querying, interviewing, collecting, and storing of pre-surgical medical images, patient demographic information as well as other pertinent data value that would assist the surgery during the procedure.

Traditionally, surgeons have been relying on their memory for localization of where the procedure should be performed. They review the MRI and X-ray images the day before surgery and studied the approach to be taken during the procedure. These images are also brought to the OR for reference. But they are displayed in hard copy in an unorganized fashion scattered throughout the OR. The next few paragraphs focus on the organization of the Pre-Op patient information

Fig. 7 (*Left*, **a**) The Pre-Op authoring module page. The *upper left hand text* list depicts the surgical data model showing the studies and procedures. After the user clicks an item in the list, the proper image, in this case, a sagittal MRI is shown on the *right*. (*Right*, **b**) The neuro-navigator tool allows the correlation of the position of the lesion in the sagittal (*left*) and the axial view (*right*). The *red lines* are the two corresponding sagittal and axial sections

which requires a preparation process. This process should not be done during the time of surgery and the information should be saved in advance with the display streamlined and organized for efficiency purposes.

Creating a surgical procedure in the pre-Op authoring toolkit The interface allows the users to create the surgical procedures by first selecting the key images as well as adding annotations to those key images as shown in Fig. 7. On this screen the PACS image and surgical procedures had been combined into one display in the Pre-Op module. Image studies related to the surgical procedure are shown on the left hand side based on the surgical data model (see Fig. 7). To view an image in a study, the users can either drag the study shown on the list from the left to the viewing pane on the right hand side or by double clicking the study from the list on the left. Figure 7 displays a sagittal MRI image with patient's ID above the image. The toolbar with icons at the top of the viewing pane allows the users to perform certain tasks accordingly to the current status of the editing module.

(1) To view images in a study: the two icons on both the right and the left sides allow the user to preview images in the study series.
(2) To perform image manipulation: the toolbar for the Pre-Op include some basic image manipulation tools such as window/level, pan, and zoom. With this functionality, the images can be displayed optimally at the exact location of the lesion.

During a minimally invasive spinal surgery operation, it is important to correlate the axial view with the corresponding sagittal view of an MRI study. The neuro-navigator tool in the Pre-Op module allows such correlation through the display as show in Fig. 7.

In addition to the input data described earlier, one type of Pre-Op data which is critical during surgery is the hand written whiteboard information located at the entrance of the OR which contains a very short summary of the patient such as name, gender, age, weight, height, any allergies, comorbidity and pain. Normally, the white board should contain all patients' information to be operated during the day. The Pre-Op authoring module described has been designed to integrate the whiteboard information onto the same Pre-Op screen for display in the OR during the surgery. The following survey measures are also included:

1. Visual analog scale (VAS): is a psychometric response scale to describe the amount of pain a patient is feeling from a specific part of her/his body.
2. Oswestry disability index: a survey to identify how the pain in the back or legs is affecting the patient in his/her daily activities.

The design concept of the ePR system is user-friendly but effective at the same time. For these reasons, the criterion of the user interface is to minimize the number of mouse clicks needed to perform a certain task and to aggregate information adequately into a single interface whenever possible. The current Pre-Op authoring module is a self-contained interface where the users can download, edit, add, and delete the

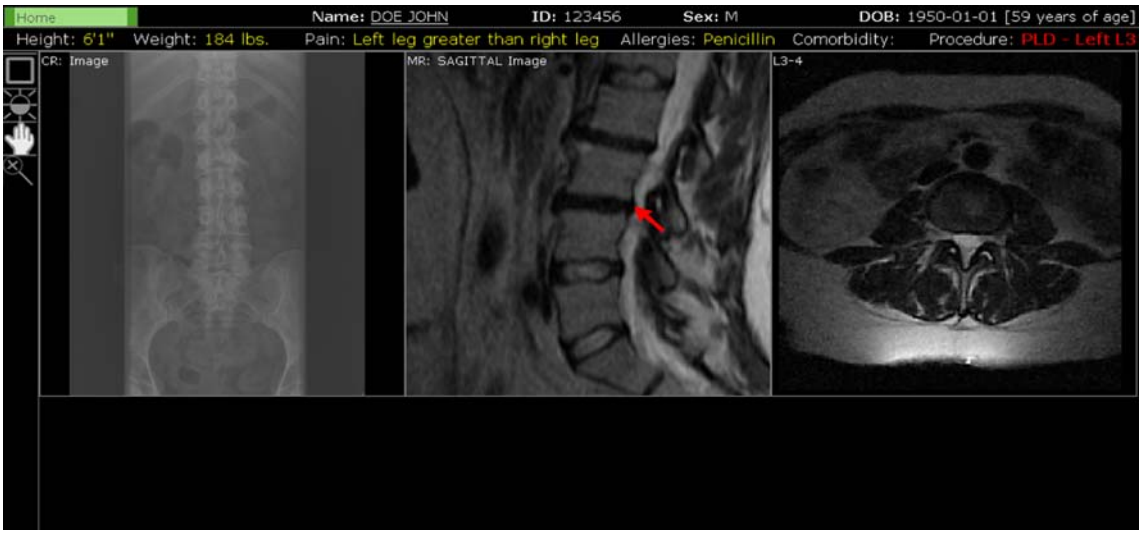

Fig. 8 The Pre-Op display organized during patient consultation as seen on the Pre-OP display monitor in the OR during Intra-OP. *Top text row* patient general information, *second text row* whiteboard information, *bottom row* images and annotation during Pre-Op consultation; *left* CR image, *middle* sagittal MRI with annotation and *right* transverse MRI

contents as needed. The Pre-Op has two major interfaces, one for editing and one for display in the OR.

Pre-Op display A minimally invasive spinal surgery procedure requires multimedia data during the Pre-Op phase including patient history, images, and consultation results. These data should be organized and displayed in the Pre-Op display during surgery. An example is shown in Fig. 8 which depicts the general patient information (first top row), whiteboard information outside of the OR (second top row), as well as the key images selected from the MRI study with their annotations during consultation (center). The term that is used for this display is the Pre-Op display since the Pre-Op authored data is actually displayed during the Intra-Op workflow Phase.

Intra-Op live display Figure 9 shows a mock up example of the Intra-Op live display with waveforms and images. The horizontal axis is time. The stream from the vital signs device is displayed at the top row (left) and to the right there are five groups of waveform: three vital signs with blood pressure, pulse oxygen concentration and pCO2, as well as BIS, IVF (intravenous fluid). Every dot in the waveform represents a data point over a one second interval. In the middle row, there are two images, the C-Arm fluoroscopic (right) and the endoscopic video images (middle), and one EMG waveform in the left. In the lower row, there is laser energy in joules. The video is updated on the Intra-Op live display with a frame rate of 30 per second (a default value).

Rule-based alert mechanism If a signal falls outside its safe range a three stage mechanism will alert personnel in the OR about that situation.

(1) Warning mode: if the numeral falls outside the safe range it will change its color to red (as seen with the PulseOX and blood pressure in the figure)
(2) Emergency mode: if the condition falls to a value greater or lower in 25% of the safe range then the Intra-Op live display will place an alert message on top of the screen.
(3) Critical mode: If the data signal value is either greater or lower in 50% to the values in the safe range then the alert message will cover the whole screen.

Post-Op module The Post-Op phase takes place after the completion of the surgical procedure, normally, the next several days after the surgery. There are three time substages: (1) patient in the recovery area and then discharged, (2) the surgeon documents the surgical results, and (3) follow up pain surveys after Post-Op for several months.

Post-Op authoring toolkit When the surgeon performs Post-Op documentation, he/she can retrieve information from the Post-Op module pertinent to the surgery using the GUI. This process involves four major steps:

(1) Finding the patient from the ePR System. The correct patient can be located from the ePR via the worklist.
(2) Selecting images. From this GUI, the surgeon can select endoscopic images that will be included in the final report by clicking the star at the top left corner of the viewing pane. As shown in Fig. 10, that image has been selected for the final report.
(3) Selecting waveforms. The waveforms are displayed at the bottom of the GUI (Fig. 10). They can be

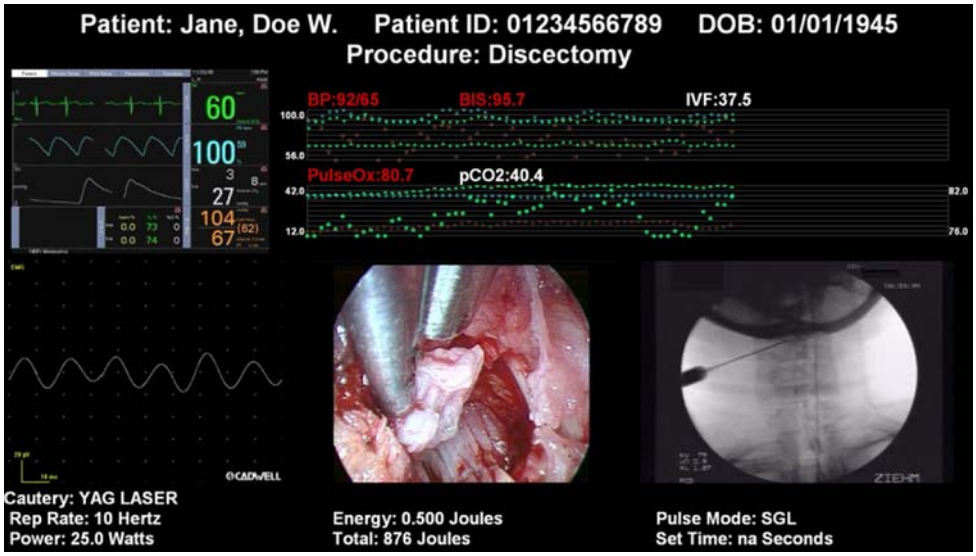

Fig. 9 A mock-up example of the Intra-Op live display as seen on the Intra-Op large monitor in OR. *Top row* from *left* to *right* video stream of vital signs and six waveforms coming from three vital signs, BIS and IVF; the *horizontal axis* is time. *Middle row* from *left* to *right* waveform of EMG, endoscopic image and fluoroscopic image. *Bottom row* laser output values

dynamically selected by clicking their corresponding boxes on the upper right side of the interface.

(4) Data synchronization. A slider at the bottom of the graph (green pointer in Fig. 10) would allow for synchronized viewing of all the image and waveform data being displayed.

The data that was displayed and selected for documentation in Fig. 10 includes a C-Arm fluoroscopic X-ray image, heart rate, diastole and systole blood pressures, respiratory rate, BIS score value, oxygen pressure and partial pressure of carbon dioxide. The curve shown at the bottom of Fig. 10 (heart rate) is a waveform obtained from another Intra-Op device. Figure 10 shown contains real-patient data with anonymized acquisition date and time and patient demographics.

Nurses and Front-desk personnel perform surveys several times after the surgery and enter the pain surveys data into the Post-Op module of the ePR system as a follow-up of the progress of the patient. The collective information can be used for future patient outcome analysis.

Results

Clinical site for developing and implementing the minimally invasive spinal surgery ePR system

The design and implementation has been in collaboration with the California Spinal Institute (CSI), Thousand Oaks, CA. CSI is a full self-sufficient independent spinal surgery institute and performs between 5 and 10 minimally invasive spinal surgeries per week. It has its own diagnostic imaging facility including conventional X-rays, CT and MRI services and a commercial PACS. CSI also provides patients with the full in-house services for spinal surgery from Pre-Op consultation to Post-OP evaluation, check-up and therapy. The concept of developing the multimedia ePR system for image-assisted Minimally Invasive Spinal Surgery was conceived 5 years ago but technologies were not available until recently [9]. The go head development decision was made in early 2007.

Many parameters used in the design were based on daily clinical experiences at CSI during the past 5 years. The ePR system can be modified for Minimally Invasive Spinal Surgery operation at other similar healthcare facilities, and image-guided surgery ORs (operation room).

System deployment

The prototype system was deployed in August 2008 to the California Spine Institute (CSI) located in Thousand Oaks, California, which is the only clinical site in Southern California that performs Minimally Invasive Spinal Surgery. This site served as an initial approach to understand the general workflow of the surgical procedure. Because the goal of the system is to be able of being installed in other locations, the workflow and implementation was kept in its more general instance, avoiding any specific-related design for CSI. In the case that a particular part of the implementation was tailored for this site, the options were configured to be flexible. The customization of the modules used in the ePR will allow having the system implemented in different locations where other vendors are used.

This section summarizes the highlights.

Planning and design phase The ePR system for minimally invasive spinal surgery was developed at the IPILab, USC. IPILab and CSI have had close collaboration for more than 5 years. There are three phases of the implementation. First,

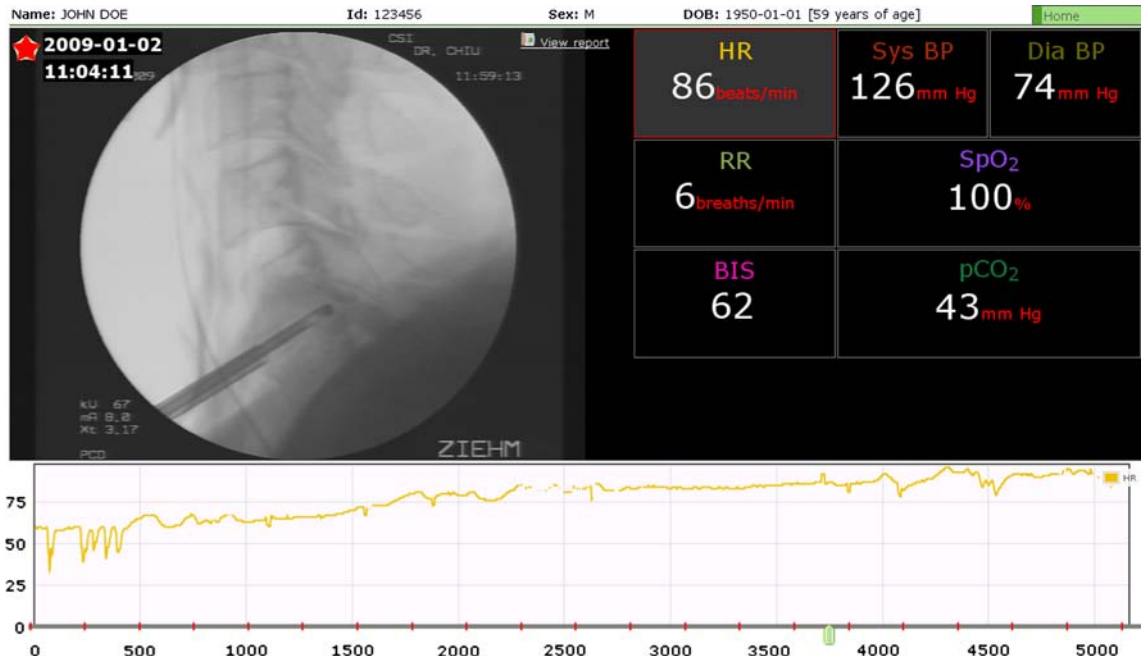

Fig. 10 The Post-Op authoring module displaying a patient case showing data acquired during the surgery. The *x* axis represent the time, while the *y* axis represent the numerical value of the data points. The *green mark* represents the time frame when this page was captured. This module can be utilized by the surgeon to create an image and waveform Post-Op results document in pdf format. The graph showed at the *bottom* is the sequence of respiratory rate values over the whole procedure time

to test the functionality of the ePR system, a prototype for each of the ePR components was developed and integrated at the CSI research facility; in addition, mockup data was collected at CSI that included an Intra-Op signal simulator for the IU device. Second, once the system was tested fully in the laboratory environment, it was then deployed in the OR to obtain user feedback and clinical evaluation. The hardware and software components consist of the Gateway Server, the ePR server, and the IU. In addition, other software packages include the ePR web pages, the IU application, the database, and the web server.

The final stage of the clinical implementation was to deploy the ePR system in the OR. This stage has been challenging, since the OR is continuous in use for minimally invasive spinal surgery, both the clinical team and the engineering team have to work together to circumvent the clinical schedule minimizing the risk of any possible disruption of the clinical service through coordinating of various tasks among the teams member; this is especially true in the final stage of implementation, when the ePR has actually been used taking care of some regular duties usually reserved by the traditional surgical method.

Hardware installation The ePR and Gateway servers were installed at CSI on a rack at their Server Room. Figure 11 shows the installation in progress and the final location of those servers.

In addition to the two servers above, the IU was also installed in one of the ORs at CSI. The IU needs to be connected to all required peripheral devices that are presented in the OR for monitoring the real-time patients' response during the clinical procedure. The IU, located in the OR, and its connection to input devices are shown in Fig. 12.

Software installation Once the servers were installed at the clinical facility, the next step was to configure all necessary software components of the ePR system. Those components include:

(1) *ePR server*. The server requires the installation of the web server (Apache) and the database (MySQL).
(2) *Gateway server*. Composed of a software DICOM listener that receives incoming DICOM studies sent from the PACS and a set of scripts to extract the metadata information and store it at the database.
(3) *Integration unit*. Software developed in C++ is utilized to make low level system calls to the different interfaces depending on performance requirements to display real-time data in the OR.

Training and support for clinical users The following users were among those trained for the use of the ePR system:

(1) *Surgeons*. They received training on the Pre- and Post-Op authoring modules. In addition, they were taught to

Fig. 11 The ePR Server installation at the server room of CSI. J. Documet was installing the servers

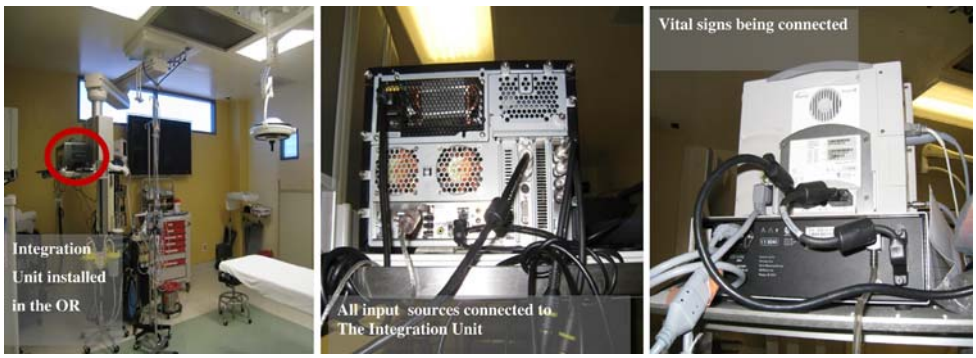

Fig. 12 Integration unit (IU, *left* inside the *red ring*) installed in the OR connected to different input sources (*middle* input units cables are connected to the back of the IU; *right* vital Signs device is being connected)

properly interpret the two large Pre-OP and Intra-Op LCD displays.

(2) *Physician assistants*. They were involved in both group and individual training sessions for Pre-Op authoring module.

(3) *Nurses*. They were trained to properly enter information related to the patient's whiteboard data and survey forms.

(4) *Front-desk assistants*. They received training for scheduling of surgical procedures, input of pain surveys for Pre-Op and Post-Op Phases as well as patient registration.

(5) *Technicians*. The training given to them was on how to correctly understand the data presented at the LCD monitor displays at the OR.

(6) *Administrative staff*. They were given training on how to add or remove a user from the ePR system and to manage the permissions for the different user types or a specific user as well.

The engineering team provided 3 months on-site baby-sitting of the ePR system as well as assisted the duty staff to prepare Pre-Op module. Figure 13 shows a typical training session. Clinical Implementation of the Post-Op module is currently ongoing.

Clinical implementation experiences

(1) The implementation phases were planned based accordingly on the three workflow stages to provide a good understanding of the features included in the ePR System and at the same time to address any positive feedback from the users. Phase one implementation was included the Pre-Op authoring and display toolkit as well as general ePR features such as worklist navigation and DICOM Query/Retrieve. Phase two implementation included the Intra-Op display as well as the Pre-Op display on large LCD monitors. Finally, phase three included the Post-Op authoring and display toolkit and is currently undergoing training sessions.
Since the ePR System was installed in August 2008 at CSI, every surgical operation has utilized the Pre-Op Display module within the OR. This is a direct result of the clinical staff performing the Pre-Op authoring one day prior to surgery. In the same amount of time, the Intra-Op live display has been used to show a centralized view of all the data obtained from peripheral devices. Data captured from the IU module is currently stored in the ePR System automatically since May 2009.

(2) Even though there was no formal evaluation from the users' training, all the people that were trained had been using the ePR with no major complaints. After a 1-year clinical operation with sufficient and meaningful data collected, a more formal user acceptance survey will be conducted targeted for a follow-up clinical experience paper.

(3) The chief surgeon who is one of the architects of this system has monthly meeting with the ePR team to provide suggestions, input and user experience for system refinement and upgrades. He has been the champion of the project.

Fig. 13 Group training in Pre-Op authoring at the consultation room

Next steps in research and development

Prototype version 2 for integration unit. The integration unit (IU) is a very critical component in the ePR system, but at the same time is very complex and needs to be refined to satisfy the ePR System requirements. The prototype version 2 of the IU has been designed to provide continuous availability, improve the performance for data collection, visualization and storage with expanded flexibility in order to support a larger set of devices and configurations.

Difference between current version and the version 2 of the integration unit. The main difference between the two versions of the Integration Unit is the capability of handling fault tolerance and continuous availability: the first prototype of the IU did not provide any fault tolerance. The second prototype provides fault tolerance by adding a second set of key pieces from the IU. This is similar to what have been done to the PACS [12]. Among the pieces added are: more robust UPS (uninterruptible power supply); NAS (network attached storage) for storage; the main processing unit is provided by means of two identical clustered blade servers. In case of any failover the recovery is done automatically. In addition, the second prototype is assembled in a self-contained mobile cart that enhances the flexibility for implementation in different environments. At the same time the second prototype has increased the number of ports to include more peripheral devices present in the operating room.

The software that acquires, displays, and stores the data also requires an update to handle the new infrastructure for the second prototype. Upon completion of the second prototype, one copy will replace the existing first prototype within CSI and the second copy will be deployed at a second clinical site to be determined.

Discussion

Lessons learned

Much of the experience gained and many lessons learned in developing the multimedia ePR for image-assisted minimally invasive spinal surgery are similar to that of early times when PACS was developed and deployed in radiology departments, and later to hospitals. However, there are some differences due to the fact that ePR users are mostly local and not hospital-wide. Among these, are listed in the following as well as any comments on the differences and similarities between them whenever appropriate.

(1) *Lack of standards from peripheral data and imaging devices used in the OR*. This was the major obstacle during the implementation phase. There are many vendors who sell peripheral devices to ORs where no data format or communication standard compliance is required. Different vendors export their data in different ways, adding complexity to the mechanisms for data retrieval and limiting the interoperability to certain vendors and products. In imaging, most ORs still use Pre-Op hardcopy for reference during the surgery. For image-assisted surgery, the Intra-Op endoscopic and C-Arm radiographic images are for assisting the surgeon during the surgery, and there is no requirement for keeping hard or soft copies for surgical document. The multimedia ePR system for minimally invasive spinal surgery, on the other hand, keeps all live data during the surgery in the database, they will be selected by the surgeon to include in the patient report during Post-Op authoring. Therefore, it had been a major challenge for acquiring data from real-time peripheral devices as well as images from endoscope and C-Arm radiography in the OR during surgery. In PACS installation, similar problems were encountered in imaging modalities connectivity, but this issue was resolved by the mandated compliance to DICOM standard in almost all the purchases in imaging systems and PACS in the late 1990s. The development of the Integration Unit (IU) in the ePR system prototype is the first step allowing all devices to be integrated. We anticipate several years down the road, surgical OR may see the advantages of data integration in the ePR and enforce vendors to output data with certain standards.

(2) *The clinical environment was different from the laboratory environment.* When the ePR prototype was moved from the laboratory environment to the clinical site, the engineering team encountered a culture shock. In the former, the laboratory environment was under control and debugging and modifications could be performed easily. Whereas in the latter, the reality of the real world

sank in, and it was very difficult to make modifications for two reasons: (1) once the ePR was installed, the clinical use of the system has always been with the highest priority, any modifications were secondary, (2) users were reluctant to continuously adopting new changes. Unlike PACS installation which has long passed this R&D mode, nowadays a prototype system would be rarely installed in the clinical site without extensive test at the manufacturer site first.

(3) *The clinical institution was not always in control of its computer and ICT (information and communication technology) equipment*. Installing new applications in clinical computers might sometimes require administrative privileges. In addition, configuring and adding new servers to CSI might need to be performed by a third party IT (information technology) team that could cause implementation issues. This issue would be encountered in many PACS installation as well.

(4) *User acceptance.* Whenever a new application in the ePR was implemented at CSI, users might be reluctant to fully embrace the new application. It is because it would temporarily disrupt their normal routine clinical workflow even if the system would ultimately improve their clinical workflow in the long run. The user acceptance is easier in PACS now since the healthcare community has gained more than 15 years of experience.

(5) *Graphical user interface challenging for new users*. When a new application was developed, training becomes crucial since users were not familiar with the interface and functionality. This issue is 100% the same as PACS when the user is first time or switches to a new PACS, or a new GUI is installed.

Design principles and reproducibility

(1) *The design principle.* The design principles of the ePR system are modularity and reproducibility. The system has three major components, Pre-Op, Intra-Op, and Post-Op, they are operated as a complete system. In order for the Post-Op to function properly, both Pre-Op and Intra-Op have to be operable. In the same token, in order for the Intra-Op to be functional, Pre-Op has to be operable. However, Pre-Op can be used without the Intra-Op and Post-Op in operation. In this case, no data from the Pre-Op would be input to the Intra-Op and Post-Op modules.

(2) *Reproducibility*. The infrastructure of the ePR system is applicable to most image-assisted minimally invasive surgical operation rooms. However, certain customization may be required. For example, different surgical input including images, waveforms and textual data may need new designs for various input device interfaces. The Integration unit (IU) infrastructure has been tested to handle up to a combined total of 12 waveforms data points, imaging inputs and video streaming sources. In addition, the Display format and GUI need to be redesigned to suit various surgical requirements.

Conclusion

A step-by-step approach was introduced to develop a multimedia ePR system for imaging-assisted minimally invasive spinal surgery. First, the clinical need for the Minimally Invasive Spinal Surgery ePR was introduced. Then, the three clinical phases of minimally invasive spinal surgery workflow in Pre-Op, Intra-Op, and Post-Op were discussed. The three-phased modules; and the four components: the input integration unit, fault-tolerant gateway server, fault-tolerant ePR server, and the visualization and display component. A prototype was built and deployed to a Minimally Invasive Spinal Surgery clinical site with user training and support for daily use. Finally, special experience gained and lessons learned from developing the system were discussed. This methodology can be extended to other image-assisted minimally invasive surgery.

References

1. Vallfors B (1985) Acute, subacute and chronic low back pain: clinical symptoms, absenteeism and working environment. Scan J Rehab Med Suppl 11:1–98
2. Chiu J, Savitz MH (2005) Use of laser in minimally invasive spinal surgery and pain management. In: Kambin P (ed) Arthroscopic and endoscopic spinal surgery—text and atlas. 2nd edn, Humana Press, New Jersey, pp 259–269
3. Chiu J (2004) Anterior endoscopic cervical microdiscectomy. In: Kim D, Fessler R, Regan J (eds) Endoscopic spine surgery and instrumentation, vol 5. Thieme Medical Publisher, New York, pp 48–58
4. Chiu J (2004) Endoscopic lumbar foraminoplasty. In: Kim D, Fessler R, Regan J (eds) Endoscopic spine surgery and instrumentation, Chap 19, Thieme Medical Publisher New York, pp 212–229
5. Chiu J, Clifford T, Greenspan M (2000) Percutaneous microdecompressive endoscopic cervical discectomy with laser thermodiskoplasty. Mt Sinai J Med 67:278–282
6. Haller JW, Ryken TC, Vanier MW (2001) Image-guided surgery of the spine. J Min Invasive Spinal Tech 1(1):87–92
7. Jaikumar S, Kim D, Kam A (2002) History of minimally invasive spine surgery. Neurosurg Supp 2002 5(2):1–14
8. Huang HK (2004) PACS and imaging informatics: principles and applications. Wiley, Hoboken, p 704
9. Huang HK (2001) PACS, informatics, and the neurosurgery command module. J Mini Invasive Spinal Tech 1:62–67
10. MySQL AB, Sun Solaris Microsystems Inc. http://dev.mysql.org
11. Apache web server, Apache software foundation http://httpd.apache.org
12. Liu BJ, Huang HK, Cao F, Zhou MZ, Zhang J, Mogel G (2004) A complete continuous-availability (CA) PACS archive server solution. Radiographics 24(4):1203–1209

RadioGraphics

Informatics in Radiology

DICOM-RT–based Electronic Patient Record Information System for Radiation Therapy[1]

Maria Y.Y. Law, PhD • Brent Liu, PhD • Lawrence W. Chan, PhD

TEACHING POINTS
See last page

Comprehensive clinical imaging data and additional relevant information are crucial for the planning and delivery of radiation therapy in patients with cancer. Multiple stand-alone systems that make use of technologic advances in imaging, treatment planning, and treatment delivery acquire or generate key data during the course of radiation therapy. However, the data are scattered in various systems throughout the radiation therapy department, thereby compromising efficient clinical work flow. In 1997 and 1999, the Digital Imaging and Communications in Medicine (DICOM) standard was extended from radiology to radiation therapy with the ratification of seven DICOM-RT objects. These objects helped set the standard for *(a)* data integration and interoperability between radiation therapy equipment and information systems from different manufacturers, and *(b)* the use of DICOM diagnostic images in radiation therapy. More recently, key radiation therapy imaging and informatics data have been integrated to form an open-architecture comprehensive radiation therapy electronic patient record (ePR) system. The benefits of such a DICOM-RT–based ePR system are threefold: it can be used as a foundation for performing effective and efficient clinical services, as a common platform for radiation therapy data exchange and expert consultation, and for medical imaging informatics research in developing innovative decision support tools and a knowledge base for improved treatment with radiation therapy.

Abbreviations: DICOM = Digital Imaging and Communications in Medicine, ePR = electronic patient record, GUI = graphical user interface, IHE = Integrating the Healthcare Enterprise, PACS = picture archiving and communications system, TPS = treatment planning system

RadioGraphics 2009; 29:961–972 • **Published online** 10.1148/rg.294085073 • **Content Codes:** IN RO

[1]From the Department of Health Technology and Informatics, Hong Kong Polytechnic University, Hung Hom, Kowloon, Hong Kong (M.Y.Y.L., L.W.C.); and Image Processing and Informatics Laboratory, Keck School of Medicine, University of Southern California at Health Sciences Campus, Los Angeles, Calif (B.L.). Presented as an education exhibit at the 2006 RSNA Annual Meeting. Received March 27, 2008; revision requested September 16; final revision received January 6, 2009; accepted January 22. All authors have no financial relationships to disclose. **Address correspondence to** M.Y.Y.L. (e-mail: *maria.law@polyu.edu.hk*).

Introduction

With advances in technology allowing more accurate treatment and better patient care, more and more images are being generated and used in radiation therapy, which is becoming increasingly image intensive. Comprehensive clinical imaging data and relevant information in radiation therapy are crucial for treatment planning and delivery in patients with cancer. Radiation therapy makes use of some of the greatest technologic advances in diagnostic imaging, image processing, therapeutic radiation, and computerization in this context. All of these advances add to the complexity of the collection and navigation of pertinent radiation therapy data. Currently in many radiation therapy departments, radiation oncologists need to go to dedicated workstations to approve treatment plans or portal images, and radiation therapists cannot view the patient's treatment plan or other images at the treatment workstation. Patient data generated during a course of treatment reside at the individual system or workstation where they are used, and thus are scattered (1). The data may be "integrated" through the hard-copy patient folder or film images; however, the data crucial for a clinical decision may be resource intensive and time-consuming to retrieve, temporarily missing, or even lost. All of these issues compromise efficient clinical work flow. One potential way of addressing these issues is to view radiology as setting the precedent in terms of its adoption of the DICOM (Digital Imaging and Communications in Medicine) imaging standard, which has led to the successful development and utilization of picture archiving and communication systems (PACS) (2).

The PACS has become an indispensable integrated imaging system in radiology and hospital operations. The field of radiation therapy has benefited from the PACS and the DICOM standard by making use of clinical images from radiology (3). However, the real benefit to a radiation therapy department is the extension of the experience and knowledge gained from integration of the PACS and different modalities to the various sources of clinical data dispersed throughout the department. A system integration infrastructure based on standards is crucial for streamlining clinical work flow and for the establishment of medical informatics research related to outcomes for future radiation therapy patients. In 1997 and 1999, the DICOM standard was extended from radiology to radiation therapy with the ratification of seven DICOM-RT objects (4–8), thereby making a patient-centric integrated solution such as an electronic patient record (ePR) system feasible. A DICOM-RT–based ePR system would be an effective and efficient "one-stop" source for tracking the treatment progress of cancer patients by integrating data from the various sources and presenting them in a graphical user interface (GUI) that is designed for ease of use. Such a system would also provide a foundation of standardized data objects, with which to build a knowledge base, and data mining tools for future clinical decision support and outcome analysis.

To date, the implementation of a DICOM-RT–based ePR system has been hindered by the complex clinical work flow and data in radiation therapy; insufficient information technology expertise in radiation therapy–related applications; and the scarcity of manufacturers in radiation therapy, each of whom is competing to be the major or sole provider. Although several manufacturers have tried to develop a more comprehensive radiation therapy information system, most of these systems have been intended for implementation with a single source vendor's equipment, and their interoperability with other vendors' equipment is at times doubtful. In this article, we review the work flow in radiation therapy; discuss and illustrate the functions and benefits of a DICOM-RT–based ePR system; and describe the development of such a system in terms of system design, implementation, testing, and evaluation.

Radiation Therapy Work Flow

Radiology work flow mainly involves the generation of images and reports, whereas radiation therapy work flow deals with much more information of different types over a much longer time span. To facilitate an understanding of the need for and benefits of an ePR system, the work flow for a patient with prostate cancer is shown in Figure 1. Radiation therapy work flow generally consists of two stages: treatment planning and treatment delivery.

Radiation treatment planning may require a few patient visits for the acquisition of images, such as the planning computed tomographic (CT) scans or magnetic resonance (MR) images and the treatment simulation image. The

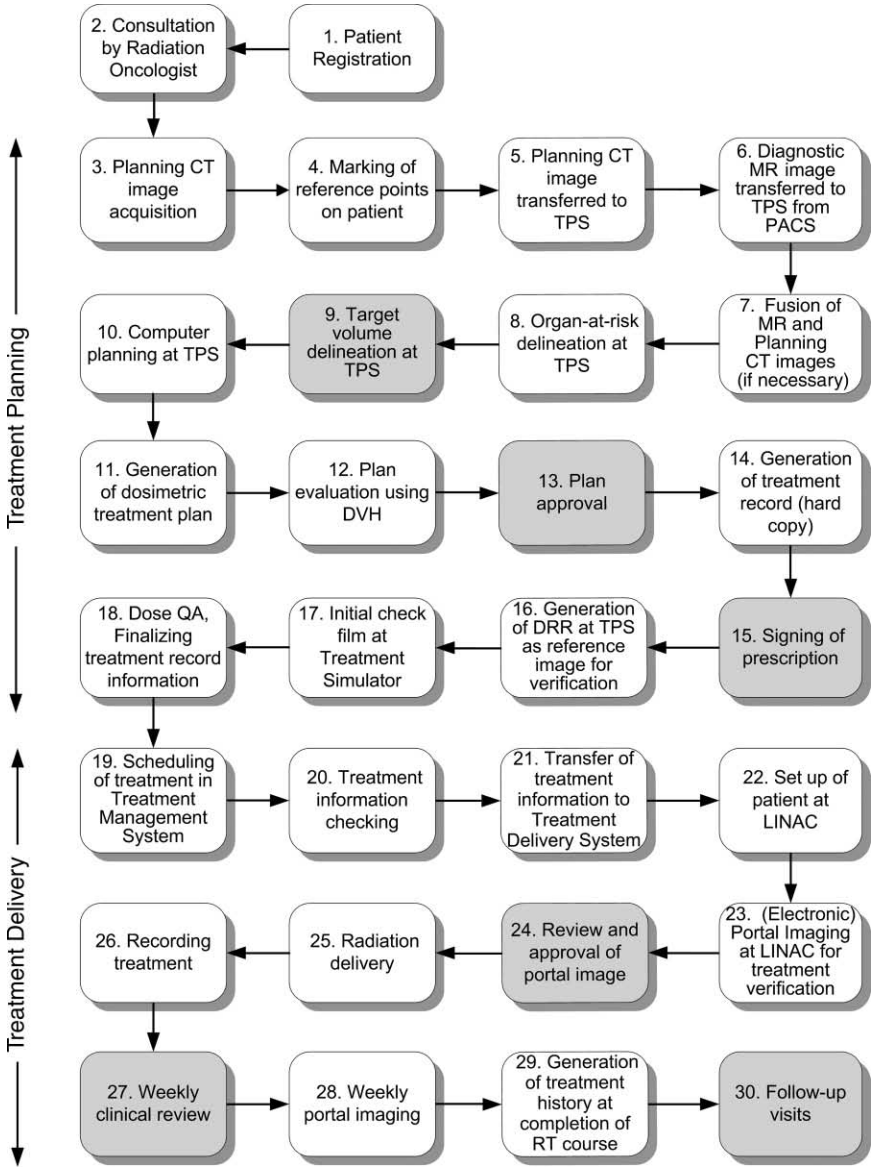

Figure 1. Chart illustrates the radiation therapy work flow for a patient with prostate cancer. The work flow consists of two stages, treatment planning (steps 1–18) and treatment delivery (steps 19–30), and is broken down into steps that can be used to evaluate the efficiency of the system once it is implemented. The work flow starts when the radiation oncologist decides at consultation that the patient is to receive radiation treatment (step 2). Gray boxes indicate steps that are performed by the radiation oncologist. Of these steps, steps 9 and 13 are incorporated into the treatment planning system (TPS) in most cases, but steps 15, 24, 27, and 30 either require hard-copy records or radiation therapy information that may not be readily accessible. *DRR* = digitally reconstructed radiograph, *DVH* = dose-volume histogram, *LINAC* = linear accelerator, *QA* = quality assurance.

CT scans or MR images will be transferred to the TPS for treatment field and dosimetric planning. This leads to the generation of DICOM objects such as the DICOM diagnostic images, RT Image, RT Structure Set, and RT Plan with or without RT Dose (Fig 1, steps 3–17). The work flow involves the participation of radiation therapists, dosimetrists or medical physicists, and radiation oncologists.

Radiation treatment can last for several weeks, during which time verification of treatment is performed on several occasions with the acquisition of portal images. This leads to the generation of RT Beams Treatment Record, RT Treatment Summary Record, and RT Image (when portal imaging is performed) (Fig 1, steps 18–29). The radiation treatment is delivered by the radiation therapist. Approval of treatment plans (Fig 1, step 13), signing of the prescription for radiation treatment (Fig 1, step 15), and approval of verification on the basis of portal imaging findings (Fig 1, step 24) are all performed by the radiation oncologist, who will also review the case on a weekly basis during the course of treatment (Fig 1, step 27) and at later follow-up visits (Fig 1, step 30). This would necessitate referencing the patient's record, including the treatment plan, images, and treatment records.

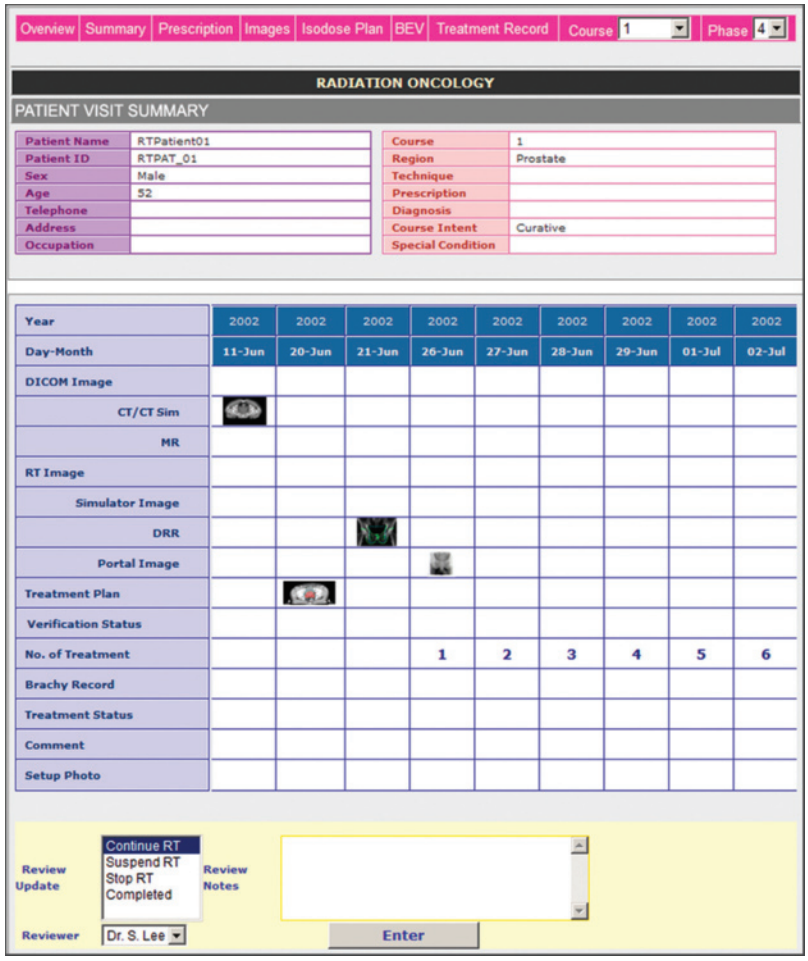

Figure 2. Screen shot of a World Wide Web client application page from the DICOM-RT–based ePR system prototype illustrates the timeline overview of the ePR for a 52-year-old man undergoing radiation therapy. In this case, CT was performed on June 11 and the CT scans transferred to the TPS, a dosimetric plan was completed on June 20, a digitally reconstructed radiograph *(DRR)* was generated on June 21, and a portal image was obtained on June 26, at which point treatment was initiated. Six radiation treatments were delivered, on June 26–29 and July 1–2, and are numbered consecutively so that the number of treatments can be seen at a glance. In addition, key data extracted from some of the DICOM-RT objects are displayed as thumbnail images for the user to select and review in greater detail using the Web client application. In Review Update (lower left), the oncologist indicates whether to continue treatment. There is also an area of free text (bottom) where the oncologist can input comments or prescribe drugs or care. *Brachy* = brachytherapy, *MR* = magnetic resonance, *Sim* = simulator.

In the current clinical environment, a patient's information is stored at the workstations or systems where they are generated, in electronic format or even as hard copies (Fig 1). Consequently, the oncologist at the clinic is unable to access any of the appropriate radiation therapy treatment plans or images except the hard-copy treatment record. On the other hand, with an ePR integrated system, all information about the patient could be accessed from a single source. Figure 2 illustrates a timeline overview of the ePR for a 52-year-old man undergoing radiation therapy. Every time a new or repeat procedure is performed, a new object is created, with the study date as one of its essential attributes. The radiation therapy information is displayed in a time sequence, which can function as a summary of the patient's visits and the procedures performed.

Functions and Benefits of a DICOM-RT–based ePR System

Functions

Figure 3 illustrates the treatment plan for the patient with prostate cancer (cf Fig 2), with isodose curves overlaid on the patient's CT scans. Figure 4 provides a detailed depiction of the setup of the treatment fields. By reviewing the treatment plan (and the details of the treatment fields) from the ePR system, the radiation oncologist was able to prescribe the radiation treatment without having to go to the treatment planning room. Note that data generated by radiation therapy equipment from different manufacturers at different steps can be integrated into a single ePR system and reviewed at one workstation.

The patient's treatment sessions were then scheduled in the treatment management system and transferred to the treatment unit. On the first

Figure 3. Screen shot (same patient as in Fig 2) illustrates the radiation dose distribution against a set of planning CT scans obtained at different levels of the pelvis. The isodense lines are decoded from the RT Dose object and are displayed with reference to the CT scans. The tumor (red) and the organs at risk (bladder [anterior to the tumor, shown in blue] and rectum [posterior to the tumor]) are decoded from the RT Structure object. All of these structures are overlaid on the planning CT scans and can be viewed together as a whole.

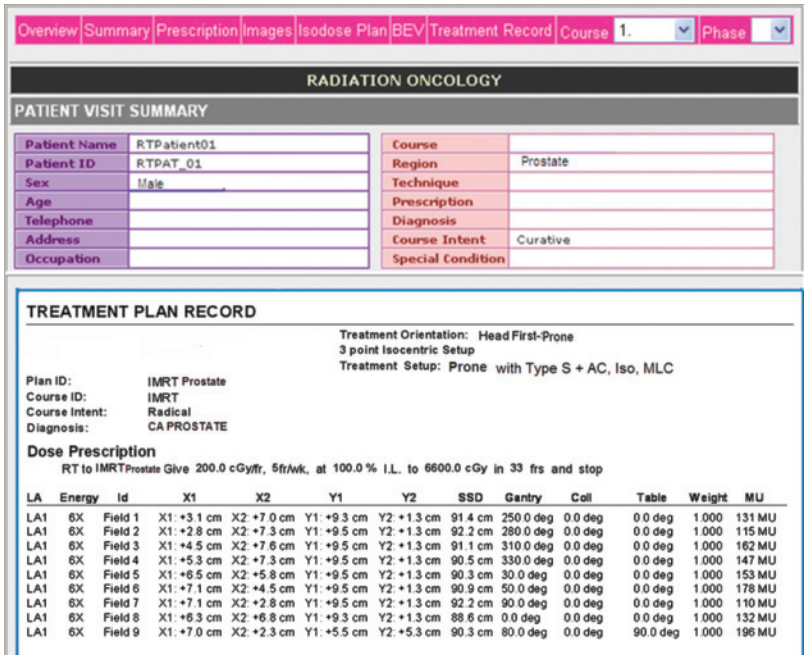

Figure 4. Screen shot (same patient as in Fig 2) illustrates a detailed prescription and plan for the radiation field. The data are extracted from the RT Plan object produced by a manufacturer's information system and are used for treatment setup at the linear accelerator.

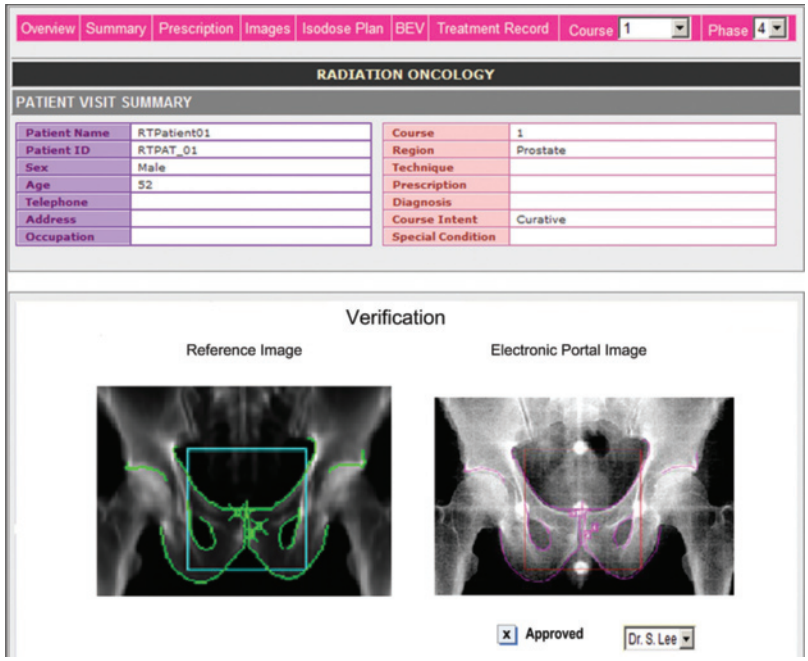

Figure 5. Screen shot (same patient as in Fig 2) illustrates how comparison of the reference image with the electronic portal image is used to verify the treatment field. The reference image (digitally reconstructed radiograph) was generated from the CT scan as an RT Image object, and the electronic portal image (also an RT Image object) was obtained at the linear accelerator. The results can then be stored in the ePR database and displayed for review. Note the "Approved" button, which allows the radiation oncologist to indicate his or her approval.

day of treatment (and weekly thereafter), portal images of the treatment fields were obtained at the linear accelerator for comparison with the reference images (digitally reconstructed radiographs) to verify the accuracy of setup (Fig 5). The radiation oncologist indicated approval by clicking on a button marked "Approved," after which treatment was begun.

Benefits

Current radiation therapy information and management systems or record-and-verify systems may contain some of the DICOM-RT data. However, an ePR system is comprehensive and more robust because it presents the entire gamut of DICOM-RT data objects in a timeline format for navigation and review of both historical and new treatment data for the cancer patient. With this system, all radiation therapy information can be reviewed at any client workstation. Because all radiation therapy–related information on the patient can be accessed and viewed from a single ePR system, the system can improve the work flow of the radiation therapy department by providing a one-stop source for viewing the data during work flow steps such as chart rounds, portal image checks, and on-treatment visits, which data currently need to be viewed by means of various stand-alone systems and paper-based folders. In addition, by using this prototype ePR system, the oncologist can approve plans, review and approve portal film images, and compare treatment images with diagnostic images to monitor treatment progress. The most important point to be gleaned from Figures 2–5, which illustrate how the ePR system is integrated with the radiation therapy work flow shown in Figure 1, is that all pertinent imaging and informatics data needed for decision making during radiation therapy are available in a single integrated system and are standardized in DICOM-RT format.

Teaching Point

The DICOM-RT–based ePR system, besides integrating all relevant local data into a single system, can enhance patient care by accepting treatment planning information from other clinical centers for real-time expert consultation. It can also serve as a common platform for cross-center clinical research in radiation therapy, since the data are now standardized in DICOM-RT format. The efficient and coherent collection of dose distribution images and dose-volume histograms generated by the TPS could pave the way for large-scale analysis of normal tissue toxicity and evaluation of treatment outcomes.

Development of a DICOM-RT–based ePR System

The mission of the ePR system is to allow all radiation therapy–related information on a patient to be viewed within a single system; that is, the pertinent imaging and informatics data (including treatment plans, graphs, images, records, and clinician remarks) can be integrated from different radiation therapy sources to form an ePR with the data standardized in DICOM-RT

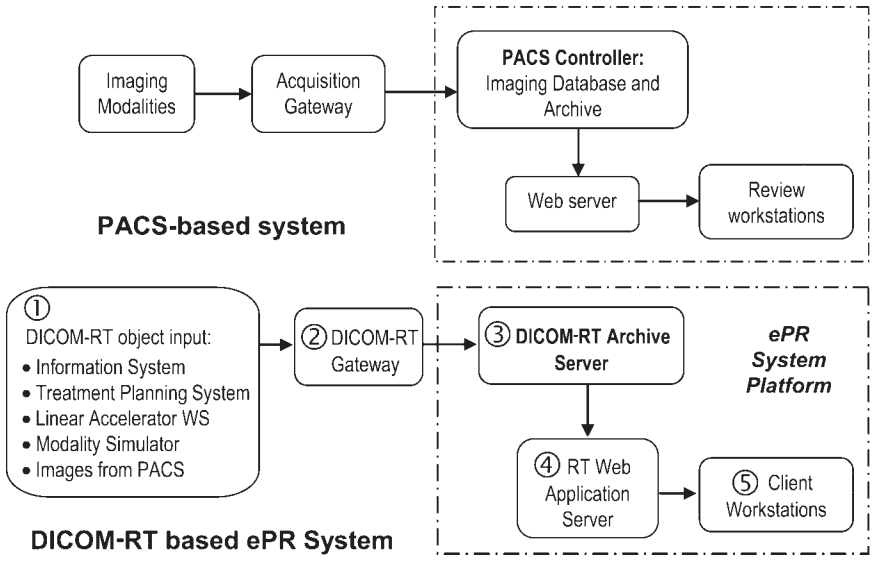

Figure 6. Top diagram illustrates PACS data flow and the key PACS components that are currently being used successfully as part of the radiology work flow. Note that the Web server is used mostly for the review of radiologic studies for the referring physician. Bottom diagram illustrates DICOM-RT–based ePR system data flow and components. Most of the radiation therapy components follow the PACS data model (modules *1*, *2*, and *3* correspond to Imaging Modalities, Acquisition Gateway, and PACS Server, respectively) due to similarities in the use of the DICOM data model. The ePR system platform is used to extract information from the DICOM-RT archive server to develop the Web-based ePR system. Note that the RT Web application server (see Fig 8) is more complex than the Web server used in the PACS data model, since the radiation therapy data contain more complex imaging and informatics data objects, whereas the PACS Web server contains only diagnostic imaging studies and reports. In addition, there are different Web application pages within the Web client workstations *(WS)* that are used in the department by oncologists, radiation therapists, and medical physicists based on their different needs.

Teaching Point

format. System development involves system design, implementation, testing, and evaluation (9–11), all of which are described in the following paragraphs.

System Design

System design consists of work flow and needs analysis and the basic architectural design of the system. The process starts with the analysis of the work flow functions, from which the needs and requirements of the users (radiation oncologists, medical physicists, and radiation therapists) are defined. For example, after a dosimetric plan has been generated, the radiation oncologist needs to approve the plan. The system designer should create a route whereby the radiation oncologist can access the system to perform such a task. In addition, the data on treatment planning and delivery are best visualized in a timeline format, along with the patient's demographic information. All pertinent events and tasks should be listed, and the framework should be drafted for the design of the GUI. This initial stage of system design provides the conceptual model for the system and requires detailed input from clinicians.

The next step is the architectural design of the data flow through the various components of the ePR system and the physical data model for central storage (the DICOM-RT archive server). Given the DICOM standard with its information object definitions defined for radiation therapy, the development of the physical data model could be similar to that of the PACS, the architecture of which could be used for the DICOM-RT–based ePR system.

PACS as a Model for Architectural Design.—A PACS consists of imaging modalities that generate images, an acquisition gateway, a PACS server-archive, and display subsystems, all of which are integrated by a network as shown in Figure 6 (2).

Teaching Point

in Figure 6 (2). The DICOM-RT objects are extensions of the DICOM standard, so that the data model and the data flow of the PACS can serve as a guide for the design of the radiation therapy data flow as shown in Figure 6 (9). Likewise, the DICOM-RT–based ePR system will receive data input from different radiation therapy information systems and equipment. These data will be integrated through DICOM-RT Gateway with the archive server to form the ePR system.

Figure 6 illustrates the similarities and differences between a PACS and the DICOM-RT–based ePR system. The latter is patterned after the generic PACS data flow design and consists of DICOM-RT Objects Input, DICOM-RT Gateway, and the DICOM-RT–based ePR system platform. The system platform in turn consists of three major components: the DICOM-RT archive server, the RT Web application server, and the Web-based client workstations. These three components correspond to the archive server, the Web server, and the review workstations in a PACS (Fig 6). The specific differences are in the design of the RT Web application server, which must handle more complex imaging and informatics data than a Web server for a PACS. The major components of the DICOM-RT–based ePR system are described in the following paragraphs.

DICOM-RT Objects Input and DICOM-RT Gateway.—From the work flow diagram in Figure 1, the radiation therapy objects are identified and are input into the ePR system (Fig 6, module *1*) through DICOM-RT Gateway (Fig 6, module *2*). The functional requirements (eg, treatment plan approval by the radiation oncologist) in the work flow review are converted into the technical details of the system based on the DICOM-RT information object definitions and the data flow of the objects. The DICOM standard service classes (eg, DICOM storage and query-retrieve) are incorporated into each component of the ePR system. After receiving the radiation therapy objects, the gateway extracts information from the objects and puts them into the radiation therapy data model as required in the DICOM-RT archive server. It also converts any nonstandard data objects to the standard required by the DICOM-RT server.

RT Archive Server.—A database schema for the DICOM-RT archive server (Fig 6, module *3*) can be constructed by following the pattern for the DICOM hierarchic structure. The schema consists of four levels—Patient, Study, Series, and RT Objects—and 11 modules (12,13), represented by the boxes in Figure 7. The schema follows the DICOM data model of the real world but includes the seven DICOM-RT data objects and the DICOM diagnostic images. It is important to note that most current PACS do not support DICOM-RT objects (except DICOM-RT Image); hence, it is necessary to have a more highly developed schema specifically for a DICOM-RT archive server. PACS manufacturers can begin to incorporate the DICOM-RT objects to turn their PACS server into a DICOM-RT archive server.

For the archive server, a SUN Ultra 2 computer (Sun Microsystems, Santa Clara, Calif) with SCSI (small computer system interface) hard disk and 100-Mbyte Ethernet adapter operating under SunOS 5.8 was used. The software included SUN Workshop Compilers CC++, a PACS programming library, and an Oracle8i release 8.1.7 database management system. The archive server is used mostly for the management and storage of objects rather than for processing the radiation therapy data (attributes) encapsulated in the objects. Upon receiving DICOM-RT objects and images from DICOM-RT Gateway, the archive server abstracts only the essential aspects of these entities for the necessary transactions and "autoroutes" all the data to the Web application server to be processed for display on the Web client application.

RT Web Application Server.—Whereas the DICOM-RT archive server is responsible for storage and transmission of DICOM images and DICOM-RT objects, the RT Web application server (Fig 6, module *4*) receives the objects, decodes them to the corresponding position in the RT Web application database, and organizes the data into the Web viewing mode for display on the client workstations (Fig 8). In this respect, the Web application server is the "brain" for the DICOM-RT–based ePR system, since all actions are processed here. Microsoft Access 2000 (Microsoft, Redmond, Wash) was used as the database for the application server. Windows Internet Information Server (Microsoft) was used for distribution of radiation therapy information, and the data were sent using hypertext transfer protocol.

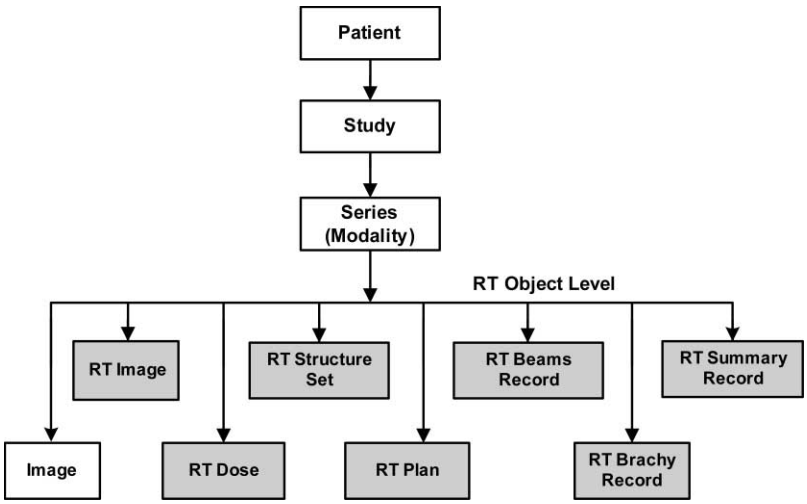

Figure 7. Schematic illustrates the DICOM-RT archive server database. The schema is based on the DICOM data model of the real world. Note that the seven DICOM-RT objects (gray boxes) are integrated within the Series (Modality) module, along with the Diagnostic Image object (white box, lower left). In other words, each object is grouped under the attribute "modality" in the "series" similar to the modality of CT or MR imaging (8). *Brachy* = brachytherapy.

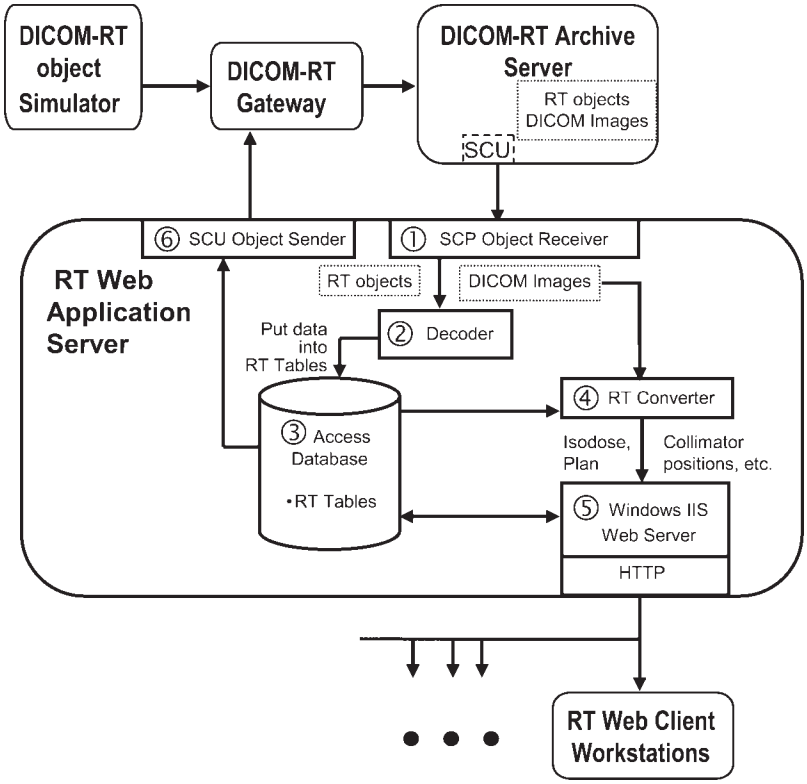

Figure 8. Diagram illustrates the architecture of the RT Web application server of the DICOM-RT–based ePR system. Six key components are shown within the server, which is more complex than a PACS Web server in that it must handle the image and informatics data from the seven DICOM-RT objects in addition to the DICOM images from diagnostic radiology. DICOM-RT objects and DICOM diagnostic images are received by Service Class Provider *(SCP)* Object Receiver *(1)*, the objects are decoded by the decoder *(2)*, and the data are arranged in RT Tables and the RT Database *(3)*. The data from the tables will be superimposed on the corresponding portions of the DICOM images by the RT Converter *(4)* and sent by the Web server *(5)* to the client workstations. Service Class User *(SCU)* Object Sender *(6)* allows updated objects to be sent to the DICOM-RT archive server via the gateway for storage. *HTTP* = hypertext transfer protocol, *IIS* = Internet Information Server.

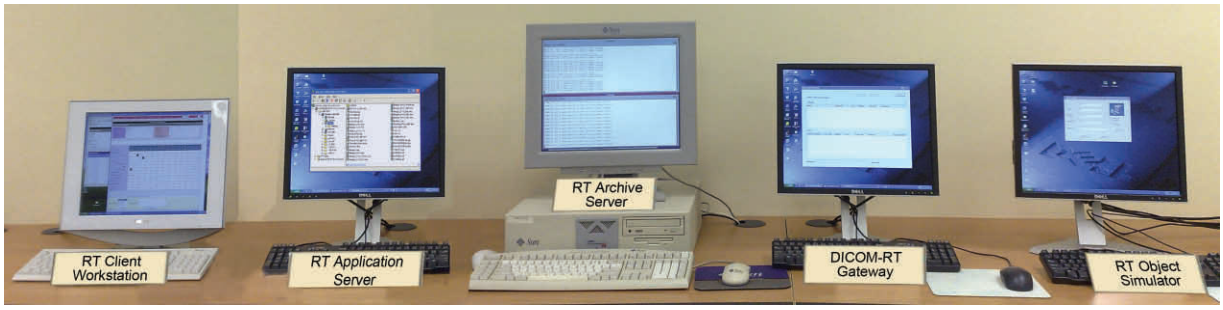

Figure 9. Photograph illustrates the DICOM-RT–based ePR system prototype. Note that the components correspond to the elements of the conceptual diagram in Figure 6.

The DICOM standard has grouped various radiation therapy attributes into modules and information object definitions (6). The overall database schema of the RT Web application server adopts what is defined by the DICOM data model and consists of 72 tables (in the prototype system) to facilitate Web viewing on the client workstations (12,13). This information includes key data items such as treatment plan parameters, beam records, isodose curves, region of interests (including tumor volume and the contours of organs at risk), dose-volume histograms, and so on. These data are parsed from the DICOM-RT objects as needed for display in the Web client application.

For the prototype system, our team designed the Web-based display and database structure at the front end, and the data objects, structure, communication protocol, and encoding-decoding with open standards at the back end. Within the Web application server, the graphical illustrations of (for example) dosimetric plans are created, stored, and displayed in a JPEG (Joint Photographic Experts Group) format. They result from the overlay of the DICOM CT Image, RT Structure Set, RT Plan, and RT Dose objects. The DICOM standard inherently provides cross-referencing among these objects. Decoding-encoding software applications were developed on the basis of the DICOM information object definitions. When multiple data items are required on a given display (eg, the dosimetric plan), the DICOM objects containing the target volumes, contours of the organs at risk, and isodose distribution are decoded to and encoded from the database records of the coordinates in the Web application server based on the definition of the DICOM sequences. These Web-based displays are created by plotting coordinates onto the referenced diagnostic CT scan.

The data objects from the Web-based application can be used to develop quantified knowledge and metadata that can be added to the database schema. Further outcomes data can also be added to the overall database schema. Therefore, it is important to design the database schema to be as flexible as possible to allow the addition of a knowledge base and outcomes data that are not part of the DICOM standard.

RT Web Client Workstation.—For the RT Web client workstations (Fig 6, module 5), the GUI is designed for users to access information within the database according to the functional requirements of radiation therapists, dosimetrists or physicists, and oncologists. On the basis of the user requirements documentation, all necessary data are included in the database tables of the Web application server. The radiation therapy work flow also serves to drive the GUI design (Figs 2–5).

System Implementation

A laboratory DICOM-RT–based ePR system prototype (Fig 9) was implemented that incorporates the infrastructure and components shown in Figure 6. Note that RT Object Simulator was used to simulate the input of DICOM-RT objects into the system.

System Testing

Development of the ePR system is subject to many iterative stages of testing, refinement, and evaluation before the system can be implemented in the clinical environment for further evaluation. The transmission of radiation therapy objects through the system was tested manually on an object-by-object basis. The real DICOM-RT objects were tested first. Next, the non-DICOM

files were translated into a DICOM object prior to evaluation. Each object type was sent through RT Object Simulator. The arrival of the object at the DICOM-RT archive server and then at the RT Web application server was tracked and the date and time of insertion examined. The system has been tested with different types of object sources from four different vendors. These object sources include VARiS Vision (Varian Medical Systems, Palo Alto, Calif); Precise and iView (Elekta, Crawley, England); Helax-TMS and Theraplan Plus (MDS Nordion; Toronto, Ontario, Canada); and Pinnacle[3] (ADAC Laboratories, Milpitas, Calif). At the time of testing, not all DICOM-RT objects had been implemented by all vendors, especially RT Dose and RT Records. However, we managed to acquire or create all of the objects from various sources.

System Evaluation

The system has been evaluated on the basis of data from 10 "virtual patients" who were created using our data sources. The arrival and integrity of all the data were verified using the GUIs at the Web client workstation. Two radiation therapists and an oncologist were invited to evaluate the system as end-users. They were asked to rate the usefulness of the system and the degree to which it improved patient service. The average rating was 8 out of 10. Suggestions for improvement and further refinement were also collected. The results indicate that the system would be very useful and quite likely to improve patient service.

Discussion

The prototype system can query-retrieve and receive diagnostic DICOM images from a commercial PACS in the same manner as a TPS. As shown in Figure 6, the entire system includes the DICOM-RT gateway, archive server, Web application server, and client workstations. During current clinical radiation therapy work flow steps, the diagnostic images within the TPS may be altered and images within the series removed, making them unavailable for future review. Our system would contain the entire diagnostic data set in case the oncologist would like to review the studies without having to access the commercial PACS application again to view them. In addition, imaging and informatics data from all the different stand-alone radiation therapy–related systems in the oncology department can be sent to the system with use of the DICOM-RT standard (Fig 6). Therefore, in an ideal situation, rather than moving from one system to another to view key treatment-related data, the decision maker (eg, the oncologist) can view all related data in one system with one application.

The DICOM-RT–based ePR system has to a certain extent demonstrated the interoperability of systems that can output DICOM-compliant information. The prototype was developed on the basis of radiation therapy work flow in daily practice so that the user can view key treatment-related data in one system.

A technical framework for implementation of established standards is currently being drafted for radiation oncology to help carry out specific clinical tasks assigned by the Integrating the Healthcare Enterprise (IHE) initiative. It identifies subsets of functional components (called "actors" [eg, Geometric Planner or Archive]) and specifies their interactions in terms of transactions. For example, after creating a geometric plan on the CT scan, the user of the Geometric Planner wants to store the plan, which involves a Geometric Plan Storage transaction. The Geometric Planner sends the newly created geometric plan to the archive for storage (14). The IHE technical framework defines only "those functions associated with integrating information systems" and not necessarily the clinical work flow in general. In this sense, the DICOM-RT–based ePR system described in this article is different from the work being done by IHE. However, the IHE technical framework would help smooth out the integration process. Although it is true that the IHE initiative has the greatest impact on work flow efficiency, without the DICOM and HL7 (Health Level 7) standards, the IHE radiology work flow profiles cannot be realized. Similarly, the challenges that exist in radiation oncology departments are related to stand-alone and proprietary systems with key data elements that are not standardized. The goal is to first standardize the data objects with DICOM-RT, and then begin integrating the DICOM-RT objects into the work flow. In fact, IHE-RO (radiation oncology) has been established to demonstrate the importance of DICOM-RT and work flow profiles for radiation oncology departments. Our radiation therapy ePR system is the first comprehensive step toward this goal. These innovations, along with our integrated ePR system, can give impetus to the movement toward full standardization among all manufacturers. In addition, our research and development team has followed these technologic

Teaching Point

advances closely, and the system will continue to be updated and refined to adhere to these newly developed IHE-RO work flow profiles once they are officially established. Our system prototype represents a major step forward in that it improves integration, since it can both convert proprietary data objects from the various stand-alone systems into DICOM-RT objects and receive developed DICOM-RT objects from other systems that have already begun to standardize their data.

Conclusions

Radiation therapy is an image-intensive treatment method for which the development and system integration of standardized data is similar to that for radiology. For prompt, accurate treatment, it is crucial to pay close attention to every detail in the radiation therapy work flow, which has an impact on patient outcomes. By providing comprehensive and up-to-date medical information, the DICOM-based ePR system can not only improve physician efficiency and the quality of patient care, but also cultivate excellence in the delivery of radiation therapy services.

DICOM-RT is the standard used to build an open-architecture DICOM-RT–based ePR system. With the DICOM-RT standard, the ePR system can enhance application interoperability among multivendor modalities, providing a truly open environment for seamless data exchange, so that a radiation therapy department will not be restricted to a single manufacturer's systems. The open architecture based on the DICOM-RT standard also facilitates consultation or clinical research across institutions. The DICOM-RT–based ePR system with standardized radiation therapy data can be leveraged for further research that can be performed to extract and quantify knowledge for decision support tools as well as outcome analysis, ultimately making this system a research and clinical tool that is even more powerful than existing clinical methods.

In summary, the benefits of a DICOM-RT–based ePR system are threefold: the system can be used *(a)* as a foundation for performing effective and efficient clinical services; *(b)* as a common platform for radiation therapy data exchange, expert consultation, and clinical research; and *(c)* for medical imaging informatics research in developing innovative decision support tools and a knowledge base for improved radiation therapy treatment.

Teaching Point

References

1. Nagata Y, Okajima K, Murata R, et al. Development of an integrated radiotherapy network system. Int J Radiat Oncol Biol Phys 1996;34(5):1105–1111.
2. Huang HK. PACS and imaging informatics: basic principles and applications. Hoboken, NJ: Wiley-Liss, 2004.
3. Schultheiss TE, Coia LR, Martin EE, Lau HY, Hanks GE. Clinical applications of picture archival and communications systems in radiation oncology. Semin Radiat Oncol 1997;7(1):39–48.
4. Digital Imaging and Communications in Medicine (DICOM) Supplement 11. Radiotherapy objects.
5. Digital Imaging and Communications in Medicine (DICOM) Supplement 29. Radiotherapy treatment record and media extensions.
6. DICOM in radiotherapy. Available at: http://medical.nema.org/dicom/geninfo/brochure/rtaapm.doc. Accessed March 1, 2007.
7. Digital Imaging and Communications in Medicine (DICOM) Part 3. Information object definitions. Available at: http://medical.nema.org/dicom/2007/. Accessed January 20, 2008.
8. Law MYY, Liu BJ. Informatics in radiology: DICOM-RT and its utilization in radiation therapy. RadioGraphics 2009 Mar 6 [Epub ahead of print].
9. Kushniruk A. Evaluation in the design of health information systems: application of approaches emerging from usability engineering. Comput Biol Med 2002;32(3):141–149.
10. Wasson CS. System analysis, design, and development: concepts, principles, and practices. Hoboken, NJ: Wiley, 2006.
11. Dennis A, Wixom BH, Roth RM. Systems analysis and design. 3rd ed. Hoboken, NJ: Wiley, 2006.
12. Law MY. A model of DICOM-based electronic patient record in radiation therapy. Comput Med Imaging Graph 2005;29(2–3):125–136.
13. Law MYY. The design and implementation of a DICOM-based integrated radiotherapy information system. Thesis. Chinese Academy of Sciences, Beijing, China, 2004.
14. ASTRO. Integrating the Healthcare Enterprise. IHE-Radiation Oncology Technical Framework Volumes 1–2: draft for trial implementation. Available at: http://www.ihe.net/Technical_Framework/upload/IHE_RO_TF_v1.pdf. Accessed August 18, 2007.

Informatics in Radiology
DICOM-RT—based Electronic Patient Record Information System for Radiation Therapy

Maria Y. Y. Law, PhD, et al

RadioGraphics 2009; 29:961–972 • **Published online** 10.1148/rg.294085073 • **Content Codes:** IN RO

Page 966
The most important point to be gleaned from Figures 2--5, which illustrate how the ePR system is integrated with the radiation therapy work flow shown in Figure 1, is that all pertinent imaging and informatics data needed for decision making during radiation therapy are available in a single integrated system and are standardized in DICOM-RT format.

Page 967
System development involves system design, implementation, testing, and evaluation.

Pages 968
The DICOM-RT objects are extensions of the DICOM standard, so that the data model and the data flow of the PACS can serve as a guide for the design of the radiation therapy data flow as shown in Figure 6 (9).

Page 971
[T]he challenges that exist in radiation oncology departments are related to stand-alone and proprietary systems with key data elements that are not standardized. The goal is to first standardize the data objects with DICOM-RT, and then begin integrating the DICOM-RT objects into the work flow.

Page 972
[T]he benefits of a DICOM-RT—based ePR system are threefold: the system can be used *(a)* as a foundation for performing effective and efficient clinical services; *(b)* as a common platform for radiation therapy data exchange, expert consultation, and clinical research; and *(c)* for medical imaging informatics research in developing innovative decision support tools and a knowledge base for improved radiation therapy treatment.

RadioGraphics

Informatics in Radiology

DICOM-RT and Its Utilization in Radiation Therapy[1]

TEACHING POINTS
See last page

Maria Y. Y. Law, PhD • Brent Liu, PhD

The Digital Imaging and Communications in Medicine (DICOM) standard is now widely implemented in radiology as the standard for diagnostic imaging. It has also been extended for use in various subspecialties. One of the first extensions was applied to radiation therapy and is known as DICOM-RT. In addition to the protocol used in the DICOM standard, seven DICOM-RT objects—namely, RT Image, RT Structure Set, RT Plan, RT Dose, RT Beams Treatment Record, RT Brachy Treatment Record, and RT Treatment Summary Record—have been created, each with a well-defined data model. The data models set the standard for integration of radiation therapy information for an electronic patient record and would facilitate the interoperability of different radiation therapy systems, thus making possible the sharing of information from different systems.

Abbreviations: CTV = clinical target volume, DICOM = Digital Imaging and Communications in Medicine, DRR = digitally reconstructed radiograph, ePR = electronic patient record, IHE = Integrating the Healthcare Enterprise, OAR = organ at risk, PACS = picture archiving and communication system, PTV = planning target volume, ROI = region of interest, TPS = treatment planning system

RadioGraphics 2009; 29:655–667 • **Published online** 10.1148/rg.293075172 • **Content Codes:** IN RO

[1]From the Department of Health Technology and Informatics, the Hong Kong Polytechnic University, Hung Hom, Kowloon, Hong Kong (M.Y.Y.L.); and Image Processing and Informatics Laboratory, Keck School of Medicine, University of Southern California at Health Sciences Campus, Los Angeles, Calif (B.L.). Presented as an Informatics exhibit at the 2006 RSNA Annual Meeting. Received August 13, 2007; revision requested November 20; final revision received November 17, 2008; accepted December 18. Both authors have no financial relationships to disclose. **Address correspondence to** M.Y.Y.L. (e-mail: *maria.law@polyu.edu.hk*).

Introduction

The Digital Imaging and Communications in Medicine (DICOM) standard is used for transmission of medical images. Its predecessor, the ACR-NEMA (American College of Radiology–National Electrical Manufacturers Association) standard, was published in 1982, followed by a second version, ACR-NEMA 2.0, in 1988 (1–3), neither of which addressed computer networking issues. A major revision named DICOM that incorporated the existing network standard was introduced in 1992, specifying standards for digital imaging systems in medicine for information handling and transmission. For details regarding the DICOM standard, readers are referred to the technical and nontechnical introduction to DICOM in two previous articles published in this journal (1,2).

DICOM is the cornerstone of the successful implementation of picture archiving and communication systems (PACS) in radiology, allowing communication between equipment from different vendors. In recent years, the DICOM standard has been extended to incorporate many medical specialties such as radiation therapy (4,5), cardiology (6,7), pathology (8,9), and ophthalmology (10,11) and allow the viewing of images together with specialty-specific information. Because radiation therapy is image intensive, it was the first specialty to be incorporated into the DICOM standard after radiology, with the creation of four DICOM-RT objects in 1997 (4) and three more in 1999 (5). In 2006, two additional objects were defined for ion therapy (12). Because this article is intended to serve as an introduction to the DICOM-RT standard, only the first seven objects for radiation therapy will be described.

For communication of radiation therapy data, the transfer protocol will largely follow the standard used in DICOM for communication of medical images, which will not be revisited in this article. It is the unique information in radiation therapy such as text, graphs, and isodose lines and their superimposition on medical images that gives rise to the creation of specific radiation therapy information object definitions and their attributes. In this article, we describe the work flow in radiation therapy compared with that in radiology and the DICOM-RT objects that are generated in the radiation therapy work flow. In addition, we discuss and illustrate the utilization of DICOM-RT in a sample case of prostate cancer and discuss the need to integrate radiation therapy information with use of DICOM-RT.

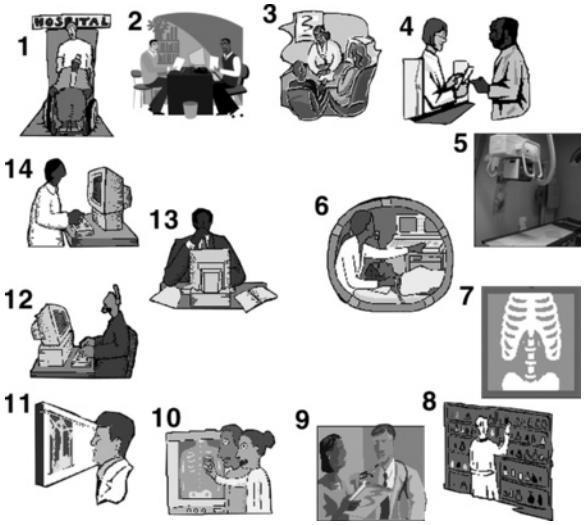

Figure 1. Chart illustrates the impact of a PACS on clinical work flow in a radiology department. Step 1, patient arrives at hospital; step 2, patient registers with hospital information system; step 3, examination is ordered at radiology information system; step 4, technologist receives information from clerk; step 5, patient is escorted into modality room; step 6, technologist performs examination; step 7, examination is completed; step 8, clerk pulls out old films; step 9, clerk prepares all necessary papers and films for radiologist; step 10, films are hung up for radiologist's review; step 11, radiologist reviews films, reads examinations, and dictates reports; step 12, transcriptionist types draft report from the dictation; step 13, radiologist reviews and signs off on report; step 14, final reports are input into radiology information system for clinical viewing. With the implementation of a PACS, steps 4, 8–10, 12, and 14 can be eliminated, making work flow more efficient. (Modified, with permission, from reference 3.)

Radiology Work Flow versus Radiation Therapy Work Flow

Radiology Work Flow

The DICOM-RT objects are extensions of the DICOM standard, which, as mentioned earlier, was first implemented for use in radiology.

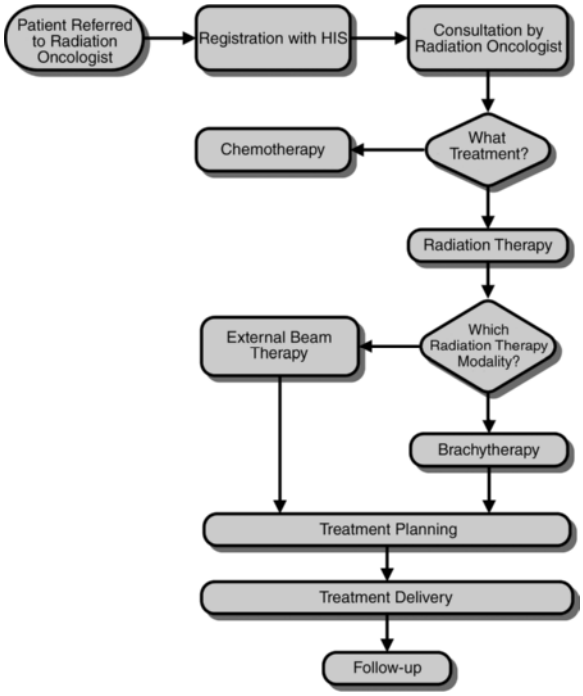

Figure 2. Chart illustrates cancer treatment work flow. Note that in some cases, the patient can receive both chemotherapy and radiation therapy as part of treatment. Whichever radiation therapy modality is chosen, the work flow involves treatment planning and delivery. *HIS* = hospital information system.

Reviewing the work flow in radiology before discussing the work flow in radiation therapy will help readers understand the similarities and differences between the information requirements of these two specialties in medicine.

Steps 1–14 in Figure 1 depict film-based radiology work flow without a PACS. With the implementation of digital radiography and a PACS, the work flow is greatly simplified. After the patient arrives at the hospital (step 1) and is registered with the hospital information system (step 2) and radiology information system (step 3), his or her personal information and the request for examination will be transmitted to the appropriate modality (step 5), saving the technologists from having to obtain the patient information from the reception counter (step 4). When the examination is performed (step 6), an image is generated (step 7). This image, together with any previous images, will be sent by the PACS to the workstation for reading by the radiologist (step 11), thereby saving steps 8–10. The prefetching of previous images by clerical staff is no longer required, and preparatory work for image reading is reduced. The radiologist can easily use some templates or a structured report at the reading workstation to type out the imaging findings (step 13), thereby saving steps 12 and 14.

In addition to saving both time and manpower in searching for old films and preparing reports, the implementation of digital radiography and a PACS allows integration of images from different modalities and vendors under the patient's unique identifier. These images can easily be retrieved without fear of losing data or film.

Radiation Therapy Work Flow

Radiation therapy consists of three modalities: external beam therapy, nuclear medicine, and brachytherapy. Upon being referred by a general physician for consultation, the patient is scheduled for an appointment. On the appointed day, the patient registers at the oncology department. The radiation oncologist sees the patient and determines the most appropriate modality for the patient on the basis of prior investigation results and treatment protocol. In general, radiation therapy entails treatment planning and delivery. Thus, when the oncologist decides that the patient should proceed with radiation therapy, the patient will be scheduled for treatment planning before undergoing treatment.

External beam therapy accounts for over 90% of the workload in a radiation therapy department. Brachytherapy often plays a supplementary role and is often used in the treatment of gynecologic cancers. Nuclear medicine has become independent of radiation therapy in many hospitals. Thus, for the sake of simplicity, only the work flow of external beam therapy will be considered. Figure 2 provides a brief overview of patient treatment in a radiation oncology department once the type of treatment has been determined. In some cases, the patient may receive both chemotherapy and radiation therapy. Figure 3 shows the general procedures involved in the planning and delivery of external beam therapy in a specific clinical case of prostate cancer.

Note how different radiation therapy data are generated within the work flow. The data are categorized and "contained" in the various DICOM-RT objects as defined by the DICOM standard (Fig 3).

Treatment Planning (Steps 1–5).—The goal of treatment planning is to deliver the highest and most uniform radiation dose possible to the tumor-bearing site but the smallest dose possible to the surrounding healthy tissue, especially critical and radiosensitive structures (the urinary bladder and rectum in cases of prostate cancer).

Information from medical images is crucial to the radiation therapy planning process. The process starts with the localization of the prostate tumor volume. For this purpose, the oncologist will order a CT study of the pelvis, performed on either the CT simulator or a CT scanner. The patient's information is delivered to the CT simulator room, where the radiation therapist positions the patient for scanning. The pelvic CT scans are generated as DICOM images and stored either in a PACS or in the workstation there (step 1). The CT scans are then transferred to a computer treatment planning system (TPS) (step 2) for radiation field planning. Previous diagnostic images, CT scans, magnetic resonance (MR) images, or positron emission tomographic (PET) scans may also be retrieved to aid in the delineation of tumor volume.

At the TPS workstation, the tumor volume and the organs at risk (OARs) (urinary bladder and rectum) are delineated. Treatment fields of appropriate size and optimal gantry or collimator angles are determined. The TPS will compute the radiation dose distribution within the body region to be treated (step 2). Determining the best radiation therapy plan requires a clinical judgment based on the balance between adequate target volume coverage and sparing of OARs. Each plan should be evaluated carefully with use of dose-volume histograms and planar dose distributions. Although they do not provide spatial information, dose-volume histograms provide a global view as to whether the resultant plan meets the dose-

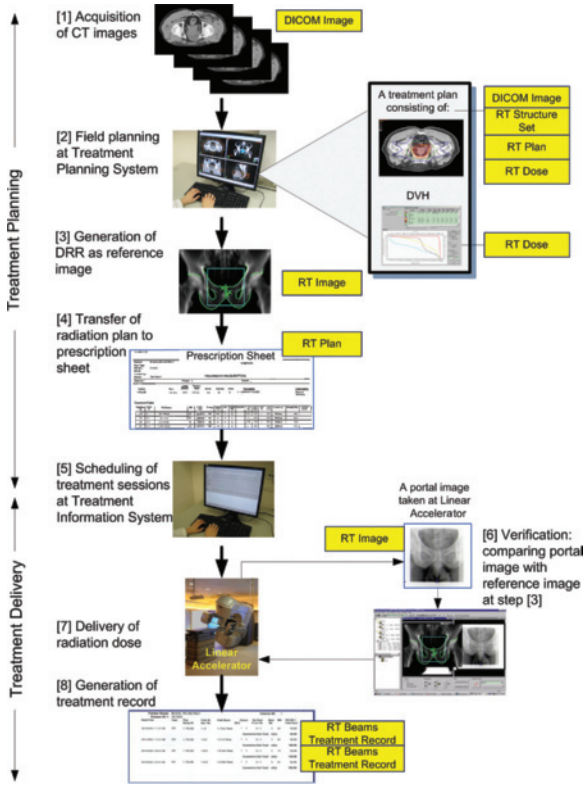

Figure 3. Chart illustrates radiation therapy work flow. Yellow boxes indicate the DICOM-RT objects that could be generated within the work flow. A radiation therapy treatment plan (step 2) with radiation dose distribution involves the superposition of the radiation therapy objects RT Plan, RT Structure Set, and RT Dose on the corresponding set of DICOM computed tomographic (CT) scans according to the coordinates in the DICOM-RT standard. Because the work flow is for external beam therapy, the RT Brachy Treatment Record information object is not shown. *DRR* = digitally reconstructed radiograph, *DVH* = dose-volume histogram.

volume criteria. A detailed slice-by-slice analysis of isodose distribution is crucial for examining target volume coverage and identifying the exact location of "hot" and "cold" spots with respect to radiation dose. When the OARs overlap with or are in proximity to the target volume, the dose is often limited by ranking the OARs in terms of relative importance.

Images similar to projectional images can be reconstructed from the CT scans to show the treatment field positions and are called digitally reconstructed radiographs (DRRs) (step 3). A DRR, or simulator image obtained for treatment planning, will serve as the reference image for treatment verification later. The finished plan is presented to the radiation oncologist for evaluation and approval. If the plan is found satisfactory, the oncologist prescribes the treatment (step 4) on the radiation therapy prescription sheet. A treatment record with all treatment details is prepared with the prescription. Treatment sessions are scheduled in the treatment information system (step 5) and transferred to the radiation treatment unit or linear accelerator, either through the department network or by manual paper delivery.

Treatment Delivery (Steps 6–12).—Before the actual radiation treatment commences, the accuracy of the treatment plan in terms of field sizes, setup, shielding positions, and so on needs to be verified at the linear accelerator. For such verification, a portal image is obtained at the linear accelerator (step 6), either as a film image or (with an electronic portal imaging device installed in the linear accelerator) as a digital portal image. The image is then compared with the reference DRR or simulator image. When the irradiated portal aligns correctly with the portal on the reference images, the oncologist will approve the verification. Radiation treatment can then proceed (step 7). Otherwise, a repeat portal image may be requested. Normally, the patient will be treated five times a week for 7–8 weeks. At each treatment session, each of the treatment beams will be recorded, as well as the radiation dose and the cumulative dose to date (step 8).

During the course of treatment, weekly verification images are acquired to ensure accuracy. The oncologist will also review the patient's progress and prescribe whatever medicine is required. Upon being completed, the patient's course of treatment will be summarized and filed. A follow-up appointment will usually be made with the patient for review purposes.

Comparison of Work Flow

Radiology mainly involves the generation of medical images and reporting of the diagnosis, whereas in radiation therapy, the images are used for treatment planning and specific kinds of images are generated for treatment verification. In radiology, the procedure is considered complete as soon as the imaging findings have been reported, but this is only the beginning for radiation therapy. Treatment planning and delivery, consultation, and follow-up are additional procedures in radiation therapy that generate information quite different from that in radiology. Table 1 compares radiology and radiation therapy in terms of the nature of the work involved and the requirements for information integration. In contrast to the radiology work flow, in which the data are mostly images and are generated together, the radiation therapy work flow entails additional imaging and informatics data that are generated over an extended period of time due to the many more steps involved. Although its framework looks similar in many areas, the DICOM information object is different. In radiology, the same DICOM image object information entity is deployed to accommodate the different modules of attributes. In radiation therapy, there are different objects to group the different types of information (Table 2).

Table 1
Requirements for Information Integration in Radiology versus Radiation Therapy

Radiology	Radiation Therapy
Imaging informatics based: image and informatics data for diagnosis, historical studies for diagnosis, computer-aided detection/diagnosis or decision support during diagnosis	Imaging informatics based: image and informatics data for treatment, historical plans for treatment planning, quantified knowledge or decision support during course of treatment
Modalities: radiography, computed radiography, CT, MR imaging, ultrasonography, PET, and so on	Modalities: external beam therapy, brachytherapy, ion therapy
Standards: DICOM, HL7, IHE Work Flow Profiles	Standards: DICOM-RT, DICOM, HL7, IHE Work Flow Profiles
Key imaging and informatics data objects: DICOM Image, DICOM-SR, other reports	Key imaging and informatics data objects: DICOM Image, DICOM-RT objects, DICOM-SR, other reports
Customers: patient, referring physician, radiologists	Customers: patient, referring physician, radiation oncologists
System integration necessary for improved work flow	System integration necessary for improved work flow
Solution: PACS	Solution: DICOM-RT electronic patient record (ePR) system

Note.—Data generated within the radiation therapy clinical work flow contain additional imaging and informatics data that are crucial for the work flow, which necessitates the DICOM-RT standard as well as an ePR system. HL7 = Health Level 7, IHE = Integrating the Healthcare Enterprise, SR = structured report.

Table 2
Image Object versus an RT Object IOD Module

Information Entity of DICOM Image Object	Module* (MR Imaging)	Information Entity of DICOM-RT Object	Module* (RT Structure Set)
Patient	Patient	Patient	Patient
Study	General Study	Study	General Study
Series	General Series	Series	RT Series
Frame of Reference	Frame of Reference	...	...
Equipment	General Equipment	Equipment	General Equipment
Image	General Image, Imaging Plane, Image Pixel, MR Image, SOP Common (13)	Structure Set	Structure Set, ROI Contour, RT ROI Observations, SOP Common (13)

*Only mandatory modules are listed. A module groups related information together. For example, the Patient module contains attributes related to the patient, such as Patient's Name, Patient ID, Patient's Birth Date, Patient's Sex, and so on. The modules for the image Information Entity depend on the modality concerned. In this table, the modality of interest is MR imaging; thus, in addition to the General Image module, Information Entity has a specific MR Image module and other related modules. Structure Set is one of the DICOM-RT objects and includes Structure Set, ROI Contour, and RT ROI Observations as its specific modules. IOD = information object definition, ROI = region of interest, SOP = service-object pair.

DICOM-RT Objects

Teaching Point

There are significant differences in the types of information required for radiology and radiation therapy as well as differences in the time at which and frequency with which the information is obtained. The different types of information require different categorization. On the basis of the standard DICOM query-retrieve model, the radiation therapy information is defined in seven information objects known as DICOM-RT objects for the transfer of data (10,11,13). These information objects include RT Structure Set, RT Plan, RT Dose, RT Image, and RT Treatment Record, which is further divided into RT Beams Treatment Record, RT Brachy Treatment Record, and RT Treatment Summary Record. Figure 4 shows these objects, how they are extensions of the DICOM model in radiology, and how they relate to each other and to the image object in radiology. The information in the DICOM-RT objects is described in the following paragraphs and illustrated in Figures 5–9.

Teaching Point

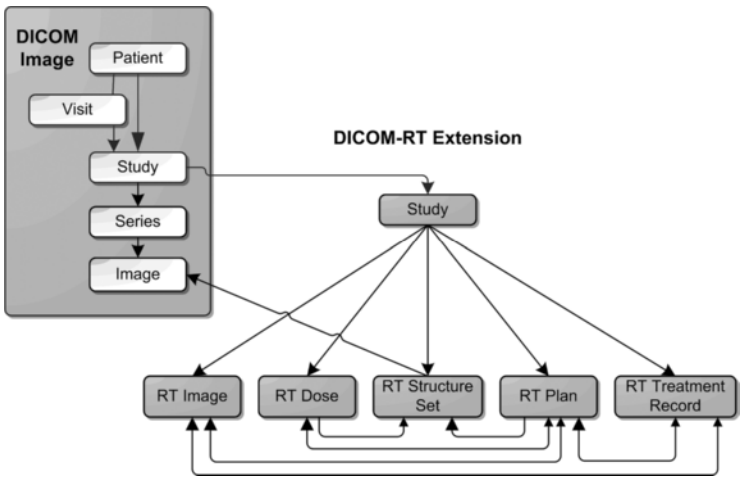

Figure 4. Chart illustrates DICOM-RT objects as an extension of the DICOM standard. Note that RT Plan, which contains all RT-related information, is an important object that is needed from the start of radiation therapy planning to the completion of treatment and is thus related to all other objects.

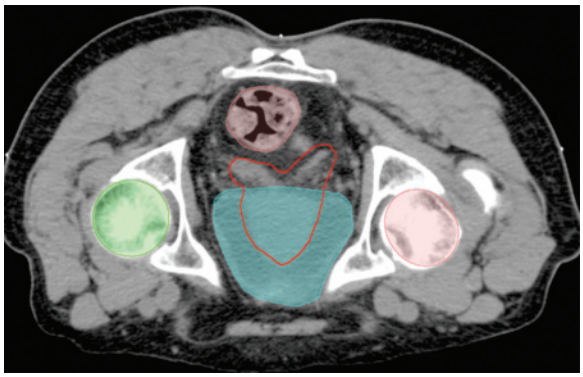

Figure 5. CT scan with superimposed color coding shows an RT Structure Set, which includes tumor volume (outlined in red), OARs (femoral heads [green and pink], rectum [purple], bladder [blue]), and body contour.

Dose Prescription												
RT to IMRT: Give 2 Gy/fr, 5 fr/wk at 100% I.L. to 76 Gy in 38 fr. and stop.												
Fields												
LA	Energy	ID	X1	X2	Y1	Y2	SSD	Gantry	Coll	Table	Weight	MU
LA2	6X	Field1	+5.8	+6.3	+4.5	+2.5	90.1	180 °	0°	0°	1.0	80
LA2	6X	Field2	+5.3	+5.5	+4.5	+2.5	85.2	110°	0°	0°	1.0	75
LA2	6X	Field3	+4.5	+5.3	+4.5	+2.5	82.8	85°	0°	0°	1.0	76
•												
•												
•												

a.

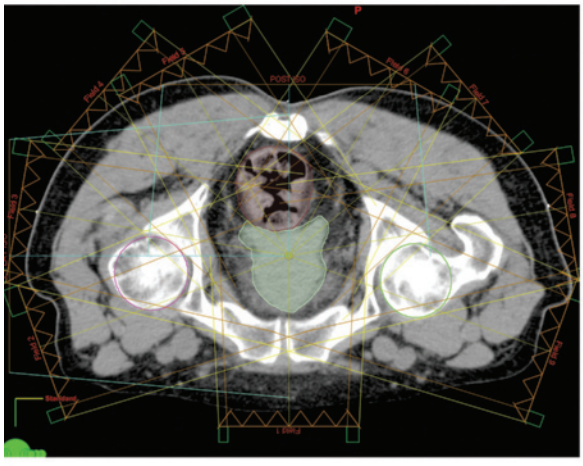

b.

Figure 6. RT Plan. **(a)** Chart illustrates an RT Plan. *Coll* = collimator rotation, *fr* = fraction, *ID* = identification, *I.L.* = isodose level, *IMRT* = intensity-modulated radiation therapy, *LA* = linear accelerator, *MU* = monitor unit, *RT* = radiation therapy, *SSD* = source-skin distance, *X* and *Y* = collimator leaves in the x and y directions. **(b)** Information from RT Plan superimposed on RT Structure Set and a CT scan. Nine radiation beams (attribute of RT Plan) are each indicated by a red label and three yellow lines.

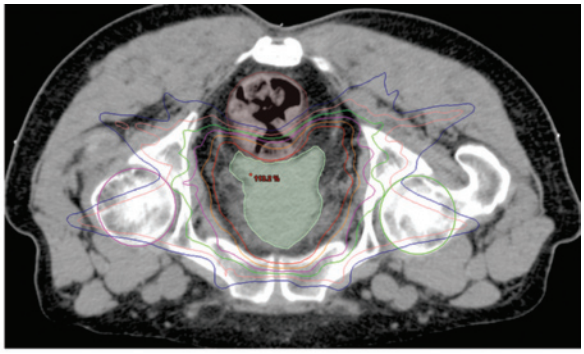

a.

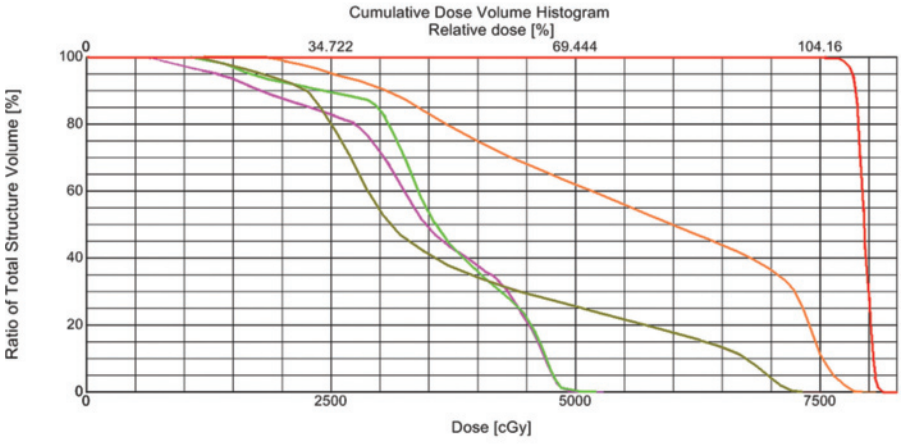

Structure	Plan	Plan Status	Course	Coverage [%/%]	Volume	Min Dose	Max Dose	Mean Dose	Modal Dose	Median Dose	Std Dev
RECTUM	TREATMENT (TREATMENT)reatment Approved	IMRT		100.0 / 100.0	53.4 [cm³]	1031.8 cGy	7517.1 cGy	3812.1 cGy	2700.0 cGy	3103.1 cGy	1671.9 cGy
RT FEMORAL HEAD	TREATMENT (TREATMENT)reatment Approved	IMRT		100.0 / 100.0	65.2 [cm³]	983.2 cGy	5157.9 cGy	3611.5 cGy	4708.8 cGy	3564.9 cGy	879.1 cGy
LT FEMORAL HEAD	TREATMENT (TREATMENT)reatment Approved	IMRT		100.0 / 100.0	67.0 [cm³]	516.4 cGy	5287.5 cGy	3455.1 cGy	4680.0 cGy	3475.3 cGy	1060.7 cGy
BLADDER	TREATMENT (TREATMENT)reatment Approved	IMRT		100.0 / 100.0	91.5 [cm³]	1639.6 cGy	8071.2 cGy	5614.4 cGy	7408.8 cGy	5999.8 cGy	1769.8 cGy
ptv-78	TREATMENT (TREATMENT)reatment Approved	IMRT		100.0 / 100.0	118.7 [cm³]	7401.4 cGy	8287.2 cGy	7950.8 cGy	7956.0 cGy	7955.8 cGy	76.9 cGy

b.

Figure 7. RT Dose. **(a)** CT scan with superimposed color coding shows radiation dose data from a TPS. Isodose curves are shown in yellow, pink, green, magenta, and blue. Red shaded area indicates tumor volume (RT Structure Set). **(b)** A dose-volume histogram (which also belongs to the RT Dose object) is used for evaluation of a treatment plan. Such evaluation is key in determining whether a proper radiation dose is being applied to the target tumor while limiting the dose to surrounding critical healthy tissue and organs. Red line indicates that most of the tumor volume is receiving over 7500 cGy of radiation. Orange, green, magenta, and yellow lines show the dose received by the rectum, right femoral head, left femoral head, and bladder, respectively (OARs). *Max* = maximum, *Min* = minimum, *Std Dev* = standard deviation.

RT Structure Set

The RT Structure Set information object (Fig 5) defines a set of areas of significance in radiation therapy, such as body contours, tumor volumes (eg, gross target volume, clinical target volume [CTV], planning target volume [PTV]), OARs, and other ROIs. The target volumes are defined in accordance with the guidelines in International Commission on Radiation Units and Measurements Reports 50 and 62. The gross target volume is essentially the gross palpable, visible, or clinically demonstrable extent and location of a tumor. The CTV contains the demonstrable gross target volume plus a margin for subclinical disease spread, which cannot be fully imaged. The PTV is a geometric concept designed to ensure actual delivery of radiation therapy dose to the CTV and contains the CTV plus a margin to take into account uncertainties due to internal organ motion, patient motion, and setup error. In cases of prostate cancer, the target volume is the prostate gland and any periglandular cancerous areas. The OARs are the urinary bladder, the rectum, and the femoral heads. Each structure will be associated with a frame of reference, with or without reference to the diagnostic images.

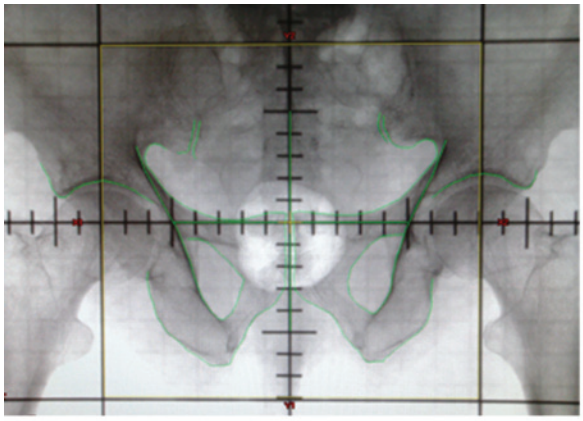

a.

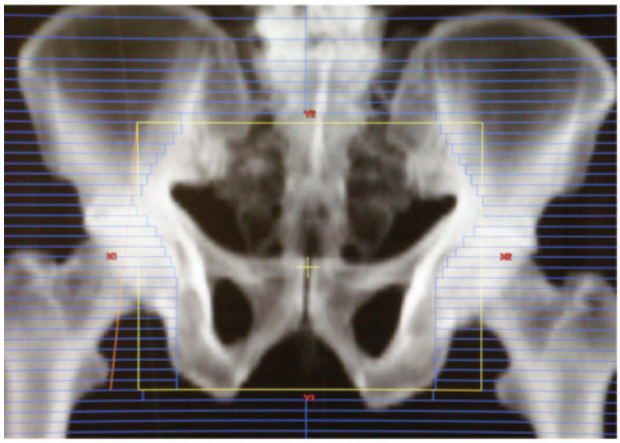

b.

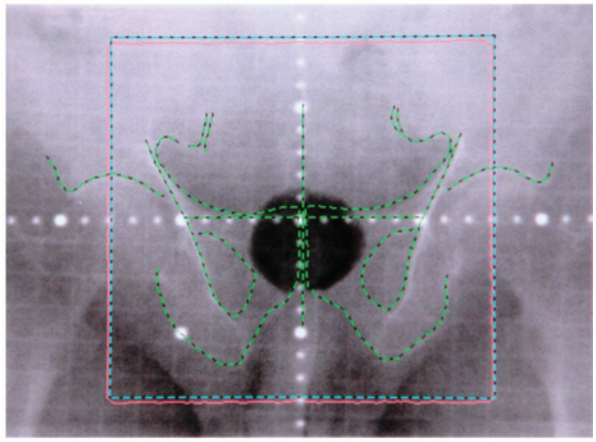

c.

Figure 8. RT Image. Projectional simulator image **(a)**, DRR from a CT scan **(b)**, and portal image acquired at a linear accelerator **(c)** show the field to be irradiated and are examples of images "acquired or calculated using conical geometry" (13). Multileaf collimators are seen on the DRR (blue lines in **b**) and are an attribute of RT Image. Portal images verify the accuracy of the placement of the treatment portal; oftentimes only the irradiated portal will be exposed. Portal images should be compared with reference images from the simulator or with the DRRs.

Field	1	2	3	4	5	6	7	8	9	10	11	12	13	14	15
Wedge	3RW60	3RW45	4RW45	4RW45	4RW45							3RW30	1vW15		3RW45
Date\MU	128	94	187	47	47	75	15	166	30	15	15	128	67	20	104
2004/06/26	128	94	187	47	47	75	15	166	30	15	15				
2004/06/27	128	94	187	47	47	75	15	166	30	15	15				
2004/06/29	128	94	187	47	47	75	15	166	30	15	15				
2004/07/02	128	94	187	47	47	75	15	166	30	15	15				
2004/07/03	128	94	187	47	47	75	15	166	30	15	15				
2004/07/04	128	94	187	47	47	75	15	166	30	15	15				
2004/07/05	128	94	187	47	47	75	15	166	30	15	15				
⋮															
2004/08/10												128	67	20	104
2004/08/11												128	67	20	104
2004/08/12												128	67	20	104
2004/08/13												128	67	20	104
2004/08/14												128	67	20	104

Figure 9. An RT Beams Treatment Record is used to record the dose (in monitor units *[MU]*) delivered to each of the radiation fields (top row) at each treatment session (dates shown in first column). The last four columns (radiation fields 12–15) show a second phase of treatment involving only four radiation fields.

RT Plan

As explained earlier, treatment planning is a process for determining the best placement of the radiation beam for optimal dose distribution. The procedure involves localization of the tumor and OARs, as well as the design (in terms of position and size) of radiation beams and their dose weighting with respect to the PTV and OARs. A clinical treatment plan may include all of the structures marked on the CT scan, the

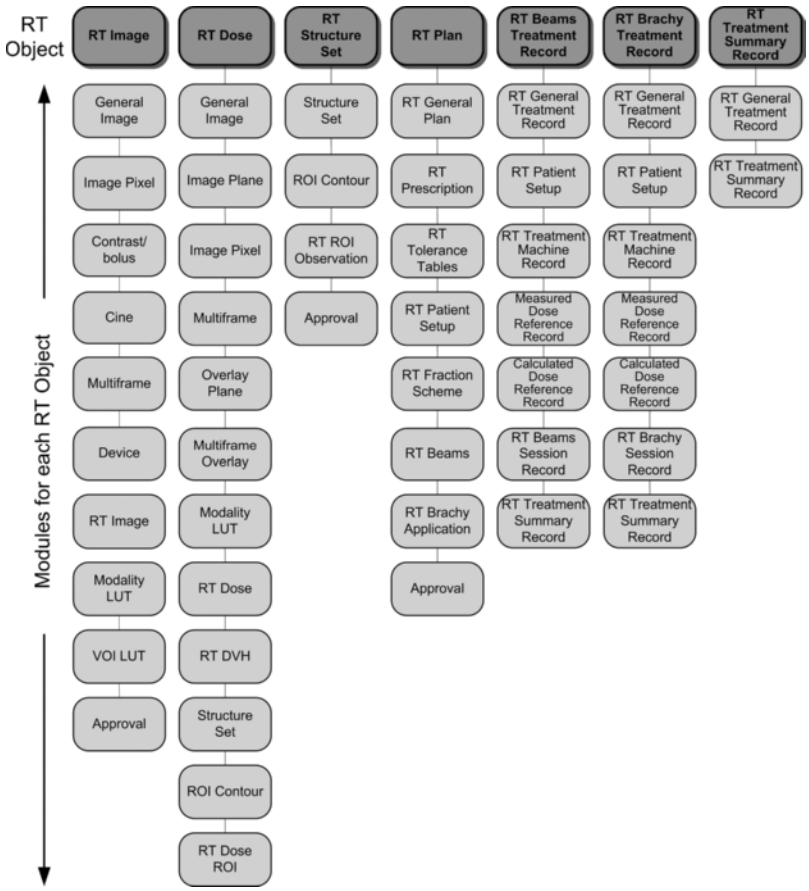

Figure 10. Chart illustrates the seven DICOM-RT objects and their associated modules. Note that the various radiation therapy data generated during the clinical work flow are distributed over the seven objects. *DVH* = dose-volume histogram, *LUT* = look-up table, *VOI* = volume of interest. Understanding how to extract key information from each of the DICOM-RT modules is crucial. The properties or attributes of each module are described in detail in reference 13.

beam positions and sizes, and the dose distribution displayed on the image. In the DICOM-RT standard, information about the structures of interest is contained in RT Structure Set and dose distribution in RT Dose, which requires the coordinates for placing their positions in relation to each other. Thus, the RT Plan object refers only to the textual information in treatment plans, whether generated manually or by a TPS. Such information includes treatment beams, fractionation scheme, prescription, accessories used, and patient setup in external beam therapy or brachytherapy (Fig 6a). In Figure 6b, information from RT Plan is superimposed on RT Structure Set and a CT scan to create a graphical presentation for better visualization.

RT Dose

The distribution of radiation dose for a treatment is represented by isodose lines expressed as a percentage or in dose units (grays). The isodose lines can be displayed in relation to the tumor volume and OARs and superimposed on images. RT Dose contains such radiation dose data from TPSs. It allows the transmission of "a 3D [three-dimensional] array of dose data as a set of 2D [two-dimensional] dose planes that may or may not be related to the CT or MR imaging planes" (Fig 7) (13).

RT Image

Teaching Point

Although RT Image has in common some of the framework used for radiology images in the DICOM standard (Table 2), it specifies the attributes of those images that are "acquired or calculated using conical geometry" (13) in radiation therapy. Such images include projectional simulator images (Fig 8a), DRRs generated from CT scans by a TPS (Fig 8b), and portal images acquired at linear accelerators (Fig 8c). Note that CT images generated with CT simulators are considered to be ordinary CT scans. In contrast to a DICOM image object, RT Image includes not only image information, but also the presentation of the image (ie, position, plane, and orientation of image; distance from radiation machine source to imaging plane). If necessary, RT Image will include the table position, isocenter position, and patient position, and the type of device used to limit the radiation therapy beam (eg, multileaf jaw pairs) (Fig 8b).

Table 3
RT Structure Set IOD Module

Entity	Module	Usage*
Patient	Patient	M
	Clinical Trial Subject	U
Study	General Study	M
	Patient Study	U
	Clinical Trial Study	U
Series	RT Series	M
	Clinical Trial Series	U
Frame of Reference	Frame of Reference	U
Equipment	General Equipment	M
RT Structure Set	Structure Set†	M
	ROI Contour†	M
	RT ROI Observations†	M
	Approval†	U
	SOP‡ Common	M

Source.—Reference 13. IOD = information object definition.
*C = conditional, M = mandatory, U = optional.
†Modules specific to the RT Structure Set DICOM-RT object. All other modules are common modules similar to those in other DICOM objects.
‡Service-object pair.

RT Treatment Record

The RT Treatment Record information object (Fig 9) includes RT Beams Treatment Record, RT Brachy Treatment Record, and RT Treatment Summary Record.

RT Beams Treatment Record.—RT Beams Treatment Record consists mainly of textual data that constitute a treatment session report. The information can be generated by a treatment verification system during the course of external beam therapy or gathered during treatment delivery. Such information includes machine used, radiation type and energy used, date and time of treatment, external beam details, treatment beam accessories, treatment fraction details, monitor units (dose), calculated dose, cumulative dose, verification image obtained, and treatment summary (optional). Each treatment is represented as an instance in an RT Beams Treatment Record object.

RT Brachy Treatment Record.—The RT Brachy Treatment Record information object is similar to RT Beams Treatment Record but consists mainly of information acquired during the course of brachytherapy, along with an optional treatment summary.

RT Treatment Summary Record.—The RT Treatment Summary Record information object summarizes cumulative information concerning the radiation treatment, including both external beam therapy and brachytherapy.

RT Object Modules

In the DICOM standard, each information object contains modules of information related to the object, including both modules that are common to all modalities in radiology (eg, Patient, General Study, General Equipment) and modules that are specific to each imaging modality (eg, CT Image module for CT, MR Image module for MR imaging). In these modality-specific modules, the properties (also known as attributes) of the images are specified. For example, the MR Image module contains both attributes that are found in other modalities (eg, Image Type, Samples per Pixel) and attributes of its own (eg, MR Acquisition Type, Magnetic Field Strength, Repetition Time, Echo Time). In radiation therapy objects, in addition to the common modules, each object contains several associated modules. Table 2 compares the modules in a DICOM image object (MR imaging) with those in a DICOM-RT object (RT Structure Set). Figure 10 shows the seven DICOM-RT objects and their associated modules.

For example, RT Structure Set includes Structure Set, ROI Contour, RT ROI Observations, and Approval modules as specific to the object (Table 3). The Structure Set module provides a framework for defining a set of areas of significance, each of which is associated with a frame of reference with or without reference to the images. If the set of structures have reference to the images, they can be displayed as an overlay on an image as in Figure 5, in which the tumor and the OARs are the ROIs, each with a unique identification number. In the ROI Contour module, the ROIs are a single contour or a sequence of two or more contours. These contours will be referenced to the ROI identification number in the Structure Set and to the CT images containing the contours (Fig 5). The RT ROI Observations module helps distinguish between individual instances or classes of ROIs specified in the previous two modules (Structure Set and ROI Contour)—for example, PTV1 and PTV2. The Approval module is a simple module that addresses the status of approval of the delineation of an important structure

(eg, the PTV), a treatment plan, or a verification image and shows the reviewer's name and the date of approval. The Approval module is also included in the RT Image, RT Structure Set, and RT Plan objects (Fig 10).

Information Encoding

All DICOM objects are composed of DICOM elements (units of information). The DICOM standard defines the attributes of each module and assigns names and data element tags to the attributes. For example, the tag for Patient's Name is (0010,0010), and that for Patient ID (identification) is (0010,0020).

During treatment planning, contours (an RT Structure Set attribute) are drawn around the ROIs (eg, bladder, rectum), which are OARs of significance. A number with its respective name is assigned to each ROI. The DICOM encoder will insert the ROI (identification) number against the element tag (3006,0022), the ROI name against (3006,0026), the contour number against (3006,0048), the contour image sequence against (3006,0016), and so on. The contour image sequence introduces the sequence of images containing the contour. Other attributes are similarly encoded into their corresponding tags as defined by the DICOM standard. With the encoded information and reference to the corresponding CT scan, the structure sets can be reproduced on the CT scan as shown in Figure 5.

Utilization of DICOM-RT Objects in a Radiation Therapy–based ePR System

In a radiation therapy department, often there are different proprietary and stand-alone information systems for single-purpose applications (eg, a separate TPS for each of several treatment modalities, such as external beam therapy, brachytherapy, or stereotactic radiation therapy–radiosurgery). Each system has its own "storage area" for the plans performed at its workstation. Oftentimes these systems are stand-alone systems and have only limited interface with other systems. Typically, the treatment plans are stored in the conventional TPS, with treatment records stored in another information system. The treatment information for a patient whose treatment involves all three systems will be stored in three different places. Currently, such treatment information is normally "linked" by a paper record or folder on the patient. The foregoing description does not take into account the hard-copy film images that are stored separately in the film library, a practice that is common in many radiation therapy departments. Even so, if the paper record is lost, the patient's treatment information "disintegrates." What is more disturbing is that treatment plans from an old TPS cannot be retrieved for review after a system upgrade. Basically, this results in the treatment plans being "lost."

The radiation therapy department needs a "bridge" system to fill the gap, integrate all the disparate data, and provide a "one-stop shop" for historical treatment plans and key related data. Ideally, information and records scattered throughout the different systems could be integrated and a live summary of the patient's treatment record could be displayed when required. Such an endeavor would help save time and effort spent in searching and minimize the loss of records and films. However, interoperability between systems from different manufacturers is an issue if there is no standard or there is noncompliance with the dedicated DICOM-RT standard. It could be argued that purchasing all equipment from a single manufacturer would solve the problem. However, the matter is not that simple. First, the department would be "tied down" to one manufacturer and would have to accept whatever service the manufacturer provides. This is not a healthy situation from the user's perspective. Second, when there is a need for the exchange of radiation therapy patient records or for research collaboration between institutions, the problem still exists.

The current trend in information technology is toward ePRs, electronic medical records, or electronic health records (14), in which all medical and health information about a patient is organized under the patient's name or identification number. When a patient's name is queried, all reports and records are displayed without the need to go into different systems. With the maturity of the DICOM standard, PACS, and IHE (Integrating the Healthcare Enterprise) work flow profiles, researchers and even manufacturers are now working toward incorporating medical images (eg, radiologic, endoscopic, and microscopic images) into the ePRs.

Teaching Point

Using the DICOM-RT standard and following the model of the PACS makes integration of radiation therapy information possible (15,16). All radiation therapy information and images from various sources can be converted to the DICOM-RT standard and integrated into a DICOM-based database. This information can be displayed as a radiation therapy ePR. From the database, connection to other radiation therapy systems and exchange of radiation therapy patient information are also possible with DICOM-RT and a DICOM-based radiation therapy ePR system. The collection of radiation therapy information in the DICOM-RT objects will lead to further initiatives in informatics research in radiation therapy.

With the increasing popularity of proton beam therapy, two more RT objects—namely, RT Ion Plan and RT Ion Beams Treatment Record—have been defined. The implementation of these objects in a proton beam therapy system is being researched, and it is hoped that, with use of the DICOM standard, information from proton beam therapy can be integrated with that from conventional radiation therapy.

Conclusions

In addition to being image intensive, radiation therapy is highly technical, and its use of radiation also involves radiobiologic factors. All of these parameters have to be recorded for future reference regarding the treatment of cancer patients with radiation therapy. Hence, along with textual information, all related treatment planning information (including isodose lines, graphs, and so on) and images need to go into a single electronic folder on the patient.

Like the DICOM standard in radiology, the DICOM-RT standard is ratified for integration, archival, and sharing of information. Given the small number of vendors and the rapidly developing technology in radiation therapy, the industry tends to focus more on technologic development; thus, the adoption of the DICOM-RT standard is slow and incomplete in most cases. For objects that have been implemented, a user interface called "DICOM export/DICOM import" may exist in some TPSs for the conversion of information from a vendor-specific format to the DICOM format. With manufacturers' collaboration, radiation therapy information can, like diagnostic images, be linked to the ePR to produce a complete radiation therapy patient record. The DICOM-based radiation therapy database can provide a platform for data sharing and for future medical imaging informatics research and outcome analysis of standardized data.

Teaching Point

References

1. Bidgood WD, Horii SC. Introduction to the ACR-NEMA DICOM standard. RadioGraphics 1992; 12:345–355.
2. Horii SC. Primer on computers and information technology. IV. A nontechnical introduction to DICOM. RadioGraphics 1997;17:1297–1309.
3. Huang HK. PACS and imaging informatics: basic principles and applications. Hoboken, NJ: Wiley-Liss, 2004; 175.
4. Digital Imaging and Communications in Medicine (DICOM) Supplement 11. Radiotherapy objects.
5. Digital Imaging and Communications in Medicine (DICOM) Supplement 29. Radiotherapy treatment records and radiotherapy media extensions.
6. Digital Imaging and Communications in Medicine (DICOM) Supplement 30. Waveform interchange.
7. Digital Imaging and Communications in Medicine (DICOM) Supplement 48. Intravascular ultrasound (IVUS).
8. Digital Imaging and Communications in Medicine (DICOM) Supplement 15. Visible light image for endoscopy, microscopy, and photography.
9. Digital Imaging and Communications in Medicine (DICOM) Supplement 122. Specimen identification and revised pathology.
10. Digital Imaging and Communications in Medicine (DICOM) Supplement 91. Ophthalmic photography SOP classes.
11. Digital Imaging and Communications in Medicine (DICOM) Supplement 110. Ophthalmic coherence tomography (OCT) storage SOP class.
12. Digital Imaging and Communications in Medicine (DICOM) Supplement 102. Radiotherapy extensions for ion therapy.
13. Digital Imaging and Communications in Medicine (DICOM) Part 3. Information object definitions. PS3.3-2008.
14. Kuzmak PM, Dayhoff RE. The use of digital imaging and communications in medicine (DICOM) in the integration of imaging into the electronic patient record at the Department of Veterans Affairs. J Digit Imaging 2000;13(2 suppl 1):133–137.
15. Law MY, Huang HK. Concept of a PACS and imaging informatics-based server for radiation therapy. Comput Med Imaging Graph 2003;27:1–9.
16. Law MY. A model of DICOM-based electronic patient record in radiation therapy. Comput Med Imaging Graph 2005;29:125–136.

DICOM-RT and Its Utilization in Radiation Therapy

Maria Y. Y. Law, PhD and Brent Liu, PhD

RadioGraphics 2009; 29:655–667 • **Published online** 10.1148/rg.293075172 • **Content Codes:** IN RO

Page 660
There are significant differences in the types of information required for radiology and radiation therapy as well as differences in the time at which and frequency with which the information is obtained.

Page 660
On the basis of the standard DICOM query-retrieve model, the radiation therapy information is defined in seven information objects known as DICOM-RT objects for the transfer of data (10,11,13). These information objects include RT Structure Set, RT Plan, RT Dose, RT Image, and RT Treatment Record, which is further divided into RT Beams Treatment Record, RT Brachy Treatment Record, and RT Treatment Summary Record.

Page 664
Although RT Image has in common some of the framework used for radiology images in the DICOM standard (Table 2), it specifies the attributes of those images that are "acquired or calculated using conical geometry" (13) in radiation therapy. Such images include projectional simulator images (Fig 8a), DRRs generated from CT scans by a TPS (Fig 8b), and portal images acquired at linear accelerators (Fig 8c).

Page 667
Using the DICOM-RT standard and following the model of the PACS makes integration of radiation therapy information possible (15,16). All radiation therapy information and images from various sources can be converted to the DICOM-RT standard and integrated into a DICOM-based database. This information can be displayed as a radiation therapy ePR.

Page 667
The DICOM-based radiation therapy database can provide a platform for data sharing and for future medical imaging informatics research and outcome analysis of standardized data.

Int J CARS (2009) 4:317–329
DOI 10.1007/s11548-009-0297-y

ORIGINAL ARTICLE

Integration of computer-aided diagnosis/detection (CAD) results in a PACS environment using CAD–PACS toolkit and DICOM SR

Anh H. T. Le · Brent Liu · H. K. Huang

Received: 15 September 2008 / Accepted: 11 March 2009 / Published online: 15 April 2009

Abstract
Purpose Picture Archiving and Communication System (PACS) is a mature technology in health care delivery for daily clinical imaging service and data management. Computer-aided detection and diagnosis (CAD) utilizes computer methods to obtain quantitative measurements from medical images and clinical information to assist clinicians to assess a patient's clinical state more objectively. CAD needs image input and related information from PACS to improve its accuracy; and PACS benefits from CAD results online and available at the PACS workstation as a second reader to assist physicians in the decision making process. Currently, these two technologies remain as two separate independent systems with only minimal system integration. This paper describes a universal method to integrate CAD results with PACS in its daily clinical environment.
Methods The method is based on Health Level 7 (HL7) and Digital imaging and communications in medicine (DICOM) standards, and Integrating the Healthcare Enterprise (IHE) workflow profiles. In addition, the integration method is Health Insurance Portability and Accountability Act (HIPAA) compliant.
Summary The paper presents (1) the clinical value and advantages of integrating CAD results in a PACS environment, (2) DICOM Structured Reporting formats and some important IHE workflow profiles utilized in the system integration, (3) the methodology using the CAD–PACS integration toolkit, and (4) clinical examples with step-by-step workflows of this integration.

Keywords PACS · Computer-aid-diagnosis (CAD) · DICOM structured reporting (SR) · CAD–PACS integration toolkit · Integrating the Healthcare Enterprise (IHE) · IHE workflow profiles

Abbreviations

CAD	Computer-assisted detection and diagnosis
CARS	Computer-assisted radiology and surgery
DICOM	Digital imaging and communications in medicine
DICOM-SR	DICOM structured reporting
FLAIR	Fluid attenuated inversion recovery
HIPAA	Health insurance portability and accountability act
HIS	Hospital information system
HL7	Health level 7
IHE	Integrating the Healthcare Enterprise
IRB	Institutional Review Board
IOD	Information object definition
KIN	Key image note
MRI	Magnetic resonance imaging
MS	Multiple sclerosis
PPM	Post-processing manager
PWF	Post-processing workflows
RIS	Radiology information system
SINR	Simple image and numeric report
SC	DICOM secondary capture
SR	Structured report object/document
WS	Workstation
XML	Extensible markup language

Presented as "Tutorial on CAD–PACS integration" at: CARS 2007, Berlin, Germany, June 27–30, 2007; and CARS 2008, CARS 2008, Barcelona, Spain, June 25–28, 2008.

A. H. T. Le (✉) · B. Liu · H. K. Huang
Image Processing and Informatics Laboratory (IPILab),
Departments of Radiology and Biomedical Engineering,
Keck School of Medicine, University of Southern California,
1450 San Pablo Street, Suite DEI 2100, Los Angeles, CA 90033, USA
e-mail: anhhle@usc.edu

Introduction

Computer-aided detection/diagnosis

Computer-aided detection (CADe) and computer-aided diagnosis (CADx) utilize computer methods to obtain quantitative measurements from medical images along with clinical information to assist clinicians and radiologists in the decision-making process of a patient. CADe is closely related to the process of automatic segmentation to indicate the location of possible abnormalities within a medical image. The classification, diagnosis, and patient care decisions are left to the radiologist. CADx involves quantification processes utilizing computer analysis to classify a region or lesion which is the ultimate goal of radiological examinations. The final diagnosis and patient care decision are also left to the radiologist [2]. The purpose of this paper is not to focus on CADe or CADx methodologies, or methods to allow CAD to directly query the Picture Archiving and Communication System (PACS) database to improve the performance of the CAD, but the integration of CADe or CADx results to facilitate PACS daily clinical service utilizing the Health level 7 (HL7) standard [7], Digital imaging and communications in medicine (DICOM) standard [17], HIS/RIS/PACS technologies, and Integrating the Healthcare Enterprise (IHE) workflow profiles [13]. Throughout this paper, we will use CAD as the generic term to represent both CADe and CADx; PACS in short for HIS/RIS/PACS as the integrated system, and DICOM for DICOM standard and IHE for IHE workflow profiles.

The need for CAD–PACS integration

Computer-aided detection and diagnosis software can be implemented within a stand-alone CAD Workstation (WS), a CAD server, or be integrated in PACS as PACS-based CAD. In order to utilize CAD results more efficiently and timely, it is commonly agreed that CAD should be integrated with the daily clinical PACS operation [2]. Currently, some PACS and CAD companies have had some success in integrating several CAD applications within the PACS operation, but the solutions are either in a CAD specific WS, or in a closed PACS operation environment using proprietary software. For example, in mammography, CAD has become an integral part of a routine clinical assessment of breast cancer in many hospitals and clinics across the United States and abroad [6]. However, the value and effectiveness of CAD applications are still hindered due to the inconvenience of the standalone CAD WS or server. The wide usage of DICOM, PACS, and IHE technologies as an integral part of daily clinical operation sheds some light on how to overcome such obstacles.

The CAD–PACS integration has many distinct advantages, among them are:

(1) PACS is a mature technology which consists of powerful computers and high speed networks dedicated to the storage, retrieval, distribution, and presentation of clinical image,
(2) the integration allows the use of built-in PACS-based easy query/retrieve tools providing user with images and related patient data obtained from CAD results,
(3) the DICOM structured reporting (SR) and IHE workflow profiles can be readily applied to facilitate the CAD–PACS integration, and
(4) CAD–PACS integration results can be directly viewed and utilized at the PACS WS together with the PACS database.

Although it is also advantageous to integrate CAD to utilize PACS data to improve the CAD algorithm resulting in better diagnosis and improved CAD performance, this paper's main focus is describing how to integrate CAD–PACS in order to achieve those aforementioned purposes. Furthermore, integrating CAD in the clinical PACS environment would facilitate radiologists and healthcare providers in their daily operation. Clinical examples to illustrate the importance and usefulness of the CAD–PACS Toolkit will be discussed in further detail in Sect. "Examples of integrating using CAD–PACS toolkit".

DICOM standard and IHE workflow profiles

CAD-HIS/RIS/PACS integration requires certain basic ingredients from HL7 [7] standard for textual data, DICOM [17] standard for image, and IHE [13] workflow profiles in order to comply with the Health insurance portability and accountability act (HIPAA) [12] requirements to be a healthcare system. Among the DICOM standard and IHE workflow profiles, DICOM structured reporting (DICOM-SR), and IHE Key image note (KIN), Simple image and numeric report (SINR), and Post-processing workflows (PWF) are important in CAD-HIS/RIS/PACS integration. Section "DICOM structured reporting (DICOM-SR)" first discusses the DICOM-SR, followed by the three IHE workflow profiles in Sect. "IHE profiles".

DICOM structured reporting (DICOM-SR)

The scope of DICOM-SR is the standardization of SR documents in the imaging environment. SR documents record observations made for an imaging-based diagnostic or interventional procedure, particularly those that describe or reference images, waveforms, or specific regions of interest (ROI). DICOM-SR was first introduced in 1994 and marked its existence when Supplement 23 was adopted into DICOM standard in 1999 as the first DICOM-SR for clinical reports [3].

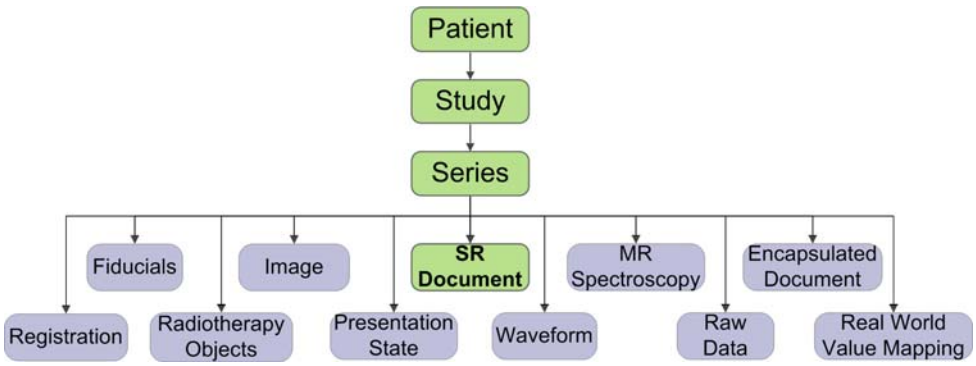

Fig. 1 DICOM structured reporting objects in the DICOM Model of the Real World. The light green box is where the SR document is located in the DICOM data module which is in the same level as DICOM Image

The DICOM Committee has initiated more than 12 supplements to define specific SR document templates. Among these, two of them related to capturing CAD results: the Mammography CAD SR (Supplement 50, 2000) [4] and Chest CT CAD SR (Supplement 65, 2001) [5] had been ratified. In practice, the use of structured forms for reporting has shown to be beneficial in reducing the ambiguity of natural language format reporting by enhancing the precision, clarity and value of the clinical document.

DICOM structured reporting is generalized using DICOM information object definitions (IODs) and services for the storage and transmission of structured reports. Figure 1 illustrates the simplified version of the DICOM Model of the real world [17], showing where DICOM-SR objects reside. The most important part of an SR object is the SR Document Content which is the "SR Templates" consisted of design with different patterns for various applications.

Thus, for example, once the CAD results with images, graphs, and text have been translated into a SR template designed for this application, the data in the specific template can be treated as a DICOM object stored in the worklist of the DICOM model (see boxes with light green background in Fig. 1) and it can be displayed for review by a PACS WS with the SR Display function. The viewing requires the original images from which the CAD results were generated so that the results can be overlaid onto the images. The SR Display function can link and download these images from the PACS archive and display them as well on the WS.

IHE profiles

Three IHE profiles useful for CAD–PACS integration are:

(1) Key image note (KIN) profile allows users to flag images as significant (e.g., for referring, for surgery, etc.) and adds a note.
(2) Simple image and numeric report (SINR) profile specifies how Diagnostic Radiology Reports (including images and numeric data) are created, exchanged, and used.
(3) Post-processing workflow (PWF) profile provides worklist, status and result tracking for post-acquisition tasks, such as Computer-Aided Detection or Image Processing.

These profiles will be used and explained in Sect. "Examples of integrating using CAD–PACS toolkit" when examples are given.

The CAD–PACS© integration toolkit

Computer-aided detection and diagnosis software can be in a stand-alone CAD WS, CAD server, or integrated within the PACS as PACS-based CAD. Regardless where the CAD software is installed, the goal is to have CAD results integrated with daily clinical PACS operation. In this section, the CAD workflow in current practice is first described followed by the presentation of a CAD–PACS integration toolkit for extending the CAD workflow to PACS environment. The CAD–PACS toolkit is a software package that has been developed and tested at Image Processing and Informatics Laboratory (IPILab) since 2006. The CAD–PACS integration applications had also been presented at RSNA Annual Meeting in 2006 and 2007 [25,16]; and given as tutorials at Computer-assisted radiology and surgery (CARS) Annual Meeting in 2007 and 2008 [8,9].

Current CAD workflow

Figure 2 depicts the PACS environment (blue box) and CAD WS/Server location (red box) which is outside the realm of PACS. These two systems are usually disjoint. When an image is needed for CAD processing (See numbers in Fig. 2), then the following occurs (See Fig. 2):

(1) CAD processes the exam ordered through Radiology information system (RIS), or directly from Modality.
(2) Technologist or radiologist transmits the original image from PACS server or PACS WS to CAD WS for

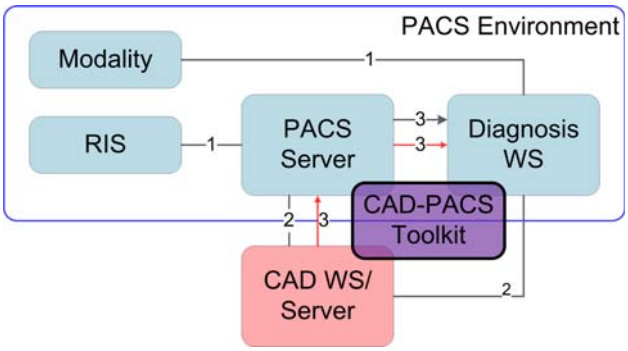

Fig. 2 CAD (*red*) Workflow (numbers, see text for detail) in the PACS environment (*blue*) with the CAD–PACS toolkit (*purple*). See color code used in Fig. 3

processing. Results are stored within the CAD domain since the CAD WS or Server is a closed system and the clinicians need to physically go to the CAD WS to view results.

(3) Consider now there exists a CAD–PACS toolkit (purple box) such that it can integrate with the PACS server, PACS WS, and the CAD Server/WS together via the DICOM standard and IHE Profiles. Then, the CAD–PACS Toolkit would provide connectivity to push CAD results to the PACS Server for archival and the PACS WS for viewing; and query/retrieve original images from PACS server to PACS WS to be overlaid with the CAD results. In addition, it could also automatically push images directly from the PACS server or PACS WS to the CAD WS for processing.

The rest of Sect. "The CAD–PACS© integration toolkit" describes the concept and dataflow of CAD–PACS toolkit; its different editions and software modules; as well as the PACS and CAD components involved.

Concept

CAD–PACS© is a software toolkit using HL7 [7] standard for textual information; DICOM standard [17] for various types of data format including images, waveform, graphics, annotations, and others; and IHE [13] workflow profiles described in the aforementioned section for the integration of CAD results within the PACS workflow. This CAD software toolkit is modularized and its components can be installed in five different configurations: (1) In a standalone CAD workstation, (2) In a CAD server, (3) In a PACS workstation, (4) In a PACS server, or (5) In a blended mixture of the previous four configurations above. In general, a CAD manufacturer would be more comfortable with the first two approaches because there is very little collaboration needed with the PACS software which is quite complex for CAD manufacturers. On the other hand, a PACS manufacturer would prefer to use an in-house CAD or acquire the CAD from outside and integrate it with its own PACS with the latter three approaches.

The infrastructure

The CAD–PACS© toolkit has three Editions: DICOM-SC™, 1st Edition; DICOM-PACS-IHE™, 2nd Edition [18, 19]; and DICOM-CAD-IHE™, 3rd Edition [15]; and five software modules: i-CAD-SC™, i-CAD™, i-PPM™, Receive-SR™, and Display-SR™ [18,19,15]. Each Edition consists of some or all of the software modules. Figure 3 shows the architecture of the toolkit.

The toolkit is classified into three different Editions for different levels of PACS integration requirements. Table 1 shows the comparisons of these three integration approaches. The 1st Edition is for simple screen capture output—the CAD quantitative results are not stored for future use. The 2nd Edition is for full CAD–PACS integration—elaborated integration efforts are needed between the CAD developer and the PACS manufacturer. This Edition will allow for the future potential for CAD to query PACS database and improving the CAD performance. The 3rd Edition does not require elaborated integration efforts between both parties—the proper use of the CAD–PACS toolkit would be sufficient which is favored by independent CAD developers.

Functions of the three editions

DICOM-SC™, 1st Edition

The first Edition utilized the i-CAD-SC™ software module which relies on the DICOM screen capture (SC) service. It is simple to design and implement but with limitation in clinical research as it uses screen capture to store CAD results for viewing purposes only.

DICOM-PACS-IHE™, 2nd Edition

The second Edition consists of four software modules: i-CAD™, i-PPM™, Receive-SR™, and Display-SR™. It utilizes the DICOM-SR service and several IHE Workflow Profiles, the methodology is elegant but requires installation of four modules within the PACS server including the i-PPM™ module (post-processing manager). This module requires thorough understanding of the entire PACS workflow which would need intensive collaboration with the PACS manufacturer during integration. The integration would require patience and perseverance from the integrator because of the protective culture of the PACS business.

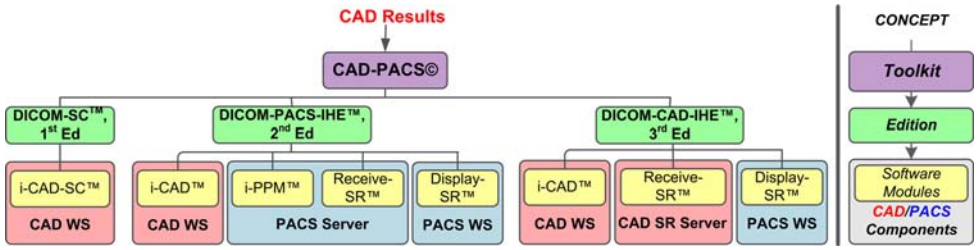

Fig. 3 *Rightmost* four levels of the CAD–PACS Integration toolkit. *Purple* CAD–PACS Integration toolkit; *green* three CAD–PACS© Editions; *yellow* five software modules; *red* CAD components and results, and *blue* PACS components. *Left* the CAD–PACS© toolkit first Edition DICOM-SC™ utilizes DICOM screen capture service to view CAD results. This Edition is easy to integrate, but the CAD output is not in a database for future retrieval. *Middle* second Edition DICOM-PACS-IHE™ utilized for integration with a full PACS. It consists of four CAD–PACS software modules. It is suitable for a PACS manufacturer to integrate an existing CAD into its own PACS. *Right* the third Edition DICOM-CAD-IHE™ utilized for integration with the CAD server. This component is independent from the PACS manufacturer as long as the PACS workstation is DICOM-SR Compliant. The CAD results can then be viewed at a PACS WS. It is favored by the CAD manufacturers or research laboratories for integration. The three modules i-CAD™, Receive-SR™, and Display-SR™ are the same in both DICOM-PACS-IHE™ and DICOM-CAD-IHE™ Editions. Post-processing manager (PPM) allows the integration of CAD results with the PACS server which is PACS specific and would require PACS vendor's assistance for implementation. In the lower level components, either in PACS or in CAD, proper toolkit software modules can be installed in the corresponding system components for CAD–PACS integration

Table 1 Comparison of the three CAD–PACS integration editions

Specifications	CAD–PACS Edition		
	DICOM-SC 1st Edition	DICOM-PACS-IHE 2nd Edition	DICOM-CAD-IHE 3rd Edition
Using secondary captured image to store CAD results	✓		
Using DICOM SR		✓	✓
PACS without SR support	✓		✓
PACS with SR support		✓	
Display referenced image	✓	✓	✓
Toggling between image and annotation		✓	✓

DICOM-CAD-IHE™, 3rd Edition

The third Edition comprises three software modules: i-CAD™, Receive-SR™, Display-SR™. It utilizes DICOM-SR and Key image note IHE profile, this method reduces the necessity of altering the current PACS Server, but CAD results are stored in the CAD server and not in PACS. DICOM-SR links PACS image/data and CAD results for viewing. This Edition is favored by CAD manufacturers because they have the ability to install the toolkit in their CAD server and integrate CAD results with the PACS clinical workflow without the complexity of the previous Edition. DICOM-SR provides the data format allowing CAD results, text, images, graphics, and annotations to be directly archived within the DICOM-SR compliant CAD server.

The second and the third Editions are the correct methods of integrating CAD with PACS because the availability of direct CAD results in daily clinical workflow would enhance the PACS operation, and allow future PACS research capability.

Data flow of the three editions

DICOM-SC™, 1st Edition

The data flow within the DICOM-SC™ is simple and straight forward. The PACS WS pushes the image to the CAD WS or CAD Server. Results are screen captured by i-CAD-SC residing in the CAD WS as a DICOM image object and sent to PACS server for archive and it can be viewed by the PACS WS. In this Edition, results can only be viewed, and data cannot be used for other purposes.

DICOM-PACS-IHE™, 2nd Edition

Figure 4 shows the workflow of this edition. The four software modules are needed to be installed in the appropriate PACS and CAD components first if those PACS components do not have the required functions. The challenge of this version is that the CAD developer has to collaborate closely with

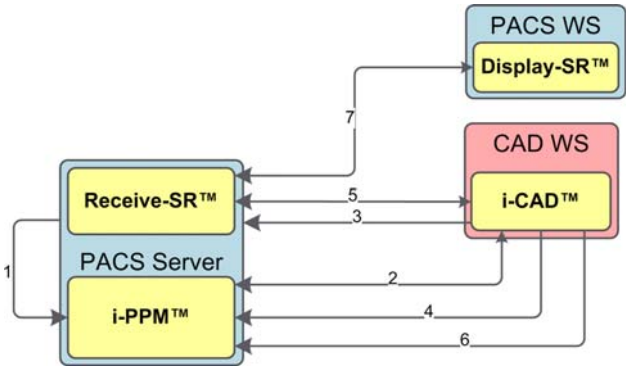

Fig. 4 Data flow of the DICOM-PACS-IHE^{TM} 2nd Edition and locations of the four modules (*yellow*) of DICOM-PACS-IHE^{TM} in the CAD and PACS components (see also color code used in Fig. 3); numbers represent data flow steps during the integration. *1* CAD Requests, *2* Query CAD worklist, work item claimed; *3* Retrieve images for CAD; *4* Worklist purpose procedure step (PPS) in PPM in the process; *5* CAD results; *6* Work item PPS completed; *7* Retrieve images/CAD results [18,19]

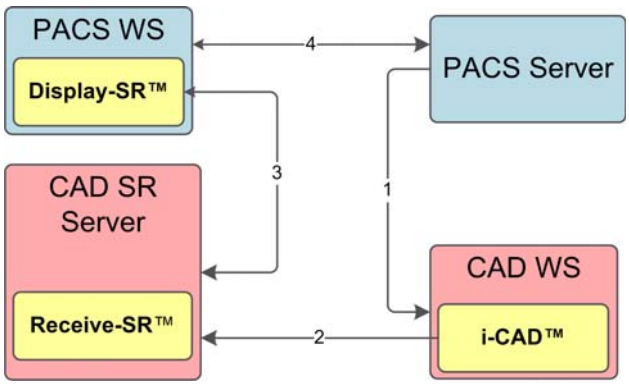

Fig. 5 The data flow DICOM-CAD-IHE^{TM} 3rd Edition shows the locations of the three software modules (*yellow*) in the CAD SR server and PACS, respectively (see also color code used in Fig. 3); and the data flow steps (numbers). *1* PACS Server pushes the CT image to CAD WS for CAD process; *2* CAD WS pushes the DICOM SR CAD results to CAD SR Server which consists of the Receive-SR^{TM} module with a SR-Database for archiving CAD results; *3* Web-based Display-SRTM at PACS WS queries/retrieves DICOM-SR CAD results from CAD SR Server; *4* The Display-SR automatically queries and retrieves original images referenced in the DICOM-SR CAD results in the PACS Server for reviewing both original images and SR. In this Edition, CAD SR Server also keeps all CAD results in SR format

the PACS server manufacturer to fully understand the PACS workflow, which is different from the CAD–PACS integration workflow. To integrate CAD results with PACS workflow using i-PPM^{TM} is not an easy task.

DICOM-CAD-IHE^{TM}, 3rd Edition

Figure 5 shows the data flow. In this edition, the CAD has two components, the CAD WS and CAD SR Server. The latter takes care of monitoring and archiving of CAD results, and retrieving original images and data from PACS.

Examples of integrating using CAD–PACS toolkit

Introduction to the examples

This section shows two different examples of integrating CAD results into PACS clinical environment using the CAD–PACS integration toolkit. DICOM-SR is the ultimate CAD output required as the exchange object for integration, and the assumption is that original images in which the CAD results were obtained are already stored in PACS. Both examples require the use of several components of the toolkit to integrate the CAD system with the PACS system. The first example is easier to integrate because the CAD developed by a manufacturer has already converted CAD results to DICOM-SR format [8]. Whereas in the second example, the CAD is developed by an R&D research laboratory and it requires the use of the toolkit to convert CAD results to DICOM-SR format first before the integration [9]. Table 2 summarizes different specifications of integration of the CAD with PACS in these two examples.

In order to have seamless integration between the two systems, CAD and PACS, the following steps and components from the toolkit are required: (1) assign a DICOM node for the SR server, (2) establish connections between PACS and SR Server for image query and retrieval, (3) activate the CAD WS/Server and the CAD SR Server to receive DICOM-SR objects, and (4) setting up Display-SR at the PACS WS.

Integration of commercial CADs with PACS

Example 1 demonstrates two CAD cases, CAD detection of lesions on chest CT images from a CAD application from GE Healthcare, Waukesha, WI (note: the algorithm was developed by R2 Technology, Inc., Santa Clara, CA and was acquired by GE Healthcare) and CAD diagnosis of breast cancer on mammogram developed by a single CAD manufacturer, Hologic's R2 Technology, Inc., Santa Clara, CA (note: the CAD method was developed by R2, the product was acquired by Hologic) [10]. In both cases available CAD outputs are already converted to DICOM-SR format by the manufacturer, and original images are already stored in PACS. The CAD–PACS integration can be summarized by these steps: (1) CAD WS or Server completes the CAD process and sends the DICOM-SR document contained CAD results to the SR Server (CAD–PACS toolkit), (2) SR Server utilizes the Receive-SR module (toolkit) to store the DICOM-SR CAD results and automatically prefetches reference images from PACS, (3) CAD results are ready for viewing on PACS WS using Display-SR module (toolkit).

Table 2 Tasks and requirements for integrating CAD with PACS systems in the two examples

Example	Tasks & Requirements		
	CAD algorithm	CAD output format	Integration tasks
1. Commercial CAD: Lesions on Chest CT & Breast Cancer on mammogram	Developed Proprietary	DICOM-SR document	Store SR files in SR server and display SR on PACS WS
2. Research CAD Multiple sclerosis (MS) on MRI	Developed Proprietary	Text or Extensible markup language (XML), Images (DICOM/Bitmap)	Create SR Template and SR files, Store SR files in SR server and display SR on PACS WS

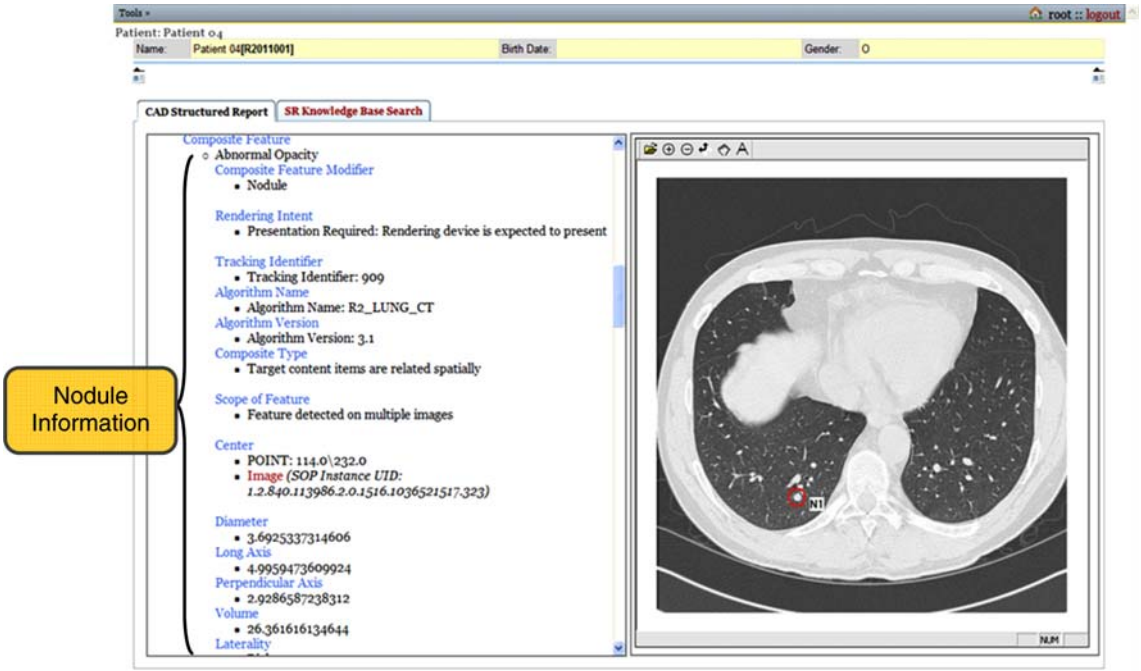

Fig. 6 Manufacturer's Chest CAD Report already in DICOM-SR format (*left*) with referenced image and annotation (*right*). Annotation (*red circle*) in the DICOM-SR allows the user to toggle it on or off. (Courtesy of: Hologic's R2 Technology, Inc., Santa Clara, CA for case materials)

Figures 6 and 7 show the screenshots of a Chest CAD and a Mammogram CAD results in DICOM-SR format displayed on a PACS WS, respectively. The top of each image shows the patient information, whereas the left side displays the structured report and the right depicts the DICOM images with nodule/lesion identified with overlaid annotations.

As shown in Fig. 6, the location of the chest nodule is extracted from DICOM-SR object and sent to the Display-SR module to display as annotations (red circle) on top of the original CT image. This information is stored separately from the DICOM images and allows annotation to be toggled on/off from the original image that is displayed. Similar for the case of mammography CAD in which the locations of the breast lesions are shown in blue crosses. The difference between Chest CAD and Mammography CAD are that (1) the CAD algorithms are different for different tissues/organs and for different modalities, and (2) the structures of DICOM-SR object are also different (see rectangular box annotation on the left of each figure). For example, Chest CAD SR does not reference the whole CT Chest Study but only those few CT images (red fonts) with nodules detected; whereas Mammography CAD DICOM-SR object includes all four images (red fonts) in a screening mammography study. One of the reasons is that a CT study has many images and the SR should only reference those images where the lesions were detected. Therefore, each CAD algorithm or CAD for a different body region should have a different SR template to present complete and precise CAD results.

Integration of research laboratory CAD with PACS

The second example is the integration of PACS with CAD of Multiple sclerosis (MS) on Magnetic resonance imaging (MRI) studies. MS is a progressive neurological disease

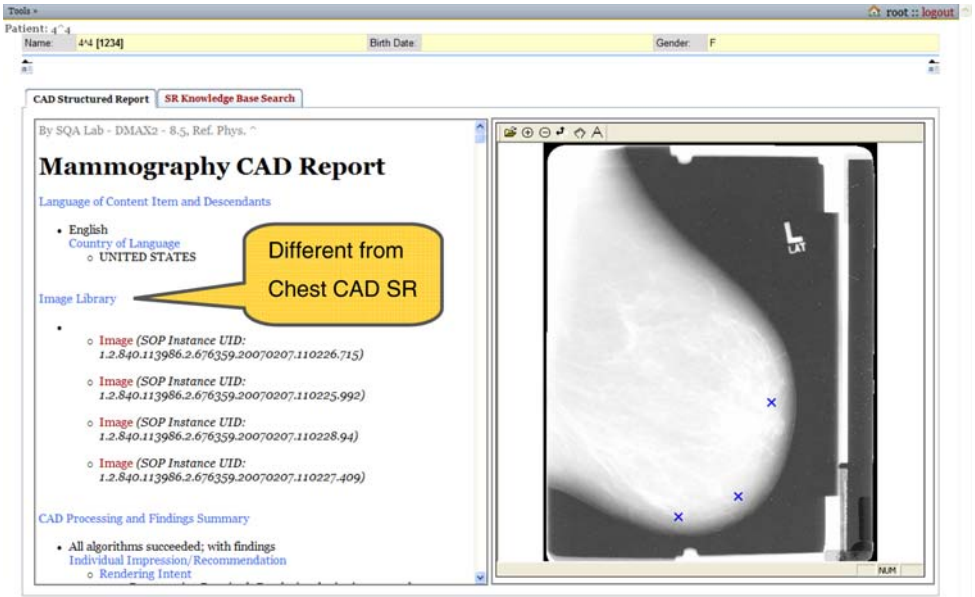

Fig. 7 Manufacturer's Mammography CAD Report already in DICOM-SR (*left*) with referenced image and annotation (*right*). Note that the DICOM-SR format is different from that in the CAD on CT (*red fonts*). Annotation (*blue crosses*) in the DICOM-SR allows the user to toggle it on or off (courtesy of: Hologic's R2 Technology, Inc., Santa Clara, CA for case materials)

affecting myelin pathways in the brain. Multiple lesions in the white matter can cause paralysis and severe motor disabilities of the affected patient. Symptoms are changes in sensation, visual problems, muscle weakness, and depression. Currently, MRI T1 and Fluid attenuated inversion recovery (FLAIR) pulse sequences are used for radiological diagnosis. In these images, MS appears as multiple white lesions in the white matter area of the brain. MRI is also used to follow-up and monitor the progress of the disease and the effectiveness of therapy after the patient is treated with drugs. Since MRI provides excellent delineation of MS, it is fairly easy for radiologists to make the diagnosis. However, due to the possibility of a large number of multiple lesions in the MRI 3-D volume set of the brain, it is tedious and time consuming to identify the 3-D aspect of each lesion and quantify the number and size of these lesions. Moreover, the quantitative reproducibility through human observers is poor. Augmenting CAD with imaging informatics methods, a 3-D CAD MS package would facilitate the physician's timely diagnosis, improve accuracy, and assess quantitatively the progress of drug therapy treatment. Figure 8 shows the most common data obtained from 3-D CAD results. The data includes the original 3-D MRI data set (Fig. 8a shows one MRI FLAIR image, CAD detected multiple lesions (Fig. 8b), radiologist identified lesions (Fig. 8c, normally not shown in the results, depicted here only for comparison purposes); color-coded MS lesions on each 2-D image (Fig. 8d, one slice; Fig. 8e, two slices; and Fig. 8f, all 26 slices). Figure 8g is the quantitative results of all lesions detected by CAD. Figure 8h is three 2-D oblique views of the brain overlaid with 26 MS lesions. The CAD results were generated through collaboration with Guardian Technologies, Inc. to develop the CAD algorithm.

Currently, these results can be shown on the specialized MS detection CAD WS, but cannot be linked or viewed in the daily clinical PACS WS. The PACS database does not contain these results as DICOM objects, and the CAD WS or database does not know what other data the patient may have within the PACS.

Generating the DICOM-SR document

In this case, the CAD generates results as shown in Fig. 8 which includes number of lesions, 3-D coordinates of the lesions, volume of each lesion, and their 2-D presentations in each detected MR slice at various oblique angles which can be used to display for 3-D viewing on a 2-D monitor. They are in a text file and not in DICOM-SR format. The first task in the integration is to convert these results to DICOM-SR format.

To convert the text file into DICOM-SR format, a special MS CAD template was first defined which was tailored to satisfy the specific need for presenting complete results. Figure 9 shows an SR template for the MS application as discussed above. Referencing to two ratified CAD SR templates for mammography and chest CT in the DICOM standard shown in Figs. 6 and 7, a new MS DICOM-SR object for this application based on the tree structure was defined, designed, and implemented. This design, which utilizes the DICOM Standard Supplement 23 and Computer Science terminologies, has a document root MS CAD (see Fig. 9) which branches into four parent nodes (detections, analyses, summary, and image library). For example, within this context, the detections performed can have one or more child nodes, detection performed $(1-n)$, with various detailed algorithms used for lesions detection. By the same token, the analyses performed

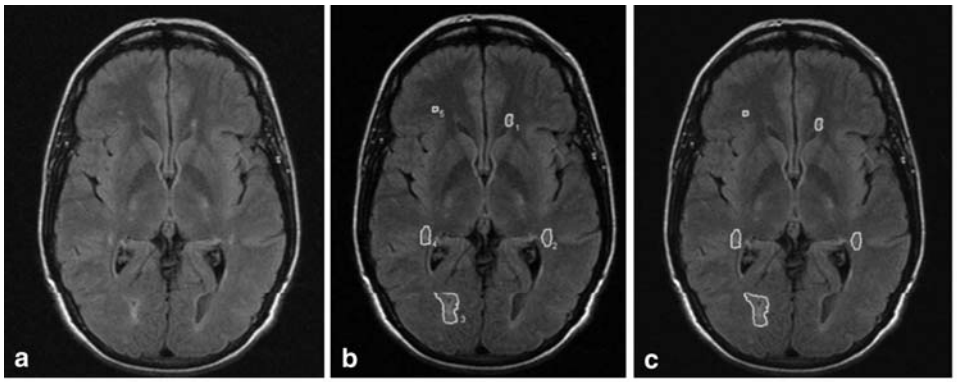

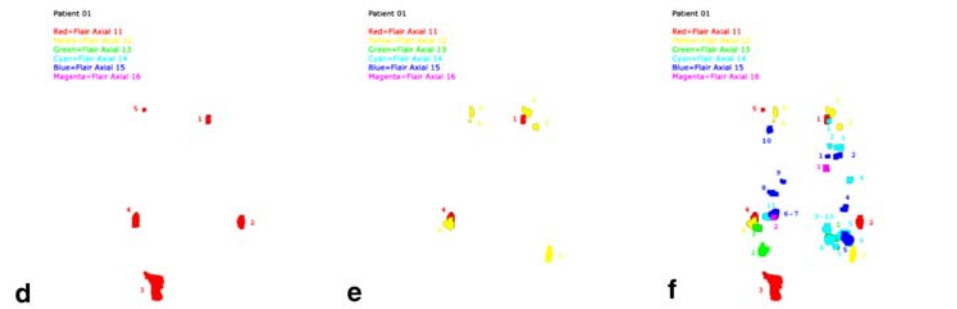

Lesion Name	Slice areas included in lesion	Total Count	Red	Yellow	Green	Cyan	Blue	Magenta
A	red 1, yellow 1	213	62	151				
B	red 2	172	172					
C	red 3	617	617					
D	red 4, yellow 4, Green 3	501	188	212	101			
E	red 5	24	24					
F	yellow 2	65		65				
G	yellow 3	194		194				
H	yellow 5	16		16				
I	yellow 6	79		79				
J	Green 1, Cyan 1, 2, 3, 10, 11* Blue 5*	1058			143	634	281	
K	Green 2	250			250			
L	Cyan 7	50				50		
M	Cyan 8	50				50		
N	Cyan 9	120				120		
O	Cyan 4	82				82		
P	Cyan 5	58				58		
Q	Cyan 6	55				55		
R	Cyan 12, Blue 6-7, Magenta 2	393				151	170	72
S	Blue 1	37					37	
T	Blue 2	111					111	
U	Blue 3	0					0	
V	Blue 4	102					102	
W	Blue 8	125					125	
X	Blue 9	52					52	
Y	Blue 10	88					88	
Z	Magenta 1	89						89

* Cyan 5 and 6 are not connected in slice 14 but join lesion J through Blue 5.

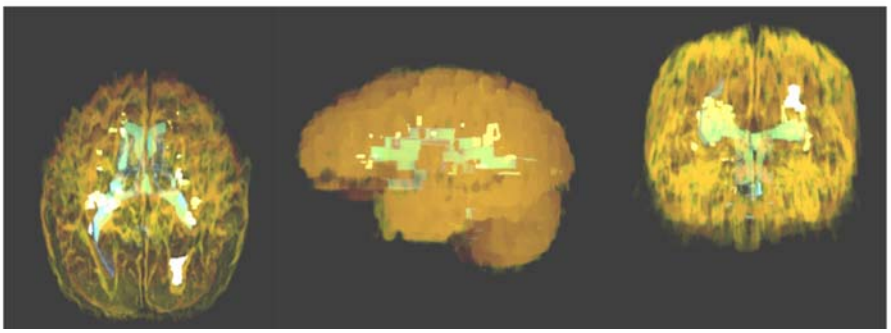

Fig. 8 The most commonly obtained data from 3-D MS CAD results. The data includes the original 3-D MRI data set. **a** A MRI FLAIR image; **b** CAD detected multiple lesions; **c** Radiologist identified lesions (normally not shown in the results, depicted here for comparison purpose only). **d** Color-coded MS lesions on a 2-D image; **e** On two slices; **f** On all slices. **g** The quantitative results of all 26 lesions detected by CAD. **h** Three oblique views of 2-D images with all 26 MS overlaid. Green color shows the ventricles (data source: courtesy of Drs. A. Gertych and B. Guo; and Guardian Technologies International Inc., Herndon, VA)

parent node describes one or more methods of quantitative analysis performed on each lesion. Each analysis performed can be further branched to one or multiple $(1-n)$ grandchild nodes, single image finding. The finding summary parent node is the most important part of an SR which includes CAD results. This node can branch into multiple child nodes $(1-n)$, each containing the name of the detection and analysis methods together with detailed results of each lesion on each single image finding. The detailed results include number, size, location, and referenced image. The Image Library parent node is optional; however, in the MS SR, it is used to reference original images where the CAD was performed

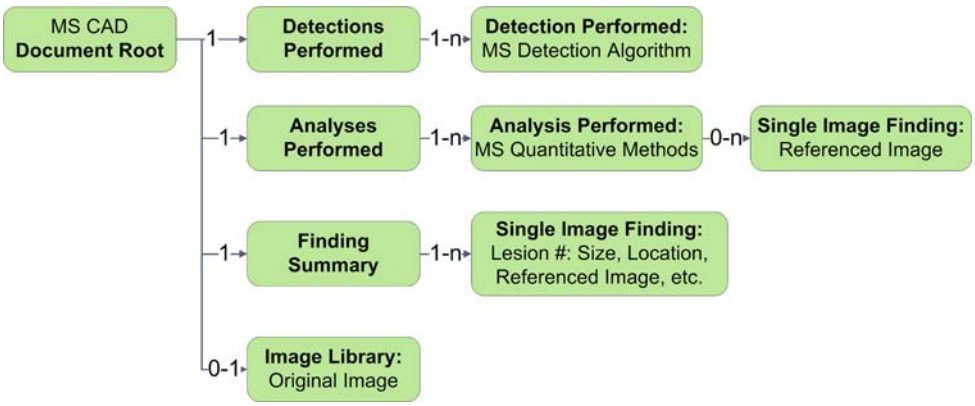

Fig. 9 Multiple sclerosis (MS) CAD SR Template. The SR template is designed following a tree structure starting from the Document Root, which branches into four parent nodes; each parent node branches to $(1 - n)$ child nodes and so forth

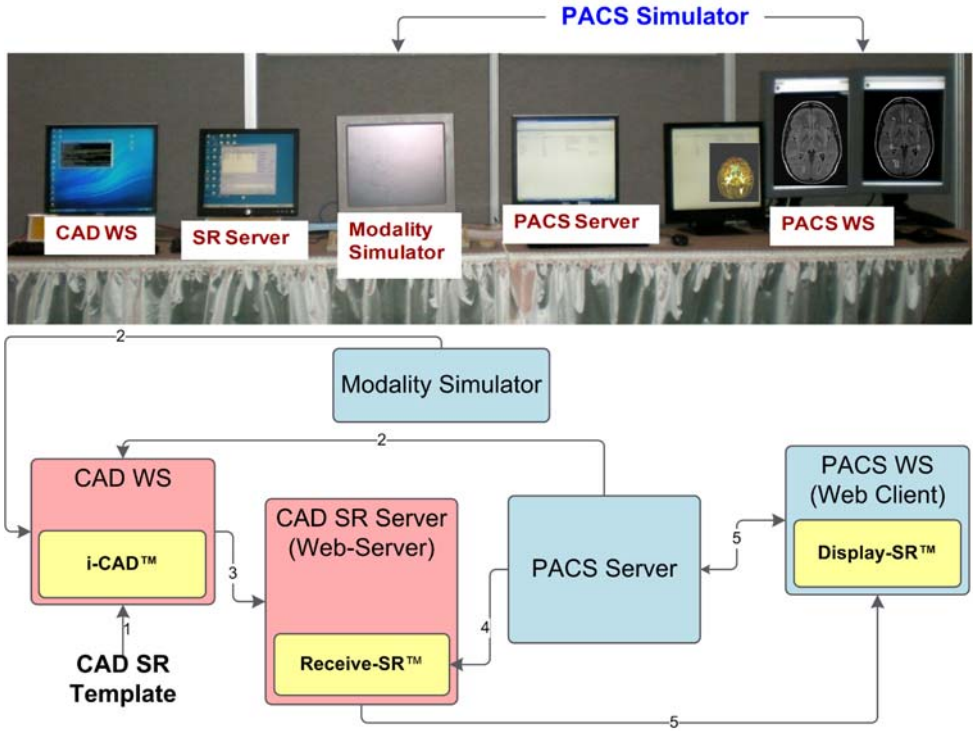

Fig. 10 Use the PACS Simulator to verify the data flow between the integrated PACS and CAD systems [18,19]. *Top* the PACS Simulator displayed at RSNA Annual Scientific Exhibit annually from 2000–2004 [1,11,20–23]. *Bottom* Workflow of CAD–PACS integration. *Blue* PACS Simulator components. *Red* CAD components. *Yellow* CAD–PACS toolkit modules. The integration steps in numerals are described in the text

on. The data structure format of each child can be obtained directly from the DICOM standard, Supplement 23.

Using the CAD–PACS toolkit

After the SR template was defined and designed, integrating the CAD with PACS can be implemented by using the toolkit. The first step is to use a PACS Simulator [1,11,20–24] to verify the data flow as shown in Fig. 10. The PACS Simulator has been a training tool for PACS and Imaging Informatics since 2000 [1,11,20–23] including to verify the HIPAA compliance [12,24] and is currently utilized as a research tool in CAD–PACS integration.

The integrating steps can be summarized as follows: (1) configuration of i-CAD module with the MS SR template and all data (measurements, nodule images, and summary) to create the DICOM-SR Object, (2) configuration of CAD WS to run the CAD application automatically after receiving DICOM images from Modality Simulator or PACS simulator, (3) based on the SR Template, i-CAD module automatically starts to create an SR upon completion of the CAD process and the results are sent in DICOM-SR format to Receive-SR for storage, (4) SR-Server prefetches referenced images from the PACS Server, and (5) CAD results are ready for viewing on PACS WS.

Figure 11 is a screenshot of CAD MS results at the PACS WS which shows an example of MS DICOM-SR Object with one 3-D view of multiple oblique 2-D images obtained using DICOM SC (see Fig. 8h). Although, this example only displays the 2-D oblique images, theoretically, the DICOM-SR specification includes image references and CAD results

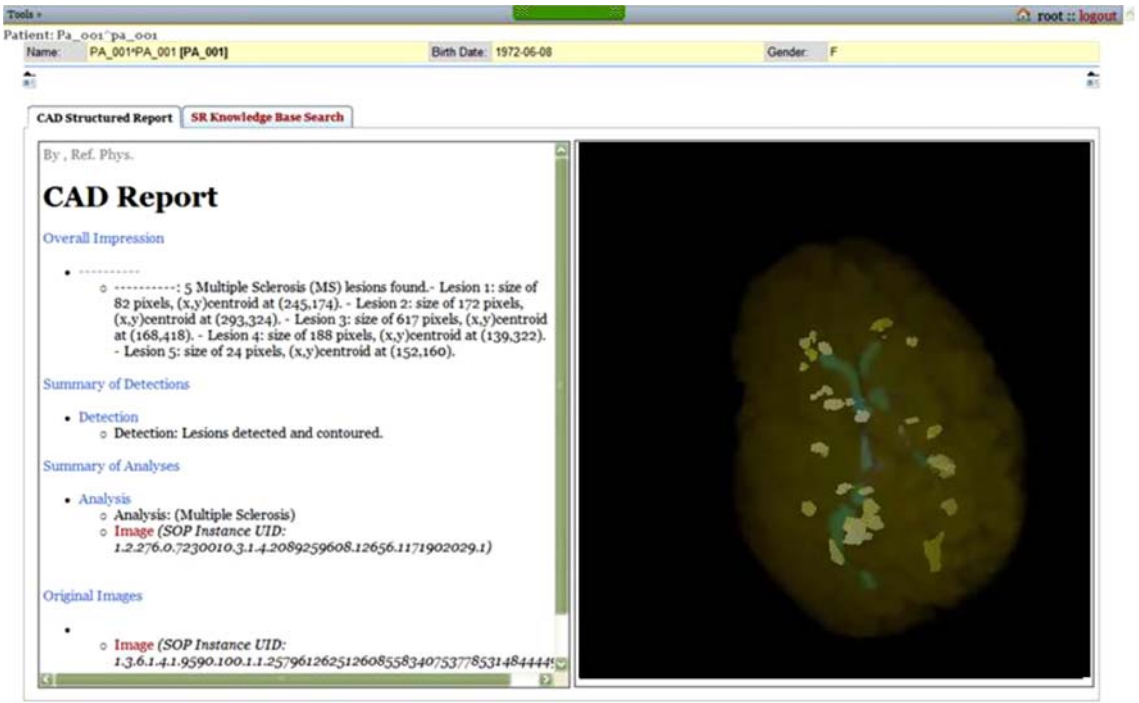

Fig. 11 Multiple sclerosis (MS) CAD Report in DICOM-SR format (*left*) and a 2-D oblique image (*right*). Refer to Fig. 8 for original images and CAD results

which can be used to display real time 3-D rendered images [9].

Discussion

Currently, CAD and PACS are two separate independent systems with only minimal communications between them. In this paper we described a CAD–PACS toolkit as a universal method to integrate CAD results with PACS in its daily clinical environment. The toolkit utilizes HL7 standard for textual data and the DICOM standard for imaging so that it follows the industrial standard for data format and communications. The method needs the DICOM-SR standard to reformat CAD results into an SR template so that they can be integrated as a component in the DICOM data mode for viewing on the PACS workstations. It also uses three IHE workflow profiles: KIN, SINR, and PWF to facilitate data transmission and communication in clinical workflow. We have shown CAD examples to illustrate explicitly how to integrate existing CAD results into PACS daily clinical operation.

Picture Archiving and Communication System is a mature healthcare technology which continues accumulating tremendous amount of imaging data daily. Unfortunately, the vast majority of this data in PACS is hardly utilized except for daily clinical service. There are many other advantages for the integrating CAD results with PACS. CAD is a growing field, its applications range from chest, breast, colon, brain, liver, skeletal, vascular, etc. Doi, in his 2007 survey [2], reports that the number of presentations in CAD at the Annual RSNA (Radiological Society of North America) Scientific Assembly increased from 59 in 2000 to 163 in 2005, and it continues to grow at a rapid rate into 2006 and 2007. At the view point of a CAD developer, PACS has tremendously large databases that can help further improve the research and development of these new CAD methods. Integrating CAD results only adds to these databases by now providing quantified results that were previously unavailable through the standard DICOM image of a PACS study. In future, the CAD–PACS integration would also allow CAD to directly assess PACS data from algorithm development and validation. However, to allow the CAD to directly query the PACS database still requires much further work mostly in administration and management issues due to patient privacy and PACS manufactures closely guarding their respective proprietary data format.

Because of the rich contents in the DICOM-SR, it benefits CAD developers to produce a comprehensive and standardized results findings and quantitative values in DICOM-SR format. The DICOM standard and template will guide the CAD developers to apply their knowledge in building a high quality and valuable reports for many other purposes.

Post-processing of medical images after generated by the imaging modalities are often performed to enhance their

diagnosis values. Post-processing of medical images are different from CAD in the sense that it produces some forms of display, some quantitative measurements, but does not provide detection nor diagnosis. To date, there are new technologies available for quantitative measurements obtained from post-processing or CAD that still reside within the post-processing workstation or the CAD server in the clinical environment. There has been some collaboration between post-processing and CAD manufacturers with PACS manufacturers to improve PACS workflow by providing an integrated PACS workstation. However, the integration has resulted in poor image quality performance and a return to standalone post-processing workstations. With the introduction of the CAD–PACS toolkit, even these results could be converted to DICOM-SR format and readily available for direct query by PACS WS and thus revolutionizing clinical workflow from single event patient-based queries to longitudinal-based queries on valuable metadata and quantitative measurements.

In addition, the trend of CAD and PACS integration is to incorporate CAD findings and DICOM key image referencing into its DICOM-compliant databases and services in the form of DICOM-SR data objects. Using DICOM-SR, content-based query/retrieval of DICOM imaging studies can be performed based on quantitative findings rather than patient identification and/or disease category; a demonstration application from our IPILab was presented at RSNA 2008 [14]. The advantages of query/retrieving content-based imaging data can be a great benefit for medical imaging research and clinical practice. The challenges we may face in this direction are several. Among them include: (1) advanced CAD methods development in data mining to search for meaningful data within PACS for specific applications, (2) addressing the Institutional Review Board (IRB) issue of using human subjects for research with almost unlimited information within the PACS database, and (3) collaboration with medical centers' PACS management and PACS manufacturers to open the PACS database for data access.

Acknowledgments This research was and has been partially supported by the National Institutes of Health (NIH), USA: NIH/NIBIB R01 EB 00298, NIH/NIBIB T32 EB 00438; and US Army Medical Research Command FY08 AAMTI – IAA, TATRC.

References

1. Cao F, Huang HK, Liu B, Zhou Z, Zhang J, Mogel G (2001) Fault-tolerant PACS server, InfoRAD exhibit. The radiological society of North America 87th scientific assembly and annual meeting, November 25–30, p 737
2. Doi K (2007) Computer-aided diagnosis in medical imaging: historical review, current status and future potential. Comput Med Imaging Graph 31(4–5):198–211. doi:10.1016/j.compmedimag.2007.02.002
3. DICOM Standard (1999) Supplement 23: Structured reporting object
4. DICOM Standard (2000) Supplement 50: Mammography CAD
5. DICOM Standard (2001) Supplement 65: Chest CAD SR SOP Class
6. Huang HK, Doi K (2007) Editorial and special issue on CAD and image-guided decision support (2007). Comput Med Imaging Graph 31(4–5):195–197. doi:10.1016/j.compmedimag.2007.02.001
7. Health Level 7 (2008). http://www.hl7.org/
8. Huang HK (2007) Tutorial on CAD–PACS integration. Computer assisted radiology and surgery, CARS 2007. Berlin, Germany, June 27–30
9. Huang HK (2008) Tutorial on CAD–PACS integration. Computer assisted radiology and surgery, CARS 2008. Barcelona, Spain, June 25–28
10. Hologic R 2 Home. http://www.r2tech.com/main/home/index.php
11. Huang HK, Cao F, Liu BJ, Zhou Z et al (2000) PACS simulator: a standalone educational tool, InfoRAD exhibit. The radiological society of North America 86th scientific assembly and annual meeting, November 26–December 1, p 688
12. HHS—Office of civil rights—HIPAA (2008). http://www.hhs.gov/ocr/hipaa
13. IHE (2008). http://www.ihe.net
14. Lee J, Le A, Liu BJ, Huang HK (2008) Integration of content-based DICOM-SR for CAD in the medical imaging informatics data grid with examples in CT chest, mammography, and bone-age assessment, education exhibit. The radiological society of North America 94th scientific assembly and annual meeting, November 30–December 5, p 912
15. Le A, Mai L, Liu B, Huang HK (2008) The workflow and procedures for automatic integration of a computer-aided diagnosis workstation with a clinical PACS with real world examples. Proc SPIE Med Imaging 6919, 69190U:1–7
16. Le A, Zhou Z, Liu BJ, Huang HK, Le A (2007) A DICOM structured report viewer and automatic workflow for CAD-PACS integration in a clinical environment based on IHE profiles. The radiological society of North America 93rd scientific assembly and annual meeting, November 25–30, p 835
17. Standards DICOM (2008). http://medical.nema.org/medical/dicom/2008
18. Zhou Z, Le A, Liu B, Huang HK (2007) PACS–CAD toolkit for integrating an independent CAD workstation to diagnosis workflow. Proc SPIE Med Imaging 6516, 651609:1–8
19. Zhou Z, Liu BJ, Le A (2007) CAD–PACS integration tool kit-based on DICOM screen capture (SC) and structured report (SR) and IHE workflow profiles. J Comput Med Imaging Graph 31(4–5):346–352. doi:10.1016/j.compmedimag.2007.02.015
20. Zhou Z, Law M, Huang HK, Cao F, Liu B, Zhang J (2002) An educational RIS/PACS simulator, InfoRAD exhibit. The radiological society of North America 88th scientific assembly and annual meeting, December 1–6, p 753
21. Zhou Z, Huang HK, Cao F, Liu BJ et al (2003) An educational RIS/PACS simulator with web-based image distribution and display system, InfoRad exhibit. The radiological society of North America 89th scientific assembly and annual meeting, November 30–December 5, p 796
22. Zhou Z, Liu BJ, Huang HK, Zhang J (2004) Educational RIS/PACS simulator integrated with HIPAA compliant architecture (HCA) for auditing, InfoRad exhibit. The radiological society of North America 90th scientific assembly and annual meeting, November 28–December 3, p 827
23. Zhou Z, Huang HK, Liu BJ, Cao F, Zhang J, Mogel G, Law MA (2004) RIS/PACS simulator with web-based image distribution and display system for education. Proceedings of the SPIE, vol 5371, pp 372–381

24. Zhou Z, Liu BJ, Huang HK, Zhang J (2005) Educational RIS/PACS simulator integrated with the HIPAA compliant auditing (HCA) toolkit. Proc SPIE 5748:491–500. doi:10.1117/12.595383
25. Zhou Z, Liu BJ, Huang HK, Le A (2006) A PACS-CAD toolkit for integrating an independent CAD workstation to diagnosis workflow based on DICOM SR and IHE profiles. The radiological society of North America 93rd scientific assembly and annual meeting, November 26–December 1, p 795

Racial Differences in Growth Patterns of Children Assessed on the Basis of Bone Age[1]

Aifeng Zhang, PhD
James W. Sayre, PhD
Linda Vachon, MD
Brent J. Liu, PhD
H. K. Huang, DSc

Purpose: To collect up-to-date data in healthy children to create a digital hand atlas (DHA) that can be used to evaluate, on the basis of the Greulich and Pyle atlas method, racial differences in skeletal growth patterns of Asian, African American, white, and Hispanic children in the United States.

Materials and Methods: This retrospective study was HIPAA compliant and approved by the institutional review board. Informed consent was obtained from all subjects or their guardians. From May 1997 to March 2008, a DHA containing 1390 hand and wrist radiographs obtained in male and female Asian, African American, white, and Hispanic children with normal skeletal development was developed. The age of subjects ranged from 1 day to 18 years. Each image was read by two pediatric radiologists working independently and without knowledge of the subject's chronologic age, and evaluation was based on their experience with the Greulich and Pyle atlas. Statistical analyses were performed with the paired-samples t test and analysis of variance to study racial differences in growth patterns. $P \leq .05$ indicated a significant difference.

Results: Bone age ($P \leq .05$) was significantly overestimated in Asian and Hispanic children. These children appear to mature sooner than their African American and white peers. This was seen in both male and female subjects, especially in girls aged 10–13 years and boys aged 11–15 years.

Conclusion: Ethnic and racial differences in growth patterns exist at certain ages; however, the Greulich and Pyle atlas does not recognize this fact. Assessment of bone age in children with use of the Greulich and Pyle atlas can be improved by considering the subject's ethnicity.

[1] From the Image Processing and Informatics Lab, Department of Radiology, University of Southern California, 1450 San Pablo St, Suite 2100, Los Angeles, CA 90292 (A.Z., B.J.L., H.K.H.); Department of Biostatistics and Radiological Sciences, University of California, Los Angeles, School of Public Health, Los Angeles, Calif (J.W.S.); and Department of Radiology, Los Angeles County Hospital and University of Southern California Medical Center, Los Angeles, Calif (L.V.). From the 2007 RSNA Annual Meeting. Received March 10, 2008; revision requested May 1; revision received April 3; accepted June 20; final version accepted July 9. Supported by National Institutes of Health grants R01 LM 06270 and R01 EB 00298: 97-08. **Address correspondence to** A.Z. (e-mail: *aifengz@gmail.com*).

Assessment of bone age is a clinical procedure used in pediatric radiology to evaluate skeletal maturity on the basis of bone growth in the left hand and wrist, as seen on a radiograph. The determination of skeletal maturity (also referred to as bone age) plays an important role in the diagnosis and treatment of endocrinologic abnormalities and growth disorders in children (1,2). In clinical practice, the method most commonly used to assess bone age is matching of a radiograph of the left hand and wrist with the Greulich and Pyle atlas (3), which contains a reference set of standard hand images collected in the 1950s in healthy white children who were members of the middle or upper class population.

Over the past 30 years, many authors have questioned the appropriateness of using the Greulich and Pyle atlas for bone age assessment in contemporary children. In 1975, Roche et al (4) showed that the average child in the United States was less physically mature than the children in the Greulich and Pyle atlas. In 1996, Ontell et al (5) examined the applicability of the Greulich and Pyle standards to ethnically diverse children. However, these studies and various others (6–8) did not provide a large-scale systematic method for validation. Thus, the purpose of our study was to collect up-to-date data in healthy children to create a digital hand atlas (DHA) that can be used to evaluate, on the basis of the Greulich and Pyle atlas method, racial differences in skeletal growth patterns of Asian, African American, white, and Hispanic children in the United States.

Advances in Knowledge

- A digital hand atlas (DHA) of 1390 hand-wrist radiographs obtained in Asian, African American, white, and Hispanic boys and girls with normal skeletal development has been developed to provide an up-to-date standard with which to assess growth and development and is accessible at *http://www.ipilab.org/BAAweb*.
- Radiologists assigned a bone age that was relatively close to the chronologic age in African American and white children; however, cross-racial differences indicated that Asian and Hispanic children mature sooner than do African American and white children, especially between 10 and 13 years of age in girls and between 11 and 15 years of age in boys.

Materials and Methods

The protocol of this retrospective study was approved and has been renewed annually by the institutional review boards of our institutions, and written informed consent was obtained from all subjects or their legal guardians. This study was compliant with the Health Insurance Portability and Accountability Act. Subject anonymity was achieved by replacing the subject name and other traceable information with a data encryption method.

Subject Recruitment

During the past 10 years (May 1997 to March 2008), a DHA has been developed that contains 1390 hand and wrist radiographs obtained in healthy Asian, African American, white, and Hispanic boys and girls. All subjects (age range, 1 day to 18 years) were recruited from public schools in Los Angeles County, California, starting in the late 1990s (9–15).

Case Selection Criteria

Before the hand was examined with radiography, a physical examination was performed to determine the health and Tanner maturity index (16) of the subject to ensure that he or she was healthy and that his or her skeletal development was normal. Height, trunk height, and weight were measured and used to calculate the body mass index.

Implication for Patient Care

- The discovery of cross-racial differences at different age ranges sheds light on the possibility that bone age assessment in children can be improved by considering a child's ethnicity, especially when accurate assessment of bone age is crucial to patient care (optimal surgical intervention in children with leg length discrepancies).

Image Acquisition

Each radiograph of the hand and wrist was obtained with a rigorous data collection protocol (9). The radiographs were obtained with an x-ray generator (Polyphos 50; Siemens, Erlangen, Germany) at 55 kVp and 1.2 mAs. The radiation dose delivered per image was less than 1 mrem (0.01 mSv), which is equivalent to approximately 1 day of natural background radiation. The hand was adjusted to the correct position, which required the subject to keep his or her fingers spread apart and maintain hand straightness as much as possible; no hand jewelry was worn. The distance between the x-ray tube and the image cassette was 40 inches. The hand of a normal child was less than 1 inch thick; therefore, the magnification factor was approximately 1.

Image Interpretation

After a radiograph of the hand was acquired in each subject, two experienced pediatric radiologists (each with more than 25 years of experience in bone age assessment) performed independent

Published online before print
10.1148/radiol.2493080468

Radiology 2009; 250:228–235

Abbreviations:
DHA = digital hand atlas
DICOM = Digital Imaging and Communications in Medicine

Author contributions:
Guarantors of integrity of entire study, A.Z., B.J.L., H.K.H.; study concepts/study design or data acquisition or data analysis/interpretation, all authors; manuscript drafting or manuscript revision for important intellectual content, all authors; manuscript final version approval, all authors; literature research, A.Z., B.J.L., H.K.H.; clinical studies, A.Z., L.V., B.J.L., H.K.H.; statistical analysis, A.Z., J.W.S., B.J.L., H.K.H.; and manuscript editing, A.Z., L.V., B.J.L., H.K.H.

Funding: This research was supported by National Institutes of Health (grant nos. R01 LM 06270, R01 EB 00298:97-08).

Authors stated no financial relationship to disclose.

readings based on Greulich and Pyle atlas standards. During reading, radiologists were blinded to the subject's chronologic age, race, and other pertinent information.

The subject's bone age, as determined by the radiologist, was compared with the subject's chronologic age. The image was selected and accepted to the DHA only if the difference between the subject's bone age, as determined by the radiologist, and the subject's chronologic age was less than 3 years. The acceptance rate was higher than 90%.

Image Digitization

For data analysis, Web-based image and data distribution, and communication in the clinical environment and public domain, each accepted radiograph (subject name and identification were covered with black tape) was digitized into the Digital Imaging and Communications in Medicine (DICOM) format by using a laser film digitizer (Array, Tokyo, Japan); furthermore, each subject's information (excluding his or her name and identification, as well as any other traceable data) was put in the DICOM header (17–19). We used the following parameters: 12 bits per pixel, optical density of 0.0–4.0, and 100-μm pixel spacing. The size of the image corresponded to the size of the original radiograph. Table 1 contains the pertinent information of four 14-year-old boys of different races. The corresponding radiographs of their hands are shown in Figure 1.

Data Collection Summary

There were two cycles of data collection, each of which had eight categories (Asian boys, Asian girls, African-American boys, African-American girls, white boys, white girls, Hispanic boys, and Hispanic girls). Each category contained 19 age groups (one for subjects younger than 1 year and 18 set at 1-year intervals for subjects aged 1–18 years). The two pediatric radiologists independently read all images obtained in each cycle. Cycle 1 consisted of 1103 digitized hand images with demographic data. Five cases for each younger age group (1–9 years) and 10 cases for each older age group (10–18 years) were included. The sample sizes were chosen to achieve a precision of approximately 0.20 for all age groups, with a 95% confidence interval when using the digital hand atlas to compare bone age with chronologic age. Precision is defined as the confidence interval width divided by the estimated mean value of chronologic age. Subjects younger than 1 year were considered infants, and their data were not used for analysis.

In order to study the active growth period in children aged 5–14 years more carefully to yield better statistics,

Figure 1

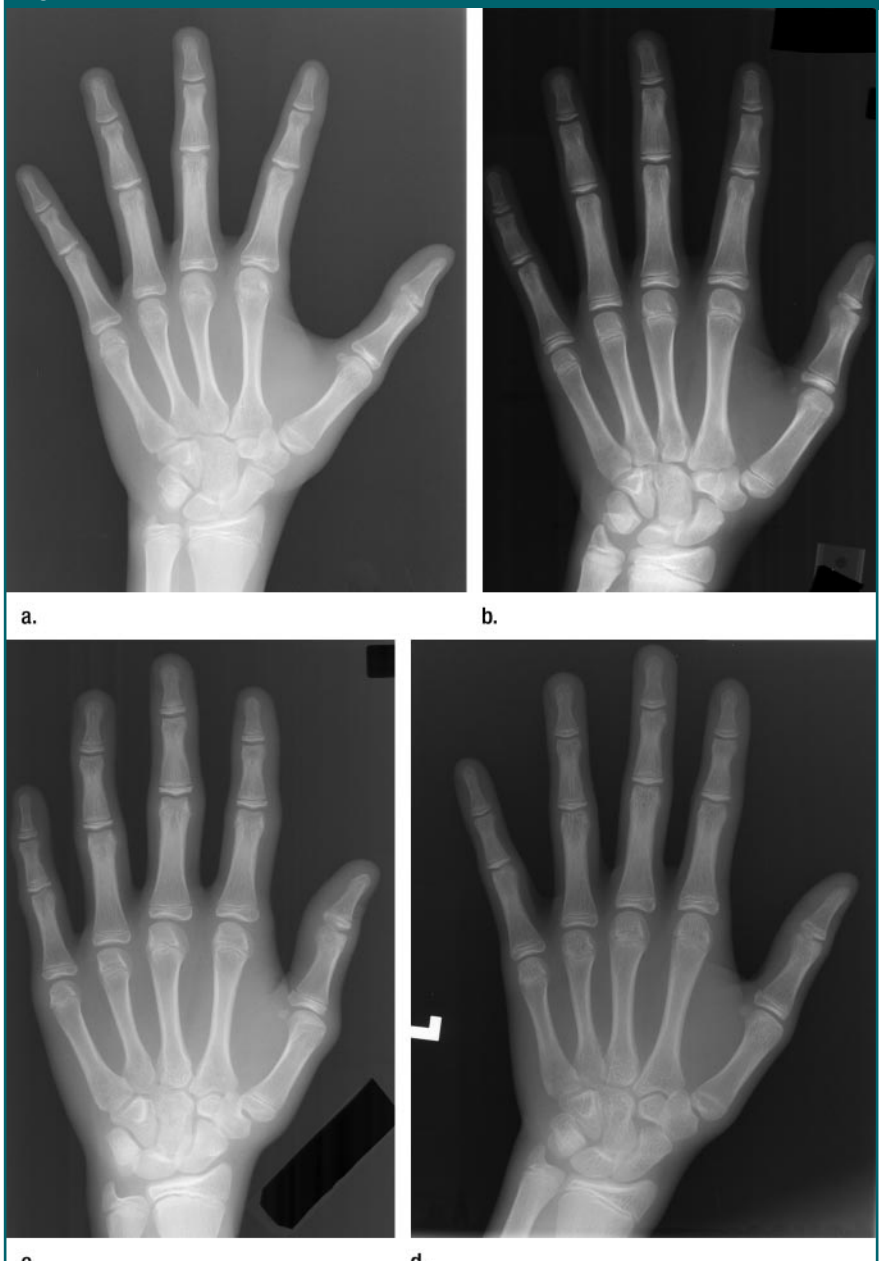

Figure 1: Examples of radiographs obtained in **(a)** a 14.13-year-old Asian boy, **(b)** a 14.46-year-old African American boy, **(c)** a 14.79-year-old white boy, and **(d)** a 14.64-year-old Hispanic boy. Corresponding demographic data and bone age, as assigned by two radiologists, are included in the DICOM image header (Table 1).

data were collected in 287 subjects during the second cycle after the first cycle had been completed. Thus, a total of 1390 cases were included in the DHA. The breakdown of cases was as follows: 167 Asian girls, 167 Asian boys, 174 African American girls, 184 African American boys, 166 white girls, 167 white boys, 183 Hispanic girls, and 182 Hispanic boys. These 1390 cases were used to derive the results described in this article.

Figure 2

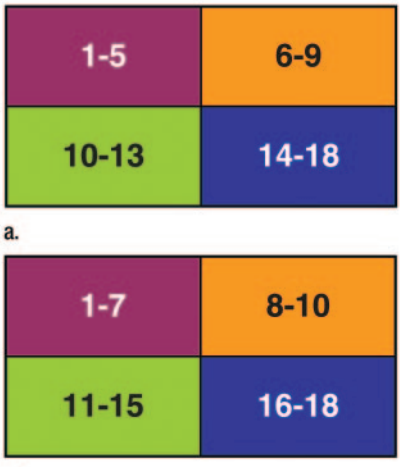

Figure 2: Charts show the four divided age subsets for **(a)** girls and **(b)** boys. These charts provide a road map for use in the study of racial differences during different growth periods. In **a**, purple indicates 1–5 years of age; orange, 6–9 years of age; green, 10–13 years of age; and blue, 14–18 years of age. In **b**, purple indicates 1–7 years of age; orange, 8–10 years of age; green, 11–15 years of age; and blue, 16–18 years of age.

Statistical Analysis

Statistical analysis was performed with computer software (SPSS, version 15.0 for Windows; SPSS, Chicago, Ill). Graphs were generated with third-party software (KaleidaGraph 3.5; Synergy Software, Reading, Pa). Two types of analysis, the paired-samples *t* test and analysis of variance, were performed by using chronologic age as the reference standard. Data from subjects in the newborn group were not used for analysis. $P \leq .05$ indicated a significant difference.

Data acquired in both cycles for each race and a given sex were combined with data for the entire age range (1–18 years), and the paired-samples *t* test was performed on a case-by-case basis to find the mean difference between the average bone age of two readings and the chronologic age. This resulted in eight categories for comparison: Asian boys, Asian girls, African American boys, African American girls, white boys, white girls, Hispanic boys, and Hispanic girls, each depicting the overall view of differences between the radiologists' average bone age reading against the chronologic age for subjects of each race and sex.

On the basis of the effects of the growth factor and sexual hormones, as well as our observations in the phalangeal, carpal, and wrist joint regions (9–15), we divided the entire growth age ranging from 1 year to 18 years into four age subsets, as shown in Figure 2. These subsets were used to study differences in growth patterns of children of different races in a given subset. Analysis of variance was used to study the cross-racial comparisons for a given subset of growth range on the basis of differences between chronologic age and bone age.

Results

Radiologist Interpretation

Table 2 shows the mean difference in age between the average bone age as-

Table 2

Mean Difference between Bone Age Assigned by Radiologists and Chronologic Age according to Race and Sex

Characteristic	Asian		African American		White		Hispanic	
	Girls	Boys	Girls	Boys	Girls	Boys	Girls	Boys
Mean difference between bone age assigned by radiologists and chronologic age (y)	0.24*	0.41*	0.03	−0.02	−0.15*	0.01	0.24*	0.30*
No. of cases†	166	165	170	179	163	164	182	178

* Mean difference between bone age assigned by radiologists and chronologic age was significant ($P \leq .05$).

† Infants (patients younger than 1 year) were excluded from analysis.

Table 1

Pertinent Information in Four 14-year-old Boys of Different Races

Subject No.	Race	Sex	Birth Date	Examination Date	Chronologic Age (y)	Tanner Maturity Index Score	Height (cm)	Trunk Height (cm)	Weight (kg)	Bone Age Assigned by Reader 1 (y)	Bone Age Assigned by Reader 2 (y)
1	Asian	Male	May 26, 1987	July 12, 2001	14.13	5	170.00	88.90	55.50	15.75	15.50
2	African American	Male	June 18, 1981	December 3, 1995	14.46	3.5	168.00	82.55	49.30	13.25	14.00
3	White	Male	July 05, 1979	April 19, 1994	14.79	4	169.00	86.70	56.00	14.00	14.50
4	Hispanic	Male	September 13, 1983	May 6, 1998	14.64	5	168.40	83.82	51.60	15.00	15.00

Note.—The DICOM header includes the subject's demographic and health-related information, as well as the bone age assigned by the radiologists. These data, along with the corresponding image, can be retrieved from the Web-based DHA.

Figure 3

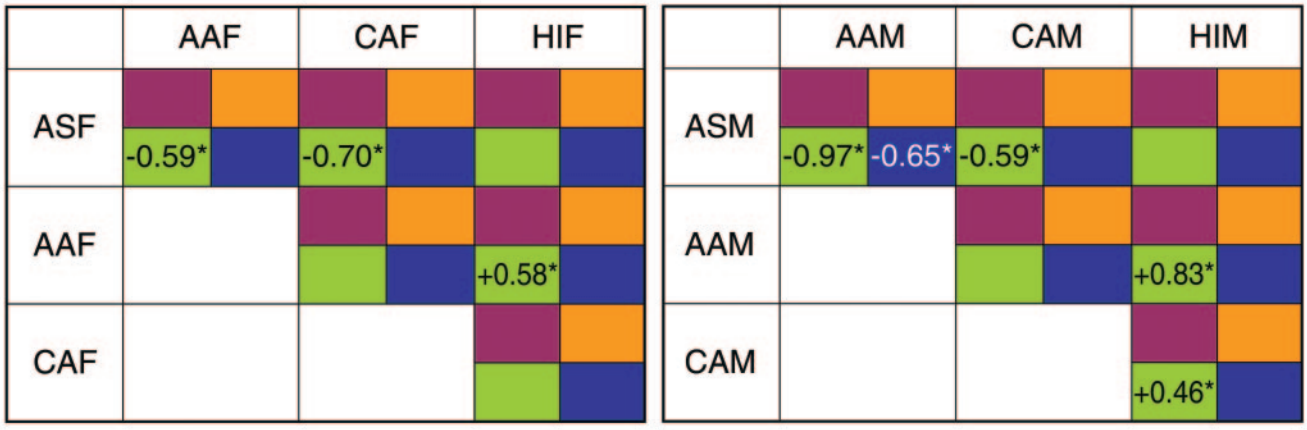

Figure 3: Charts show cross-racial comparisons of **(a)** girls and **(b)** boys. Data are shown only if differences are significant ($P \leq .05$). Each racial block was divided into four age groups, as described in Figure 2. The plus and minus signs indicate under- and overestimation of bone age, respectively, by radiologists in comparing rows with columns. *AAF* = African American girl, *AAM* = African American boy, *ASF* = Asian girl, *ASM* = Asian boy, *CAF* = white girl, *CAM* = white boy, *HIF* = Hispanic girl, *HIM* = Hispanic boy.

signed by two radiologists and the chronologic age for each of the eight categories separated by race and sex. Since we collected data in children with normal skeletal development, the differences with asterisks shown in Table 2 are within 2 standard deviations between the normal chronologic age and the average bone age (see the Case Selection Criteria section) and may not be important from a clinical perspective. However, we were able to conclude that the radiologists had a slight tendency, which was statistically significant, to overestimate bone age in the Asian and Hispanic populations as a whole.

Cross-racial Comparisons

The cross-racial differences assessed with analysis of variance among the four races in the four divided age subsets (Fig 2) are presented in Figure 3.

Figure 3a shows that in girls, significant mean differences of average reading between races were observed in the third age subset (10–13 years). Radiologists overestimated bone age in Asian girls in comparison with their African American and white peers by approximately 0.59 year and 0.70 year, respectively. Similarly, radiologists overestimated bone age by 0.58 year in Hispanic girls when compared with African American girls. Figure 4 shows plots of bone age versus chronologic age in Asian girls versus white girls, Asian girls versus African American girls, and Hispanic girls versus African American girls. In each comparison, the figure on the left covers the entire age range (1–18 years), whereas the figure on the right shows a close-up view of the third age subset (10–13 years).

Similar patterns were also observed in boys (Fig 3). In the third age subset (11–15 years), significant overestimation of bone age of 0.97 year and 0.83 year was observed in Asian and Hispanic boys, respectively, when compared with African American boys. Overestimation of 0.65 year continued until the fourth age subset (16–18 years) when Asian boys were compared with African American boys. Furthermore, comparison of white boys with Asian and Hispanic boys in the third age subset (11–15 years) resulted in significant overreading of 0.59 year and 0.46 year, respectively. Figure 5 shows bone age versus chronologic age in four racial pairs: *(a)* Hispanic boys versus African American boys, *(b)* Asian boys versus African American boys, *(c)* Asian boys versus white boys, and *(d)* Hispanic boys versus white boys.

Discussion

An up-to-date DHA for four ethnic groups has been developed with 1390 hand and wrist radiographs obtained in Asian, African American, white and Hispanic boys and girls with normal skeletal development aged between 1 day and 18 years. Each case was read by two pediatric radiologists working independently on the basis of the Greulich and Pyle atlas standard. The normality and consistency of the data were ensured by radiologists' readings and a rigorous quality assurance data collection protocol. Hand radiographs were digitized and stored in the DICOM format, which facilitates image viewing and transmission in the clinical environment for training and image-assisted daily clinical operation.

Previous studies, in which researchers examined the applicability of the Greulich and Pyle atlas for use in contemporary children, have been performed: Mora et al (7) examined 534 children of European and African de-

scent, and Ontell et al (5) collected data in 765 trauma patients of four races. Both of these studies are similar to our study in that they involved use and evaluation of the Greulich and Pyle atlas in each of the racial groups. However, in neither study did the authors compare cross-racial differences. Our study differed from the aforementioned studies in that our study consisted of a robustly designed database of 1390 carefully chosen healthy subjects and we compared cross-racial growth differences.

By using the DHA, we observed differences in the readings of two pediatric radiologists in subjects of four races on the basis of the Greulich and Pyle atlas standard, and we recorded these differences systematically. Our results show the cross-racial differences between skeletal growth patterns of Asian and Hispanic children and skeletal growth patterns of white and African American children. Radiologists assigned a bone age that was relatively close to the chronologic age of African American and white children. However, bone age and chronologic age were significantly different in Asian and Hispanic children. Cross-racial differences in four age subsets indicate that Asian and Hispanic children mature earlier than African American and white children. This holds true for girls and boys, especially those aged 10–13 years and 11–15 years, respectively.

Genetic differences, diet, and nutritional intake may influence variations in the bone growth pattern. This calls into question the applicability of the Greulich and Pyle atlas as a reference for children of different races. Our results suggest that bone age assessment in children can be improved by considering the ethnic population. An institutional review board–approved clinical validation study of the usefulness of the DHA is being performed at our institution (Los Angeles County Women's and Children's Hospital, Los Angeles, Calif).

Our study had limitations that should be considered in future research. First, all subjects enrolled in this study were from the Los Angeles metropolitan area. Further studies with data collection from different geographic regions are necessary to study regional factors in skeletal development. Second, mixed ethnicity was not considered. This issue should be addressed in future studies, with a view toward comparison of skeletal development in children with mixed ethnicity with that in children of their parents' ethnicities. Third, we investigated the effect of ethnicity in only those children whose skeletal development was considered normal on the basis of the Greulich and Pyle atlas. Fourth, a subject's ethnicity is usually unavailable in daily

Figure 4

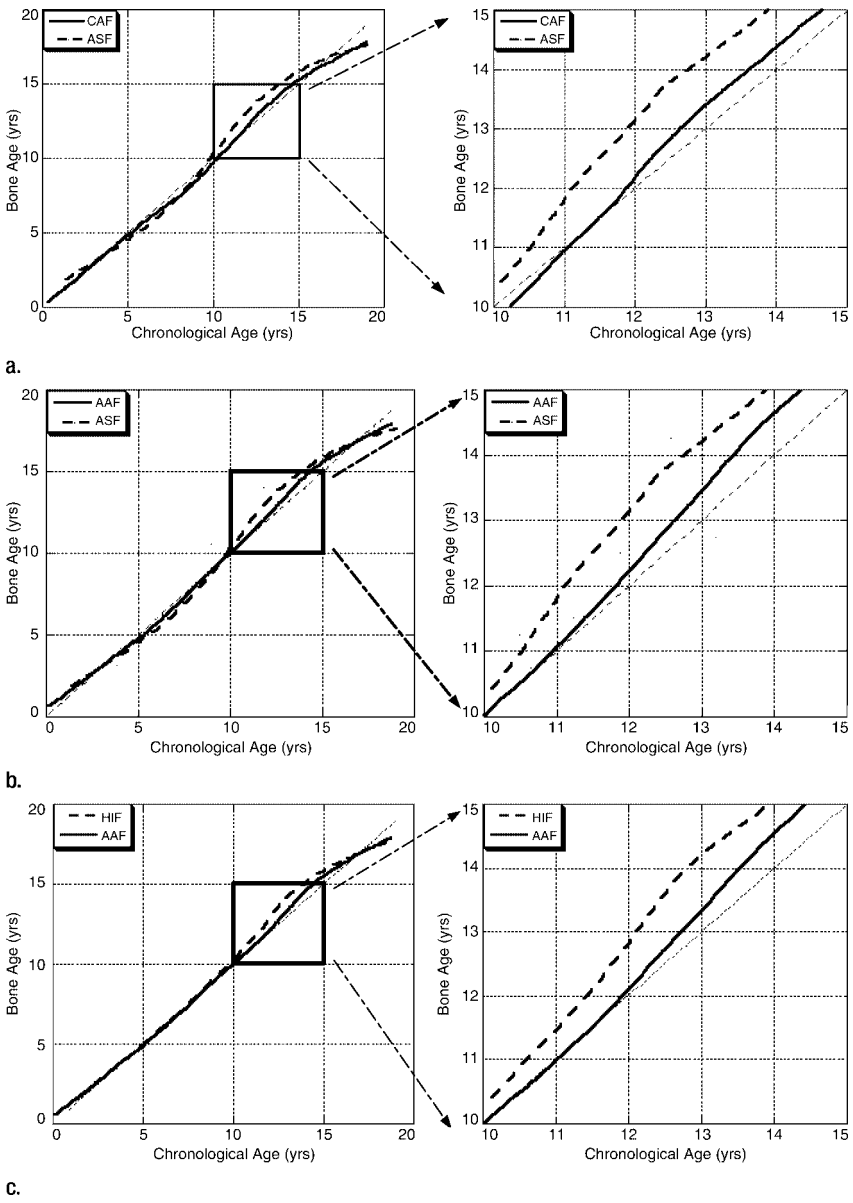

Figure 4: Graphs show comparisons of three racial pairs. The x-axis shows the chronologic age, the y-axis shows the average bone age, and the thin 45° dotted line shows the normal standard comparison in **(a)** Asian girls *(ASF)* versus white girls *(CAF)*, **(b)** Asian girls versus African American girls *(AAF)*, and **(c)** Hispanic girls *(HIF)* versus African American girls. The graphs on the left show the plots for the entire age range, whereas the graphs on the right are close-up plots for the third age subset (10–13 years).

practice. This limits future applications of the DHA in clinical practice. This issue needs to be addressed in patient care when enough attention has been brought to the racial factor in bone age assessment in children.

The DHA provides an up-to-date standard with which to classify normal bone growth and development in children. Currently, the DHA is accessible from the World Wide Web for online learning and teaching. Also, a computer-assisted bone age assessment system for use with the DHA has been developed and distributed to several international institutions (20) for use in a multicenter study.

Acknowledgments: We thank the National Institutes of Health for supporting this research; the Bone Development Group at the Childrens Hospital, Los Angeles, Calif, for data collection; and James Hill, MD, JD, for his assistance in the literature search and manuscript revision.

References

1. Tanner JM, Healy MJR, Goldstein H, Cameron N. Assessment of skeletal maturity and prediction of adult height (TW3 method). London, England: Saunders, 2001.
2. Kirks D. Practical pediatric imaging. In: Diagnostic radiology of infants and children. Boston, Mass: Little, Brown, 1984; 198–201.
3. Greulich WW, Pyle SI. Radiographic atlas of skeletal development of the hand and wrist. Stanford, Calif: Stanford University Press, 1959.
4. Roche AF, Roberts J, Harnill PV. Skeletal maturity of children 6–11 years: racial, geographic area and socioeconomic differentials. In: National Health Survey. Rockville, Md: Health Resources Administration, National Center for Health Statistics, 1975; 1–38.
5. Ontell FK, Ivanovic M, Ablin DS, Barlow TW. Bone age in children of diverse ethnicity. AJR Am J Roentgenol 1996;167:1395–1398.
6. Loder RT, Estle DT, Morrison K, et al. Applicability of the Greulich and Pyle skeletal age standards to black and white children of today. Am J Dis Child 1993;147:1329–1333.
7. Mora S, Boechat MI, Pietka E, Huang HK, Gilsanz V. Skeletal age determinations in children of European and African descent: applicability of the Greulich and Pyle standards. Pediatr Res 2001;50:624–628.

Figure 5

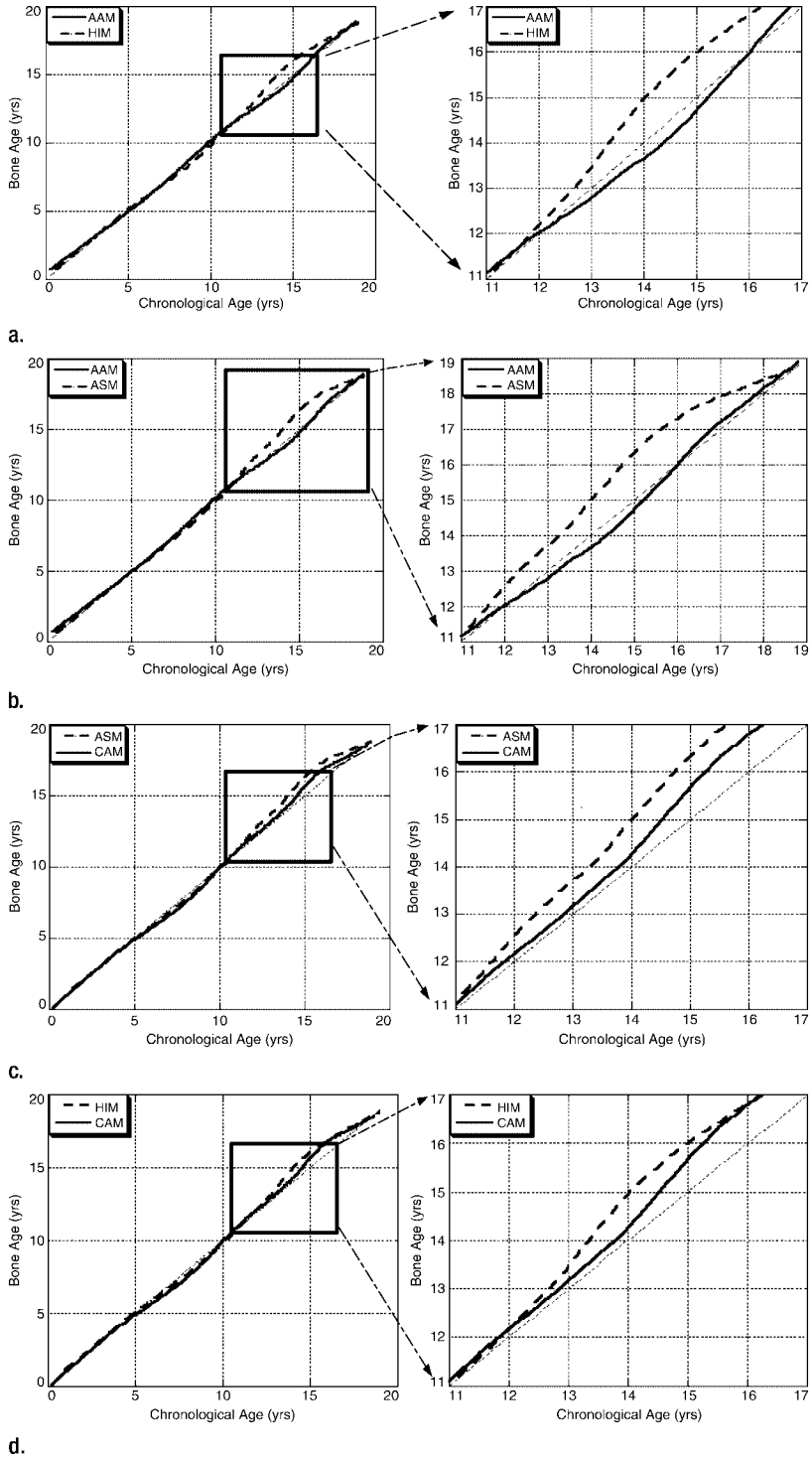

Figure 5: Comparisons (as in Fig 4) of **(a)** Hispanic *(HIM)* versus African American boys *(AAM),* **(b)** Asian *(ASM)* versus African American boys; **(c)** Asian versus white boys *(CAM);* and **(d)** Hispanic versus white boys. Left: entire age range. Right: third age subset (11–15 years) **(a, c, d)** and third and fourth age subsets (11–18 years) **(b)**.

8. Masse G, Hunt EE. Skeletal maturation of the hand and wrist in West African children. Hum Biol 1963;35:3–25.

9. Gertych A, Zhang A, Sayre J, Pospiech-Kurkowska S, Huang HK. Bone age assessment of children using a digital hand atlas. Comput Med Imaging Graph 2007;31:322–331.

10. Zhang A, Tsao S, Sayre J, Gertych A, Liu BJ, Huang HK. Is Greulich and Pyle atlas still a good reference for bone age assessment? In: Horii SC, Andriole KP, eds. Proceedings of SPIE: medical imaging 2007—PACS and imaging informatics. Vol 6516. Bellingham, Wash: International Society for Optical Engineering, 2007; 65161H.

11. Pietka E, Pospiech-Kurkowska S, Gertych A, Cao F, Huang HK. Computer-assisted bone age assessment: image analysis and fuzzy classification [abstr]. Radiology 2002;225(P):751.

12. Pietka BE, Pospiech S, Gertych A, Cao F, Huang HK, Gilsanz V. Computer automated approach to the extraction of epiphyseal regions in hand radiographs. J Digit Imaging 2001;14:165–172.

13. Zhang A, Gertych A, Liu BJ. Automatic bone age assessment for young children from newborn to 7-year-old using carpal bones. Comput Med Imaging Graph 2007;31:299–310.

14. Huang HK, Zhang A, Liu BJ, et al. Data grid for large-scale medical image archive and analysis. Proceedings of the 13th ACM International Conference on Multimedia. Singapore: Association for Computing Machinery, 2005; 1005–1013.

15. Zhang A, Gertych A, Liu BJ, Huang HK. Data mining and visualization of average images in a digital hand atlas. In: Ratib OM, Horii SC, eds. Proceedings of SPIE: medical imaging 2005—PACS and imaging informatics. Vol 5748. Bellingham, Wash: International Society for Optical Engineering, 2005; 65–72.

16. Tanner JM. Growth at adolescence. Oxford, England: Blackwell Scientific Publications, 1962.

17. Huang HK. PACS and imaging informatics: basic principles and applications. Hoboken, NJ: Wiley, 2004; 504–507.

18. Zhang A, Zhou Z, Gertych A, Liu BJ, Huang HK. Integration of bone age assessment CAD results with the PACS diagnostic workflow utilizing DICOM structure report [abstr]. In: Radiological Society of North America scientific assembly and annual meeting program. Oak Brook, Ill: Radiological Society of North America, 2006; 909.

19. Zhou Z, Liu BJ, Le AH. CAD-PACS integration tool kit based on DICOM secondary capture, structured report and IHE workflow profiles. Comput Med Imaging Graph 2007; 31:346–352.

20. Law M, Chan T, Tang FH, Lau TY, Huang HK, Zhang A. A retrospective study of bone age assessment of Chinese children in Hong Kong using a digital hand atlas [abstr]. In: Radiological Society of North America scientific assembly and annual meeting program. Oak Brook, Ill: Radiological Society of North America, 2006; 909.

Journal of Digital Imaging

Feature Selection and Performance Evaluation of Support Vector Machine (SVM)-Based Classifier for Differentiating Benign and Malignant Pulmonary Nodules by Computed Tomography

Yanjie Zhu,[1] Yongqiang Tan,[1] Yanqing Hua,[2] Mingpeng Wang,[2] Guozhen Zhang,[2] and Jianguo Zhang[1]

There are lots of work being done to develop computer-assisted diagnosis and detection (CAD) technologies and systems to improve the diagnostic quality for pulmonary nodules. Another way to improve accuracy of diagnosis on new images is to recall or find images with similar features from archived historical images which already have confirmed diagnostic results, and the content-based image retrieval (CBIR) technology has been proposed for this purpose. In this paper, we present a method to find and select texture features of solitary pulmonary nodules (SPNs) detected by computed tomography (CT) and evaluate the performance of support vector machine (SVM)-based classifiers in differentiating benign from malignant SPNs. Seventy-seven biopsy-confirmed CT cases of SPNs were included in this study. A total of 67 features were extracted by a feature extraction procedure, and around 25 features were finally selected after 300 genetic generations. We constructed the SVM-based classifier with the selected features and evaluated the performance of the classifier by comparing the classification results of the SVM-based classifier with six senior radiologists' observations. The evaluation results not only showed that most of the selected features are characteristics frequently considered by radiologists and used in CAD analyses previously reported in classifying SPNs, but also indicated that some newly found features have important contribution in differentiating benign from malignant SPNs in SVM-based feature space. The results of this research can be used to build the highly efficient feature index of a CBIR system for CT images with pulmonary nodules.

KEY WORDS: Feature selection, content-based image retrieval, classification, CT images, lung diseases

INTRODUCTION

Solitary pulmonary nodules (SPNs) are common findings in thoracic imaging. The volumetric computed tomography (CT) technique has introduced spiral scans which shorten the scan time and, when used in thoracic imaging, reduce the artifacts caused by partial volume effects, cardiac motion, and unequal respiratory cycles. For these reasons, spiral CT is useful in identifying and characterizing SPNs.

However, it is still difficult for radiologists to distinguish malignant from benign nodules. Differentiating malignant nodules from benign ones by visual examination is subjective and the results vary between different observers and in different cases. In general, experienced radiologists classify nodules more accurately than resident radiologists. The necessity for reliable and objective analysis has prompted the development of computer-aided systems.

It is reported that two radiologists working together outperform any independent radiologist. The computer-assisted diagnosis and detection (CAD) system can provide a "second opinion," which might improve the radiologist's performance. One study has demonstrated that radiologists more accurately classified SPNs (as measured by area under the receiving operating characteristic

[1]*From the Shanghai Institute of Technical Physics, Chinese Academy of Sciences, 500 Yu Tian Road, Shanghai, 200083, China.*

[2]*From the Department of Radiology, Huadong Hospital, Shanghai, China.*

Correspondence to: Jianguo Zhang, Shanghai Institute of Technical Physics, Chinese Academy of Sciences, 500 Yu Tian Road, Shanghai, 200083, China; tel: +86-21-55510087; fax: +86-21-63248028; e-mail: jzhang@mail.sitp.ac.cn

Online publication 26 February 2009

doi: 10.1007/s10278-009-9185-9

(ROC) curve (AUC)) with CAD assistance.[1] Recent studies have focused on the role of CAD in differentiating and characterizing pulmonary nodules. These reports discuss characteristics of nodules demonstrated to be relevant to their classification.[2–8] For example, the presence of calcification and/or fat indicates that the nodule is likely to be benign, while irregular margins and heterogeneous attenuation are signs of malignancy.[9] Another way to improve accuracy of diagnosis on new images is to recall or find images with similar features from archived historical images which already have confirmed diagnostic results,[10] and content-based image retrieval (CBIR) technology is now proposed for this purpose in digital imaging and management environment.[11,12]

Selecting the right features and constructing the higher performed classifier of pulmonary nodules are very important in developing the qualified CAD and CBIR systems. For example, most of the CAD systems consist of two steps: feature extraction and classification. In CBIR, the large amount of visual features such as shape, texture, and granulometry are usually included to build the searching index.[13]

Some studies have been done on finding and selecting features and evaluating the performance of classifiers of lung nodule and tissues for CAD and CBIR purposes.[14–20] In feature selection studies, most researches focused on differentiating the visual features of pulmonary nodules and tissues, and there were few considerations about the differentiating features for classifying benign from malignant SPNs. In classifier construction studies for lung CAD, linear discriminant analysis (LDA) and artificial neural networks (ANN) were studied intensively.[2–8] However, in LDA, the complex decision surface might not be linear. In ANN, it was difficult to determine the number of units in the hidden layer and its gradient-based algorithm might be trapped in local minima.

In this paper, we present a method for selecting pattern features of pulmonary nodules of CT images and evaluate the performance of support vector machine (SVM)-based classifiers in differentiating benign from malignant SPNs. We constructed the SVM-based classifier with the selected features using a genetic generation procedure and evaluated the performance of the classifier by comparing the classification results of the SVM-based classifier with two groups of senior and junior radiologists′ observations, as well as the results of the neural-network-based classifier. The results of this research are not only helpful to improve CAD for diagnosis on SPNs but also useful to build the highly efficient feature index of a CBIR system for CT images with pulmonary nodules. We discussed the impacts of nodule segmentation results and kernel function selection on the performances of SVM-based classifier in differentiating benign from malignant SPNs.

MATERIALS AND METHODS

Materials

High-resolution scans of 77 patients with solitary pulmonary nodules mostly less than 3 cm performed between October 1999 and December 2006 were included in our study. The selection criteria included the following: nodules were solitary, and there was no calcification or artifacts from cardiac motion or beam hardening from adjacent bone. Definitive diagnoses were obtained in each case by cytological or histopathological examination of surgical specimens and CT-guided transthoracic needle aspiration biopsy or based on clinical data such as no radiological evidence of nodular growth during two or more years of follow-up.

Among the 77 patients, 48 were men and 29 were women (age range, 27–86 years; mean, 57.97 years). There were 43 malignant cases (27 adenocarcinoma, nine squamous cell carcinoma, four small cell carcinoma, and three adenosquamous carcinoma). Thirty-four cases were benign (17 pulmonary hamartomas, eight cases of pulmonary tuberculosis, five cases of inflammatory pseudotumor, and four cases of pneumonia). Four of the 77 cases were larger than 3 cm. The largest was 4.48 cm; the smallest was 0.54 cm and the mean diameter was 1.90 cm. Among the 77 cases, 31 were larger than 2 cm, while seven out of the 31 cases were benign and 24 were malignant. Large nodules were inclined to be malignant, which dovetailed with the radiologists' knowledge.

The images were obtained by Somatom Plus (Siemens AG, Germany) and Somatom 16 (Siemens AG, Germany) CT scanners with the following parameters: 120 kV, 100 mA, 1-s

scanning time, and a standard reconstruction algorithm for the Somatom Plus scanner and 120 kV, 250 mA, 0.5-s scanning time, and a standard reconstruction algorithm (B41f) for the Somatom 16 scanner. Some patients had additional scans covering the tumors.

Nodule Segmentation

We used two methods to perform nodule segmentation in our study: the region-grow and the snake techniques. First, we can identify the boundary of most nodules by using the region-grow method from a user-specified seed point inside the nodule with adjustable thresholds. This region-grow method has also been used in other lung nodule segmentation applications.[2,7] However, the region-grow technique could not be applied if the nodule contacted with vessels or the chest wall. In those cases, we applied the snake approach after using region grow. We have 77 cases of images; 61 of these case images can be segmented by using region grow, and 14 should be segmented by using both region-grow method and snake approach, and only two cases of images must be segmented by user interactively. The times required to segment a nodule with our region-grow software program were about 4 s averagely. Figure 1 shows two examples of nodules for which the borders were identified by each of these two techniques.

Due to partial volume averaging effects, the spikes of some nodules had much lower attenuations than the center of the nodule. As a result, the border of the spikes identified by the region-grow method was not sharp. The snake method depended on its initial border and did not trace the exact border of the nodule in some cases, but, in such cases, we reinitialized the process to get a satisfied result. The segmentation results covered most of the nodule area and captured most characteristics of the borders. In our study, the segmentation results were all approved by an experienced radiologist.

Feature Extraction

In image pattern recognition, feature extraction is the first step in image classification. The visual features of lung nodules, such as the size, shape, and internal texture, were considered in our study, as such characteristics would be considered by the radiologist when classifying a nodule as malignant or benign. For example, nodules with calcification or fat are more likely to be benign, whereas irregular borders suggest malignancy. To characterize nodules, we also tried to capture other features that may suggest malignancy, such as attenuation statistics, Gabor filter responses, wavelet decomposition features, multiscale Hurst parameters, and so on.

We performed specific feature extraction of lung CT images with nodules based on the following

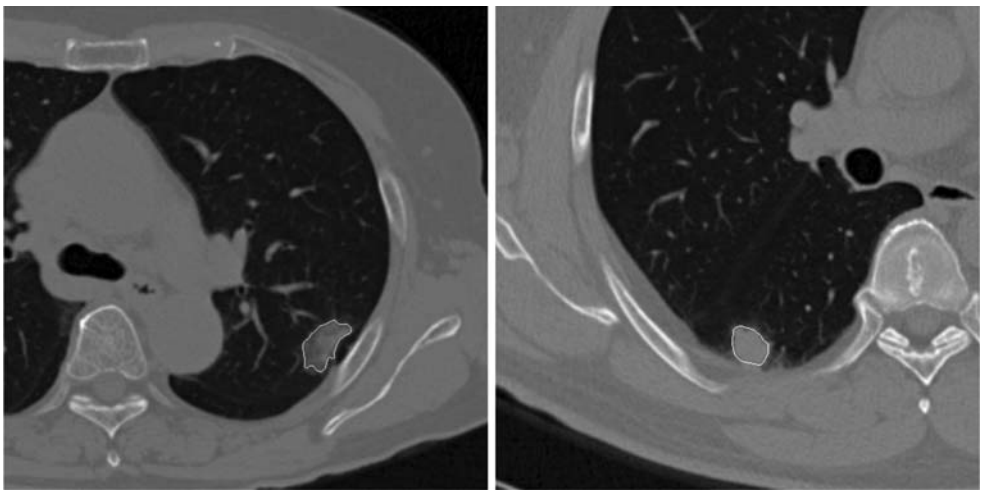

Fig 1. The segmentation results of two pulmonary nodules.

parameters: the first-order statistics features (feature 1 to feature 14) describe the attenuation distribution and the shape of the histogram; the second-order statistics features (feature 15 to feature 34) describe the spatial dependency of pixel values, particularly, entropy features represent the smoothness of the region of interest (ROI); the Gabor features (feature 35 to feature 46) capture the directional information at different scales; the wavelet frame decomposition features (feature 47 to feature 55) represent the energy of the decomposed image; the multiscale Hurst features (feature 56 to feature 61) describe the roughness of the ROI at different scales; and shape features represent the area, perimeter, irregularity of the border, and size of the ROI. A complete list of the features is provided in Table 1. Some features have good discriminant power, while other features contribute little to the classification. Therefore, the extracted features must be subjected to an optimal selection procedure before being used in classification. This selection procedure is further described in the next section.

Table 1. A Complete List of Features Extracted for Lung Nodules in CT Images

Feature extraction methods	Feature no.	Feature name
	1~10	HIST1, HIST2,...HIST10
	11	MEANV
	12	STDV
	13	KURT
First-order statistics	14	SKEW
	15~19	ASM1, CONT1, CORR1, IDM1, ENTR1
	20~24	ASM2, CONT2, CORR2, IDM2, ENTR2
	25~29	ASM3, CONT3, CORR3, IDM3, ENTR3
Second-order statistics	30~34	ASM4, CONT4, CORR4, IDM4, ENTR4
Gabor filters	35~46	GAB1, GAB2, ...GAB12
Wavelet frame decomposition	47~55	WF1, WF2, ...WF9
	56~58	HM1, HM2, HM3
Fractal parameters	59~61	HS1, HS2, HS3
	62	AREA
	63	PERI
	64	COMP
	65	MEAND
	66	MIND
Shape features	67	MAXD

Algorithms of Feature Selection, Statistical Classification, and Analysis

We enrolled 77 cases of SPNs in this study and extracted 67 features for each image. Thus, there was a high possibility of overfitting during the classification step due to the low number of samples relative to the number of features extracted. For this reason, it was necessary to reduce the high dimensionality of the input feature vectors.

In this study, we employed a genetic-algorithm-based feature selection technique to recreate multiple groups of feature subsets with different numbers of features (between five and 30 of the total 67 features were used in each analysis). This allows us to evaluate the performance of each classifier built by different groups of feature subsets. We also introduced the support-vector-machine-based classifier in this section to classify the SPNs as well and its related algorithm. In order to evaluate the performance of the classifiers in differentiating the malignant nodules from SPNs, the ROC analysis was also included in this section.

Genetic Algorithm for Feature Selection

Feature selection is a combinational optimization approach to a problem that is difficult to solve directly. The genetic algorithm is a general optimization method that is useful especially for computation-intensive applications. It mimics the evolution process in biology by representing the solution of the problem as genomes. The crossover of good genomes (indicated by small fitness value) tends to yield better results, and a certain probability of mutation allows for exploration of the whole solution space. After many generations of crossover and mutation, the algorithm yields an acceptable solution.

In this study, each generation had the same number of features, and the fitness function was defined as the misclassification rate of a tenfold cross-validation procedure. In this procedure, the samples were divided randomly into ten groups, while one group was used as test data; the rest of the samples were used to fit a multivariate normal-density function. The test data were classified based on likelihood ratios. After each group had acted as test group exactly once, the fitness function was calculated as the misclassification

rate. The smaller the value was, the better the was fitness of the genome. Figure 2 showed an evolution process of mean fitness and best fitness with the increasing of generations, in which the number of features was fixed to 25, and the number of genomes in each population was 100, and the number of generations was 300. It demonstrates that both the mean fitness and the best fitness values drop drastically after about 50 generations.

Support Vector Machine

Support vector machine is based on the structural risk minimization principle. It is reported that SVM outperforms other classifiers in many studies.[21,22] The SVM approach enjoys many attributes. It is less computationally intense in comparison to artificial neural networks. It performs well in high-dimensional spaces and also well on both training data and testing data but does not suffer from the small size of training dataset as do other kinds of classifiers since the decision surface of SVM-based classifier is determined by the inner product of training data.

The basic idea of SVM is to construct a hyperplane that maximizes the margin between negative and positive examples. The hyperplane is determined by the examples called support vectors that are closest to the decision surface. The decision surface is determined by the inner product of training data, which enables us to map the input vectors through function Φ into a higher-dimensional inner product space called feature space. The feature space could be implicitly defined by kernel $K(x, y)$. To tolerate noise and outliers and to avoid overfitting, slack variables ξ_i are introduced which allows the margin constraints to be violated.[23]

Consider the training samples (x_i, y_i), $i=1,\ldots,m$, where each point x_i is an input vector with label $y_i \in \{-1, 1\}$. The decision surface has the form:[23]

$$y = \kappa(x, w) + b \tag{1}$$

The decision surface is the solution of the following optimization problem:

$$\text{minimize} : \frac{1}{2}\kappa(w, w) + C\sum_{i-1}^{l}\xi_i \tag{2}$$

$$\text{subject to} : y_i[\kappa(w, x_i) + b] \geq 1 - \xi_i, i = 1...l$$
$$\xi_i \geq 0, i = 1...l \tag{3}$$

where $C>0$ is a parameter chosen by the user to penalize decision errors and φ is the mapping

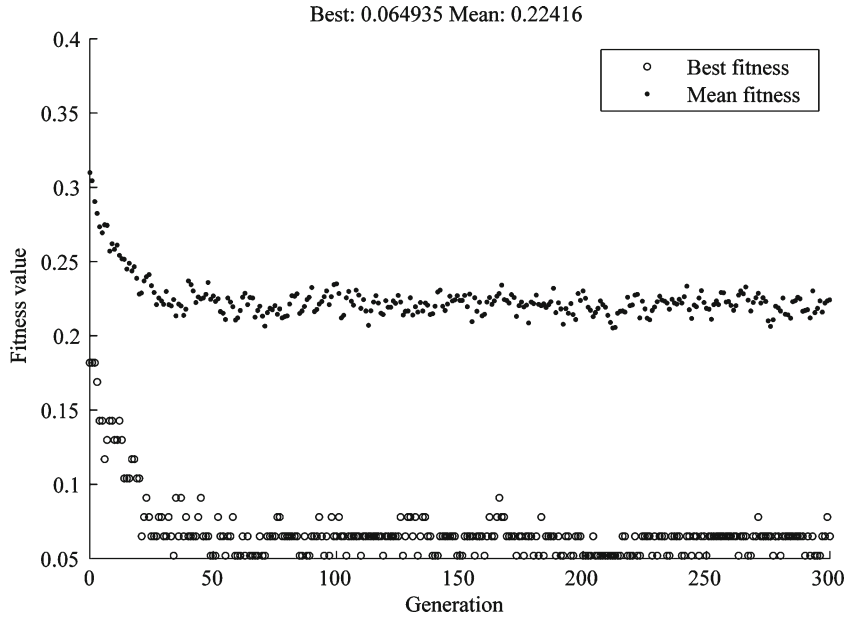

Fig 2. The evolution of best fitness and mean fitness value with increasing numbers of generations, in which the number of features was fixed to 25; the number of genomes in each population was 100, and the number of generations was 300.

determined by the kernel function. The most popular kernel is the Gaussian kernel function which is defined by:

$$\kappa(x,y) = e^{-\gamma\|(x-y)\|^2} \quad (4)$$

where γ is also chosen by the user.

In our study, the value of C was chosen to be 50 and the value of γ was chosen to be 1, and those values had good performance in the application. We will discuss in more detail why we choose Gaussian kernel function in "Reliability of Nodule Segmentation and Its Impact on the SVM-Based Classifier."

ROC Analysis

An ROC graph is a technique for visualizing the performance of classifiers and is useful to compare the performance of different classifiers in medical decision-making systems. The graph depicts the tradeoff between the true-positive and false-positive rates. While an ROC graph is a two-dimensional description of classifier performance, it is often useful to reduce it to one scalar value. The AUC is largely adopted to represent the expected performance of a classifier. The AUC of a classifier is equivalent to the probability that the classifier will rank a randomly chosen positive instance higher than a randomly chosen negative instance.[24]

RESULTS

Feature Selection of CT Images with SPN

We enrolled 77 cases in this study as described in "Materials" and extracted 67 features for each SPN. Since the dimensionality of the feature space is comparable to the number of samples, feature selection was carried out using a genetic algorithm as mentioned in "Genetic Algorithm for Feature Selection." The results of some selected feature subsets are shown in Table 2. There are about 30 subsets and each of the subset contains the number of selected features from five to 30. The next step is to determine the relevance of each selected feature to the process of differentiating benign and malignant nodules.

During the evaluation process by using the genetic algorithm, some features may be selected many times as the number of generation increases. The more times it was selected, the more important it contributed to the final generation of selected features. The number of times each feature was selected is provided in Table 3. From Table 3, we see that HIST1, HIST4, HIST10, ENTR3, ENTR4, GAB2, COMP, and MEAND were present in more than half of the feature subsets. The feature selection results were consistent with the knowledge of the radiologists. For example, the fourth histogram feature which indicated the presence of fat existed in most feature subsets. This is consistent with radiologists' knowledge that the presence of fat suggests that a SPN is benign. We will discuss the selected features and compare them with previous reported studies further in "Discussion."

Table 2. The Subsets of Feature Selection Carried Out by Using a Genetic Algorithm Mentioned in "Genetic Algorithm for Feature Selection" with The Evolution of Best Fitness and Mean Fitness Value of Genetic Generations as Indicated by Fig. 2

Subset num.	Label num. (#) of selected features
5	1, 6, 10, 15, 36
6	10, 11, 23, 32, 33, 36
7	1, 4, 6, 10, 14, 18, 31
8	2, 3, 10, 11, 17, 23, 33, 36
9	1, 4, 10, 13, 29, 33, 34, 45, 64
10	4, 10, 11, 13, 20, 29, 34, 36, 62, 65
…	…

There are about 30 subsets and each of subset contains the number of selected features from five to 30. The no. of subsets means that there are five features in this subset if the no. is five, and the selected features in each subset means that the kinds of the features listed in Table 1 are contained in this subset

SVM-Based Classifiers for CT Images with SPN

The basic idea of using SVM to classify the patterns in SVM-based feature space is to construct a hyperplane that maximizes the margin between negative and positive examples. The hyperplane is determined by the examples called support vectors that are most close to the decision surface. We employed the SVM-KM toolbox[25] as the SVM implementation based on the decision surface solution given by Eqs. 1 to 4 and the features selected in "Feature Selection of CT Images with SPN" to construct SVM-based clas-

sifier. The parameter C was set to be 50 and γ set to be 1 throughout this study.

Figure 3 showed the decision surface of SVM-based classification by using HIST1 and HIST10 in SVM-based feature space. The upper-right part in Fig. 3 indicates that the output of the classifier is positive, and down-left part indicates that the output of the classifier is negative. The circle symbol "o" indicates true-positive samples and plus symbol "+" represents true-negative samples, the features of which were used to train the SVM-based classifier. All the features are scaled to the range [0, 1]. The HIST1 feature represents the percentage of pixels in the nodule that are less than −185 HU, and the feature is scaled to the range [0, 1]. Higher values of HIST1 mean that a higher percentage of pixels are in a single bin of the histogram. The HIST10 represented the percentage of pixels above 136 HU which was in the range of calcification and indicated that high percentage of calcification and low attenuation pixels suggested that the nodule was benign.

Performance Evaluation of SVM-Based Classifiers for Differentiating SPNs

Comparison of SVM- and BP-ANN-Based Classifiers

In classifier construction studies for lung CAD, the ANN was usually used,[3,4] so we compared the performance of SVM-based classifier with ANN-based in the following. We employed a two-layered feedforward neural network which contained one input layer, one hidden layer, and one output layer. The number of inputs in the input layer equaled the dimensionality of the input vector. The output layer contained one unit to output a score that indicated the malignancy of an input nodule, and the number of units in the hidden layer was chosen from three to 18 so that the area under the ROC curve was maximized. The neural network toolbox of Matlab® was used in this study

Now, we compared the performance of SVM and back propagation (BP)-ANN in differentiating solitary pulmonary nodules in terms of AUC using the selected feature subsets with leave-one-out procedure.

A leave-one-out procedure was carried out in which one nodule was used for test purpose and

Table 3. The Number of Times each Feature Was Selected in the 300 Genetic Generation Procedure

Feature name	HIST1	HIST2	HIST3	HIST4	HIST5	HIST6	HIST7	HIST8	HIST9	HIST10	MEANV	STDV	KURT	SKEW	ASM1
Selected times	18	3	4	22	6	3	2	2	5	25	13	2	21	10	3
Feature name	CONT1	CORR1	IDM1	ENTR1	ASM2	CONT2	CORR2	IDM2	ENTR2	ASM3	CONT3	CORR3	IDM3	ENTR3	ASM4
Selected times	2	11	7	11	7	2	8	7	12	2	5	5	4	18	3
Feature name	CONT4	CORR4	IDM4	ENTR4	GAB1	GAB2	GAB3	GAB4	GAB5	GAB6	GAB7	GAB8	GAB9	GAB10	GAB11
Selected times	6	5	10	21	3	17	2	4	2	2	1	3	3	3	5
Feature name	GAB12	WF1	WF2	WF3	WF4	WF5	WF6	WF7	WF8	WF9	HM1	HM2	HM3	HS1	HS2
Selected times	11	5	1	4	3	3	1	3	0	3	2	2	3	3	3
Feature name	HS3	AREA	PERI	COMP	MEAND	MIND	MAXD								
Selected times	11	11	13	18	20	4	1								

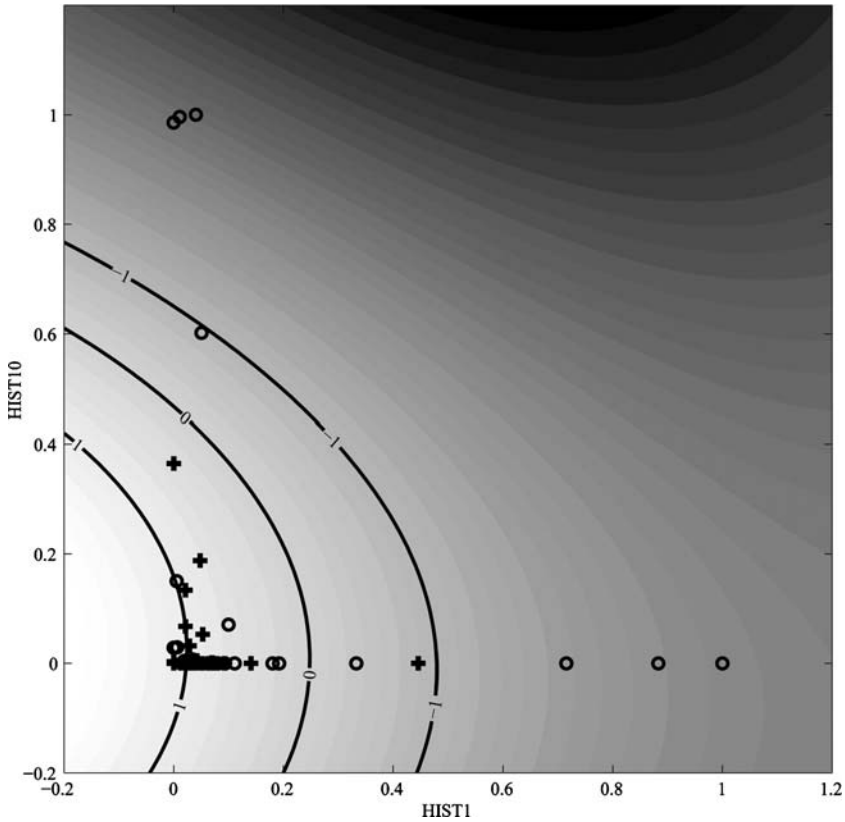

Fig 3. The decision surface of SVM is indicated in feature space by using HIST1 and HIST10. The *upper-right part* in the figure indicates that the output of the classifier is positive, and *down-left part* indicates that the output of the classifier is negative. The *circle symbol* indicates true-positive samples and *plus symbol* represents true-negative samples, the features of which were used to train the SVM-based classifier. This figure indicated that the high percentage of calcification and low attenuation pixels suggested that the nodule was benign.

the others were used for training the SVM- and ANN-based classifiers until each example was used for test only once. For a subset of features, the AUCs of SVM and ANN could be calculated using ROCKET.[26] Thus, the AUCs of SVM and ANN using different feature subsets were calculated. We selected 26 subsets of features, which contained different number of features, ranging from five to 30. Each subset of features was used to train the SVM and ANN classifiers and differentiate nodule(s) by a leave-one-out procedure, and the AUCs of the two classifiers were calculated and listed in Table 4, and the related bar graph was shown in Fig. 4 and Fig. 5 illustrated the ROC curves of SVM and ANN with ten selected features. From Figs. 4 and 5, we see that the performance of SVM-based classifier in differentiating SPNs is better than that of the ANN-based classifier.

Comparison of SVM-Based Classifier with the Radiologists' Observation

In order to evaluate the performance of SVM-based classifier in differentiating SPNs compared to radiologists' observation, we set up an experiment to let two groups of radiologists read the 77 cases of CT images with SPNs. Group one had three senior radiologists who had more than 20 years of experience in reading lung CT images in radiology department of Huadong Hospital in Shanghai; group two had three junior radiologists who had 2 to 5 years in reading lung CT images. All of these two groups of radiologists had never read these images before. They used PACS diagnostic workstations with high-resolution monitors to read these images and marked the pathology of nodules as benignancy with −1 and malignancy with 1 independently. The senior radiologists had

Table 4. The AUC of SVM and ANN by Leave-one-out Procedure Using Different Feature Subsets

Subset num.	5	6	7	8	9	10	11
SVM	0.8714	0.8208	0.8721	0.8639	0.8865	0.8673	0.868
ANN	0.7825	0.7839	0.7592	0.8406	0.8406	0.7975	0.7613
Subset num.	12	13	14	15	16	17	18
SVM	0.8953	0.814	0.8598	0.8345	0.8871	0.8693	0.8748
ANN	0.8865	0.764	0.8256	0.7661	0.7497	0.7811	0.7674
Subset num.	19	20	21	22	23	24	25
SVM	0.8194	0.8632	0.8385	0.8433	0.7886	0.7879	0.8549
ANN	0.7661	0.7462	0.7763	0.7654	0.8358	0.7531	0.7798
Subset num.	26	27	28	29	30		
SVM	0.8296	0.8310	0.7968	0.8091	0.7393		
ANN	0.7832	0.7558	0.71	0.8187	0.816		

better performance in differentiating SPNs than juniors. To represent the performance of senior and junior radiologists respectively, we used the averaged results of senior radiologists and junior radiologists, respectively, as the likelihood of malignancy to generate the ROC curves for them. Figure 6 illustrated the ROC curves of senior and junior radiologists' performance, as well as the SVM-based classifier with 17 selected features. From Fig. 6, we see that the SVM-based classifier had better performance in differentiating SPNs than radiologists.

DISCUSSION

Comparison of the Selected Features with Other Reported Results

CAD studies have offered insight in differentiating benign and malignant SPNs. For example, McNitt-Gray et al.[2] considered density distribution, area, and texture to classify 31 nodules by means of linear discriminant analysis, achieving an accuracy of 90.3%. As presented in "Feature Selection of CT Images with SPN," these most

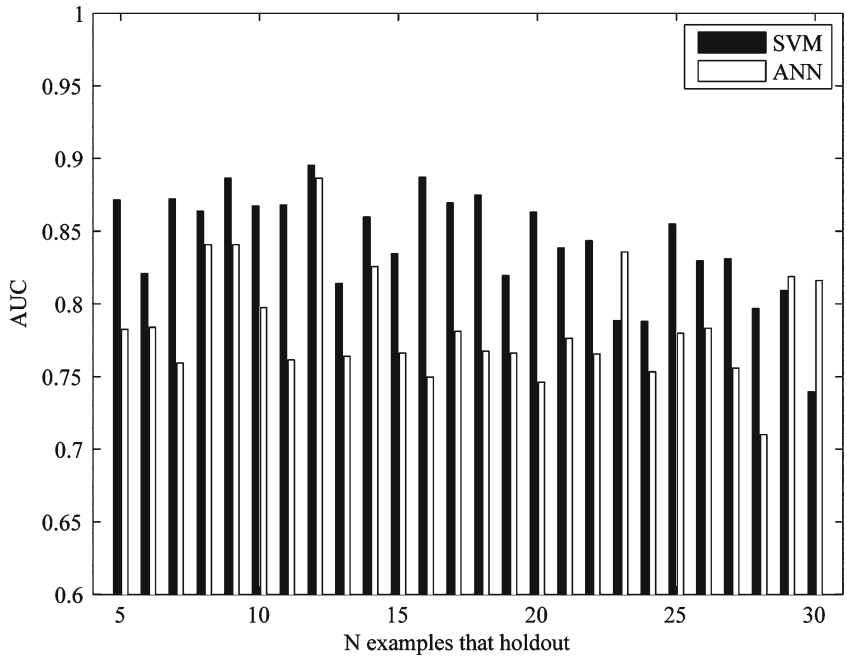

Fig 4. The ROC curves of SVM- and BP-ANN-based classifiers using ten selected features by the leave-one-out method.

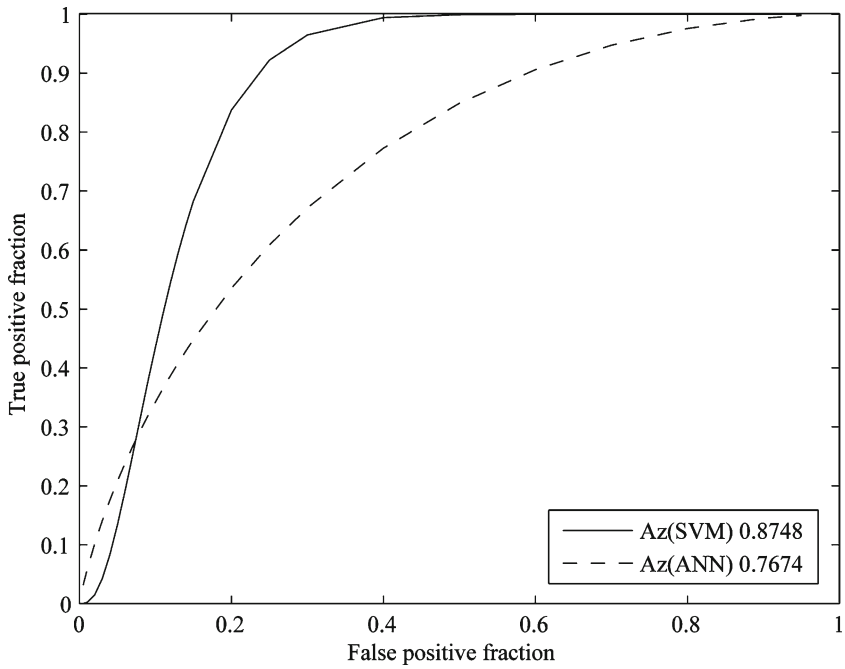

Fig 5. The AUCs of SVM- and BP-ANN-based classifiers by the leave-one-out method using different feature subsets.

frequently selected features in our research are the characteristics most commonly considered by radiologists in distinguishing benign from malignant nodules and also are consistent with data in the published literature.[3,5,6,9] Except for these, we found that seven new features (GAB2, CORR1, HS2, CORR2, CORR4, GAB12, and HM3) represented in SVM-based feature space also have

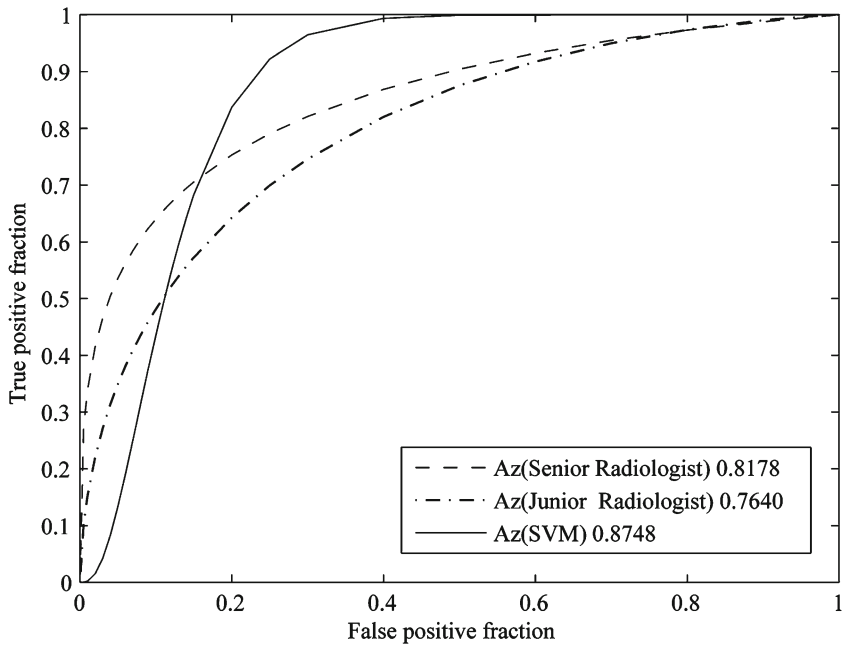

Fig 6. The ROC curves of radiologists' average performance and the SVM-based classifier with 13 selected features. The SVM-based classifier had better performance in differentiating SPNs than average of radiologists.

important impact on differentiating SPNs, and these newly found features should be included in feature index of a CBIR system for SPNs. Table 5 gives the comparison of the features selected (including times selected in evaluation process by using the genetic algorithm) in our research with the published literature.

Kernel Function Selection in SVM Classifier Construction

Although we chose the Gaussian kernel function to construct the SVM-based classifier in "ROC Analysis," the feature distributions of selected features in SVM-based feature space depend on the kernel functions which map the selected features to SVM feature space. So, the performance of SVM-based classifier in differentiating SPNs may rely on selected kernel function. In this section, we will select the different kernel functions to construct and evaluate the SVM-based classifiers to see whether there is significant difference between these kernel functions in differentiating SPNs. Usually, there are multiple kernels that can be selected, and the potential candidate kernels can be linear, multiple polynomial, Gaussian, and sigmoid, such as:

$$\text{Linear kernal}: \quad K(x,y) = <x,y> \tag{5}$$

$$\text{Polynomial kernal}: K(x,y) = (<x,y> + 1)^P \tag{6}$$

$$\text{Gaussian kernal}: K(x,y) = \exp\left(-\frac{\|x-y\|^2}{2\sigma^2}\right) \tag{7}$$

$$\text{Sigmoid kernel}: K(x,y) = \tanh(\gamma <x,y> - \delta) \tag{8}$$

We used these kernel functions one by one to construct the SVM-based classifiers with different selected feature sets and then used these classifiers to classify the SPNs.

We used a leave-one-out procedure to carry out the evaluation in which one nodule was used for test purpose and the others were used for training the SVM-based classifiers until each example was used for test only once, same as Comparison of SVM- and BP-ANN-Based Classifiers. For a subset of features, the AUCs of SVM could be calculated using ROCKET.[26] Table 6 gives the evaluation results of AUCs of SVM-based classifiers with different kernel functions on six subsets with feature numbers from five to 30. From Table 6, we can see that there is no significant difference between these kernel functions in differentiating SPNs since the average AUCs of SVM-based classifiers with different kernel functions are almost the same.

The reasons of selecting Gaussian kernel function in our research are: (1) the Gaussian model only has one parameter, and it is easy to construct the Gaussian SVM classifier compared to polynomial model which has multiple parameters; (2) the linear kernel function is a specific example of Gaussian model; (3) although both Gaussian and sigmoid models can realize the nonlinear mapping in high-dimensional space, there is less limitation in using Gaussian kernel function, but sigmoid may have invalidation values in some parameters. So, it is reasonable to choose Gaussian kernel function in constructing SVM-based classifier.

Reliability of Nodule Segmentation and Its Impact on the SVM-Based Classifier

Since the segmentation results of lung CT images with nodules would impact the feature extraction and selection for constructing SVM- or ANN-based classifiers, we should investigate the reliability of segmentation methods used in our research. In the following, we will perform some steps to evaluate whether our segmentation methods are reliable and how they impact on the SVM-based classifier.

In region-grow method, the threshold 800 was used as common value to perform the segmentation, but a user can adjust the threshold on individual case of image a little bit based on his or her visual evaluation on the results of segmented nodules. We chose four users to perform the segmentation on 77 cases of images, respectively. These four users can identify the boundary of most nodules by using the region-grow method from a user-specified seed point inside the nodule with adjustable thresholds or apply snake approach to refine the segmentation results on some (14 images) nodule images. So, we got four groups of segmented 77 cases of images which may have different segmentation results on these images. We performed feature extraction and feature selection

Table 5. The Comparison of the Features Selected in SVM-based Space in Evaluation Process by Using the Genetic Algorithm in our Research with Published Literature. Seven New Features Represented in SVM-based Feature Space have been Found to be Important on Differentiating SPNs, and these Features should also be Included in Feature Index of a CBIR System for SPNs

Feature name	Times selected	Literature published	Description	Significance
HIST10	24	Matsuki et al.[1]	Pixel range [136 HU, ~]	Calcification
KURT	23	Matsuki et al.,[1] McNitt-Gray et al.,[2] Nakamura et al.,[3] Kawata et al.,[5] Shah et al.[7]	Kurtosis of the nodule	Shape
HIST4	22	Nakamura et al.,[3] Kawata et al.[5]	Pixel range [−104 HU, −65 HU]	The range of fat
ENTR4	21	McNitt-Gray et al.[2]	The entropy of averaged concurrence matrix, step = 4	Uniformity or complexity of the texture
MEAND	19	Matsuki et al.[1], McNitt-Gray et al.,[2] Nakamura et al.,[3] Kawata et al.,[5] Shah et al.[7]	Mean diameters of the nodule	Shape
HIST1	18	McNitt-Gray et al.,[2] Shah et al.[7]	Pixel range [~, −185 HU]	Low attenuation pixels
ENTR3	18	McNitt-Gray et al.[2]	The entropy of averaged concurrence matrix, step = 3	Uniformity or complexity of texture
GAB2	17		Small Gabor filter responses at 45°	The spectrum of local image
COMP	16	Nakamura et al.[3]	Compactness of nodule	Roundness of the nodule
ENTR1	13	McNitt-Gray et al.[2]	The entropy of averaged concurrence matrix, step = 1	Uniformity or complexity of the texture
PERI	12	Matsuki et al.,[1] McNitt-Gray et al.,[2] Nakamura et al.,[3] Kawata et al.,[5] Shah et al.[7]	Perimeter of the nodule	Shape
ENTR2	11	McNitt-Gray et al.[2]	The entropy of averaged concurrence matrix, step = 2	Uniformity or complexity of the texture
MEANV	10	Matsuki et al.,[1] McNitt-Gray et al.,[2] Nakamura et al.[3]	Mean of the nodule pixels	Mean of nodule density
CORR1	10		The correlation of averaged concurrence matrix, step = 1	Correlation of local image
HS2	10		The standard deviation of Hurst parameters, scale = 2	Roughness of an image
CORR2	8		The correlation of averaged concurrence matrix, step = 2	Correlation of local image
CORR4	8		The correlation of averaged concurrence matrix, step = 4	Correlation of local image
GAB12	8		Small Gabor filter responses at 135°	The spectrum of local image
HIST3	7	Nakamura et al.,[3] Kawata et al.[5]	Pixel range [−144 HU, −105 HU]	Nodule density
HIST5	7	Nakamura et al.,[3] Kawata et al.[5]	Pixel range [−64 HU, −25 HU]	Nodule density
IDM2	7	Nakamura et al.[3]	The inverse difference moment of averaged concurrence matrix, step = 2	Homogeneity of the texture
IDM3	7	Nakamura et al.[3]	The inverse difference moment of averaged concurrence matrix, step = 3	Homogeneity of the texture
HM3	7		The mean of Hurst parameters, scale = 3	Roughness of an image

Table 6. The AUCs of SVM-based Classifiers with Different Kernel Functions by Leave-one-out Procedures Using Different Feature Subsets

Feature num. in a subset	AUCs of SVM with Gaussian	AUCs of SVM with linear	AUCs of SVM with polycon (power = 2)	AUCs of SVM with polycon (power = 3)
5	0.825581395	0.870725034	0.856361149	0.893296854
10	0.859097127	0.863885089	0.834473324	0.892612859
15	0.856361149	0.831737346	0.744186047	0.865253078
20	0.868673051	0.831053352	0.800273598	0.881668947
25	0.807797538	0.765389877	0.794801642	0.79753762
30	0.819425445	0.883036936	0.764021888	0.763337893
Average	0.830106282	0.844286015	0.801720509	0.832789645

on each of these four groups of images and used the selected features from each of the four groups to construct SVM-based classifier, respectively, then used leave-one-out procedure to calculate AUCs of these four SVM-based classifiers to evaluate their performance on differentiating SPNs. Table 7 shows the results of the comparison between four feature groups related to four user nodule segmentation results with region-grow and snake methods.

From Table 7, we can see that our nodule segmentation methods are reliable for different qualified users to segment the SPNs on most lung CT images since the differences of segmentation results from different users with region-grow and snake segmentation methods have no significant impact statistically on the results of differentiating SPNs by using the SVM-based classifier.

Selected Features Potentially Used in CBIR System

In a medical CBIR system, the large amount of visual features and low-level image character features such as shape, texture, and granulometry are usually included to build the image-searching index,[13] which is a multiple-dimension feature vector database and is linked to an image database storing related historical images with confirmed diagnostic results. The working principle of CBIR is to look for candidate images from the CBIR image database, the features of which are similar with that of an input image. As the numbers of character features of an image are usually very large such as more than hundreds or thousands, some of features are useful to label the image characters, and some are not. The image-searching efficiency (iteration times and costs of similarity calculation of every searching) of finding the right images from CBIR system are mostly dependent on the dimension numbers of feature vectors and selected correct features used to label image characters.[10] The fewer the dimension numbers of feature vectors are, the less are the costs of similarity calculation of every searching. The more correct the features used to label image characters are, the more few are the itinerate searching times in CBIR searching procedure. So, it will greatly improve the performance of a CBIR system if we used more correct features to label image characters with fewer numbers of the features in building image-searching index.

With the results of this paper, we can use selected pattern features of SPNs to build searching index in a CBIR system for lung cancer CT images, which would have more searching efficiency than that without optimally selecting pattern features of SPNs from CT images,[12] as the number of selected features are reduced from 67 to 17 without sacrificing the performance of classifiers in differentiating lung nodules.

CONCLUSIONS

In this paper, we presented a method for optimally selecting pattern features of SPNs from

Table 7. The AUCs of SVM-based Classifiers Constructed from Four Groups the Features of which were Extracted and Selected Based on Four Users' Nodule Segmentation Results, Respectively

Feature num. in a subset	User 1	User 2	User 3	User 4
5	0.870041	0.863885	0.762654	0.825581
10	0.881669	0.889193	0.857729	0.859097
15	0.876197	0.856361	0.810534	0.856361
20	0.844733	0.853625	0.844049	0.868673
25	0.79959	0.850889	0.861833	0.807797
30	0.80301	0.790698	0.759234	0.819425
Average	0.837762	0.851705	0.82545	0.830106

CT images, determined the usefulness of various selected pattern features for a CAD in differentiating SPNs or for a CBIR system in searching similar feature nodules, and evaluated the performance of support-vector-machine-based classifier in differentiating lung nodules.

Seventy-seven biopsy-confirmed CT cases of SPNs were included in this study. A total of 67 features were extracted by a feature extraction procedure, and 25 features were finally selected from these 67 features after 300 genetic generations. We constructed the SVM-based classifier with the selected features and evaluated the performance of the classifier by comparing the classification results of the SVM-based classifier with six radiologists' observations and ANN-based classifier. The evaluation results showed that the SVM-based classifier had good performance in differentiating the benign from malignant SPNs compared to an average performance of radiologists in our research and was more accurate than the ANN-based classifier in distinguishing benign from malignant SPNs. This study results not only showed that most of the selected features are characteristics frequently considered by radiologists in classifying SPNs which are also consistent with the finding of CAD analyses previously reported but also indicated that some newly found features have important contribution to differentiating benign from malignant SPNs in SVM-based feature space.

The results of this research are not only helpful to improve CAD for diagnosis on SPNs but also useful to build the highly efficient feature index of a CBIR system for CT images with pulmonary nodules. We discussed the impacts of nodule segmentation results and kernel function selection on the performances of SVM-based classifier in differentiating benign from malignant SPNs.

ACKNOWLEDGEMENTS

The project was supported by the grants from the National Nature Science Foundation of China (grant no. 30570512) and Shanghai Science and Technology Committee (grant no. 064119658, 06SN07111). The authors would like to thank Dr. Xiaojun Ge for providing the CT images used in this study.

REFERENCES

1. Matsuki Y, Nakamura K, Watanabe H, Aoki T, Nakata H, Katsuragawa S, Doi K: Usefulness of an artificial neural network for differentiating benign from malignant pulmonary nodules on high-resolution CT: evaluation with receiver operating characteristic analysis. Am J Roentgenol 178 (3):657–663, 2002

2. McNitt-Gray MF, Hart EM, Goldin JG, Yao CW, Aberle DR: A pattern classification approach to characterizing solitary pulmonary nodules imaged on high resolution computed tomography. Proc SPIE 2710:1024–1034, 1996

3. Nakamura K, Yoshida H, Engelmann R, MacMahon H: Computerized analysis of the likelihood of malignancy in solitary pulmonary nodules with use of artificial neural networks. Radiology 214:823–830, 2000

4. Shiraishi J, Abe H, Englemann R, Aoyama M: Computer-aided diagnosis to distinguish benign from malignant solitary pulmonary nodules on radiographs: ROC analysis of radiologists′ performance–initial experience. Radiology 227:469–474, 2003

5. Kawata Y, Niki N, Ohmatsu H, Kusumoto M, et al: Hybrid classification approach of malignant and benign pulmonary nodules based on topological and histogram features. In: Proc MICCAI 297–306, 2000

6. Silva AC, Paiva AC, Oliveira ACM: Comparison of FLDA, MLP and SVM in diagnosis of lung nodule. Lect Notes Comput Sci 3587:285–294, 2005

7. Shah SK, McNitt-Gray MF, Rogers SR: Computer aided characterization of the solitary pulmonary nodule using volumetric and contrast enhancement features. Acad Radiol 12 (10):1310–1319, 2005

8. Yamashita K, Matsunobe S, Tsuda T, Nemoto T: Solitary pulmonary nodule: preliminary study of evaluation with incremental dynamic CT. Radiology 194:399–405, 1995

9. Siegelman SS, Khouri NF, Leo FR: Solitary pulmonary nodules: CT assessment. Radiology 160:307–312, 1986

10. Müller H, Michoux N, Bandon D: A review of content-based image retrieval system in medical applications-clinical benefits and future directions. Int J Med Informatics 73(1):1–23, 2004

11. Fisher B, Deserno T, Ott B, et al: Integration of a research CBIR system with RIS and PACS for radiological routine. Proc SPIE 6919:691914–1–691914-10, 2008

12. Tan Y, Zhang J, Hua Y, Zhang G: Content-based image retrieval in picture archiving and communication system. Proc SPIE 6145:614515–1–614515-8, 2006

13. Deserno T, Antani S, Long RL: Ontology of gaps in content-based image retrieval. J Digit Imaging (in press), 2007

14. Depeusinge A, Lavindrasana J, Hidki A, et al: A classification framework for lung tissue categorization. Proc SPIE 6919:69190C1–69190C12, 2008

15. Silva AC, Carvalho PCP, Gattass M: Diagnosis of lung nodule using semivariogram and geometric measures in computerized tomography images. Comput Methods Programs Biomed 79:31–38, 2005

16. Haralick RM: Statistical and structural approaches to texture. Proc IEEE 67:786–804, 1979

17. Clausi DA, Jernigan ME: Designing Gabor filters for optimal texture separability. Pattern Recogn 33:1835–1849, 2000

18. Manjunath B, Ma W: Texture features for browsing and retrieval of image data. IEEE Trans Pattern Analysis Mach Intell 18(8):837–842, 1996

19. Unser M: Texture classification and segmentation using wavelet frames. IEEE Trans Image Processing 4:1549–1560, 1995

20. Kaplan LM, Murenzi R: Texture segmentation using multi-scale Hurst features. IEEE Int Conf Image Process 3:205–208, 1997

21. Joachims T: Text categorization with support vector machines. In: Proceedings of European Conference on Machine Learning (ECML), 1998

22. Brown M, Grundy W, Lin D, Cristianini N, Sugnet C, Furey T, Ares M, Haussler D: Knowledge-based analysis of microarray gene expression data using support vector machines. 1999. http://www.cse.ucsc.edu/research/compbio/genex/genex.html. Santa Cruz, University of California, Department of Computer Science and Engineering

23. Shawe-Taylor J, Cristianini N: Kernel methods for pattern analysis, Cambridge: Cambridge University Press, 2004

24. Fawcett T: ROC graphs: notes and practical considerations for data mining researchers. Technical report HPL-2003-4 HP Labs, 2003.

25. Canu S, Grandvalet Y, Guigue V, Rakotomamonjy A: SVM and kernel methods Matlab toolbox, Rouen: Perception Systèmes et Information, INSA de Rouen, 2005

26. Metz CE: ROCKIT software. http://xray.bsd.uchicago.edu/krl/index.htm, 2006

SELECTED BOOK EXCERPT

The definitive guide to PACS—now with more clinically applicable material

In recent years the field of picture archiving and communications systems—PACS—and image informatics has advanced due to both conceptual and technological advancements. This edition of *PACS and Imaging Informatics: Basic Principles and Applications* addresses the latest in this exciting field. In contrast to the previous edition, this updated text uses the framework of image informatics, not physics or engineering principles, to explain PACS. It is the only resource that thoroughly covers the critical issues of hardware/software design and implementation in a systematic and easily comprehensible manner.

To strengthen and update the book, the author:

- emphasizes clinical applications of PACS and integrates clinical examples throughout the text
- reflects the many changes in the field, with new chapters on web-based PACS, security, integrating the healthcare enterprise, clinical management systems, and the electronic patient record
- uses the framework of imaging informatics to explain PACS, making the book accessible to those without advanced knowledge of physics, engineering, math, or information technology
- explains how PACS can improve workflow, therapy, and treatment

With the most systematic and thorough coverage of practical applications available, this text is the complete guide for all those involved in designing, implementing, and using PACS. Professionals in medical and allied health imaging informatics; radiologists and their technical staff; surgeons and oncologists and their teams; medical and electronic engineers; medical informaticians; and fellows, graduate students, and advanced undergraduates will all benefit from this valuable resource.

"An excellent book for people involved in the design, implementation, or simply the operations of PACS and an appropriate textbook."
— from a review of the previous edition in *IEEE Engineering in Medicine and Biology*

"The strength of the book lies in the vast experience of the author, who has implemented PACS at numerous institutions in the United States and abroad."
— from a review of the previous edition in *Radiology*

WILEY-BLACKWELL
www.wiley.com/wiley-blackwell

ISBN 978-0-470-37372-9
90000
9 780470 373729

Huang

Second Edition

PACS and Imaging Informatics

Basic Principles and Applications

WILEY-BLACKWELL

Second Edition

PACS and Imaging Informatics

Basic Principles and Applications

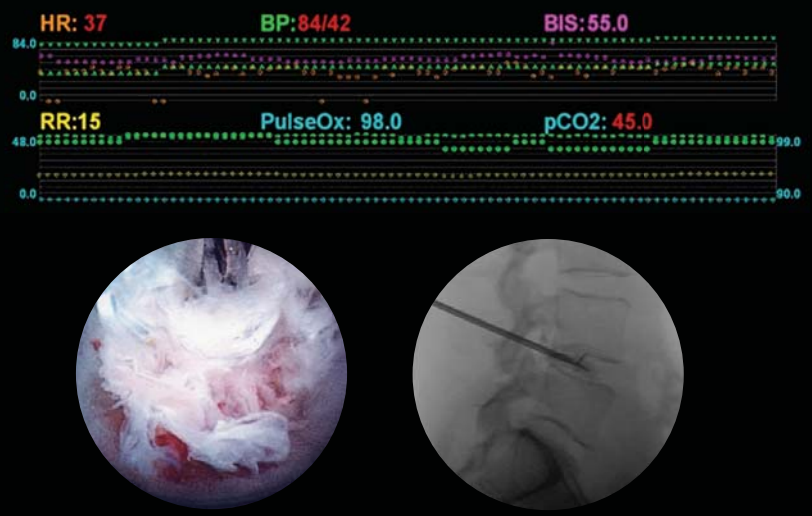

H. K. Huang, D.Sc., FRCR (Hon.), FAIMBE

WILEY-BLACKWELL

ACKNOWLEDGMENTS

Many people have provided valuable assistance during the preparation of this book, in particular, many of my past graduate students, postdoctoral fellows, and colleagues, from whom I have learned the most. Chapter 1, Introduction, and Part I, Medical Imaging Principles (Chapters 2–6), have been revised substantially from the original book *PACS and Imaging Informatics: Basic Principles and Applications*, published, 2004. Part II, PACS Fundamentals (Chapters 7–13), consists of materials based on revised industrial standards and workflow profiles, updated technologies, and current clinical experience of other researchers and ourselves. Part III, PACS Operation (Chapters 14–19), are mostly our group's personal experience over the past six years in planning, design, implementation, and operating large-scale PAC systems. Part IV, PACS-based and DICOM-based Imaging Informatics (Chapters 20–28), presents systematic overview of current trends in medical imaging informatics research learned from colleagues and other researchers, as well as our own research and development.

Materials retained from the last edition were contributed by K. S. Chuang, Ben Lo, Ricky Taira, Brent Stewart, Paul Cho, Shyh-Liang Andrew Lou, Albert W. K. Wong, Jun Wang, Xiaoming Zhu, Johannes Stahl, Jianguo Zhang, Ewa Pietka, X. Q. Zhou, F.Yu, Fei Cao, Brent Liu, Maria Y.Y. Law, Lawrence Chan, Harold Rutherford, Minglin Li, Michael F. McNitt-Gray, Christopher Carr, Eliot Siegel, Heinz Lemke, Kiyonari Inamura, and Cammy Huang.

For the new materials, I am thankful for contributions by the following individuals: Brent Liu (Chapters 7, 18, 19, 24, Sections 9.4, 9.5, 11.6, 18.6, 18.7.1, 18.7.2, 18.7.3, 18.8, 19.2, 19.3, 19.4, 21.4, 28.3.1), Jianguo Zhang (Sections 12.7), Maria Y.Y. Law (Chapter 23, Section 28.3.2), Cammy Huang (Section 28.5), Michael Z. Zhou (Chapter 17, Sections 8.6, 21.3, 21.4, 21.5, 26.3, 28.2), Lucy Aifeng Zhang (Sections 20.4.3, 26.7, 26.8), Jorge Documet (Sections 8.6, 14.6, Chapter 24, Chapter 27), Anh Le (24.3, 26.3, 26.5), Jasper Lee (Sections 4.9, 5.4.4, 21.6), Kevin Ma (Section 26.8), Bing Guo (Chapter 27, Sections 12.8, 26.5, 26.6), Kevin Wong (Sections 18.7.3, 19.4), John Chiu (Chapter 24), NT Cheung (Sections 16.11, 22.3), Tao Chan (Sections 16.11, 25.4, 25.5), Anthony Chan (Sections 18.7.4). Paymann Moin and Richard Lee contributed discussions in clinical radiology and some art work and images. A special thank you must go to Mariam Fleshman and Ashley Sullivan who contributed some creative art work, read through all chapters to extract the lists of acronyms and the index, and organized the references, to Angelica Visgen for editorial assistance, to Jim Sayre for numerous data collections and statistical analysis, and to Maria Y. Y. Law, who read through and edited the Introduction, and Part I and Part IV chapters.

This book was written with the assistance of the following staff members and consultants of the Imaging Processing and Informatics Laboratory, USC:

Brent J. Liu, Ph.D.
Associate Professor, USC

Jianguo Zhang, Ph.D.
Professor, Shanghai Institute of Technical Physics,
The Chinese Academy of Science,
Visiting Professor, USC

Maria Y. Y. Law, Ph.D. M.Phil., BRS., Teach Dip.,
Associate Professor, Hong Kong Polytechnic University
Visiting Associate Professor, USC

Jorge Document, Ph.D.
Postdoctoral Fellow, USC

Camillan Huang, Ph.D
Director of Scientific Outreach, WGLN; and Virtual Labs Project Director
Center for Innovations in Learning
Lecturer, Department of Computer Science, Stanford University

H. K. HUANG SHORT BIOGRAPHY

H. K. (Bernie) Huang, FRCR(Hon.); FAIMBE; Professor of Radiology and Biomedical Engineering; Director, Division of Imaging Informatics, Department of Radiology; and Director MS Program, Medical Imaging and Imaging Informatics, Department of Biomedical Engineering, University of Southern California, Los Angeles, Chair Professor of Medical Informatics, The Hong Kong Polytechnic University; and Honorary Professor, Shanghai Institute of Technical Physics, The Chinese Academy of Sciences.

Dr. Huang pioneered in picture archiving and communication system (PACS) and imaging informatics research. He developed the PACS at UCLA in 1991, and the hospital-integrated PACS at UCSF in 1995, and started imaging informatics research in 1999. Dr. Huang has taught at Georgetown University (1971–80); University of Iowa (1981–82); UCLA (1982–92); UC Berkeley and UC San Francisco (1992–99); Hong Kong Polytechnic University (2000–present); and the University of Southern California (2000–present). His current research interests are in tele-imaging and telemedicine, fault-tolerant PACS server, PACS ASP model, Internet 2, PACS-based CAD and surgery, imaging informatics, image recovery during disaster, image integrity, Data Grid, grid computing, HIPAA compliance, patient tracking system, radiation therapy information system, PDA Web-based image management and distribution, ePR, and image-guided minimally invasive spinal surgery. He has co-authored and authored eight books, published over 200 peer-reviewed articles, and received several patents. His book: *PACS and Imaging Informatics* published by John Wiley & Sons in 2004 has been the only textbook in this field. Over the past 25 years Dr. Huang has received over U.S. $21 million dollars in PACS, medical imaging informatics, tele-imaging, and image processing related research grants and contracts, as well as imaging informatics training grants from the U.S. federal and state governments, and private industry. He has mentored 24 PhD students and over 30 postdoctoral fellows from around the world. Dr. Huang has been a consultant for many national and international hospitals, and imaging manufacturers in the design and implementation of PAC systems, enterprise-level ePR with image distribution, and image-based therapy and treatment ePR systems.

Dr. Huang was inducted into the Royal College of Radiologists, London as an Honorary Fellow, for his contribution in PACS research and development, in November 1992; the American Institute of Medical and Biological Engineering as a Founding Fellow, for his contribution in medical imaging, in March 1993; the EuroPACS Society as an Honorary Member for his contribution in PACS, in October 1996; Honorary President, 2003 International CARS Congress, London; and President, 2007 First Iranian Imaging Informatics Conference. Dr. Huang has been Visiting Professor in many leading universities around the world, and a Board Member in leading medical imaging manufacturers.

PACS AND IMAGING INFORMATICS
BASIC PRINCIPLES AND APPLICATIONS

Second Edition

H. K. Huang, D.Sc., FRCR (Hon.), FAIMBE

Professor of Radiology and Biomedical Engineering
University of Southern California

Chair Professor of Medical Informatics
The Hong Kong Polytechnic University

Honorary Professor, Shanghai Institute of Technical Physics
The Chinese Academy of Sciences

WILEY-BLACKWELL
A John Wiley & Sons, Inc., Publication

Published by John Wiley & Sons, Inc., Hoboken, New Jersey
Published simultaneously in Canada

Library of Congress Cataloging-in-Publication Data:

Huang, H. K., 1939–
PACS and imaging informatics : basic principles and applications / H.K. Huang. – 2nd ed. rev.
p. ; cm.
Includes bibliographical references and index.
ISBN 978-0-470-37372-9 (cloth)
1. Picture archiving and communication systems in medicine. 2. Imaging systems in medicine. I. Title. II. Title: Picture archiving and communication system and imaging informatics.
[DNLM: 1. Radiology Information Systems. 2. Diagnostic Imaging. 3. Medical Records Systems, Computerized. WN 26.5 H874p 2010]
R857.P52H82 2010
616.07′54–dc22

2009022463

Printed in the United States of America

10 9 8 7 6 5 4 3 2 1

To my wife, Fong, for her support and understanding,
my daughter, Cammy, for her growing wisdom and ambitious spirit, and my
grandchildren Tilden and Calleigh, for their calming innocence.

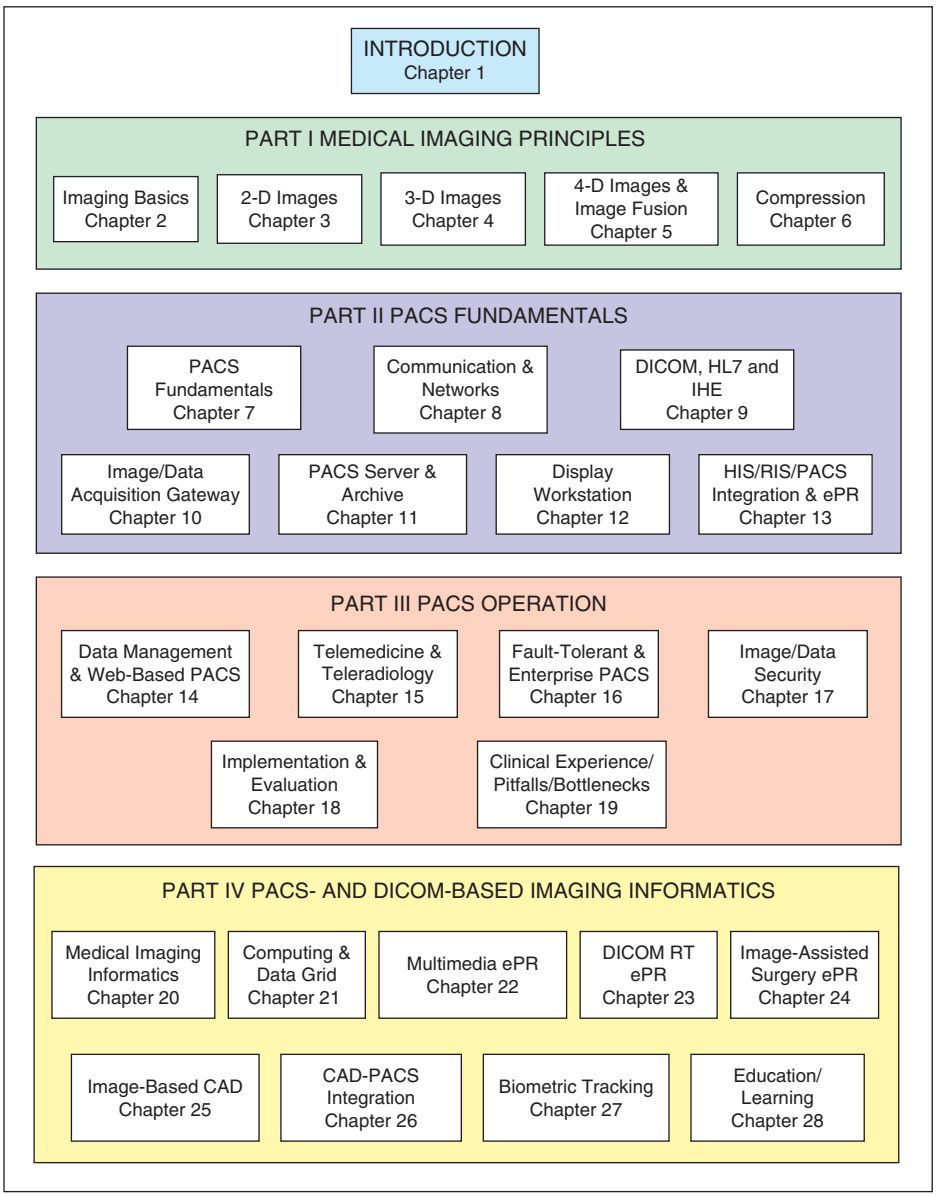
INTRODUCTION
Chapter 1
PART I MEDICAL IMAGING PRINCIPLES
Imaging Basics
Chapter 2
2-D Images
Chapter 3
3-D Images
Chapter 4
4-D Images &
Image Fusion
Chapter 5
Compression
Chapter 6
PART II PACS FUNDAMENTALS
PACS
Fundamentals
Chapter 7
Communication &
Networks
Chapter 8
DICOM, HL7 and
IHE
Chapter 9
Image/Data
Acquisition Gateway
Chapter 10
PACS Server &
Archive
Chapter 11
Display
Workstation
Chapter 12
HIS/RIS/PACS
Integration & ePR
Chapter 13
PART III PACS OPERATION
Data Management
& Web-Based PACS
Chapter 14
Telemedicine &
Teleradiology
Chapter 15
Fault-Tolerant &
Enterprise PACS
Chapter 16
Image/Data
Security
Chapter 17
Implementation &
Evaluation
Chapter 18
Clinical Experience/
Pitfalls/Bottlenecks
Chapter 19
PART IV PACS- AND DICOM-BASED IMAGING INFORMATICS
Medical Imaging
Informatics
Chapter 20
Computing &
Data Grid
Chapter 21
Multimedia ePR
Chapter 22
DICOM RT
ePR
Chapter 23
Image-Assisted
Surgery ePR
Chapter 24
Image-Based CAD
Chapter 25
CAD-PACS
Integration
Chapter 26
Biometric Tracking
Chapter 27
Education/
Learning
Chapter 28